Phytoplankton Production In Lake Victoria, East Africa

by

Gregory M. Silsbe

A thesis
presented to the University of Waterloo
in fulfillment of the
thesis requirement for the degree of
Master of Science
in
Biology

Waterloo, Ontario, Canada, 2004

I hereby declare that I am the sole author of this thesis. This is a true copy of this thesis, including any required final revisions, as accepted by my examiners.

I understand that my thesis may be made electronically available to the public.

Abstract

This thesis develops, validates and applies an empirical model that provides the first spatially explicit estimates of gross and net phytoplankton production in Lake Victoria. Gross and net phytoplankton production are in turn used to estimate the maximum sustainable yield (MSY) of Lake Victoria's fishery following an empirical formula and the carbon efficiency transfer method.

Chapter 2 presents results from three inshore areas where diurnal and sub-seasonal gross and net phytoplankton production was derived using an adapted version of the phytoplankton production model developed by Fee (1990). Spatial and temporal trends of chlorophyll (chl), PI parameters, the vertical attenuation of PAR (k_{PAR}), Secchi depths (SD) and respiration rates are identified. k_{PAR} and SD are highly correlated to chl within the euphotic zone, as well as to each other. Furthermore, the two PI parameters, P_{BM} and α_B, exhibit a strong linear relationship and both decline along an increasing chl gradient, presumably due to increased light-limitation, a taxonomic shift from diatoms to cyanobacteria with increasing chl as well as an increased need for biologically fixed nitrogen. These hypotheses are supported by observed synchronous changes in the PSII:PSI ratio of phytoplankton and changes in the chl-specific attenuation of PAR (k_{chl}). Relationships are also derived between biomass-specific respiration rates (R_B) with chl and P_{BM}; similar to PI parameters R_B decreases with increasing chl. Owing to these correlative trends, only one parameter is required to estimate gross phytoplankton production through the empirical model developed in this thesis.

The empirical model predicts that gross phytoplankton production increases in a near linear fashion between chl of 0 to 10 $mg.m^{-3}$, begins to flatten out as chl approaches 20 $mg.m^{-3}$ and then slightly decreases when chl exceeds 40 $mg.m^{-3}$ where the maximum PP_G of 13.1 g $O_2.m^{-2}.day^{-1}$ is reached and is in close agreement with a theoretical argument proposed by Talling (1965). Areal respiration and consequently net phytoplankton production are sensitive to chl within the mixed layer as well as mixed layer depths. Overall, the lakewide averages of gross and net phytoplankton production are 9.68 and 2.2 g $O_2.m^{-2}.day^{-1}$ respectively.

Significant temporal variability was observed on sub-seasonal scales within the inshore of Lake Victoria, and changes in limnological parameters coincided with changes in water column temperatures in each of the three bays. In Fielding Bay, the availability of meteorological data revealed that strong nocturnal wind events decreased both the water column temperature and chl, while both parameters generally increased in the absence of any such wind event. Lateral exchange of water with deeper areas through strong wind events essentially flushes Fielding Bay causing the observed decreases in both the water column temperature and chl; this hydrodynamic event also influences other limnological parameters according to their respective correlative regression equations with chl. Spatial trends were also observed between inshore areas. The deepest area, Napoleon Gulf, has the lowest values of chl while the shallowest area, Inner Murchison Bay, has the highest chl as the mean depth of a bay sets an approximate upper limit on chl. With respect to diurnal variability, PI parameters decline through the day, k_{PAR} increases over the day and no statistically valid trends were ascertained for chl and R_B.

Chapter three examined spatial and seasonal patterns of chlorophyll fluorescence, temperature, dissolved oxygen and water transparency from four lakewide cruises. Significant spatial variability of each parameter confirmed that lakewide data is required to generate spatially explicit estimates of phytoplankton production. Complex patterns in the thermal structure during each cruise illustrated that physical processes in Lake Victoria are at times more complex that a previously stated unidirectional hypothesis of warm water in the north and cool water in the south (Spigel and Coulter 1996), and these patterns influence spatial patterns in dissolved oxygen and Secchi depths. Similar to Chapter 2, estimates of chl within the mixed layer were highly correlated to mixed depths, while lakewide averages of chl are lower than previously reported offshore values (Mugidde 1993, 2001).

Acknowledgements

I would like to thank my supervisors, Drs. Bob Hecky and Stephanie Guildford for their patience, guidance and financial support throughout my Masters degree and for allowing a civil engineer to enter a biology program. I would further like to thank them for fostering a dynamic academic environment at the University of Waterloo and for providing opportunities to work abroad, for which many of their students have benefited both intellectually and culturally. I am grateful to my committee members Drs. Bill Taylor and Ralph Smith for their thoughtful suggestions early on in my degree and for their revision of this thesis.

Throughout this degree, and the year and a half leading up to it, I have had the pleasure to participate in different research projects in conjunction with several African research institutes. I am particularly indebted to many scientists and technicians from these institutes who have made my research enjoyable and productive. Foremost, I am grateful to the mentoring and kindness of Dr. Rose Mugidde at the Fisheries Research and Resources Institute (FIRRI) without whom this thesis would never have been possible. Lakewide data presented in Chapter 3 was collected through the Lake Victoria Fisheries Research Project (LVFRP) in conjunction with the Tanzanian Fisheries Research Institute (TAFIRI). I would particularly like to thank the LVFRP project manager Martin Van der Knapp for his enthusiasm and for organizing valuable research cruises. TAFIRI scientists Johanna Budeba and Charles Ezekiel primarily collected the lakewide data with the assistance of myself, Katherine Mackenzie and Brynn Upsdell through youth internship programs funded by the Canadian International Development Agency (CIDA).

Most of the fieldwork presented in Chapter 2 was performed in conjunction with FIRRI, I would like to thank former director Dr. Richard Ogutu-Ohwayo and current director Dr. John Balirwa for their intellectual and logistical support. William Okello, Godfrey Magezi and Simon Kikonyogo helped ease the load of field and lab work and provided friendship while David Balidawa, Musana and Charles Balisse provided reliable transportation. Data collection in Inner Murchison Bay was carried out with the National Water and Sewerage Corporation (NWSC) with assistance from

Kennedy Ara and Jill Aitken. Fieldwork in 2001 and 2002 were financially supported through Lake Victoria Environmental Program (LVEMP) and a CIDA Innovation grant respectively. I am grateful to an NSERC grant awarded to my supervisors that funded my M.Sc. while in Waterloo.

I would like to acknowledge The Centre for Learning & Teaching Through Technology (LT3) at the University of Waterloo whose Learning Innovation Grant financially supported the development of the adapted version of Fee's phytoplankton production model employed throughout this thesis. I am particularly grateful to the support of Dr. Ralph Smith and Dr. Jane Holbrook for guiding me through grant process and to Dr. Stephanie Guildford, Mangaleso Gondwe and Serghei Bocaniov for discovering more errors in the program than I would care to admit. I would like to thank Linda Campbell whose International Development Research Award funded the digitizing of the Lake Victoria bathymetric map. I am grateful to Sally MacIntyre for generously lending me several thermistor chains and for forgiving me when they disappeared from the lake.

I am grateful to colleagues within the University of Waterloo Aquatic Ecology Group (UWAEG) for their friendship and for the many thoughtful discussions we have enjoyed. Dr. Piet Verburg, Scott Higgins, Mohammed Mohammed, Vicky Jackson, Jane Almond, Rebecca North and Paul Weidman have been particularly helpful throughout the course of this degree. I would like to thank Sairah Malkin for her love, friendship and support throughout my Master's as well as providing a critical review of several sections of this thesis.

I thank my family and I wish to dedicate this thesis to my grandfather Walter Silsbe, who passed away in May of 2004.

Table of Contents

List of Figures

List of Tables

Chapter 1: General Introduction

1.1 Lake Victoria: Background

Lake Victoria, in terms of surface area, is the world's second largest freshwater lake and the largest of all tropical lakes. Similar to the other African Great Lakes, its geological history is linked to the formation of the East African Rift Valley. Lakes located within the Rift Valley (i.e. Lake Malawi and Tanganyika) are characteristically long and narrow, deep, steep-sided and meromictic. Lake Victoria, on the other hand, is located atop a broad topographical depression between the western and eastern branches of the rift valley system (Scholz 1998) it is shallow, broad and experiences annual offshore overturns (Talling 1957b). Table 1.1 offers a comparative geographical and geopolitical view between Lake Victoria and some of the world's other Great Lakes. Apart from morphological and hydrological differences between Lake Victoria and Lakes Malawi and Tanganyika, there is also an obvious economic disparity between the riparian countries of African lakes and other Great Lakes. From this simple fact, one might infer large gaps in comprehensive knowledge of African lake ecosystems due to depressed research infrastructure as well as political and economical instability. Although this is true to a certain extent, Lake Victoria has nonetheless benefited from a significant amount of research that has revealed a fascinating ecological history.

Recent paleolimnological studies conducted on Lake Victoria through the International Decade of East African Lakes (IDEAL) program have elucidated the recent geological history of the lake. The precise timing of when Lake Victoria was formed remains uncertain. More importantly, the IDEAL program revealed that the lake was completely desiccated around 12,400 years before present (Johnson et al. 1996), as East Africa was significantly drier and cooler during the last ice age. Evidence of ecosystem evolution since this drying event stems from additional paleolimnology studies and early observations of Lake Victoria's fisheries. Kendall (1969) showed that since

Table 1.1: Geographical and geopolitical features of Great Lakes

Lake	Surface Area (km^2)	Volume (km^3)	Maximum Depth (m)	Mean Depth (m)	Drainage Basin (km^2)	Combined GDP of Riparian Countries (US$ Billions)[4]
Victoria[1]	66,368	2,598	75	39	195,000	82.1 (Kenya, Uganda, Tanzania)
Malawi[2]	28,800	8,400	706	273	22,490	46.6 (Malawi, Mozambique, Tanzania)
Tanganika[2]	32,600	18,880	1,471	580	198,400	66.3 (Burundi, DRC, Tanzania, Zambia)
Superior[2]	82,100	12,200	406	149	128,000	11,005 (Canada, USA)
Erie[3]	25,657	484	64	19	58,800	11,005 (Canada, USA)
Baikal[3]	31,500	23,000	1,637	730	540,000	1,270 (Russia)

[1] Silsbe 2003
[2] Spigel and Coulter 1996 and references therein.
[3] Crul 1995 and references therein.
[4] CIA 2002

the desiccation of Lake Victoria, *Coelastrum* spp. were the dominant green algal taxa, and the diatom community fluctuated between dominance by *Stephanodiscus astraea*, *Aulocisira* spp. and *Nitzschia* spp. Stager (1998) attributes these observed fluctuations in diatom species to global scale warming and cooling trends, suggesting that algal communities in Lake Victoria have been inherently dynamic, albeit on long time scales. The most remarkable occurrence since the desiccation of Lake Victoria 12,400 years ago has been the appearance of a superflock of haplochromine cichlid fish; at the turn of the last century at least 500 species inhabited Lake Victoria (Seehausen et al. 1997b). Competing hypotheses have proposed that either the superflock evolved from one ancestral species within Lake Victoria (Seehausen et al. 1997a) or that past geological alterations allowed for two seeding lineages of haplochromines originating from Lake Kivu to recolonize Lake Victoria after the recent desiccation (Verheyen et al. 2003 and references therein). Regardless of which hypothesis is correct, drastic anthropogenic effects within the past 40 years have led to the rapid mass extinction of many of these same species (Ogutu-Ohwayo 1985, Ogutu-Ohwayo 1990, Witte et al. 1992).

In a successful effort to increase commercial fish production, the large voracious piscivore Nile Perch (*Lates niloticus*) and the detritivore tilapia (*Oreochromis niloticus*) were introduced into Lake Victoria during the 1950s and early 1960s (Ogutu-Ohwayo 1985). At the same time, human population in the Lake Victoria basin was sharply increasing (United Nations 1995) and correlated with similar increases in agricultural production (Verschuren et al. 2002). Watershed activities including increases in municipal and industrial effluents, greater subsistence agricultural practices, deforestation and human encroachment of the shoreline leading to wetland degradation have collectively given rise to higher nutrient fluxes into the lake (Bugenyi and Balirwa 1989, Hecky 1993, Scheren et al. 2000). So as Lake Victoria's ecosystem was being purposefully manipulated through exotic fish introductions, it was also unintentionally being subjected to historically unprecedented nutrient loadings (Hecky 1993). Fortunately near the onset of these occurrences, surveys of the fisheries (Graham 1929; Beverton 1959), limnology (Talling 1957a; Talling 1957b; Talling 1965) and

hydrology (Fish 1957; Talling 1957b; Newell 1960) were conducted on Lake Victoria. This historical research has acted as a benchmark allowing present-day scientists to quantify subsequent changes in Lake Victoria's ecosystem, and infer causal relationships to help explain how 40 years of human activities could so quickly alter biological communities over 12,000 years in the making.

One of the best-documented changes in Lake Victoria since the 1960's, and one that is central to this thesis, is the increase in biomass and taxonomic shift of the phytoplankton community. At the time of the historic surveys, Lake Victoria was mesotrophic with a diatom-dominated community (Talling 1965). The mobilization of high amounts of nutrients into the lake brought forth an 4 and 8-fold increase in phytoplankton biomass offshore and inshore respectively while phytoplankton production doubled throughout the lake (Mugidde 1993). Phosphorus (P) loading increased disproportionately to non-biologically fixed nitrogen (N) loading while soluble reactive silica (SRSi) loadings remained constant (Hecky 1993). The decrease in N:P and P:Si ratios caused a taxonomic shift from siliceous diatoms to N-fixing cyanobacteria (Kling et al. 2001). This shift is further apparent with the concurrent depletion of dissolved silica in the water column, the disappearance of the historically persistent diatom *Aulacosira* (Hecky 1993), higher frequency of cyanobacterial blooms (Ochumba and Kibaara, 1989) and the current dominance of biologically fixed N in the N budget of Lake Victoria (Mugidde 2001, 2003; Mugidde et al. 2003).

The eutrophication of Lake Victoria, specifically the increase in algal biomass, has altered physical dynamics and dissolved oxygen content within the lake. As there are now higher amounts of organic material in the epilimnion, solar radiation is more rapidly absorbed through shallower depths (Imberger 1985). This is evident in the twofold decrease in the euphotic zone (Mugidde 1993), and stronger diurnal thermoclines exhibiting greater temperature increases over smaller depths (Talling 1957; MacIntyre et al. 2002). These changes in light penetration and diurnal stratification alter the light exposure and mixing dynamics of phytoplankton, which in turn affects their production, respiration and growth. The increase in phytoplankton biomass has also increased the amount of

organic material available for heterotrophic decomposition in the hypolimnion, dramatically increasing the volume of seasonally anoxic water (Hecky et al. 1994).

Changes in both the clarity and oxygen content of Lake Victoria have had profound impacts on other trophic levels. In response to longer and more intense seasonal anoxia, the benthic invertebrate community has shifted from anoxia-intolerant to more tolerant species (Verschuren et al. 2002). With respect to zooplankton, it is possible that primary producers now dominating the lake offer a poorer food quality than the previous diatom dominated community (Sterner et al. 1993), which could potentially depress production by zooplankton (and also planktivorous cichlids). This theory is supported by the data in Lehman and Branstator (1993), who showed negligible phytoplankton grazing by zooplankton and suggested that grazing by microheterotrophs on bacteria may now be a more important trophic pathway.

The synchronous increase of the piscivorous Nile Perch with the extinction of endemic cichlid species led many researchers to hypothesize top-down food web control, even though the extinction of endemic cichlid species occurred approximately 20 years after the Nile Perch's introduction (Ogutu-Ohwayo 1990). The endemic flock of haplochromine cichlid species occupied highly specialized ecological niches (Fryer and Iles 1972) and aforementioned changes in lower trophic levels could have undoubtedly played a role in many of the extinctions. Unlike the generalist Nile Perch, haplochromines are specialists (Witte et al. 1992) and many species may have been disadvantaged by the changes at the base of Lake Victoria's food web (Hecky 1993). Similar to the benthic invertebrate community, increased anoxia would have also dispersed several species of deep-water dwelling cichlids and removed a deep-water refugium (Kudhongnia and Cordone 1974). Also, Seehausen et al. (1997a) showed that mate selection amongst cichlid fish species is based on coloration, and that decreased water clarity in Lake Victoria hinders sexual selection, thereby inhibiting the ability of cichlids to maintain their diversity. Overall, this decrease in biodiversity has simplified the food web as there are now fewer trophic levels separating phytoplankton, the base of the food web, from the top predator the Nile Perch (Ogutu-Ohwayo 1990).

Although the introduction of the Nile Perch and Tilapia and eutrophication of Lake Victoria has been an ecological disaster, it has also been a economic success: The Nile Perch and Nile Tilapia are now two of the three dominant commercial species, and Lake Victoria's fishery increased seven-fold between 1968 to its peak in 1990 when an estimated 787,899 tonnes of fish were landed (Mkumbo and Cowx 1999), making it the world's largest freshwater fishery. However, by 1995 there was a 48% decline in the fish landed (Mkumbo and Cowx 1999). Furthermore, a fourfold increase in fishing boats during the past decade (FSTC 2000) and the continual emergence of new fish processing plants are leading to growing concern amongst stakeholders that current fishery efforts in Lake Victoria may not be sustainable (Ntiba et al. 2001). As thousands of fishermen earn the majority of their household income by fishing, and in turn provide the most inexpensive source of dietary protein in the Lake Victoria basin as well as a major export commodity, a collapsed fishery would be detrimental to the entire region.

1.2 Thesis Rationale

To provide an independent estimate of potential fisheries yield for the lake, regional scientists are applying a mass-balance food web model that requires production estimates of all trophic levels (Pauly et al. 2000). As the base of the aquatic food web, an estimate of annual lakewide phytoplankton production is essential in determining a valid and sustainable target for Lake Victoria's fishery. The purpose of this thesis is to generate an estimate of annual lakewide phytoplankton production through the investigation and advancement of relevant limnological processes in Lake Victoria.

Phytoplankton production estimates through space and time in large lakes and oceans are numerous and methodologically variable, but can be classified into two general approaches. In the first approach, most commonly applied to large lakes, time and site-specific phytoplankton production estimates are computed from chlorophyll, the vertical attenuation of irradiance and photosynthetic-irradiance parameters using a program such as that developed by Fee (1990, see Section 2.1.1), and are then extrapolated through space and time. For example, Millard et al.'s (1999)

estimates of phytoplankton production for Lakes Erie and Ontario were derived by dividing each lake into approximately 40 geographical regions with one station per region: At each station the required limnological data for Fee's program was collected in the spring, summer and fall and the subsequent 120 (40 stations x 3 seasons) independent estimates of phytoplankton production were then spatially and temporally assumed representative of each region and season respectively to derive lakewide estimates. Similar approaches have been ascribed to African Great Lakes, although financial logistics have inhibited the frequency and spatial coverage of data collection. Patterson et al. (2000) sampled chlorophyll and the vertical attenuation of irradiance at one station 15 times annually in both 1992 and 1993 to estimate phytoplankton production in Lake Malawi, and Hecky and Fee (1981) collected data chlorophyll, the vertical attenuation of irradiance and photosynthetic-irradiance parameters at 38 stations in two different seasons to compute annual phytoplankton production for Lake Tanganyika. The process of scaling finite estimates through space and time to generate annual and regional phytoplankton production is methodologically simple, but requires several assumptions and is valid if it can be proven that the distinct sets of measurements accurately encompass the spatial and temporal variability through which they have been extrapolated (Hecky and Fee 1981).

The second general approach used to estimate phytoplankton production, increasingly used in the oceanographic community, is to develop empirical relationships between data that can be remotely sensed with other data paramount to phytoplankton production that can only be obtained through field research. For example, Behrenfeld and Falkowski (1997) developed an empirical model that predicts maximum phytoplankton carbon fixation rates as a function of remotely sensed sea-surface temperature (SST). This model was tested against field data, physiologically justified in that temperature dependant enzymatic activities influence the Calvin cycle and then used with remotely sensed chlorophyll data to estimate oceanic phytoplankton production.

There are only a handful of published studies examining limnological parameters relevant to phytoplankton production, and only two studies directly examining phytoplankton production in Lake Victoria (Talling 1965; Mugidde 1993). Empirical relationships such as the relationship between

algal biomass and euphotic depth have not been developed for Lake Victoria, there are no-modern day published accounts of spatial limnological patterns in the offshore and consequently no study has yet provided an estimate of annual lakewide phytoplankton production.

Chapter two presents results from nearshore phytoplankton production research conducted during the course of this thesis and introduces novel adaptations to the phytoplankton production model developed by Fee (1990). Spatial, temporal and correlative trends of the data required to compute phytoplankton production are identified, compared to historical data on Lake Victoria and discussed in the context of their respective effect on phytoplankton production. Chapter three examines spatial and seasonal patterns of chlorophyll fluorescence, temperature, dissolved oxygen and water transparency from four lakewide cruises while discussing the implications for these distributions on the physical limnology, phytoplankton production and respiration in Lake Victoria. Chapter four develops a modeling framework for phytoplankton production based upon the results of chapter two, and is applied to the lakewide dataset presented in chapter three to facilitate lakewide estimates of phytoplankton production.

Each chapter is written in manuscript format with individual sections for an introduction, materials and methods, results, discussion and work cited. This thesis draws upon a multitude of historical research as outlined in the each introductory section, and is discussed in context with the specific results of each chapter. When possible, scanned figures and tables or relevant past research is placed in appendices along with the complete datasets gathered in this thesis on CD-Rs, to better facilitate use by others.

1.3 Work Cited

Behrenfeld, M.J. and P.G. Falkowski. 1997. Photosynthetic rates derived from satellite-based chlorophyll concentrations. Limnology and Ocanography. 42: 1-20.

Beverton, R.J.H. 1959. Report on the state of the Lake Victoria fisheries. Fisheries Laboratory, Lowestoft, UK.

Bugenyi, F.W.B. and J.S. Balirwa. 1989. Human intervention in natural processes of the Lake Victoria ecosystem - the problem, p. 311-340. In J. Solanki and S, Herodek (eds.) Conservation and management of lakes. Symp. Biol. Hung. 38. Akademiai Kiado, Budapest.

CIA. 2002. The world fact book. http://www.cia.gov/cia/publications/factbook/index.html

Crul, R.C.M. 1995. Conservation and management of the African Great Lakes Victoria, Tanganika and Malawi. UNESCO/IHP-IV. Project M-5.1.

Fee, E.J. 1990. Computer programs for calculating in-situ phytoplankton photosynthesis. Can. Tech. Rep. Fish. Aquat. Sci. No. 1740.

Fish, G.R. 1957. A seiche movement and its effects on the hydrology of Lake Victoria. *Fish. Publ. Lond.* 10: 1-68.

Fryer, G. and T.D. Iles. 1972. The cichlid fishes of the Great Lakes of Africa: Their Biology and Evolution. Oliver and Boyd. Edinburg.

FSTC. 2000. Frame survey technical committee draft report on Lake Victoria fisheries frame survey. Part 1: Main Report. Lake Victoria Fisheries Organization. Jinja. Pp. 63-87.

Graham, M. 1929. The Victoria Nyanza and its fisheries. A report on the fish survey of Lake Victoria 1927-1928 and Appendices. Crown Agents for the Colonies, London. 255 pp.Fish, G.R. 1957. A seiche movement and its effect on the hydrology of Lake Victoria. *Fish Publ. Lond.* 10.

Hecky, R.E. 1993. The eutrophication of Lake Victoria. International Association of Theoretical and Applied Limnology. 25: 39-48.

Hecky, R.E. and E.J. Fee. 1981. Primary production and rates of algal growth in Lake Tanganyika. Limnology and Ocanography. 26: 532-547.

Hecky, R.E., F.W.B. Bugenyi, R. Ochumba, J.F. Talling, R. Mugidde, M. Gophen and L. Kaufman. 1994. The deoxygenation of Lake Victoria. Limnology and Oceanography. 39: 1476-1481.

Imberger, 1985. The diurnal mixed layer. Limnology and Oceanography. 30: 737-770.

Johnson, T.C., C.A. Scholz, M.R. Talbot, K. Kelts, R.D. Ricketts, G. Ngobi, K. Beuning, I. Ssemmanda and J.W. McGill. 1996. Late Pleistocence desiccation of Lake Victoria and rapid evolution of cichlid fishes. Science. 273: 1091-1093.

Kendall, R.L. 1969. An ecological history of the Lake Victoria basin. Ecological Monographs. 39: 121-176.

Kling, H.J., R. Mugidde and R.E. Hecky. 2001. Recent changes in the phytoplankton community of Lake Victoria in response to eutrophication. In: M. Munawar and R.E. Hecky (eds). The Great Lakes of the World (GLOW): Food-web, health and integrity. 47-65.

Kudhongania, A.W. and A.J. Cordone. 1974. Bathospatial distribution patterns and biomass estimates of the major demersal fishes in Lake Victoria. *Afr. J. Trop. Hydrobiol. Fish.* 3: 15-31.

Lehman, J.T. and D.K. Branstrator. 1993. Effects of nutrients and grazing on the phytoplankton of Lake Victoria. International Association of Theoretical and Applied Limnology. 25: 850-855.

MacIntyre, S., Romero, J.R. and G.W. Kling. 2002. Spatial-temporal variability in surface layer deepening and lateral advection in an embayment of Lake Victoria, East Africa. Limnology and Oceanography. 47: 656-671.

Millard, E.S., E.J. Fee, D.D. Myles and J.A. Dahl. 1999. Comparison of phytoplankton photosynthesis methodology in Lakes Erie, the Bay of Quite and the Northwest Ontario Lake Size Series. In: Sate of Lake Eries (Sole) – Past, Present and Future. Eds. Munawar, M., T. Edsall and I.F. Munawar. 441-468.

Mkumbo, O.C. and I.G. Cowx. 1999. Cath trends from Lake Victoria. In: Cowx, I.G. and D. Tweddle (Eds.). Report of the Fourth FIDAWOG Workshop held at Kisumu. LVFRP/TECH/99/07. Lake Victoria Fisheries Research Project, Jinja, pp. 99-102.

Mugidde, R. 1993. The increase in phytoplankton primary productivity and biomass in Lake Victoria (Uganda). International Association of Theoretical and Applied Limnology. 25: 846-849.

Mugidde, R. 2001. Nutrient status and phytoplankton nitrogen fixation in Lake Victoria, East Africa. Ph.D. Thesis, University of Waterloo, Waterloo, Canada.

Mugidde, R, R.E. Hecky, L.L. Hedzel and W.D. Taylor. 2003. Pelagic Nitrogen Fixation in Lake Victoria (East Africa). Journal of Great Lakes Research: 29(2): 76-88.

Newell, B.S. 1960. The hydrology of Lake Victoria. Hydrobiologia. 15: 363-383.

Ntiba, M.J., W.M. Kudoja and C.T. Mukasa. 2001. Management issues in the Lake Victoria watershed. Lakes and Reservoirs: Research and Management. 6: 211-216.

Ochumba, P.B. and D.I. Kibaara. 1989. Observations on blue-green algal blooms in the open waters of Lake Victoria, Kenya. African Journal of Ecology. 27: 23-34.

Ogutu-Ohwayo, R. 1985. The effects of predation by Nile Perch, *Lates niloticus*. Introduced into Lake Kyoga (Uganda) in relation to the fisheries of Lake Kyoga and Lake Victoria. FAO. Fish. Rep. 335: 18-39.

Ogutu-Ohwayo, R. 1990. The decline of the native fishes of lakes Victoria and Kyoga (East Africa) and the impact of introduced species, especially the Nile perch, *Lates niloticus*, and the Nile tilapia, *Oreochromis niloticus*. Environmental Biology of Fishes. 27: 81-96.

Patterson, G., R.E. Hecky and E.J. Fee. 2000. Effect of hydrological cycles on planktonic primary production in Lake Malawi/Niassa. Advances in Ecological Research. 31: 421-430.

Pauly, D., V. Christensen and C. Walters. 2000. Ecopath, Ecosim, and Ecospace as tools for evaluating ecosystem impact of fisheries. ICES Journal of Marine Sciences. 57: 697-706.

Scheren, P.A.G.M., H.A. Zanting and A.M.C. Lemmens. 2000. Estimation of water pollution sources in Lake Victoria, East Africa: Application and elaboration of the rapid assessment methodology. Journal of Environmental Management. 58: 235-248.

Scholz, C.A., T.C. Johnson, P. Cattaneo, H. Malinga and S. Shana. 1998. Initial results of 1995 IDEAL seismic reflection survey of Lake Victoria, Uganda and Tanzania. *In* Environmental Change and Response in East African Lakes. 47-57.

Seehausen, O., J.J.M. Van Alphen and F. Witte. 1997a. Cichlid fish diversity threatened by eutrophication that curbs sexual selection. Science. 277: 1808-1811.

Seehausen, F. Witte, E.F. Katunzi, J. Smits and N. Bouton. 1997b. Patterns of the remnant cichlid fauna in Southern Lake Victoria. Conservation Biology. 11: 890-904.

Silsbe, G.M. 2003. A new digital map for Lake Victoria. Bulletin of the International Decade for East African Lakes (IDEAL). http://www.d.umn.edu/llo/Ideal/Su03.pdf.

Spigel, R.H. and G.W. Coulter. 1996. Comparison of hydrology and physical limnology of the East African Great Lakes: Tangyanika, Malawi, Victoria, Kivu and Turkana (with reference to some North American Great Lakes. In. Johnson, T.C. and E. Odada [eds]. The limnology, climatology and paleoclimatology of the East African Lakes.

Stager, J.C. 1998. Ancient analogues for recent environmental changes at Lake Victoria, East Africa. In Environmental Changes and Responses in East African Lakes. Edited by J.T. Lehman.

Sterner, R.W., D.D. Hagemeir, W.L. Smith and R.F. Smith. 1993. Phytoplankton nutrient limitation and food quality for *Daphnia*. Limnology and Oceanography. 38: 857-871.

Talling, J.F. 1957a. Diurnal changes of stratification and photosynthesis in some tropical African waters. *Proc. Roy. Soc. B*. 147: 57-83.

Talling, J.F. 1957b. Some observations on the stratification of Lake Victoria. Limnology and Oceanography. 2: 213-221.

Talling, J.F. 1965. The photosynthetic activity of phytoplankton in East African lakes. *Int. Revue ges. Hydrobiol.* 50: 1-32.

United Nations. 1995. World population prospects: The 1994 revision. New York: United Nations.

Verheyen, E., W. Salzburger, J. Snoeks and A. Meyer. 2003. Origin of the superflock of cichlid fishes from Lake Victoria, East Africa. Science. 300: 325-329.

Verschuren, D, T.C. Johnson, H.J. Kling, D.N. Edgington, P.R. Leavitt, E.T. Brown, M.R. Talbot and R.E. Hecky. 2002. History and timing of human impact on Lake Victoria, East Africa. Proceedings of the Royal Society of London - B - Biological Sciences. 269: 289-294.

Witte, F., T. Goldschmidt, J.H. Wanick, M.J.P. Oijen, P.C. Van Goudswaard, E.L.M. Witte-Maas and N. Bouton. 1992. The destruction of an endemic species flock: Qualitative data on the decline of the haplochromine cichlids of Lake Victoria. Environmental Biology of Fishes. 34: 1-28.

Chapter 2: Temporal Patterns of Phytoplankton Production in Three Inshore Bays in Lake Victoria, East Africa

2.1 Introduction

This chapter is an examination of diurnal and sub-seasonal temporal variance of inshore gross and net phytoplankton production and the limnological parameters that influence it. This chapter provides valuable information for the derivation of annual lakewide phytoplankton, resolves diurnal variations of gross and net phytoplankton production in an African Great Lake, introduces novel adaptations of the phytoplankton production program of Fee (1990) to facilitate these objectives and employs historic datasets to validate results.

Phytoplankton production estimates are obtained through an adapted version (Silsbe 2003a) of the program originally developed by Fee (1990). Fee's model has been widely used to provide estimates of phytoplankton production in the Laurentian Great Lakes (Millard et al. 1996, 1999), Canadian Shield lakes (Carignan et al. 1998), lakes of various size and trophic status (del Giorgio and Peters 1994), as well as Lakes Malawi (Bootsma 1993; Patterson et al. 2000) and Tanganyika (Hecky and Fee 1981). The revised model provides independent calculations of gross phytoplankton production (PP_G) and areal respiration (AR), which are then used to determine net phytoplankton production (PP_N). AR is a function of chlorophyll specific respiration rates (R) and chlorophyll (chl); PP_G is a function of chl, photosynthesis-irradiance (PI) parameters, vertical attenuation coefficient of PAR (k_{PAR}) and theoretical or measured incident irradiance (I_o). Theoretical information on the model is provided in Materials and Methods and a list of commonly used symbols is given in Table 2.1.

Only one study (Mugidde 1993) has examined modern-day PP_G in Lake Victoria, while AR and consequently PP_N have not been measured. Several studies have however independently examined spatial or temporal patterns of one or more of the parameters required to calculate PP_G, of which chl has been the most thoroughly studied in Lake Victoria.

Table 2.1: Symbols, definitions and units.

Symbol	Definition	Units
Physical Parameters		
PAR	Photosynthetically Active Radiation	
I	Irradiance	$\mu mol \cdot m^{-2} \cdot s^{-1}$
I_o	Incident irradiance	$\mu mol \cdot m^{-2} \cdot s^{-1}$
k_{PAR}	Vertical attenuation coefficient of PAR	m^{-1}
k_{chl}	Chlorophyll specific attenuation coefficient	$m^2 \cdot mg\ chl^{-1}$
Z_{eu}	Euphotic depth	m
SD	Secchi depth	m
T_{WC}	Average water column temperature	°C
N	Buoyancy frequency	hr^{-1}
Z_{mix}	Surface mixed layer depth	m
Biological Parameters		
P_G	Gross photosynthesis	$g\ O_2 \cdot mg\ Chl^{-1} \cdot hr^{-1}$
P_N	Net photosynthesis in the euphotic zone	$g\ O_2 \cdot mg\ Chl^{-1} \cdot hr^{-1}$
PP_G	Gross areal phytoplankton production	$g\ O_2 \cdot m^{-2} \cdot day^{-1}$
$PP_{N[Zeu]}$	Net areal phytoplankton production in the euphotic zone	$g\ O_2 \cdot m^{-2} \cdot day^{-1}$
$PP_{N[WC]}$	Net areal phytoplankton production in the water column	$g\ O_2 \cdot m^{-2} \cdot day^{-1}$
chl	Chlorophyll concentration	$mg \cdot m^{-3}$
chl_{Zeu}	Average chlorophyll concentration in the euphotic zone	$mg \cdot m^{-3}$
Chl_{WC}	Average chlorophyll concentration in the mixed layer	$mg \cdot m^{-3}$
chl_F	Chlorophyll inferred fluorescence	$mg \cdot m^{-3}$
chl_F:chl	Ratio of chl_F to chl	unitless
R	Respiration rate	$mg\ O_2 \cdot m^{-3} \cdot hr^{-1}$
R_B	R normalized to chl	$mg\ O_2 \cdot mg\ Chl^{-1} \cdot hr^{-1}$
$AR_{[Zeu]}$	Areal Respiration in the euphotic zone	$g\ O_2 \cdot m^{-2} \cdot day^{-1}$
Photosynthesis-irradiance (PI) curve parameters		
α	Light-limited slope of the PI Curve	$mg\ O_2 \cdot \mu mol^{-1} \cdot m^{-1}$
P_M	Light-saturated rate of photosynthesis	$mg\ O_2 \cdot m^{-3} \cdot hr^{-1}$
α_B	α normalized to chl	$mg\ O_2 \cdot mg\ Chl^{-1} \cdot \mu mol^{-1} \cdot m^2$
P_{BM}	P_M normalized to chl	$mg\ O_2 \cdot mg\ Chl^{-1} \cdot hr^{-1}$
I_k	Half irradiance-saturation index = P_M/α	$\mu mol \cdot m^{-2} \cdot s^{-1}$
Photochemical Parameters		
PSII	Oxygen-evolving Photosystem II complex	
PSI	Photosystem I complex	
n_{PSII}	Concentration of PSII complexes	$mg\ O_2 \cdot mg\ Chl^{-1}$
n_{PSI}	Concentration of PSI complexes	$mg\ O_2 \cdot mg\ Chl^{-1}$
σ_{PSII}	Functional absorption cross-section of PSII	$nm^2 \cdot quanta^{-1}$
τ	Electron turnover rate of rate-limiting component at light saturation	s^{-1}

Modern-day limnological studies in Lake Victoria have shown that seasonal and spatial patterns of chl occur through relative changes in the light and nutrient environment, which in turn are both strongly influenced by the dynamics of Lake Victoria's thermal structure (Hecky 1993; Hecky et al. 1994; Mugidde 2001; Kling et al. 2001; Guildford et al. 2003). Table 2.2 provides a spatial comparison of inshore (< 20 m) and offshore (≈ 60 m) chl and examines seasonality through the coefficients of variance of chl within, between and irrespective of seasons. Four important spatial and temporal trends can be observed from Table 2.2. Chl is on average nearly 2-fold higher in the inshore than the offshore. A common seasonality can be observed for the both inshore and offshore data; in both regions chl is highest between September and December, and lowest between May and August. The coefficient of variance between seasonally averaged data is significantly larger in the offshore than the inshore, implying that seasonality is more pronounced in the latter and relatively muted in the former. Finally, regardless of season the coefficient of variance of non-seasonally partitioned data is high in both regions.

Table 2.2: Average and coefficient of variance (CV) of chlorophyll (mg.m^{-3}) in the inshore and offshore within, between and irrespective of seasons (Data from Mugidde 1992). Sample size is given in parentheses.

	Within Season			CV of Seasonal Averages	All Data
	Sep-Dec	Jan-Apr	May-Aug		
Inshore Average	52.4 (6)	45.6 (10)	39.8 (17)	-	46.0 (33)
Inshore CV	11%	22%	32%	14%	27%
Offshore Average	33.0 (4)	25.4 (5)	14.8 (4)	-	24.5 (13)
Offshore CV	30%	37%	42%	37%	44%

Examining the specific mechanisms that cause these spatial and temporal trends of chl allows hypotheses to be formulated concerning sub-seasonal temporal variation and inshore spatial variation. Annual offshore time-series have shown that Lake Victoria has a seasonal, vertically transient metalimnion and hypolimnion (Talling 1957a, 1966; Hecky et al. 1994) although some inter-annual variability in the demarcation of seasons as described below has been observed (Hecky 1993; Ramlal 2002). During September to December, the water-column exhibits rising temperatures due to

successive deepening of diurnal thermoclines. By January a prominent metalimnion forms and remains in the water-column through to April while the months encompassing May to August are delineated by near isothermal conditions. When the lake is stratified high rates of organic decomposition deplete hypolimnetic oxygen forming an oxic-anoxic interface (Hecky et al. 1994) below which bioavailable nitrogen (N) can be lost through denitrification (Seitzinger 1988; Hecky et al. 1996) and bioavailable phosphorus (P) is enriched through its release from reduced iron oxide complexes (Boostma and Hecky 1996; Guildford and Hecky 2000; Mugidde 2001). Consequently, relative changes in vertical mixing and nutrient stoichiometry enact seasonal shifts in light-limitation (Mugidde 1993), N and possibly P-limitation (Mugidde 2001) on the offshore phytoplankton community as follows: During September through December shallow surface mixing layers and a stable water column provide a suitable light climate for both photosynthesis and N-fixation, allowing for a large phytoplankton crop dominated by the N-fixing genera *Anabaena* to develop (Hecky 1993, Mugidde 2001; Kling et al. 2001). Between January and April, metalimnetic depths are generally deeper than the previous period (Mugidde 2001) as thermal stability begins to decrease in February (Hecky 1993). Consequently, lower phytoplankton biomass during this period may in part be due to increased light-limitation (Mugidde 1993), and *Microcystis* and *Cylindrospermopsis* succeed *Anabaena* as the dominant phytoplankton genera (Kling et al. 2001; Mugidde 2001). It is uncertain why *Cylindrospermosis* becomes the dominant N-fixer at this time, but *Microcystis* is better adapted than *Anabaena* to low-light environments through the potential physiological presence of phycoerythrin pigments (De Nobel et al. 1998; Otsuku et al. 1998), gas vesicles that allow positive buoyancy (Reynolds et al. 1987), as well as its ability to store nutrients (Kilham and Hecky 1988). Around May thermal stratification ceases and deep waters are reoxygenated, thus preventing further denitrification while releasing hypolimnetic P into the entire water column (Hecky et al. 1996), which remains nearly isothermal until the end of August. During this phase, surface mixing is deepest (Hecky 1993; Mugidde 2001; Chapter 3), and extreme light-limitation is thought to cause relatively low phytoplankton biomass (Mugidde 1993; Hecky 1993; Kling et al. 2001). The pennate diatom

Nitzschia becomes the dominant offshore phytoplankton during this phase (Mugidde 2001), which reflects adequate P and Silica (Si) availability (Kilham et al. 1986). N-fixing cyanobacteria are either absent (Mugidde 2001) or in very low abundance (Kling et al. 2001) during this period, and the concurrent annual maxima of dissolved inorganic nitrogen suggest that N is not limiting at this time (Mugidde 2001).

An annual time series of the inshore thermal structure in Lake Victoria has yet to be conducted, but sporadic temperature and dissolved oxygen profiles in the shallow waters (< 20 m) of the northern archipelago of Lake Victoria (Talling 1965; Mugidde 2001; Ramlal et al. 2001) indicate that complete mixing to depth occurs approximately once every two or three days, consistent with other shallow tropical lakes (Hare and Carter 1984; Powell et al. 1984). The increased frequency of complete water-column mixing in the inshore inhibits the long-term formation of an oxic-anoxic interface and sets a finite limit on the surface mixing depth. Hecky (1993) and Hecky et al. (1996) hypothesize that diminished denitrification, due to the absence of an inshore oxic-anoxic interface in the water column, increases the amount of bioavailable N and consequently maintains the higher inshore phytoplankton biomass shown in Table 2.2. Moreover, turbulence at boundary layers is a critical mechanism in facilitating resuspension of nutrients and phytoplankton into the euphotic zone (MacIntyre 1998) while lateral advection through differential heating and cooling (Imberger and Parker 1985) serves to transport nutrients from turbulent regions to other areas. Both processes are more likely to occur in inshore areas with variable morphometry, further supporting the hypothesis of increased nutrient cycling within the inshore (Hecky 1993). Overall, morphometric differences between inshore and offshore regions remove the main mechanisms responsible for phytoplankton seasonality observed in the offshore.

Although inshore surface mixing depths are shallower than in the offshore, they follow the same seasonal trend as described for the offshore (Mugidde 2001). Decreased light penetration in the inshore due to higher phytoplankton biomass offsets this shallower mixing and can impose the same degree of light-limitation as in the offshore (Mugidde 1993). Furthermore, despite hypothesized

increased inshore nutrient cycling, N-fixing cyanobacteria are prevalent in the inshore between September and April and compromise a higher percentage of total phytoplankton biomass than in the offshore (Mugidde 2001). Increased light levels and PP_G during this period (Mugidde 1993) rapidly draw down dissolved nutrient pools and result in N-deficiency (Guildford et al. 2003). Light-limitation of photosynthesis and N-fixation through self-shading may establish upper limits on inshore phytoplankton biomass during this period. Conversely, epilimnetic inshore waters in the May-August period have been shown to be nutrient replete and accordingly the phytoplankton community is nutrient sufficient (Mugidde 2001). Even in the inshore, this period is delineated by complete mixing, suggesting that light-limitation of photosynthesis controls phytoplankton production at this time (Mugidde 1993).

From these general observations, simple hypotheses concerning sub-seasonal and spatial variance are proposed: Shallower bays should be able to maintain higher phytoplankton biomass because of a shallower maximum mixing depths and increased nutrient cycling. Secondly, sub-seasonal changes in phytoplankton biomass should be correlated with changes in the thermal structure: Periods of deep mixing should decrease chl through light-limitation, periods of minimal mixing should increase chl and effect corresponding changes in the PI parameters. As the prominent mechanisms in Lake Victoria causing deep and shallow surface mixing are convective cooling and intense diurnal heating respectively (MacIntyre et al. 2002b), changes in chl should specifically be correlated with temperature changes in the water column.

On a diurnal time scale, variations in the vertical distribution of phytoplankton through changes in cell density and hydrodynamics affect the irradiance exposure of phytoplankton and can consequently influence PP_G estimates (Marra 1978). When the timescale for sinking or rising of a phytoplankton cell (a function of cell density) exceeds the timescale for mixing (a function of the coefficient of eddy diffusivity), the cell's motility determines its position, or when the opposite occurs the cell will follow the flow depending on the turbulent Froude number (MacIntyre 1998; Ivey and Imberger 1991). Furthermore, thermocline deflection through intrusions, surface overflows and

internal waves also affects the vertical position of phytoplankton in the water-column. The vertical eddy diffusion coefficient has not been directly measured in Lake Victoria, but measurements of the surface mixed layer (Z_{mix}), and turbulent velocity scales suggest that diurnal stratification inhibits turbulence below the shallow surface mixed layer during the day and nocturnal cooling produces turbulence during the night that deepens the surface mixed layer (MacIntyre et al. 2002b). In the same study, thermocline upwelling and downwelling through lateral advection of water masses in Pilkington Bay commonly occurred, presumably through differential heating and cooling.

In Lake Victoria the dominant cyanobacteria possess the competitive advantage of being able to manipulate their buoyancy through gas vacuoles, allowing cells to ascend in the water-column to a favourable light environment in the absence of strong turbulent mixing. This control is delicate and subject to rapid alteration depending on environmental conditions (Reynolds 1972). For example, Walsby (1976) found that formation of gas vacuoles in *Anabaena* was stimulated by low light intensities but high light intensities collapsed the vacuoles. Diurnal variations in phytoplankton biomass in Lake Victoria was first observed by Talling (1957b) who noted that the diatom *Aulacoseira* was uniformly distributed in the water column except at times of intense diurnal heating when negligible water column turbulence caused the negatively-buoyant diatom to sink. In a tropical reservoir Talling (1957b) noted that the cyanobacterium *Anabaena* was often in greatest concentrations at the surface of the water in the late afternoon and was only uniformly distributed in the water column for brief periods of isothermal mixing. Ganf (1974a) examined vertical fine-scale diurnal changes in chl in the tropical eutrophic Lake George and noted that cyanobacteria were generally evenly distributed at dawn but accumulated at depth over the course of the day although Ganf (1974a) noted that horizontal velocity currents from lateral advection complicates this interpretation.

As shown in Figure 2.1, experiments have repeatedly shown that the rate of photosynthesis versus irradiance can be approximated by a rectangular hyperbola (PI curve) that can be mathematically defined by two parameters (Jassby and Platt 1976). The asymptote of the hyperbola

represents the maximum photosynthetic rate P_M, while the initial linear slope of light-dependent photosynthesis is symbolically known as α. A third term in a PI curve is I_k, defined mechanistically as half of the saturation irradiance (I_{sat}) where photon absorption is equivalent to electron transport (Falkowski and Raven 1997) or empirically as the quotient of P_M and α (Talling 1957c). PI parameters are useful indicators of photosynthetic physiology (Henley 1993) and relative changes in P_M and α have been classified as either I_k-dependent or I_k-independent (Behrenfeld et al. 2004). I_k-dependent changes arise through a disproportionate increase or decrease in one of the PI parameters relative to the other, whereas I_k-independent changes arise through a proportionate increase or decrease in both α and P_M. In physiological studies, changes in PI parameters are often described in terms of their photochemical parameters. Equation 2.1 shows that α is a product of the concentration of photosystem II (PSII) complexes (n_{PSII}) and their functional absorption cross-section (σ_{PSII}), Equation 2.2 shows that P_M is a function of n_{PSII} and the inverse of their maximum potential turnover rate (τ^{-1}) (Falkowski and Raven 1997). Mugidde (1993) normalized P_M and α to chl to facilitate comparisons of PI parameters for measurements of different biomass, symbolically noted as P_{BM} and α_B. Berhrenfeld et al. (2004) express chl as a production of the number of PSII centres with the average chl per PSII centre plus the product of the number of PSI centres and the average chl per PSI centre as shown in Equation 2.3. All units are given in Table 2.1.

Equation 2.1) $\alpha = n_{PSII} \times \sigma_{PSII}$

Equation 2.2) $P_M = n_{PSII} \times \tau^{-1}$

Equation 2.3) chl = number of PSII x chl/PSII + number of PSI x chl/PSI

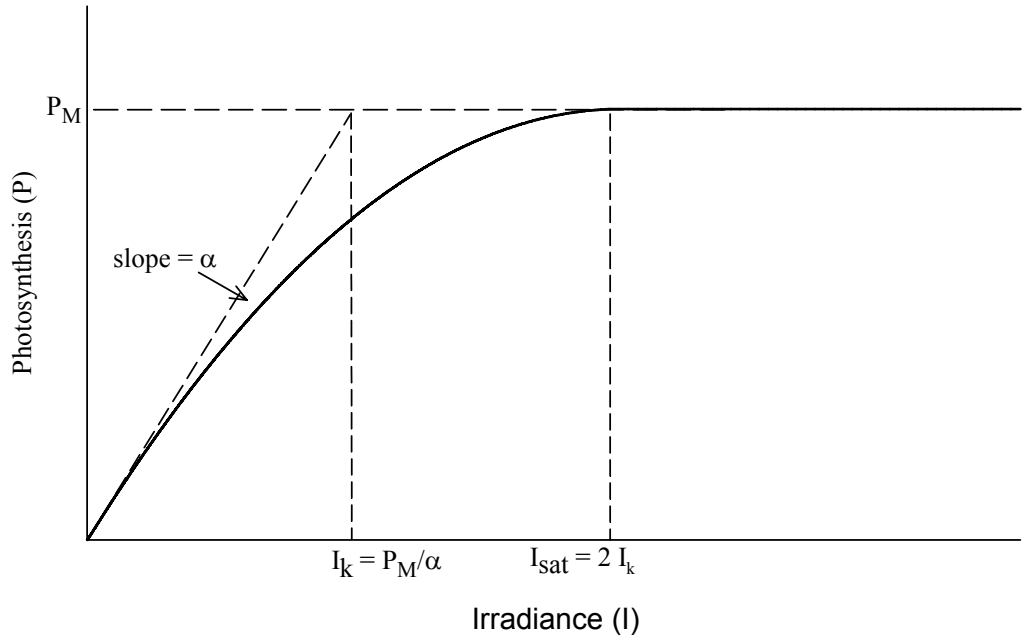

Figure 2.1: PI curve (Modified from Jassby and Platt 1976 and Kalff 2001)

The most common manifestation of an I_k-dependent change occurs on a diurnal scale through photoacclimation: Phytoplankton cells in a low-light environment increase their photosynthetic capacity by increasing σ_{PSII} through state transitions and non-photochemical quenching (Falkowski and Raven 1997), which increases α relative to P_M. Accordingly, cells acclimated to lower irradiances have smaller values of I_k than cells acclimated at high irradiances. Phenotypic adjustments of chl content per cell also occur in response to the light environment (Falkowski and La Roche 1991): Phytoplankton acclimated to lower irradiances have more chl per cell, such that P_{BM} and α_B appear lower relative to the assemblage acclimated to higher irradiances with less chl content per cell (Geider 1987). This specific adaptation may not be prevalent in Lake Victoria, as the dominant cyanobacteria are more likely to photoacclimate by adjusting phycobilisome pigments instead of chl pigments (MacIntyre et al. 2002a).

With respect to I_k-independent changes in PI parameters, the chl-specific attenuation coefficient (k_{chl}) and the PSII:PSI ratio link P_{BM} and α_B at the level of basic photochemistry and variations in either cause parallel changes in both PI parameters (Behrenfeld et al. 2004). The

PSII:PSI ratio varies between phytoplankton taxa: In one study examining three diverse phytoplankton species, the PSI:PSII ratio was 1:2, 1:1 and 2:1 in a diatom, a green alga and a cyanobacterium respectively (Berges et al. 1996). According to the above relationship this would mean that under the same environmental conditions PI parameters normalized to chl would be highest in diatoms and lowest in cyanobacteria, assuming that chl:PSI and chl:PSII is roughly the same (Behrenfeld et al. 2004). This hypothesis is supported by the historic taxonomic shift from diatoms to cyanobacteria in Lake Victoria (Kling et al. 2001) and concomitant decrease in P_{BM} and α_B (Mugidde 1993). Changes in the PSII:PSI ratio can also occur within a taxon along gradients of nutrient stress. Table 2.3 lists four potential physiological states of phytoplankton, cites under what conditions each state has been shown to most likely occur in Lake Victoria and describes the anticipated response of a phytoplankton community (assumed to be a cyanobacterium) in terms of P_{BM} and the PSII:PSI ratio. Superscripts provide the referenced source.

Table 2.3: Physiological States with their potential occurrences in Lake Victoria, and expected responses of P_{BM} and PSII/PSI Ratio along increasing gradients of these states.
([1]Guildford and Hecky 2000; [2]Mugidde 2001; [3]Mugidde 1993; [4]Ramlal et al. 2001; [5]Healey 1985; [6]Berges et al. 1996; [7]Kana et al. 1992; [8]Nimer et al. 1998, [9]Geider et al. 1996; [10]MacIntyre et al. 2002a; [11]Kawamuru et al. 1979; [12]Murukami and Fujita 1991; [13]Miskiewicz et al. 2002)

Physiological State	Occurrence in Lake Victoria	Response to Increasing Limitation	
		P_{BM}	PSII:PSI
N-Limitation	Inshore and Offshore when the water column is thermally stratified[1,2]; N-fixation increases with Chlorophyll[2]	Decrease[5]	Decrease[6,7]
C-Limitation	May occur in diurnally stratified and productive water[4]	Decrease[8]	?
P-limitation	Inshore with high algal biomass and thermal stratification[2]	Decrease[5]	?
Light-limitation	Offshore when Zmix >> Zeu; Inshore due to self shading[1,3]	Decrease[9,10]	Decrease[11,12,13]

Recent research in Lake Victoria has demonstrated the potential of nutrient-limitation generally arises when chl is high. Mugidde (2001) found a positive correlation between N-fixation

and chl ($r^2 = 0.65$), inferred limitation from N-debt and P-debt assays when ambient chl was above average, and Ramlal et al. (2001) hypothesized that C-limitation can occur in stratified and highly productive inshore areas. Inshore light-limitation in Lake Victoria is caused by self-shading (Mugidde 1992), especially in shallow embayments that allow high concentrations of chl to develop and cause comparatively rapid attenuation of light in the water column. Regardless of the limiting resource, phytoplankton should respond with a decrease in P_{BM} through a decreased demand for photosynthate (Healey 1985; Nimer et al. 1998; Geider et al. 1996; MacIntyre et al. 2002a). In cyanobacteria, the PSII:PSI ratio is expected to decline through N and light-limitation through the selective degradation of PSII-serving phycobilisomes (Kawamuru et al. 1979; Kana et al. 1992; Berges et al. 1996).

The general correlation between PI parameters and chl from historic research in conjunction with hypothesized temporal and spatial changes in chl with mixing depth facilitates hypotheses for changes in PI parameters: High inshore chl, as hypothesized to occur when the mixed layer is shallow, should coincide with relatively low PI parameters. Low inshore chl, as hypothesized to occur when surface mixing is deep, should coincide with relatively high PI parameters. These hypotheses underscore the influence of phytoplankton biomass on physical processes and nutrient cycling in Lake Victoria: Meteorological variability aside, intense diurnal thermoclines are more likely to occur when chl is high through relatively shallower attenuation of light (Imberger 1985). Strong diurnal thermoclines inhibit water column turbulence (MacIntyre 1998) that in turn can dampen physical processes that assist nutrient cycling (MacIntyre et al. 1999). Conversely, low phytoplankton biomass will allow deeper attenuation of light, less intense diurnal thermoclines and potentially greater nutrient cycling through increased turbulence. Therefore aside from the increased nutrient demand from a large standing crop of phytoplankton, the relative quantity of phytoplankton themselves can alter physical processes and nutrient cycling within a water body.

Temporal and spatial trends in k_{PAR} should be related to changes in chl, as k_{PAR} is the sum of the partial attenuation coefficients due to water (k_w), chl (k_{chl}·chl) and particulate and dissolved detritic substances as shown in Equation 2.4 (Lorenzen 1972).

Equation 2.4) $k_{PAR} = k_w + k_X + k_{chl}$·chl

Partial attenuation coefficients of the first two parameters have not been previously measured in Lake Victoria and cannot be individually addressed in the chapter. The partial attenuation coefficient of chl, k_{chl}, can vary by up to four orders of magnitude (Kirk 1994). k_{chl} is expected to change with phytoplankton cell morphology, chloroplast size and distribution, the degree of stacking and optical properties of thylakoid membranes and changes in the relative abundance of chl and accessory pigments (Berner et al. 1989). High linear correlation between k_{PAR} and chl has been shown in several studies (Tilzer et al. 1995; Krause-Jensen and Sand-Jensen 1998), and one study containing a comparable range of chl to Lake Victoria showed a decreased dependence of k_{PAR} along an increasing chl gradient presumably due to an increased dominance of phycocyanin-rich cyanobacteria (Voros et al. 1998). Reanalysis of k_{PAR} and chl from Mugidde's (1992) dataset revealed that an S curve ($\ln(k_{PAR}) = 0.32 - 15.0.chl^{-1}$) had the best fit ($r^2 = 0.73$, $p < 0.001$, $n = 44$). Similar to Voros et al. (1998), this statistical relationship predicts a decreasing dependence of k_{PAR} along an increasing chl gradient.

Incident irradiance (I_o) can be either obtained by direct measurement from a meteorological station or estimated as a function of day of the year and latitude (to determine daylength and solar declination) and two coefficients to estimate absorption of irradiance in the atmosphere by particles and by cloud cover respectively (Kirk 1994). As the equator bisects Lake Victoria, daylength and solar declination are relatively constant year round and most daily variability in I_o is due to cloud cover (Yin et al. 2000).

There is a paucity of respiration rate (R) measurements in tropical African Lakes, as phytoplankton production measurements in Lakes Malawi (Patterson et al. 2000) and Tanganyika

(Hecky and Fee 1981) employed the C_{14} method. In Lake Victoria, Talling (1965) states that R is 'generally 1/3 of optimal photosynthetic rates'. Positive correlations between R per unit chl (R_B) and P_{BM} have been shown in the marine cyanobacterium *Trichodesmium* (Carpenter and Roenneberg 1995) and in tropical lakes Xolotlan (Erikson 1999) and George (Ganf 1974b), both of which are eutrophic and dominated by cyanobacteria. The link between R_B and P_{BM} follows the concept of gross respiration being comprised of two components: A basal maintenance respiration rate and a respiration rate proportional to a cell's growth rate as influenced by its photosynthetic production (Langdon 1988) that is particularly pronounced in cyanobacteria (Padan et al. 1971; Sentzova et al. 1975).

2.2 Materials, Methods and Data Analysis

This study was undertaken in three inshore bays, Napoleon Gulf, Inner Murchison Bay and Fielding Bay, all located in northern Lake Victoria. Figure 2.2 illustrates the location of sampling stations within the bays, and Table 2.4 provides a morphological summary of each bay. Average depths within a specified radius of each station were determined using a digital map of Lake Victoria (Figure 2.2). The proximity of Napoleon Gulf and Fielding Bay to the Fisheries Research and Resources Institute (FIRRI) in Jinja and Inner Murchison Bay to National Water and Sewerage Corporation (NWSC) in Kampala allowed collected samples to be immediately transported to the respective research institute for preservation or analysis, with the exception of phytoplankton photosynthesis in Inner Murchison Bay which was transported (~2 hours) and determined at FIRRI. Diurnal studies were conducted seven times in Inner Murchison Bay and Fielding Bay and eight times in Napoleon Gulf. The sampling regime was repeated three times a day in the early morning, early afternoon and again in the late afternoon, except in Murchison Bay, which was usually sampled twice a day owing to its distance from FIRRI.

Table 2.4: Location, Depth and Proximal Bathymetry of Sampling Stations

Station	Latitude	Longitude	Depth (m)	Average Depth (m) Within Specified Radius		
				1 km	5 km	10 km
Fielding Bay	0° 26’ 51”N	33° 16’ 28”E	7.5	5.1	6.0	9.4
Napoleon Gulf	0° 24’ 05”N	33° 14’ 53”E	14	8.8	7.7	12.4
Inner Murchison Bay	0° 15’ 08”N	32° 39’ 36”E	6	4.9	2.2	3.5

SD was measured with a white 25 cm diameter secchi disk as the average depth at which the disk was no longer visible upon lowering and raising it in the water column on the shaded side of the boat. A flat-plate LI-COR quantum sensor (LI-COR Biosciences, Lincoln NB) was used to determine underwater irradiance in the photosynthetically active waveband (λ 400 to 700 nm). Measurements

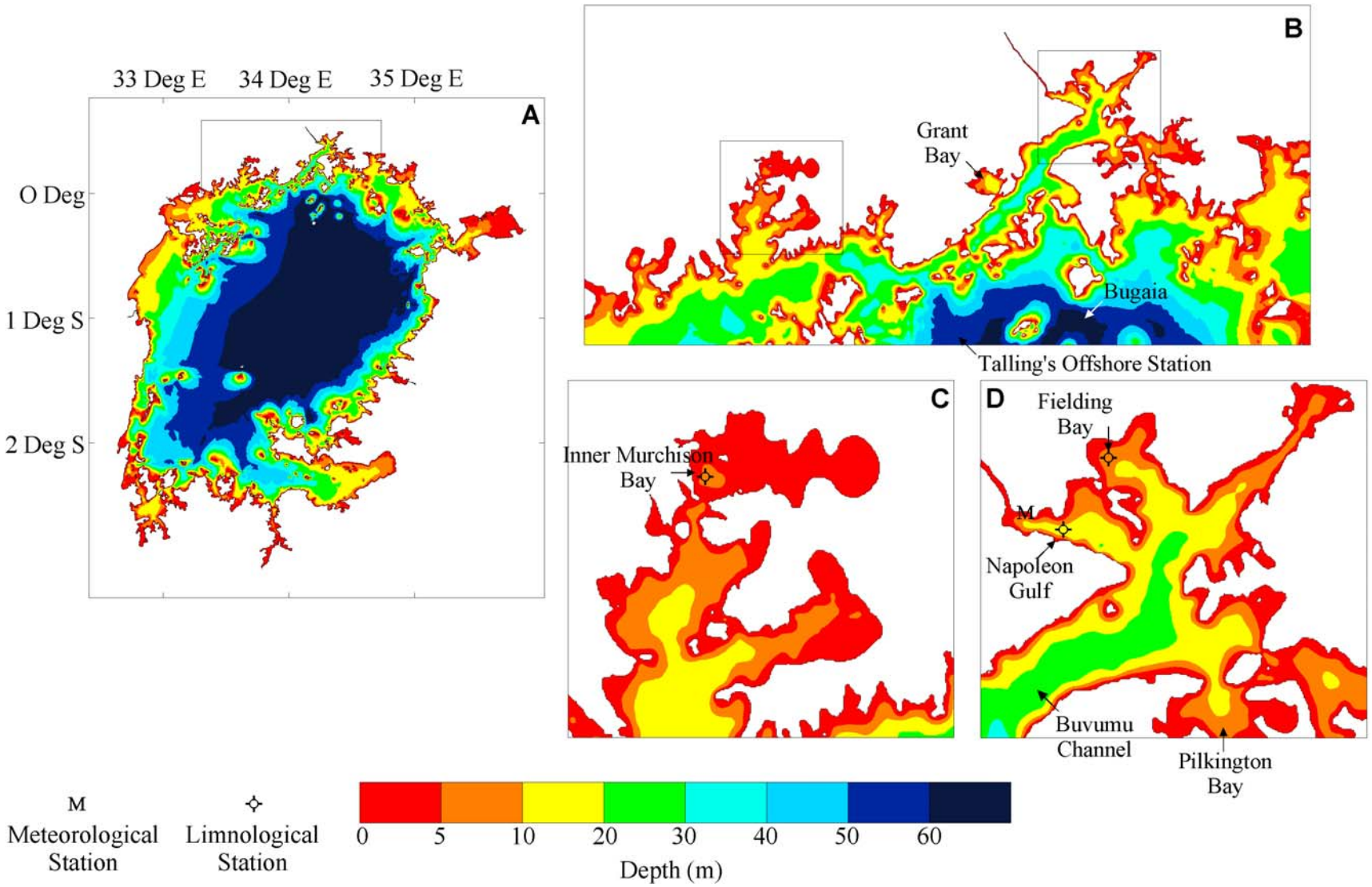

Figure 2.2: Bathymetric maps of A) Lake Victoria, B) Northern Lake Victoria, C) Inner Murchison Bay, D) Napoleon Gulf and Fielding Bay. Digital map from Silsbe (2003b).

were taken above and below the air-water interface to ascertain surface reflection, and every 0.5 m thereafter to a depth of approximately 0.1% surface irradiance to determine k_{PAR} (Kirk 1994).

A SBE-19 CTD profiler (Sea-Bird Electronics Inc., Bellevue WA) equipped with a Beckman dissolved oxygen sensor and a WetStar chlorophyll fluorometer (WetLabs, Philomath OR) collected profiles at each station. The CTD sampled at a 2 Hz interval and was lowered at an approximate descent rate of 0.2 $m.s^{-1}$ allowing for measurements of temperature, conductivity, oxygen and chlorophyll fluorescence every 0.1 m. The conductivity, temperature and pressure (depth) sensors on the CTD have very sensitive resolutions and are extremely stable (Seabird 2001, 2002), however the dissolved oxygen sensor required calibration: The internal electrochemistry of the oxygen sensor changes with successive measurements, thus recorded values undergo a linear and gradual departure from the actual concentrations (Carlson 2002). To accommodate for this sensor drift, independent measurements of dissolved oxygen using the Winkler method (method detailed below) were performed in duplicate in conjunction with phytoplankton production assessment. The observed departures in sensor and Winkler measurements were then entered into an algorithm (Owens and Millard 1985) designed to perform post-collection calibration.

Chl in the euphotic zone (chl_{Zeu}) was determined as the average of independent measurements taken from the surface and euphotic depth using a Niskin water sampler. Duplicate samples of 200 ml of water were passed through Whatman GF/F filters (0.4 μm) that were then extracted in 20 ml of 95% methanol at 4°C for 24 hours. Extract was placed in a Jenway spectrometer (Barloworld Scientific, Essex UK) at wavelengths of 665 and 750 nm following Talling and Driver (1963). Extracted chl samples were then acidified with 1N HCl and reread at the same wavelengths to determine the contribution of pheo-pigments, but the percentage decline in absorbance in every sample was never below the criteria specified by Lorenzen (1967) so no correction for pheo-pigment contribution was applied.

The WetStar fluorometer measures *in vivo* chl fluorescence (range 0.06-150 chl $mg.m^{-3}$, sensitivity ≥ 0.03 $mg.m^{-3}$) and can be used to estimate extractable chl (Lorenzen 1966) with certain assumptions. The fluorometer is factory calibrated with a dilution series of Coprophophyrin stock solution (solution is equivalent to 50 $mg.m^{-3}$ of chl-a) to ascertain the linear relationship between voltage measured by a photodiode and the corresponding chl of the stock solution. In order to infer chl from *in* vivo fluorescence, several assumptions are required. Light energy impinging on phytoplankton chloroplasts can be used for one of three processes, photochemistry, non-photochemistry (thermal dissipation or transfer of the energy to an adjacent pigment) or fluorescence; each process is in direct competition with the other two, so an increased efficiency in one decreases the efficiency in the other two (Maxwell and Johnson 2000). The first assumption is that the efficiency of fluorescence is maximal beneath the photic zone where low light energy minimizes photochemical and non-photochemical processes, and therefore most representative of actual pigment measurements (Gilbert et al. 2000; Marra 1997). Secondly, fluorescence per unit chl, or fluorescence yield, is highly variable as optical properties of phytoplankton are a function of taxonomic composition (i.e. pigmentation) and physiological status (Cullen et al. 1988). Virtually all fluorescence originates from chl bound to PSII (left hand term of equation 2.3), as rates of excitation transfer in PSI and accessory pigments are approximately 5 times faster than PSII and therefore have a negligible contribution to fluorescence yield (Owens 1991). Extracted chl is compared to chl_F through the ratio chl_F:chl for samples taken near the bottom of the euphotic zone. Assuming chl/PSII and chl/PSI are equivalent (Behrenfeld et al. 2004), manipulation of Equation 2.3 yields Equation 2.4.

Equation 2.4) $chl_F:chl = (1 + PSI:PSII)^{-1}$

From Equation 2.4 and approximate PSI:PSII ratios for diatoms (1:2) and cyanobacteria (2:1), a lake dominated by cyanobacteria will have a lower chl_F:chl than a lake dominated by diatoms, as a shown by Heaney (1978). Chl_F measurements beneath the euphotic depth were divided by

chl_F:chl to provide high resolution estimates of extractable chl distributions. These distributions were combined with chl_{Zeu} to estimate chl_{WC}, necessary for accurate estimates of $AR_{[WC]}$ and $PP_{N[WC]}$.

The oxygen method (Carignan et al. 1998) was used to quantify phytoplankton respiration and photosynthesis. In Fielding Bay the procedure outlined below was repeated three times a day, whereas in Napoleon Gulf and Inner Murchison Bay, determination of phytoplankton photosynthesis and respiration was performed once per day. Water was collected at the surface and at the base of the euphotic zone (usually assumed to be 3 metres) using a Niskin water sampler and siphoned into separate 5L acid-washed carboys using a long tube to minimize aeration. Carboys were transported to the lab, gently shaked to ensure a homogenous sample and water was gently siphoned into two series of 14 BOD bottles by placing a tube at the bottom of the bottle and flushing it with approximately three times the bottle volume. Ten bottles per sample were placed in the light-gradient incubator for three hours, two bottles per sample were immediately fixed to provide initial dissolved oxygen concentrations, and two bottles were placed in the dark for the duration of the incubation to ascertain respiration. At the end of the incubation, the methodology of Carignan et al. (1998) was followed and reagents for the Winkler method were prepared following Stainton et al. (1977) to determine the final dissolved oxygen concentrations of the BOD bottles. The only alteration was that the end point of the titration was determined using colourimetric analysis with a HACH digital titrator (HACH Company, Loveland CO; accuracy = 0.00125 ml) to dispense sodium thiosulphate. Irradiance in the incubator was determined at each bottle position using a LI-COR 4π quantum sensor and the volumes of the BOD bottles were routinely determined as the difference between dry weight and weight after being filled with deionized water.

In Fielding Bay, thermistors were deployed using a float, rope and concrete anchor on each individual sampling day and recorded temperature on 30-second intervals. A TR-1050 thermistor (Richard Brankner Research Ltd., Ottawa ON; accuracy ±0.002°C, resolution 0.00005°C) was deployed at 0.1 m, and 5 Tidbit Stowaway thermistors (Onset Computer Corporation, Bourne MA;

accuracy 0.44°C, resolution = 0.3°C, 90% response time in 5 minutes) at 1.0m, 2.0m, 3.0m, 4.5m and 6m. An inter-comparison calibration at the beginning and end of the field season was performed by placing all thermistors in a warm water bath that progressively cooled. All Stowaway thermistors recorded identical temperatures, although small differences with the RBR thermistor (~0.2°C) occurred owing to the lower precision and slower response time of the Stowaway thermistors.

Meteorological data were provided courtesy of the Directorate of Water Development from the Campbell Scientific met station shown in Figure 2.2D. Wind speed, wind direction and air temperature were measured at an approximate height of 3 m above lake level at the Jinja Pier aboard a stationary vessel. Data are used in comparison with limnological measurements from Fielding Bay, approximately 6 km east. As shown in Figure 2.2D, the met station is more sheltered from the open lake than Fielding Bay, and therefore only provides an approximation of actual meteorological conditions in Fielding Bay.

Figure 2.3 provides a conceptual diagram of the phytoplankton production model with relevant equations. The first step in determining PP_G requires quantifying underwater irradiance (I) along user-specified time (t) and depth (z) intervals shown as grey lines in Figure 2.3C. Equation 1 quantifies I at each interval of t and z as a function of I_0 (Figure 2.3A) and k_{PAR} (Figure 2.3B). $I_{[t,z]}$ is then extrapolated to a PI curve (Figure 2.3E) to determine $P_{B[t,z]}$, and each of these values are then multiplied by $chl_{[t,z]}$ (Figure 2.3E, Eqn. 2) to determine $P_{[t,z]}$. PP_G is calculated as the double integral (Eqn. 3) of $P_{[t,z]}$ through the euphotic depth ($0 \rightarrow z_{eu}$) and time ($t_0 \rightarrow t_1$). As PP_G is light dependent, integrations are constrained to the euphotic depth; however AR is light independent and can be integrated through any depth. The subscript Zeu refers to AR (and consequently PP_N) integrated through the euphotic depth and the subscript WC refers to AR integrated through the entire water column. To minimize any variability between days, PP_G in this thesis is calculated using cloud-free conditions and an atmospheric effect coefficient of 0.30 (as calculated following Fee (1990)).

The revised model allows PI parameters, k_{PAR} and chl to vary within a day, whereas in the previous model the same parameters were assumed to be diurnally static. Fee (1975) shows that accounting for diurnal variations of PI parameters reduced annual production estimates by 11% in a set of small oligotrophic-mesotrophic lakes, but argues that the effect of variation is often exceeded by the errors associated with sampling and data analysis. Observed diurnal variations of chl (Ramlal et al. 2001) and transparency (Wanink and Kashindye 1998) in Lake Victoria suggest diurnal variations in the input parameters may have an appreciable effect on production estimates. The linear interpolation and static extrapolation rules of the original model now also pertain to diurnal variations. For example, if chl is found to be 30, 40 and 35 $mg.m^{-3}$ at 9:00, 12:00 and 17:00 hrs, chl at 10:00 and 14:00 hrs are interpolated as 33.3 and 38 $mg.m^{-3}$ respectively, while values at 8:00 and 18:00 remain at 30 and 35 $mg.m^{-3}$. Daily averaged diurnal data presented in the results section are calculated using these interpolation rules to give appropriate weighting to each value.

Raw data for all figures are located on the accompanying CD in the folder ‘Chapter 2’.

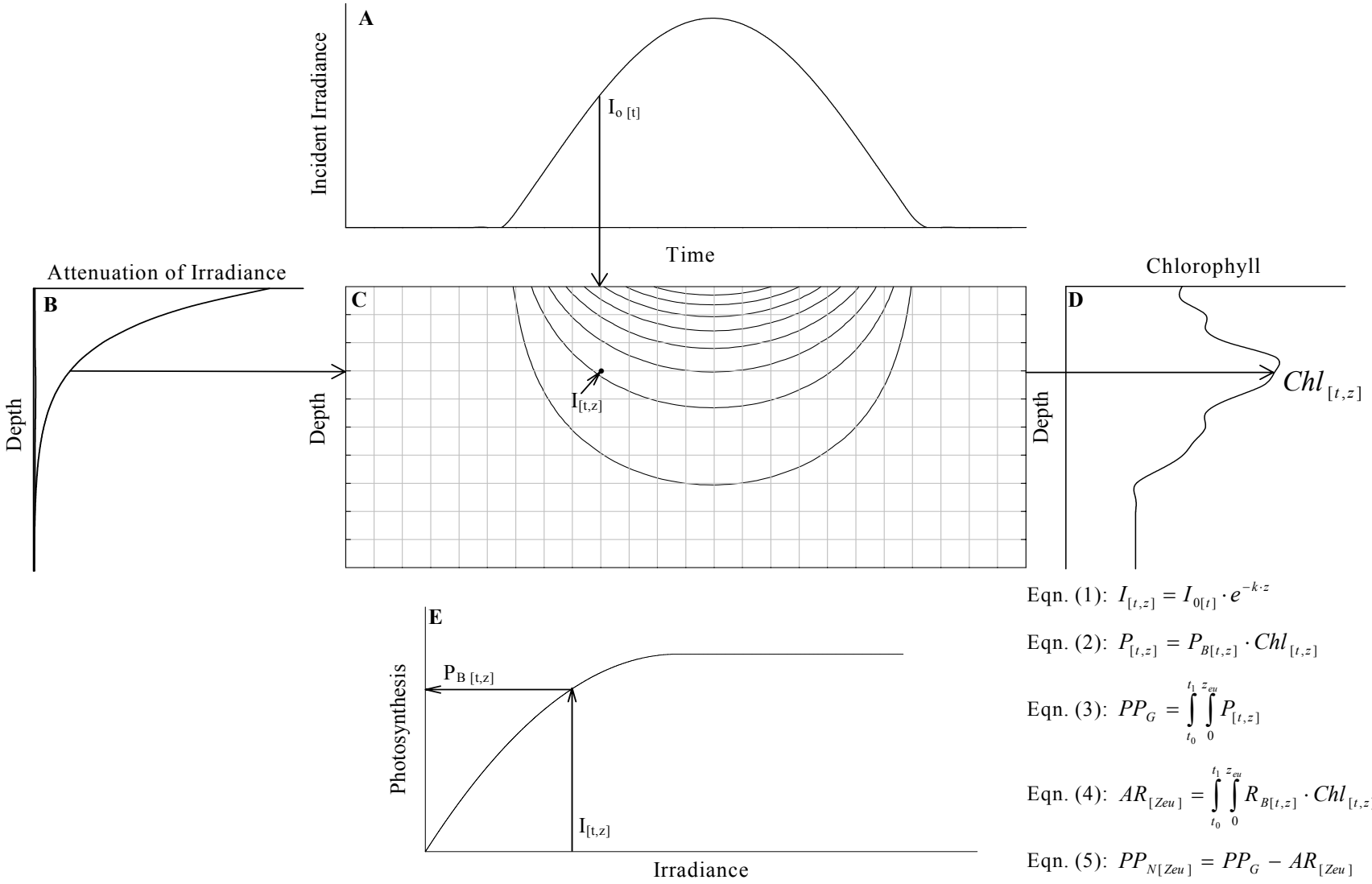

Eqn. (1): $I_{[t,z]} = I_{0[t]} \cdot e^{-k \cdot z}$

Eqn. (2): $P_{[t,z]} = P_{B[t,z]} \cdot Chl_{[t,z]}$

Eqn. (3): $PP_G = \int_{t_0}^{t_1} \int_{0}^{z_{eu}} P_{[t,z]}$

Eqn. (4): $AR_{[Zeu]} = \int_{t_0}^{t_1} \int_{0}^{z_{eu}} R_{B[t,z]} \cdot Chl_{[t,z]}$

Eqn. (5): $PP_{N[Zeu]} = PP_G - AR_{[Zeu]}$

Figure 2.3: Conceptual Diagram of Gross Phytoplankton Production Model: A) Incident Irradiance, B) in-situ irradiance, C) under-water irradiance field, D) chlorophyll profile and E) PI curve.

2.3 Results

Figure 2.4 depicts the temporal variation of chl_{Zeu} and chl_{WC} in each of the three bays, with points corresponding to daily averages and error bars encompassing the diurnal range. On average and as summarized in Table 2.6, Inner Murchison Bay had the highest chl, followed by Fielding Bay and the lowest chl was in Napoleon Gulf. The near 3-fold difference of average chl between Napoleon Gulf and Inner Murchison Bay demonstrates significant spatial variability, as both bays were sampled over the same time period in 2001. Temporal trends in these two bays also differed, as generally the highest chl in Inner Murchison Bay occurred at the same time as the lowest chl in Napoleon Gulf (Figure 2.4). Chl in each bay exhibited strong temporal variability, as the coefficients of variance for daily averaged chl_{WC} were 35%, 26% and 42% for Inner Murchison Bay, Napoleon Gulf and Fielding Bay respectively. In each bay, chl_{zeu} and chl_{WC} followed similar temporal patterns, and the largest difference between the two was in Fielding Bay. The most rapid temporal changes in chl also occurred in Fielding Bay, where the daily averaged chl_{WC} decreased 3.7-fold between days of the year 270 and 278 followed by a 3.3-fold increase between days of the year 278 and 289 (Figure 2.4).

Figure 2.5 shows the temporal variation of average Z_{eu} and SD in each of the three bays, with points corresponding to daily averages and error bars encompassing the diurnal range. On average, both Z_{eu} and SD were deepest in Napoleon Gulf, followed by Fielding Bay and were shallowest in Inner Murchison Bay. In each bay, SD and Z_{eu} exhibited similar temporal patterns, as k_{PAR} is linearly correlated to the inverse SD shown in Figure 2.6C. Data from the Lake Victoria Ecosystem Project (NSF Grants DEB-9318085 and DEB-9553064) have been added to supplement this relationship, as the project's dataset is more spatially extensive with several offshore stations having deeper Z_{eu} and SD relative to inshore sites. Both SD and k_{PAR} were strongly correlated with average euphotic chl (chl_{zeu}) as seen in Figure 2.6A and B respectively, and both curves became increasingly asymptotic as chl increased. Due to these relationships with chl, temporal and spatial patterns of Z_{eu} and SD are similar to the patterns exhibited by chl in each bay. Data from the Lake Victoria Ecosystem Project

also supplements the correlations in Figure 2.6A and B, as does the historic data of Talling (1965) added to Figure 2.6B.

Figure 2.7 depicts the temporal variation of the thermal structure in each bay. To minimize the influence of diurnal heating, early morning profiles in each bay were used to interpolate between sampling dates identified with inverted triangles. As summarized in Table 2.5, Fielding Bay had the highest average water column temperature (T_{WC}) and was the most stratified as indicated by the largest buoyancy frequency (N calculated following Fischer et al. 1979) of the three bays. Napoleon Gulf and Inner Murchison Bay had similar T_{WC}, but Inner Murchison Bay (the shallowest of all bays) had the lowest N and was almost completely isothermal each morning of sampling. With respect to temporal variability over the length of study periods, T_{WC} ranged by approximately 1.5°C in each bay.

Time specific annually averaged meteorological data for 2002 demonstrates a diel pattern (Appendix I, Figure 6.1) with wind speed and air temperature reaching a maximum in the late afternoon, consistent with a strong lake breeze (Flohn and Fraedrich 1966; Asnani 1993). Average wind speed for the 24 hours previous to each morning (09:00 previous day to 09:00 current day) had a small coefficient of variance and was not correlated to early morning T_{WC} as shown in Figure 2.8A and Table 2.8. Northern areas of Lake Victoria are occasionally subjected to strong overnight wind events, such that a 3-hour wind event with an average wind speed of 4 $m.s^{-1}$ has a statistical return time of 11.3 days, based on Pearson Type III frequency analysis using 2002 meteorological data. Figure 2.8B depicts the maximum 3-hour overnight wind event for each day, and as summarized in Table 2.8, overnight wind regimes are better correlated to T_{WC} than daily averaged wind speeds.

Figure 2.9 depicts the temporal variation of PI parameters in each of the three bays, with points corresponding to daily averages and error bars encompassing the diurnal range for the Fielding Bay dataset. On average and as summarized in Table 2.6, both P_{BM} and α_B were highest in Napoleon Gulf, followed by Fielding Bay and were lowest in Inner Murchison Bay. In each bay, P_{BM} and α_B exhibited similar temporal patterns as α_B was significantly correlated to P_{BM}, as depicted in Figure

2.10A. PI parameters from the more spatially extensive dataset of Mugidde (1992) shown in Figure 2.10B also demonstrate positive linear covariance; however a student t-test showed that the regression equations in Figure 2.10A and B were not statistically similar. I_k values can be determined using the regression equations of each dataset. Both curves predict an I_k value of 169 $\mu mol.m^{-2}.s^{-1}$ when P_{BM} is 16.6 mg $O_2.m^{-3}.hr^{-1}$, however the regression equation of Figure 2.10A predicts that I_k decreases as P_{BM} increases, whereas the dataset of Mugidde's (1992) predicts the opposite. Figure 2.10C shows PI parameters measured on specific days in Fielding Bay, with data points labeled as the day of the year on which they were acquired. Although PI parameters in Fielding Bay exhibit positive linear covariance ($r^2 = 0.81$, $n = 41$, $p < 0.0001$), covariance of PI Parameters within a day was variable with the r^2 for P_{BM} and α_B ranging from 0.02 on day of the year 296 to 0.85 on day of the year 302. Furthermore, the average coefficients of variance for diurnal measurements of P_{BM} and α_B were 12% and 16% respectively, lower than those calculated over the study period shown in Table 2.6.

α_B and P_{BM} showed significant correlation to chl when fitted with equations shown in Figure 2.11A and B respectively. Therefore in each bay when chl was high, PI parameters were low and when chl was low PI parameters were high. Historic P_{BM} and chl data was used to validate this relationship as seen in Figure 2.11C. Although there is increased unexplained variance in the historic datasets, a student t-test of the linearly transformed regression equation was statistically similar to the current dataset ($\alpha = 0.05$).

Figure 2.12A shows an estimation of k_{chl}, the partial attenuation coefficient due to chl, plotted against chl. k_{chl} was determined by assuming the partial attenuation coefficients unrelated to chl (Equation 2.4) were constant and equivalent to the offset of the regression equation (0.11 m^{-1}) presented Figure 2.6B, a value that was then subtracted from all values of k_{PAR} that were then divided by the corresponding measurement of chl. Similar to the relationship of SD versus chl (Figure 2.6A), k_{chl} shows a strong statistical relationship to chl when fitted with a hyperbolic decay equation. As shown in Figure 2.12B and C, k_{chl} is linearly related to the PI parameters. 53% and 47% of the

variation in P_{BM} and α_B, respectively, is explained by changes in k_{chl}. Furthermore, 40% of the variation in P_{BM} is explained by changes in chl_F:chl, an approximate indicator of the PSII:PSI ratio (Equation 2.6) shown in Figure 2.13C. As chl_F:chl increases there is a shift in the PSII:PSI ratio towards oxygen evolving PSII centres, and accordingly P_{BM} also increases. Despite this correlation, Figure 2.13A illustrates that chl_F and chl are weakly correlated as the regression coefficient is small. However, as shown for Fielding Bay in Figure 2.13B, diurnal variability of chl_F:chl is small (average coefficient of variance = 10%), such that on a given day chl_F:chl can be applied to chl_F measurements to give a reasonable approximation of chl below the euphotic zone in the absence of photochemical and non-photochemical quenching.

Figure 2.14 shows volumetric rates of P_{Opt} and R in each bay. Similar to chl, both P_{Opt} and R are highest in Inner Murchison Bay and lowest in Napoleon Gulf. A positive covariance is seen between the two parameters, although the relationship is not strong when they are normalized to chl as shown in Figure 2.15A. R_B has a stronger correlation to chl (Figure 2.15B), and generally decreases as chl increases. The statistical significance of this relationship increases when diurnal averages of the two parameters are taken (Figure 2.15C). No historical data is available to validate these relationships although Talling (1966) noted that R is usually 0.33 of P_{Opt}, higher than the approximate 0.16 P_{Opt}:R ratio derived from Figure 2.14.

Table 2.7 provides the mean and coefficient of variance for the average PP_G, $AR_{[Zeu]}$ and $AR_{[WC]}$ for each bay, including the production to respiration ratio (P:R) in both the euphotic zone and for the entire water column. On average PP_G is highest in Napoleon Gulf and lowest in Inner Murchison Bay, similar to the spatial averages of Z_{eu} and opposite to the spatial averages of chl. Conversely, both $AR_{[Zeu]}$ and $AR_{[WC]}$ are highest in Inner Murchison Bay and lowest in Napoleon Gulf. The P:R ratio within the euphotic zone is greater than one in each bay and highest in Napoleon Gulf, indicating that within the euphotic zone each station is net autotrophic. However when respiration below the euphotic zone is taken into account, all stations are net heterotrophic. These patterns are further illustrated in Figure 2.16, showing the temporal variation of PP_G, $AR_{[Zeu]}$ and

$AR_{[WC]}$ in each bay. In Fielding Bay, the euphotic zone was net autotrophic on each sampling day but the water column was net heterotrophic on all days except day of the year 330, when PP_G reached its maximum over the study period. In Napoleon Gulf the euphotic zone was always net autotrophic while the water column varied between autotrophy and heterotrophy. In Inner Murchison Bay the euphotic zone was net autotrophic for the first 3 sampling days but became net heterotrophic after that, coinciding with the increase in chl (Figure 2.4) and the large concurrent increase in $AR_{[WC]}$.

Temporal variation of the P:R ratio for the entire water column within each bay is shown in Figure 2.17. Also in this figure is the critical depth (Z_{cr}), the depth at which PP_N is zero for each individual 24-hour calculation for each bay, as well as the average depth within a 5 km radius of each station. When Z_{cr} is less than the average depth of each bay, the bay is net heterotrophic but when Z_{cr} is greater than the average depth of each bay the bay is net autotrophic, assuming each parameter of the model is approximately spatially homogeneous on each day within a 5 km radius. According to Figure 2.17A, Fielding Bay was varied between autotrophy and heterotrophy, and the average Z_{Cr} of the study period was equal to 6 m the average depth (6 m). In Napoleon Gulf the larger P:R sets a deeper Z_{Cr} relative to the other two bays. The average Z_{Cr} in Napoleon Gulf of 13.2 m exceeds the average depth of 8 m, indicating that Napeleon Gulf was net autotrophic over the sampling period. Finally the low P:R ratio in Inner Murchison Bay causes the lowest values of Z_{Cr} relative to the other three bays. On average Z_{Cr} is approximately twice the average depth in Inner Murchison Bay indicating net autotrophy. The temporal patterns of Z_{Cr} in both Napoleon Gulf and Inner Murchison Bay follow the same general trend as chl. Specifically in Inner Murchison Bay when Z_{Cr} exceeds the mean depth of 2.2 m chl increases, and when Z_{Cr} approaches the mean depth chl generally levels off as well.

Table 2.5: Mean and coefficient of variance for physical parameters in Fielding Bay (FB), Napoleon Gulf (NG) and Inner Murchison Bay (IMB).

Site	T_{WC} (Deg C)		N (hr^{-1})		Zeu (m)		SD (m)	
	Mean	C.V.	Mean	C.V.	Mean	C.V.	Mean	C.V.
FB	26.26	1.6%	28.0	36.0%	3.28	16.4%	0.87	26.1%
NG	24.55	2.0%	15.6	56.9%	5.39	15.7%	1.35	18.4%
IMB	24.71	1.6%	39.1	78.3%	3.10	21.3%	0.76	13.6%

Table 2.6: Mean and coefficient of variance for biological parameters in Fielding Bay (FB), Napoleon Gulf (NG) and Inner Murchison Bay (IMB).

Site	Chl_{Zeu} ($mg.m^{-3}$)		Chl_{ML} ($mg.m^{-3}$)		R_B (mg O_2.mg $Chl^{-1}.hr^{-1}$)		PI Parameters			
							P_{BM} (mg O_2.mg $Chl^{-1}.hr^{-1}$)		α_B (mg O_2.mg $Chl^{-1}.\mu mol^{-1}.m^2$)	
	Mean	C.V.	Mean	C.V.	Mean	C.V.	Mean	C.V.	Mean	C.V.
FB	55.8	43.3%	49.3	42.4%	2.1	36.5%	14.7	27.9%	22.7	50.3%
NG	24.3	32.3%	22.2	25.6%	2.3	24.7%	20.4	12.1%	34.5	24.6%
IMB	69.5	30.5%	65.6	35.0%	2.0	16.7%	12.1	30.5%	16.9	43.5%

Table 2.7: Mean and coefficient of variance for phytoplankton production and respiration in Fielding Bay (FB), Napoleon Gulf (NG) and Inner Murchison Bay (IMB).

Site	PP_G (g $O_2.m^{-2}.day^{-1}$)		AR				P:R			
			Zeu (g $O_2.m^{-2}.day^{-1}$)		WC (g $O_2.m^{-2}.day^{-1}$)		Zeu		WC	
	Mean	C.V.	Mean	C.V.	Mean	C.V.	Mean	CV	Mean	CV
FB	12.9	19.6%	8.2	29.6%	16.3	39.9%	1.66	27.9%	0.87	36.1%
NG	14.0	24.8%	7.4	24.2%	16.3	36.0%	1.95	17.5%	0.99	31.7%
IMB	13.0	22.4%	11.8	48.7%	20.4	40.2%	1.27	44.0%	0.76	53.6%

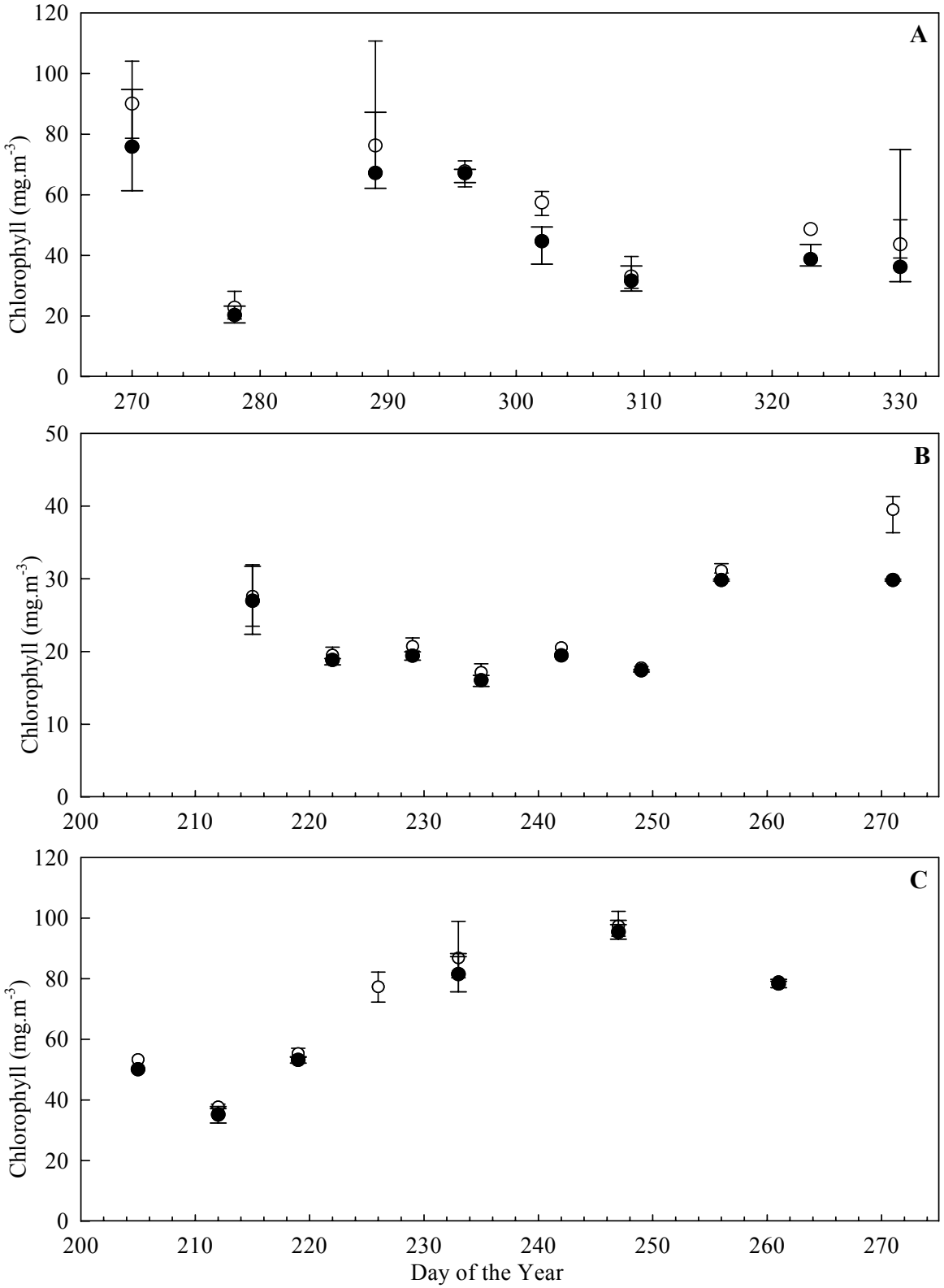

Figure 2.4: Temporal variation of chl_{zeu} (open circles) and chl_{WC} (closed circles) in A) Fielding Bay, B) Napoleon Gulf and C) Inner Murchison Bay. Points correspond to daily averages and error bars represent the range of data on that day.

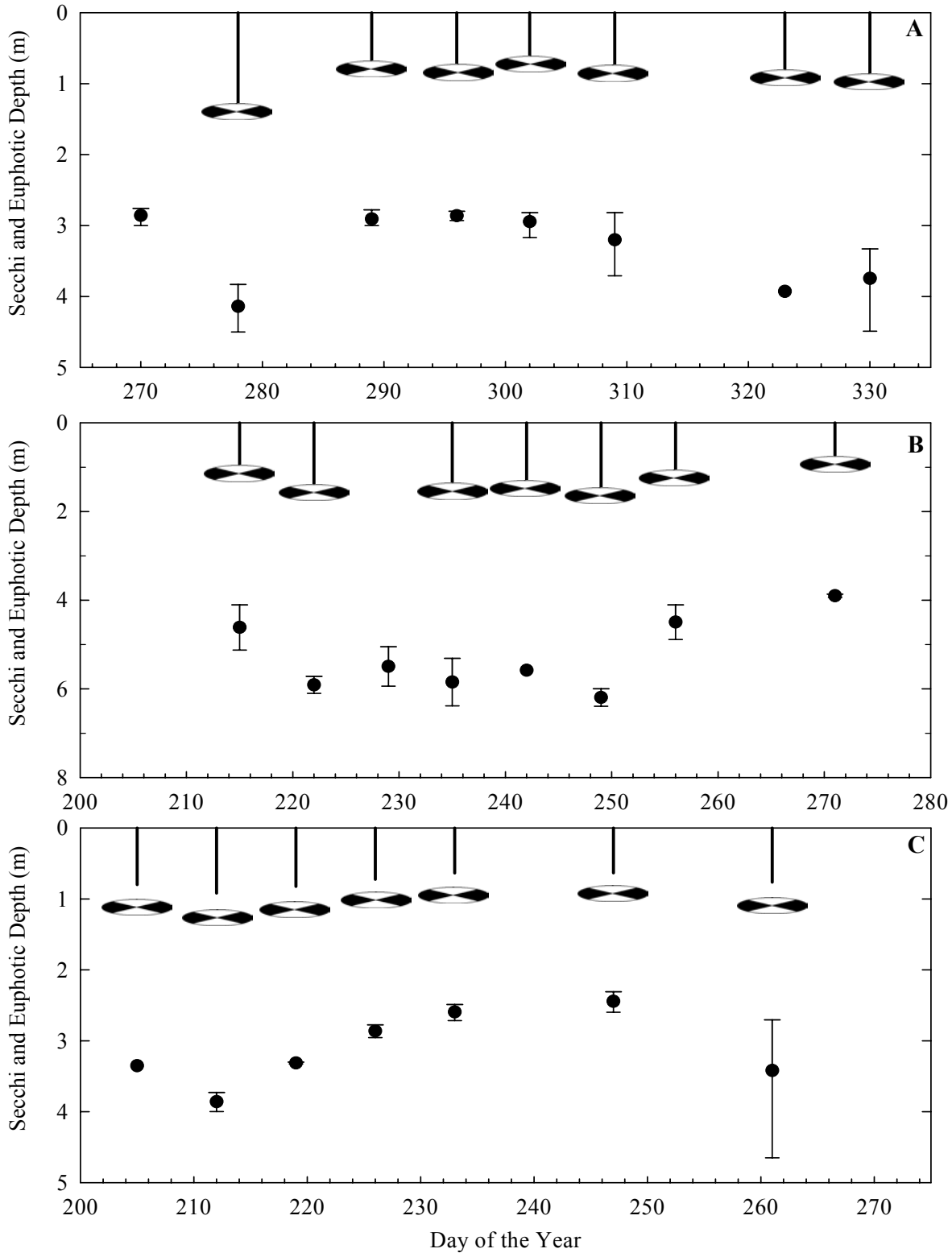

Figure 2.5: Temporal variation of z_{eu} (closed circles) and SD (black and white disks) in A) Fielding Bay, B) Napoleon Gulf and C) Inner Murchison Bay. Points correspond to daily averages and error bars represent the range of data on that day.

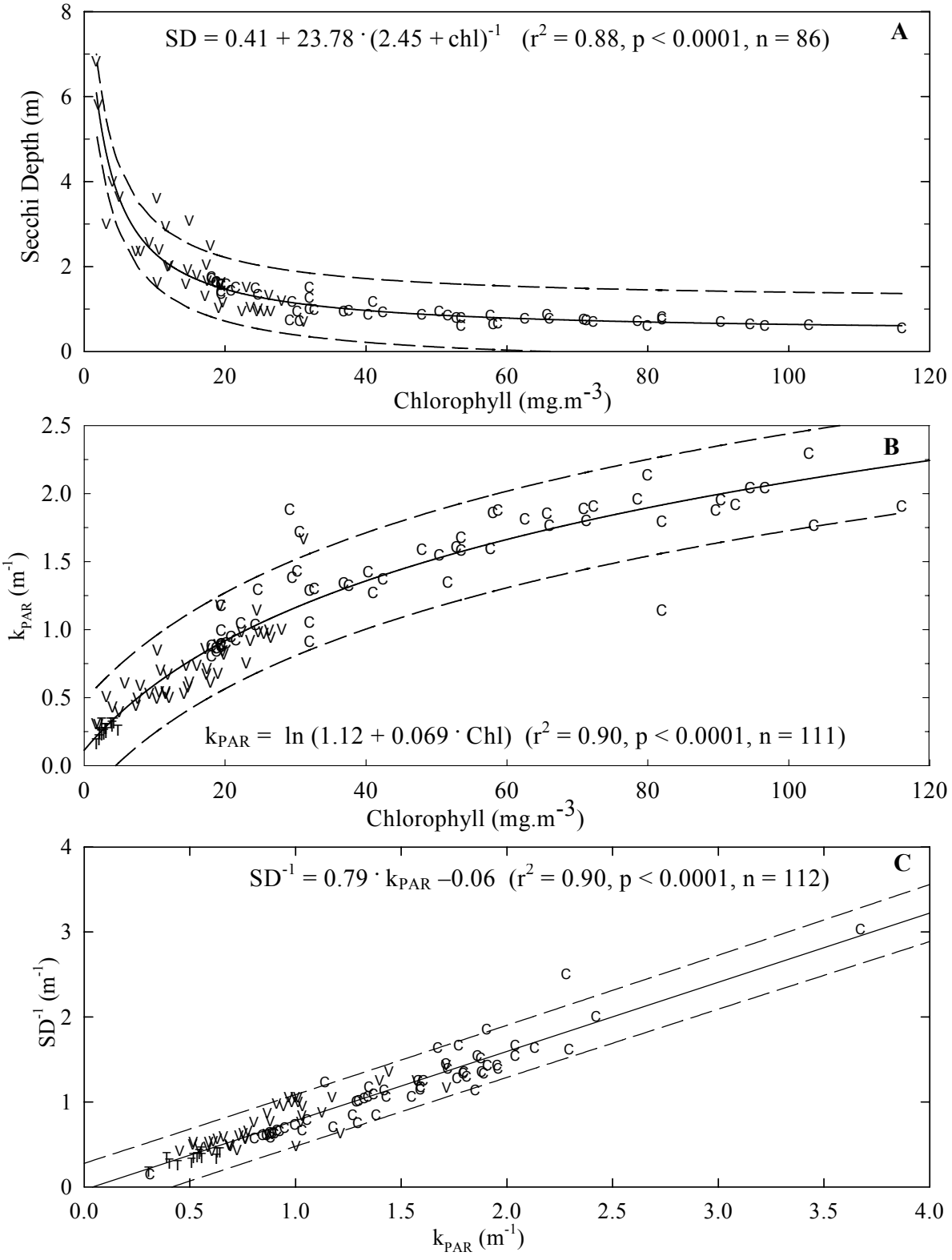

Figure 2.6: Regression of A) SD and B) k_{PAR} versus chl_{zeu} and C) SD^{-1} versus k_{PAR}. Dashed lines are prediction intervals.

(C – Current Dataset, T – Talling 1965, V – Lake Victoria Ecosystem Project).

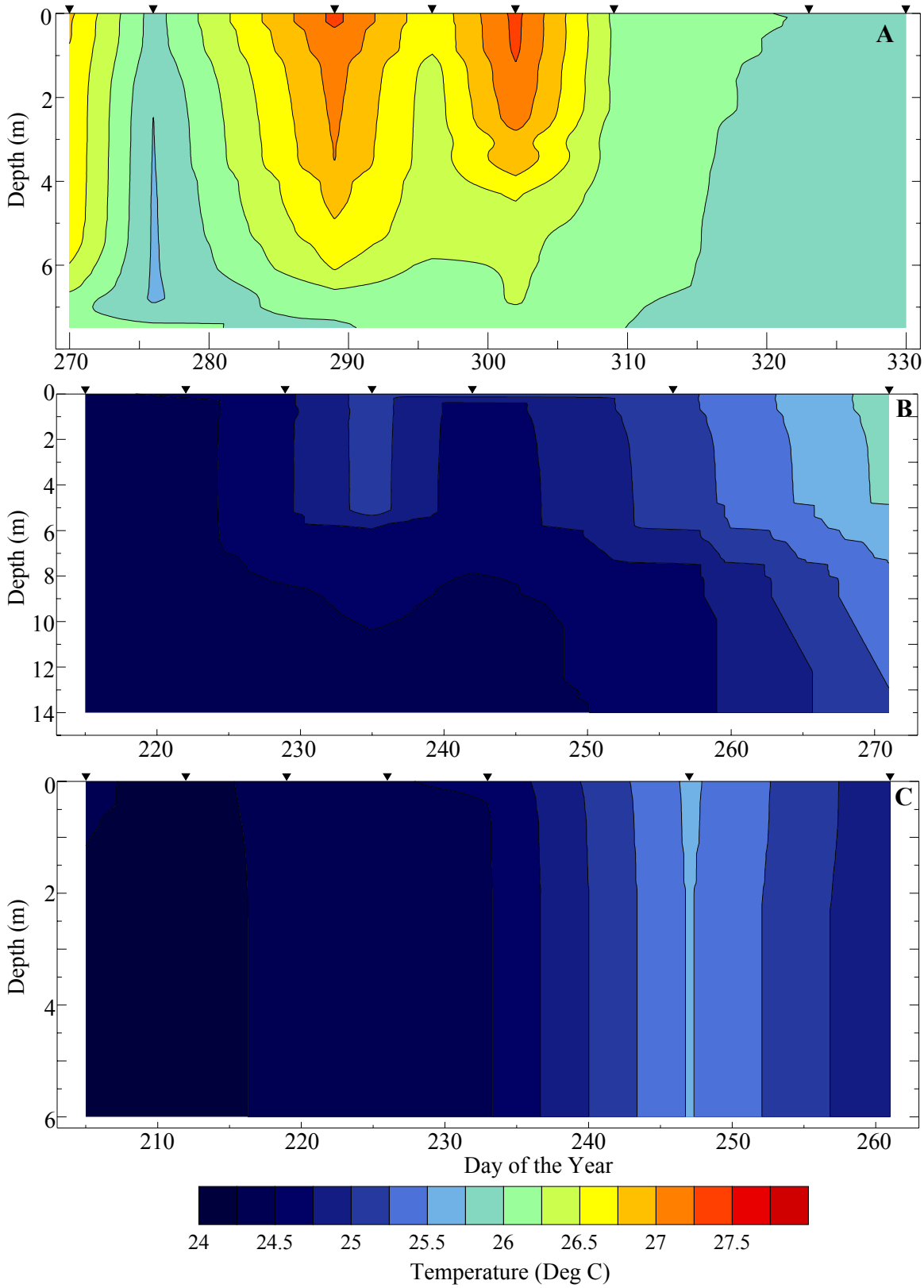

Figure 2.7: Temporal variation of water column temperature as measured in the early morning to minimize the influence of diurnal heating in A) Fielding Bay, B) Napoleon Gulf and C) Inner Murchison Bay. Inverted triangle represents water column profile.

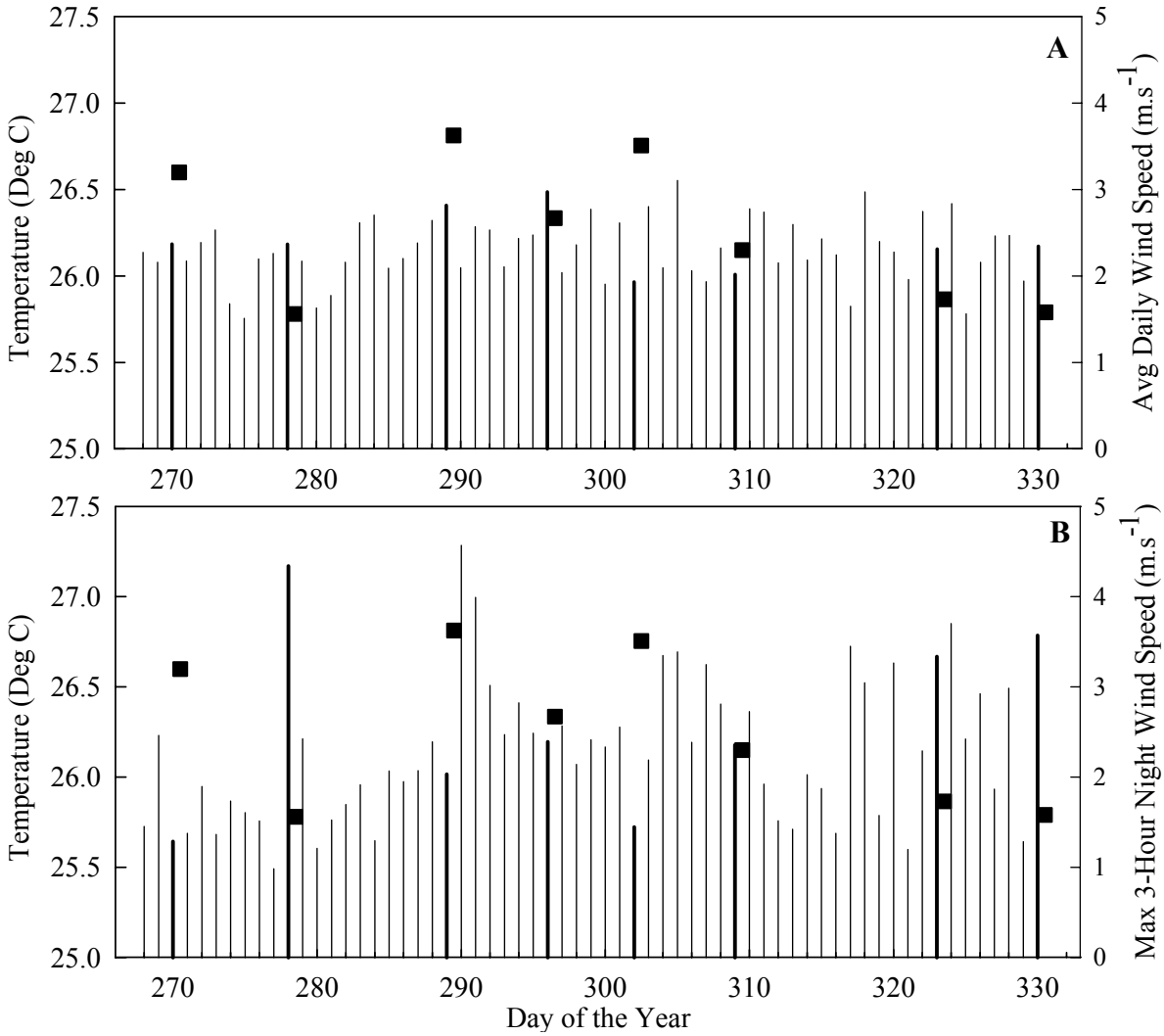

Figure 2.8: Temporal variation of T_{WC} (solid squares) and average wind speed A) over 24 hours and B) maximum 3-hour overnight wind event. Events prior to profiles shown in bold.

Table 2.8: Diel Wind Regimes and their correlation to early morning T_{WC}

Wind Regime	r^2 versus T_{WC}	Return Period for Event with average speed of 4 $m.s^{-1}$ (days)
24 Hours	0.02	168.3
4 Hour Wind Event	0.78	21.8
3 Hour Wind Event	0.77	11.3
2 Hour Wind Event	0.79	8.7
1 Hour Wind Event	0.78	5.0

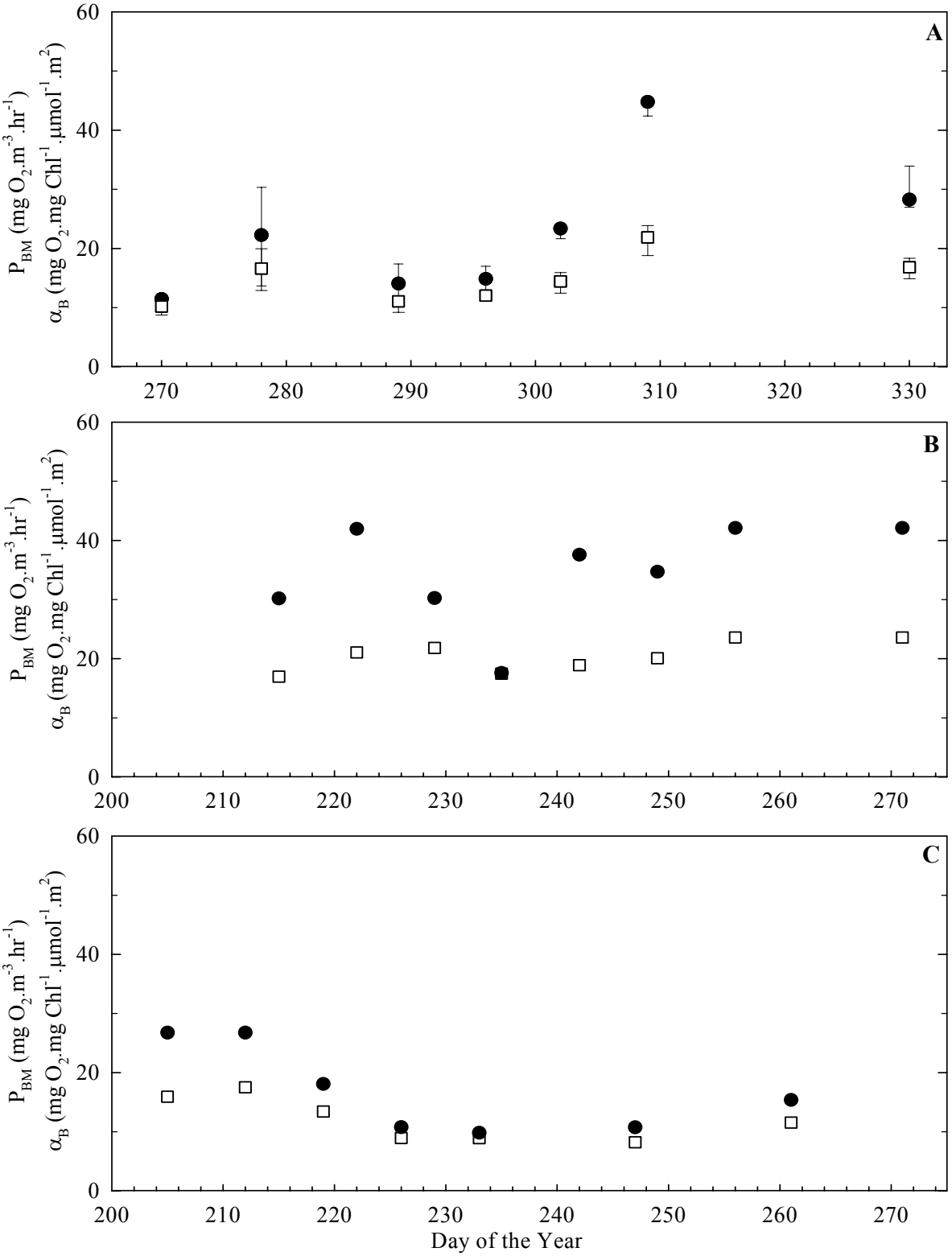

Figure 2.9: Temporal variation of water-column averages of P_{BM} (open squares) and α_B (closed circles) in A) Fielding Bay, B) Napoleon Gulf and C) Inner Murchison Bay. Points correspond to daily averages and error bars represent the range of data on that day.

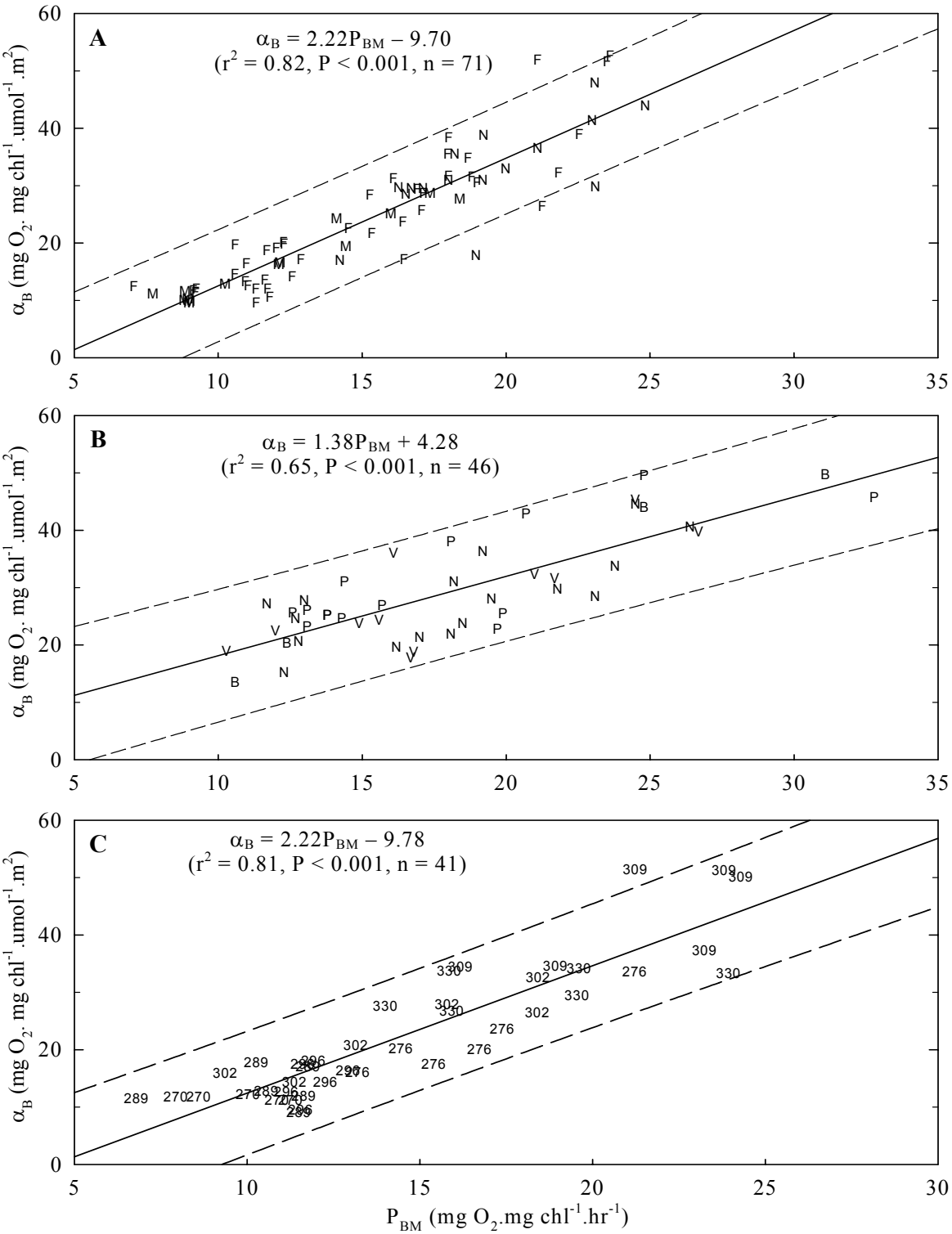

Figure 2.10: Regression of P_{BM} versus α_B from A) this dataset B) Mugidde (1992) and C) Fielding Bay measurements where label represents day of the year. Dashed lines are prediction intervals.

(B – Bugaia, F – Fielding Bay, M – Inner Murchison Bay, N – Napoleon Gulf, P – Pilkington Bay, V –Buvumu Channel).

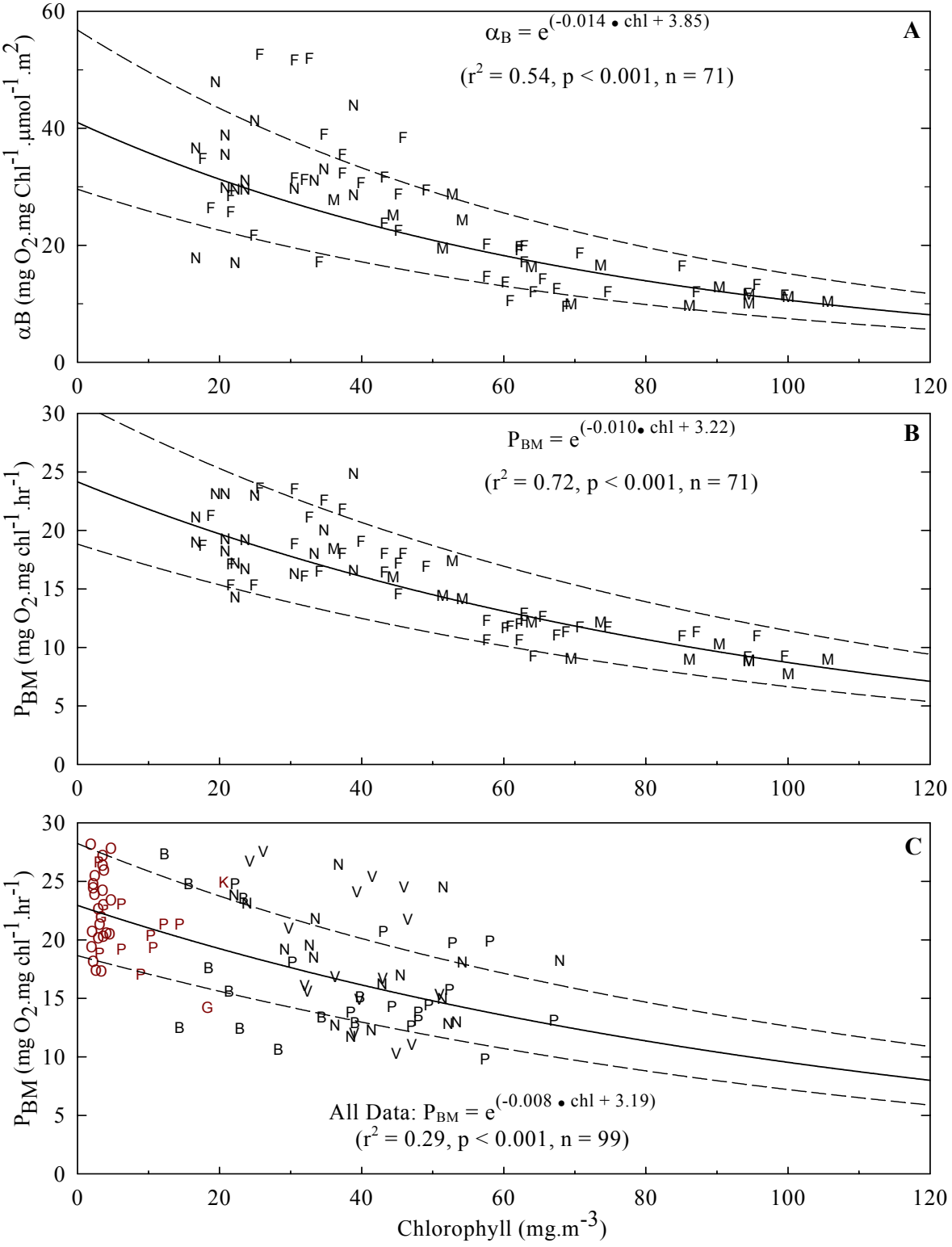

Figure 2.11: Regression of A) α_B and B) P_{BM} from this dataset and C) Historic P_{BM} versus chl_{zeu} (Talling 1965; Mugidde 1992).

(B – Bugaia, F – Fielding Bay, G- Grant Bay, K – Kavirondo Gulf, M – Inner Murchison Bay, N – Napoleon Gulf, O – Offshore Station, P – Pilkington Bay, V –Buvumu Channel).

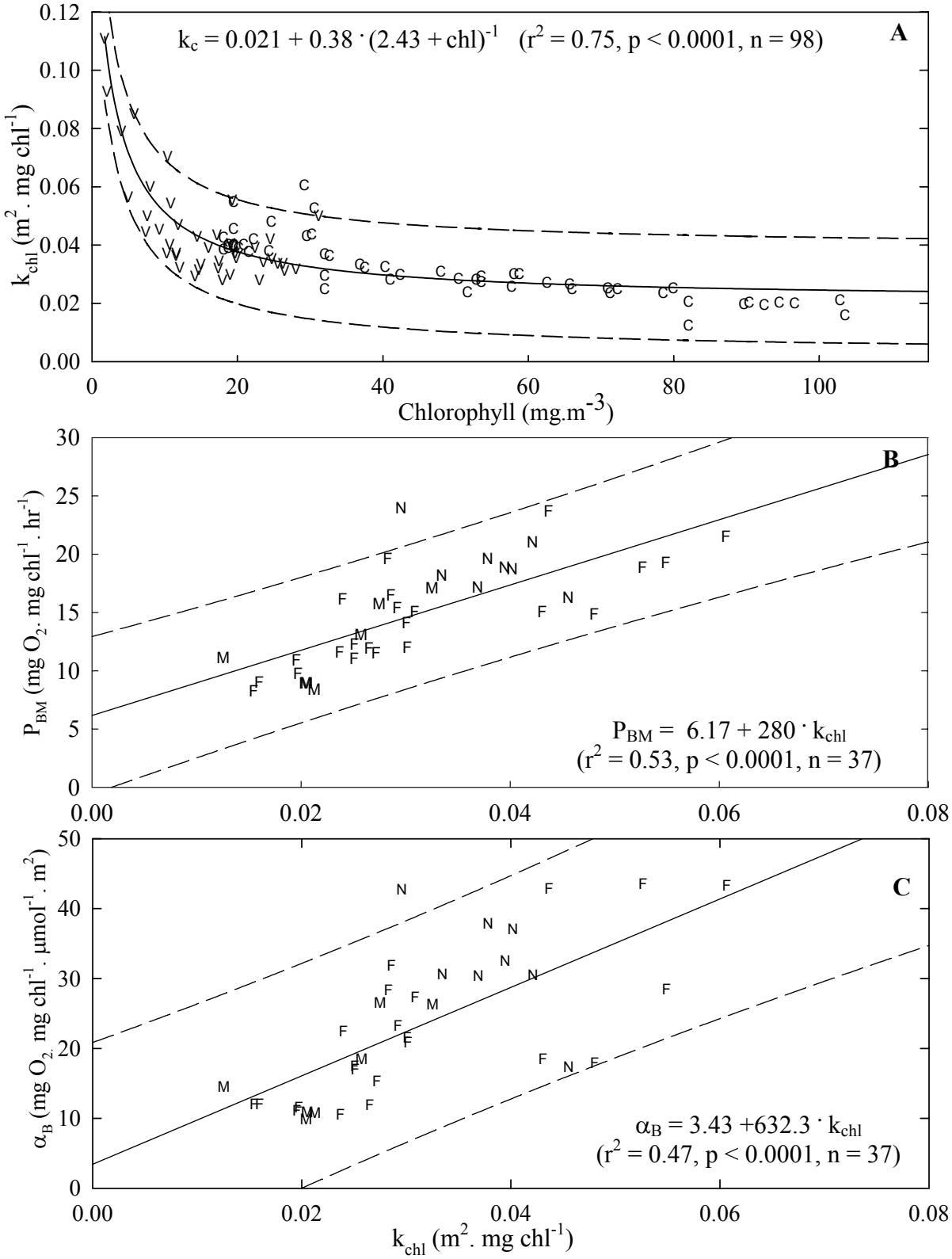

Figure 2.12: Regression of k_{chl} versus A) chl_{zeu} B) P_{BM} and C) α_B. Dashed lines are prediction intervals.

(F – Fielding Bay, M – Inner Murchison Bay, N – Napoleon Gulf).

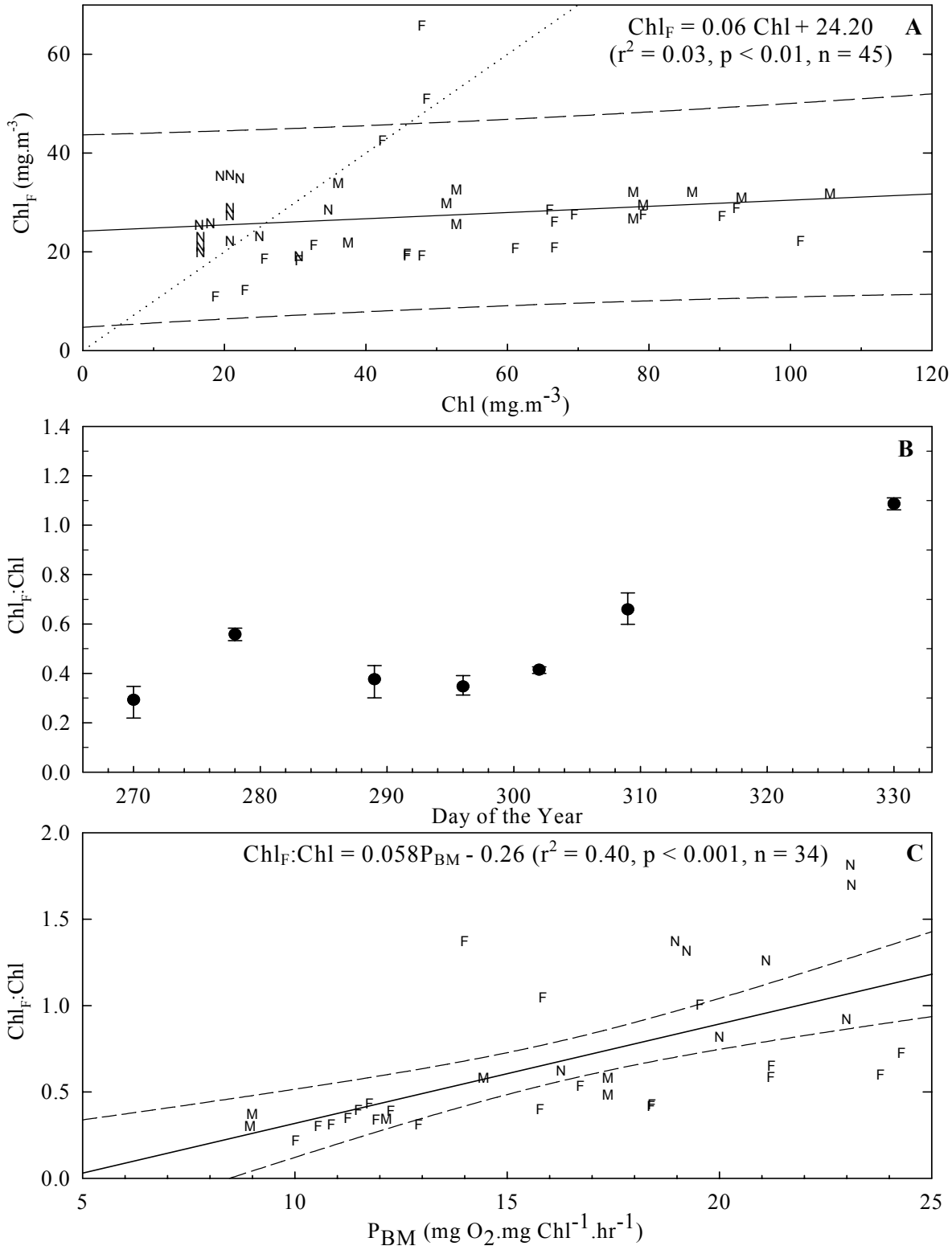

Figure 2.13: A) Regression of chl_F versus chl, dotted line is the 1:1 line. B) Temporal variation of chl_F:chl in Fielding Bay C) Regression of chl_F:chl versus P_{BM}. Dashed lines are prediction intervals.

(F – Fielding Bay, M – Inner Murchison Bay, N – Napoleon Gulf)

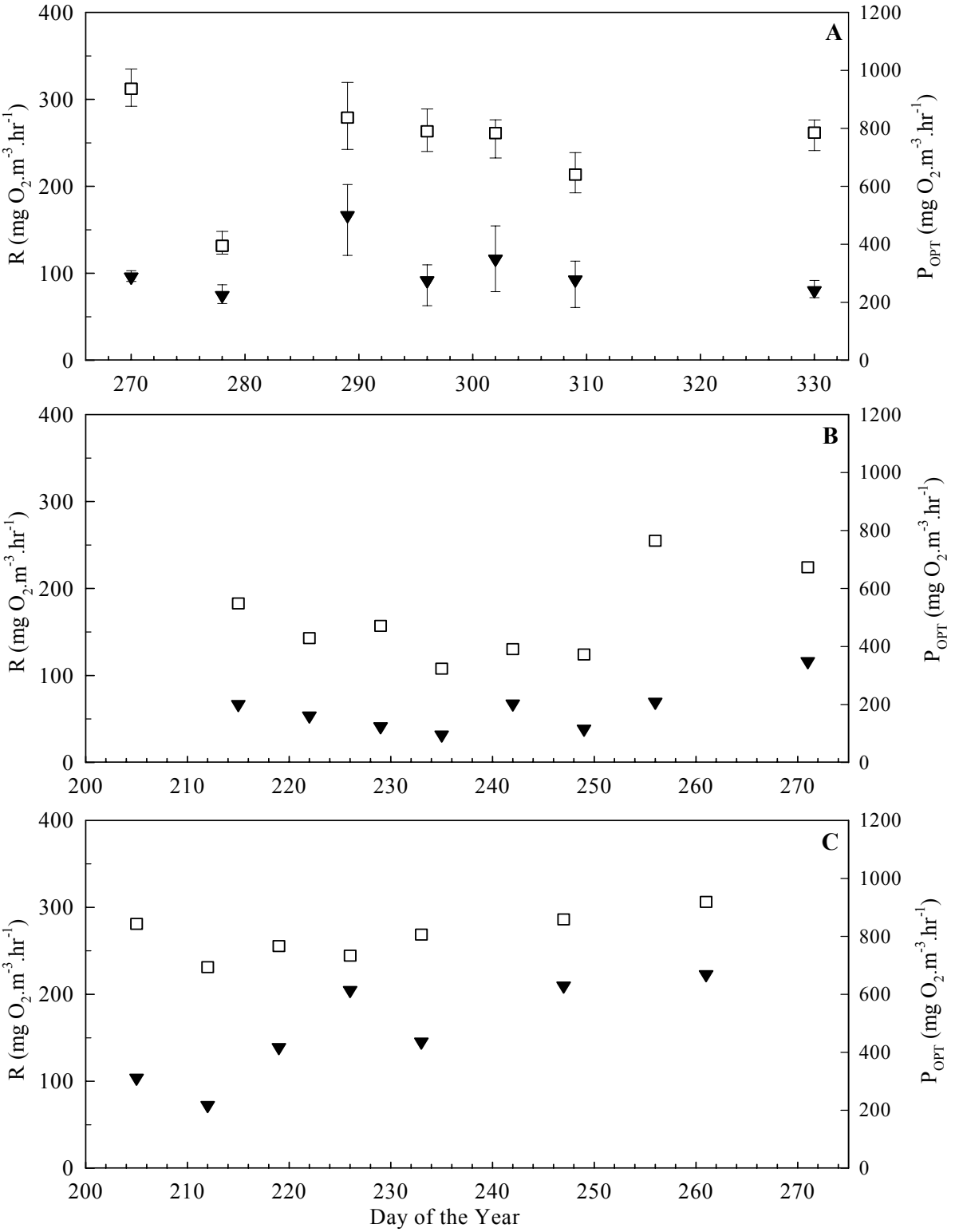

Figure 2.14: Temporal variation of P_{Opt} (open squares) and R (closed triangles) in A) Fielding Bay, B) Napoleon Gulf and C) Inner Murchison Bay. Points correspond to daily averages and error bars represent range of data over diurnal scale.

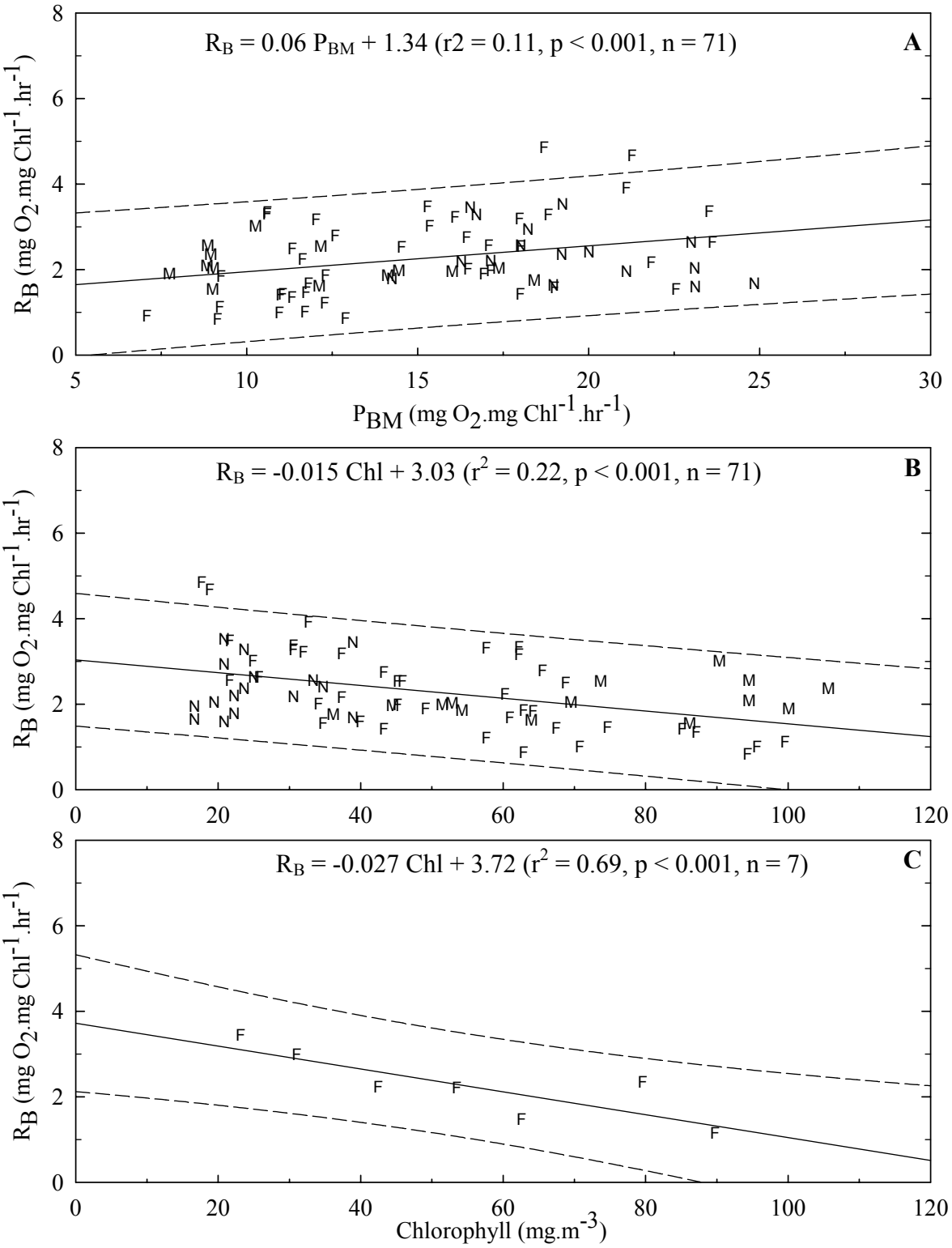

Figure 2.15: Regression of R_B versus A) P_{BM}, B) chl_{zeu} and C) diurnally averaged R_B versus diurnally averaged chl_{zeu}. Dashed lines are prediction intervals.
(F – Fielding Bay, M – Inner Murchison Bay, N – Napoleon Gulf)

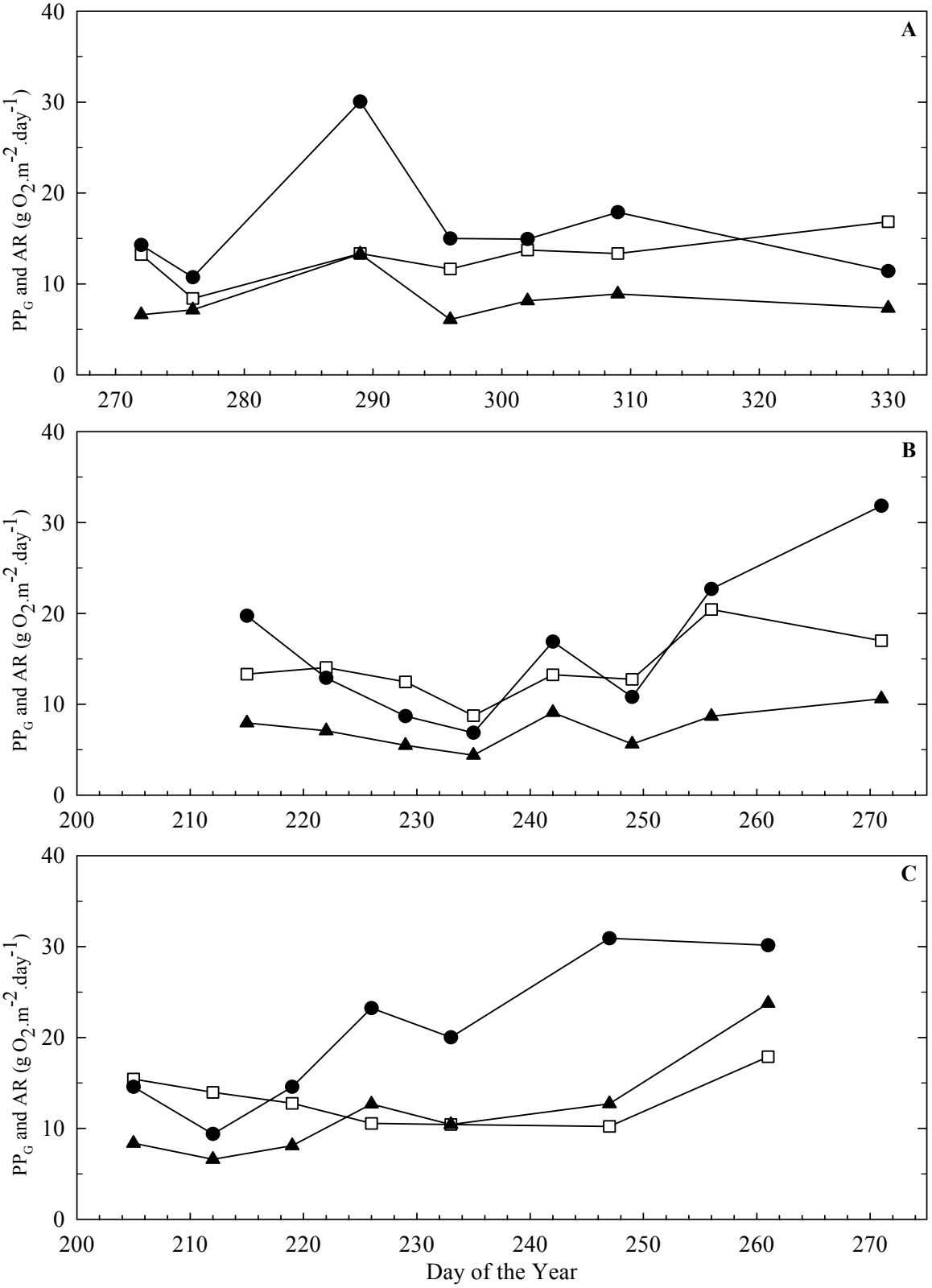

Figure 2.16: Temporal variation of PP_G (open squares), $AR_{[Zeu]}$ (closed triangles) and $AR_{[WC]}$ (closed circles) in A) Fielding Bay, B) Napoleon Gulf and C) Inner Murchison Bay.

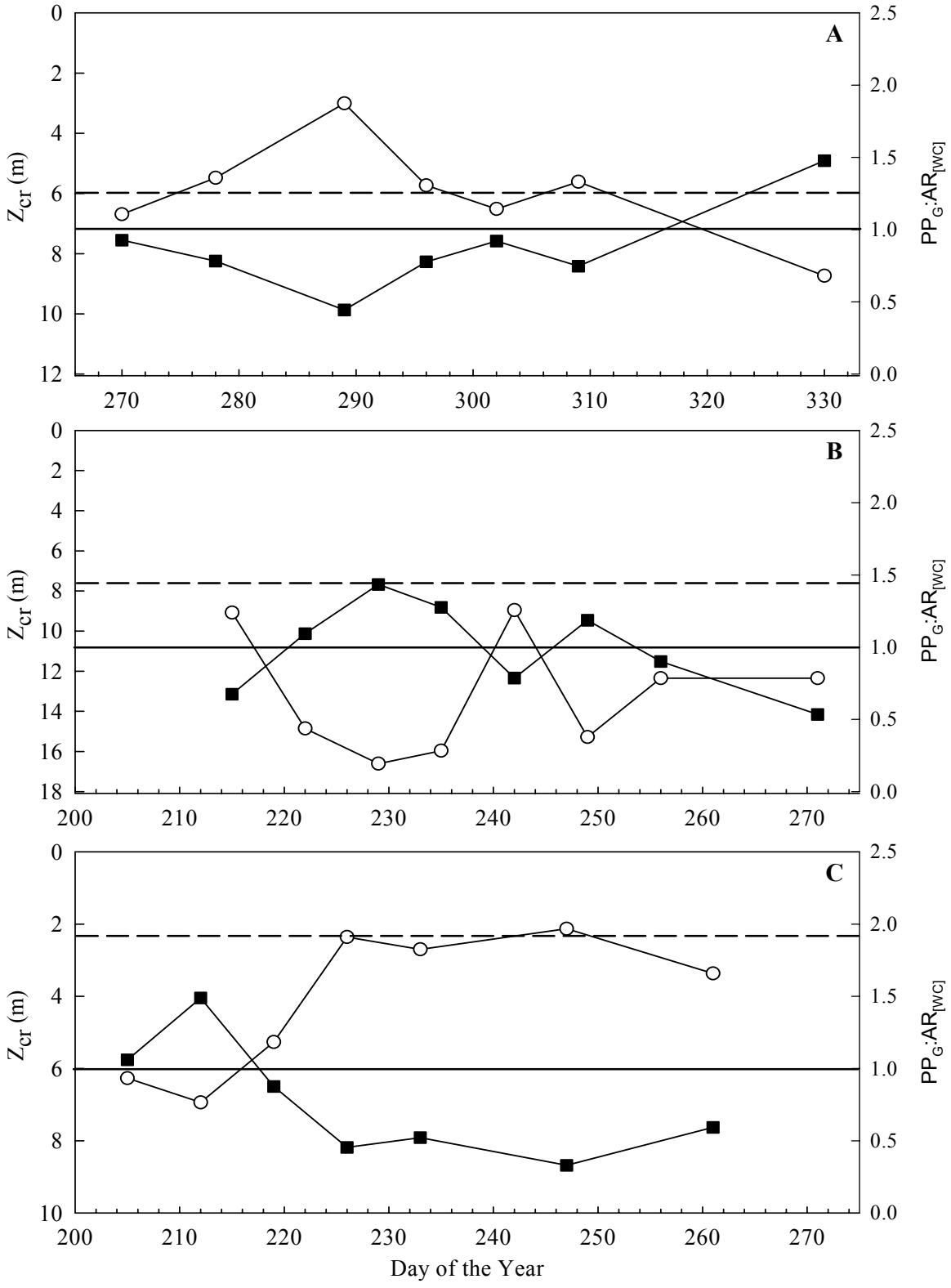

Figure 2.17: Critical depth where PP_N is 0 (open circles) and PP_G:$AR_{[WC]}$ ratio (closed squares) in A) Fielding Bay, B) Napoleon Gulf and C) Inner Murchison Bay. Dashed line represents average depth within a 5 km radius of station, solid line corresponds to PP_G:$AR_{[WC]}$ of 1.0.

Diurnal Patterns

Diurnal lateral advection of water masses in Fielding Bay can be inferred from up and downwelling of isotherms below the surface mixed layer (MacIntyre et al. 2002b). A comparison of concurrent diurnal changes in meteorological and temperature data (Appendix I: Figure 6.2 to 6.15) reveals some general patterns: On days of the year 270, 289, 302 southerly winds reached their daily maximum speed (> 4m.s^{-1}) during the afternoon (13:00-16:00 hrs) consistent with the average diurnal pattern of late afternoon lake winds (Appendix I: Figure 6.1). On each of these days, upwelling of cooler isotherms coincides with these meteorological events. Conversely, on days of the year 276, 309 and 330 a strong afternoon wind event either occurs later on or not all and consequently there is negligible deflection of isotherms over the day at depth. Day 296 does not conform to these two scenarios as deeper isotherms show downwelling over the course of the course of the day. The meteorological record on day 296 is unique in that relatively high wind speeds (3-4 m.s^{-1}) persist throughout the day and reach the daily maxima in mid-morning.

All parameters required to calculate primary production are presented in Figure 2.18 to Figure 2.20. To remove long-term variability shown in the preceding section, each parameter measured at a specific time is normalized to its diurnal average for a given day and are thus presented as unitless. As shown in Figure 2.18A and B, both PI parameters show a general decline from the morning through to late afternoon, a trend that is more pronounced in α_B. The greater magnitude of decrease in α_B relative to P_{BM} means that I_k generally increases over the day. Of the declines in PI parameters, a two-tailed t-test (α=0.05) showed that only the differences between morning and late afternoon population means were statistically significant for both α_B and P_{BM}. A diurnal pattern in R_B was not apparent in this study as shown in Figure 2.18C.

The diurnal patterns of chl_{Zeu} and chl_{WC} are given in Figure 2.18A and B. In general both parameters are highest around midday, vary on a day-by-day basis and show some correlation with Fielding Bay's thermal structure. For example on days of the year 278, 309 and 330 where wind

speeds were low and there was no substantial deflection in isotherms, late afternoon measurements of chl_{Zeu} and chl_{WC} were above the daily average. Conversely on days of the year 270, 289 and 302 with late afternoon wind events and upwelling of isotherms, late afternoon chl_{zeu} and chl_{WC} were equivalent or below their daily average. Figure 2.19C depicts the vertical distribution of chl on each day and time by normalizing chl values sampled near the bottom of the euphotic zone to surface chl samples. On average the vertical distribution was relatively consistent over the day, with average surface chl samples being 14%, 13% and 12% higher than samples at depth in the morning, midday and late afternoon respectively. It is difficult to correlate changes with concurrent changes in the thermal structure, however on days of the year 270, 289 and 302 the observed upwelling decreased the vertical heterogeneity of chl between midday and late afternoon.

k_{PAR} generally increased over the day and therefore euphotic depths become shallower (Figure 2.20A). Differences between morning and late afternoon are statistically significant (two-tailed t-test, α=0.05). Overall, decreases in PI parameters and shallower euphotic depths should serve to decrease PP_G on a diurnal scale, however changes in chl_{zeu} and the vertical distribution of chl may offset this trend. Diurnal changes in PPG and $P:R_{[WC]}$ were investigated by running the primary production model using all diurnal data as well as three model runs using only data from the morning, midday and afternoon respectively. As shown in Figure 2.20B, PP_G does decrease over the day, with differences between calculations based on morning and late afternoon being statistically significant. Based on the magnitude of change relative to diurnally averaged data, potential errors in using only time-specific data approximately range from a 20% overestimation to a 20% underestimation. Using the time-specific averaged population means, morning samples overestimate diurnal production by 5%, midday samples are equivalent to the diurnal average and late afternoon samples are 11% lower. Figure 2.20C shows the $P:R_{[WC]}$ ratio increasing over the day, although changes between morning and late afternoon are not statistically significant.

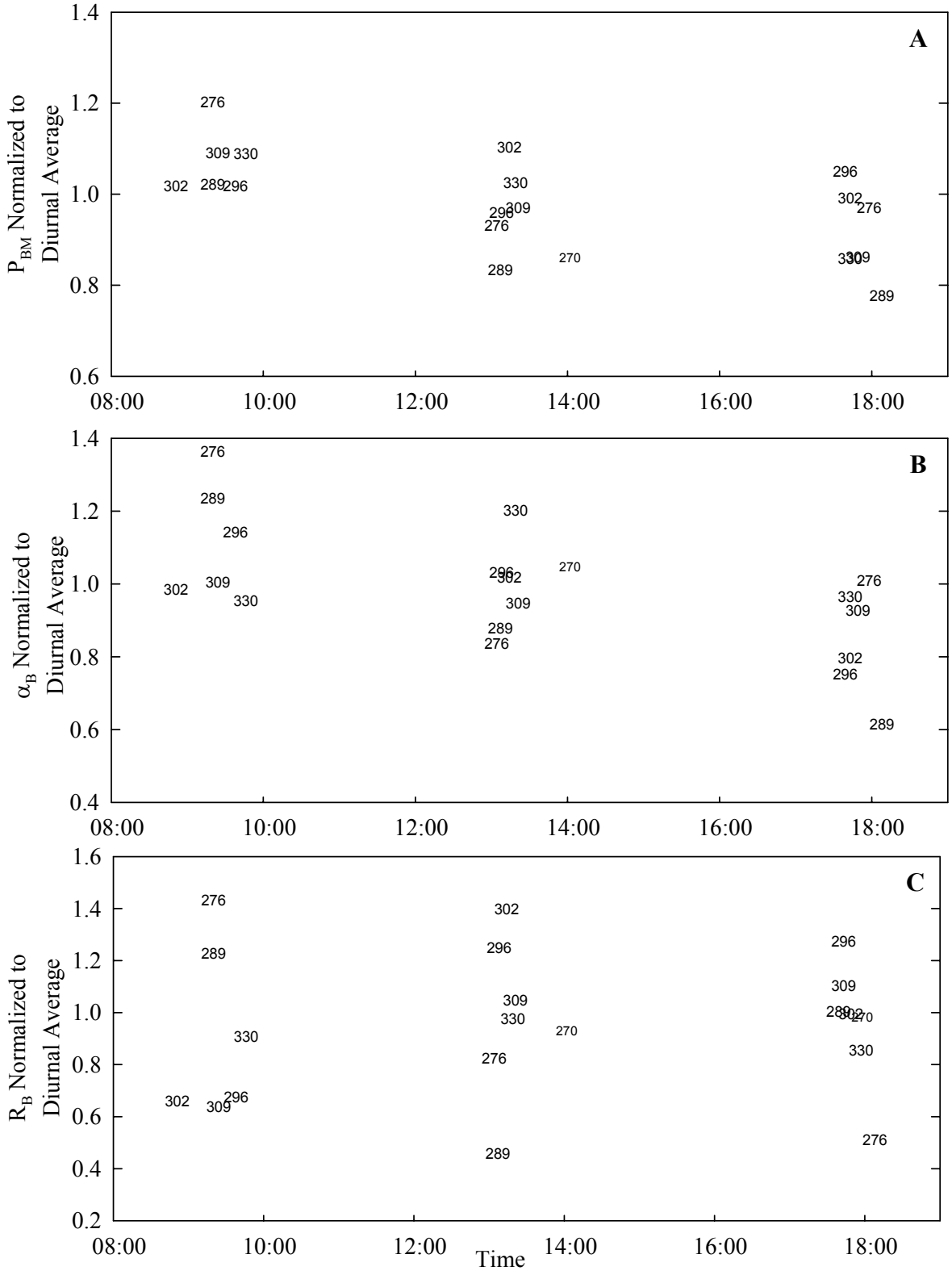

Figure 2.18: Time specific measurements of A) P_{BM}, B) α_B and C) R_B normalized to diurnal averages. Labels represent day of measurement, all data from Fielding Bay.

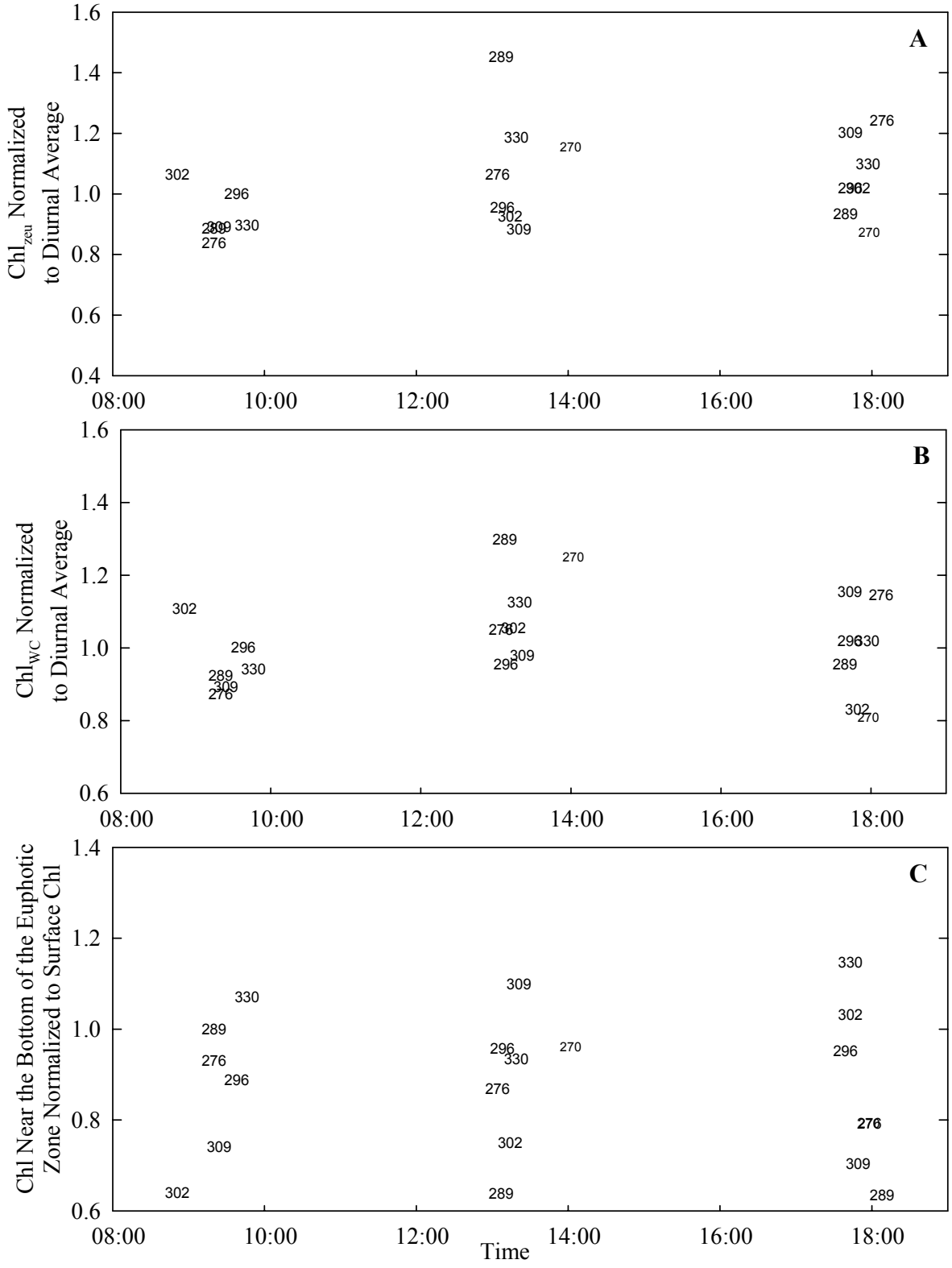

Figure 2.19: Time specific measurements of A) Chl_{Zeu} and B) Chl_{WC} normalized to diurnal averages and C) Chl near the bottom of the euphotic zone normalized to surface chl. Labels represent day of measurement, all data from Fielding Bay.

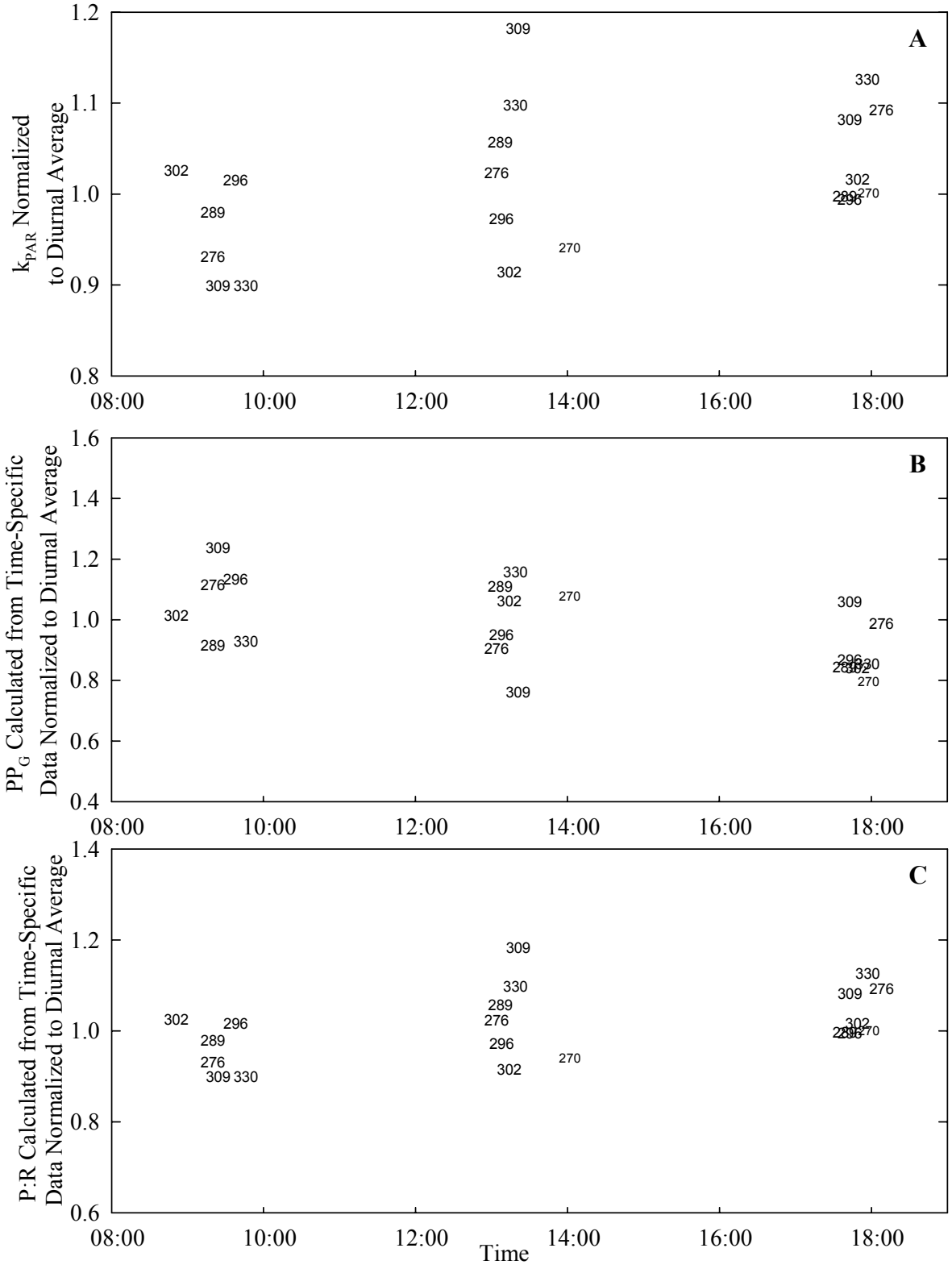

Figure 2.20: Time specific measurements of A) k_{PAR} normalized to diurnal averages. B) PP_G and C) P:R calculated using only time-specific data normalized to calculations using all diurnal data. Labels represent day of measurement, all data from Fielding Bay.

2.4 Discussion

Table 2.6 confirms the hypothesis that deeper inshore areas in Lake Victoria will have less phytoplankton biomass than shallower inshore areas. Inner Murchison Bay is the shallowest bay in this study and has the highest average chl while Napoleon Gulf is the deepest inshore area and has the lowest average chl. As 25% of Lake Victoria's surface area is less than 20 m, this spatial observation is important when extrapolating phytoplankton production measurements over the lake, as average chl concentrations are expected to reflect bottom depths of inshore areas.

Temporal variation of chl, as inferred by the coefficient of variance (c.v.), over the study period of each bay was large and generally exceeded the variance of Mugidde's (1992) dataset showed in Table 2.2. Fielding Bay had the largest c.v. for both chl_{zeu} and chl_{WC} and demonstrated that, similar to seasonal trends in both the inshore and offshore of Lake Victoria, increases and decreases in chl occur contemporaneously with similar changes in water column temperature. The relationship between changes in T_{WC} and % change in chl_{WC} was linearly positive in each bay and best correlated in Fielding Bay ($r^2 = 0.71$, $n = 8$, $p < 0.001$). Furthermore, as was shown in Figure 2.8 and summarized in Table 2.8, T_{WC} in Fielding Bay was not strongly influenced by average daily wind speeds but was highly correlated with strong overnight wind events with statistical return periods of 5 to 22 days. Decreases in water-column temperatures and subsequent decreases in both chl_{Zeu} and chl_{WC} in response to strong nocturnal wind events suggest hydrodynamic mechanisms regulate phytoplankton biomass. Strong overnight wind events blew from the north to the south, consistent with observed nocturnal land winds over Lake Victoria (Flohn and Fraedrich 1966; Asnani 1993). According to hydrodynamic theory, a northerly nocturnal wind stress over Fielding Bay would cause water from Fielding Bay to laterally advect south to deeper areas of the lake (i.e. Buvumu Channel in Figure 2.2) while causing a return flow at depth (Monismith et al. 1990), effectively flushing Fielding Bay. As deeper areas of a lake are generally cooler (Imberger and Parker 1985) and as already shown are expected to have lower chl, hydrological flushing of Fielding Bay would decrease both T_{WC} and

chl. This theory is best exemplified in Fielding Bay between days of the year 270 and 278, where T_{WC} decreased by 1°C and both chl_{Zeu} and chl_{WC} exhibited 4-fold decreases after a 3-hour nocturnal wind event with an average northerly wind speed over 4 $m.s^{-1}$. Moreover, in the absence of strong nocturnal wind events between days of the year 278 and 289, both water column temperature and chl increased by 1°C and 3.5-fold respectively, suggesting a decreased exchange with water from deeper areas.

Assuming lateral advection and exchange of water masses from deeper areas of Lake Victoria is the prominent mechanism causing synchronous decreases in T_{WC} and chl, several insights concerning phytoplankton production can be made: First of all, higher temporal resolution meteorological data can improve temporal interpolation of phytoplankton biomass within a bay. For example, Fee's model would normally linearly interpolate chl on day of the year 274 as the mean of days of the year 270 and 278. However if lateral advection through nocturnal wind events is the prominent cause of observed decreases in chl, phytoplankton biomass on day of the year 274 is probably much closer to that of day of the year 270 owing to the absence of any large wind event in the preceding 4 days. Secondly, this theory implies that connectivity of a bay to offshore areas will affect temporal variability of chl. Areas that are more open to the offshore (i.e. Fielding Bay and Napoleon Gulf in Figure 2.2) favor greater exchange of water than areas that are more constricted such as Pilkington Bay (MacIntyre et al. 2002b) and Inner Murchison Bay. The decreased connectivity of Inner Murchison Bay may explain its lower coefficient of variance of chl shown in Table 2.6 as compared to Fielding Bay.

Hydrodynamic mechanisms also appear to influence chl on a diurnal scale. As shown in Figure 2.19 and in Appendix I (Figure 6.2 to Figure 6.15) on days of the year 270, 289 and 302 strong afternoon lake breezes caused cooler water to enter the Fielding Bay station at depth and occurred contemporaneously with decreases in chl_{Zeu} and chl_{WC}, where the decrease in chl_{Zeu} between midday and late afternoon averaged 22.2 $mg.m^{-3}$ for the three days. The hydrodynamics of this event has

been observed in nearby Pilkington Bay, where comparable afternoon wind speeds also resulted in a upward deflection of deep isotherms at a midbay station (MacIntyre et al. 2002b, Figure 2D and 7 between 14:00 and 16:00 hrs on April 24). Drogue measurements from that same study showed that in response to a wind event, surface currents propagate in the opposite direction to currents at 3 and 6 m, leading to downwelling at the downwind site and upwelling at the upwind site. Based on this scenario, and the fact that chl_{Zeu} is higher than chl below the euphotic depth (Figure 2.19), it can be hypothesized that the decrease in chl between midday and late afternoon during days with strong lake winds is due to lateral advection of chl upwind that is replaced with cooler water from depth that consequently has less chl. In the absence of a strong late-afternoon wind event on days of the year 276, 309 and 330, there were no comparable deflections of isotherms below the euphotic zone and chl_{zeu} increased on average by 4.0 $mg.m^{-3}$ between midday and late afternoon on these three days, presumably due to the production of new chl in the absence of lateral advection.

The vertical distribution of chl within the euphotic zone influences modeled estimates of PP_G. A water column with more chl at the surface than at the bottom of the euphotic depth compared to a situation where chl is uniformly distributed within the euphotic zone will have higher PP_G as more chl is exposed to higher irradiances. The ratio of chl at the bottom of the euphotic zone to chl at the surface is shown in Figure 2.19C and was not correlated to any physical or biological parameters including Z_{mix}, N, wind speed and chl_{Zeu}. Spatial heterogeneity of k_{PAR} in Fielding Bay (Appendix I) suggests similar heterogeneity of chl following the regression equation of Figure 2.6B. Diurnal horizontal currents in inshore areas of Lake Victoria can synchronously propagate in different directions through depth (Ochumba 2002; MacIntyre et al. 2002b). Accordingly, entrainment of different concentrations of phytoplankton through depth complicates any interpretation of the vertical distribution of chl despite anticipated changes in cell buoyancy (Reynolds et al. 1987), and impedes the formulation or application of relevant empirical models (i.e. O'Brien et al. 2003). Surface chl was on average 13% higher than chl at the base of the euphotic zone (Figure 2.19C), opposite to the

general pattern shown in Lake George, where chl was lower in surface waters than the bottom of the euphotic zone (Ganf 1974a). In the absence of any other data, the vertical distribution of chl cannot be accurately predicted in Lake Victoria at this time; however, the average 13% increase from the base of the euphotic zone to the surface is not large enough to significantly alter PP_G estimates.

Of the three bays in this study, only Napoleon Gulf has recent chl measurements to allow a comparison to historic data. The average chl_{zeu} in Napoleon Gulf of 24.3 $mg.m^{-3}$ shown in Table 2.6 is lower than reported by Mugidde (1992, 41.5 $mg.m^{-3}$, n = 18) but within the annual range (22.1 $mg.m^{-3}$ to 67.9 $mg.m^{-3}$) and higher than that reported by Ramlal et al. (2001, 19.1 $mg.m^{-3}$, n =7) measured in August and September 1995. Overall, inshore temporal changes in chl, whether on seasonal, sub-seasonal or diurnal scales are tightly coupled with hydrodynamic properties. Seasonal variations occur through general changes in the thermal structure and mixing depths, sub-seasonal variability can be influenced by the frequency of large scale exchange with deeper areas and diurnal variability can be influenced by periodic lateral advection of water within a bay's immediate vicinity.

The correlation of chl with SD (Figure 2.6B), k_{PAR} (Figure 2.6C), α_B (Figure 2.11A), P_{BM} (Figure 2.11B) and R_B (Figure 2.15A) facilitates spatial and temporal analysis of each parameter according to their derived regression equation with chl and provides the basis for extrapolation of these parameters over a large range of chl data, whether historic, current or acquired through remote sensing. As the derived parameters then satisfy the input requirements of Fee (1990), it is now possible to obtain a rapid estimate of phytoplankton production from chl data alone (Chapter 4). Physiological and physical explanations will now be developed and discussed for each relationship in conjunction with historic research conducted in Lake Victoria.

Figure 2.6B depicts a hyperbolic relationship between k_{PAR} and chl using data from this chapter, the Lake Victoria Ecosystem Project and data from Talling (1965), providing a mathematical representation for the previously reported increases of chl and k_{PAR} through eutrophication (Mugidde 1993). Similar to the reanalyzed dataset of Mugidde (1992), the hyperbolic relationship also

demonstrates a decreasing dependence of k_{PAR} along an increasing gradient of chl. According to Equation 2.4 and as shown in Figure 2.12A, a decrease in k_{chl} along an increasing chl gradient may cause the asymptotic nature of this curve and can occur through a taxonomic shift from diatoms to cyanobacteria (Kirk 1994) or an increase in cellular pigment concentration through the package effect (Dubinsky et al. 1986). Phytoplankton increase cellular content of light-harvesting pigments in response to light-limitation, which in Lake Victoria can occur when high quantities of algal biomass cause self-shading of the population (Mugidde 1993) while temporal patterns of chl in the offshore show that diatoms dominate when chl is low and are increasingly displaced with cyanobacteria as chl increases (Kling et al. 2001). From Figure 2.12A, k_{chl} decreases from 0.043 m^2. mg chl^{-1} at 15 $mg.m^{-3}$ chl to 0.026 m^2. mg chl^{-1} at 70 $mg.m^{-3}$ chl. The latter value is typical for a mixed population of cyanobacteria, although the former is higher than those measured for other phytoplankton (Kirk 1994). Measurements of attenuation and scattering due to non-algal material and dissolved organic carbon (DOC) would be beneficial to validate or improve the regression equation of Figure 2.6C and Figure 2.12A.

In Lake Victoria, SD also exhibits a decreasing non-linear dependence on chl along an increasing gradient of chl as shown in Figure 2.6A, presumably due to the aforementioned affect on k_{PAR} and k_{chl} which are components of SD visibility. Accordingly, k_{PAR} and the inverse secchi depth (SD^{-1}) demonstrate a positive linear relationship (Figure 2.6C). The slope of the relationship ($k_{PAR} = 1.27 \cdot SD^{-1}$) is lower than that found in a variety of lakes ($k_{PAR} = 1.77 \cdot SD^{-1}$; Idso and Gilbert 1974) or turbid oceanic water ($k_{PAR} = 1.44 \cdot SD^{-1}$; Holmes 1970). SD is commonly referred to as a measure of water transparency (Weztel 2001); however more specifically it is the maximum depth at which the light reflected off the disk can be visually resolved. The human eye has the greatest spectral sensitivity centred around 550 nm, therefore the lower slope between k_{PAR} and SD^{-1} in Lake Victoria than other studies is possibly attributed to the dominance of phycobilisome-containing cyanobacteria

whose absorption spectra are markedly higher in the 550 nm range than those of other phytoplankton taxa (Kirk 1994).

As shown in Figure 2.9, Figure 2.10 and Figure 2.18 discernable diurnal and sub-seasonal patterns of PI parameters occur in Lake Victoria relative to the time of day and chl concentrations respectively. A review of several studies examining diel or diurnal periodicity of PI parameters states that P_{BM} is generally highest in the morning or midday (Henley 1993), while diurnal changes in α_B are directly correlated to P_{BM} in some studies (Harding et al. 1987) and independent of P_{BM} in other studies (Henley et al. 1991). The decline of PI parameters in Fielding Bay through the day shown in Figure 2.18 is consistent with these general findings, and with diurnal patterns of photosynthesis in tropical Lake George (Ganf and Horne 1975). Figure 2.18 also shows that α_B experiences a greater decline relative to P_{BM} on a diurnal scale, and this decoupling of PI parameters leads to an increase in I_k over the day. A diurnal increase in I_k demonstrates that phytoplankton are photoacclimating to high irradiances (Senger and Fleischhacker 1978). By decreasing σ_{PSII}, the most common manifestation of photoacclimation (Falkowski and Raven 1997), α_B decreases independently of P_{BM} (Equation 2.1) and may be the prominent mechanism through which photoacclimation occurs Lake Victoria. This diurnal pattern of decreasing PI parameters and the proposed mechanism causing it are consistent with observed circadian rhythms of cell division and growth in cyanobacteria (Mori et al. 1996).

Figure 2.10C demonstrates that variability of PI parameters on sub-seasonal scales is large and mostly I_k-independent as compared to diurnal variability. Further to sub-seasonal covariation in PI parameters, Figure 2.11 shows that PI parameters decline along an increasing chl gradient that can be modeled with a negative exponential curve. These relationships confirm the general findings reported in Table 2.3 as well as the hypothesis that relatively high and low PI parameters will coincide with low and high chl respectively. The validity of the derived relationship between P_{BM} and chl in Lake Victoria is enhanced when combined with the more spatially robust data of Mugidde (1992) and historical data of Talling (1965) and provides an empirical relationship describing the

effect of eutrophication on phytoplankton photosynthetic capacity in Lake Victoria. Covariation of PI parameters is consistent with observed linear covariance shown for both aquatic and terrestrial plants using seasonal datasets (Enriquez et al. 1996; Behrenfeld et al. 2004) as well as other datasets for Lake Victoria (Figure 2.10B). Decreases in PI parameters along an increasing chl gradient has not been explicitly shown in any other tropical lake, as very few of these lakes experience such a wide range in chl. However a reanalysis of P_{BM} and chl data from eutrophic Lake Awassa (Belay and Wood 1984; chl ranges from 20 to 45 $mg.m^{-3}$) shows that a negative growth model with a regression equation $P_{BM} = e^{(-0.04.chl + 3.56)}$ was statistically significant ($r^2 = 0.59$, $n = 18$, $p = 0.0002$) but not statistically similar to the regression equation of this dataset (t-test, $\alpha = 0.05$).

The correlations between P_{BM} and the chl_F:chl (an approximation of PSII:PSI ratio, Figure 2.13C) as well as the correlation of both PI parameters with inferred values of k_{chl} (Figure 2.12A) suggest that the underlying mechanism(s) causing covariance of PI parameters and their decline along an increasing chl gradient are related to pigment allocation between photosystems, pigment content per cell and/or packaging effects. Increasing N-deficiency and a taxonomic shift from diatoms to cyanobacteria are proposed to cause these associated changes. The first hypothesis follows evidence of N being the dominant limiting nutrient in Lake Victoria (Talling 1965; Guildford and Hecky 2000), observed coupling between cellular N-content and light availability in cyanobacteria (Healey 1985), evidence of stoichiometric shifts in the PSII:PSI ratio of N-limited cyanobacteria (Berges et al. 1996), studies showing rapid depletion of phycobilisome pigments in cyanobacteria grown in N-deplete media (Allen and Hutchison 1980) concurrent with a decline in chl-specific gross oxygen evolution (Kana et al. 1992), as well as recognition that phycobilisomes function as both cellular N reservoirs and photosynthetic pigments (Boussiba and Richmond 1980). Changes in k_{chl} directly related to nutrient status in cyanobacteria have not been addressed in the literature. However, Barlow et al. (2002) found k_{chl} (at λ 440 and 490 nm) decreased with ambient nitrate concentrations along two meridional transects in the Atlantic Ocean. Secondly, a taxonomic shift from diatoms to

cyanobacteria along an increasing chl gradient, as has been shown in temporal offshore studies (Mugidde 2001), can also be argued to cause the decrease in PI parameters. Such a taxonomic shift would also cause a decrease in the PSII:PSI ratio (Burges et al. 1996), a decrease in k_{chl} (Kirk 1994) and decreased phytoplankton growth rates (Kilham and Hecky 1988). These two hypotheses are in fact complementary: Studies have shown that as N:P ratios in ecosystems decline (increasing N-deficiency) cyanobacteria increasingly displace diatoms as the dominant taxa (Reynolds 1984), such that both factors are likely responsible for the observed changes. These theories sufficiently justify the use of the regression equations of Figure 2.15 in an empirical model (Chapter 4), although future research relating PI parameters to community composition and phycobilisomes in Lake Victoria can further validate these relationships.

Figure 2.15 demonstrates that R_B increases with P_{BM} and decreases with chl, and taking diurnal averages of R_B and chl increases the regression coefficient. The correlation between R_B and P_{BM} supports observations for the marine cyanobacteria *Trichodesmium* (Carpenter and Roenneberg 1995) and similar measurements in tropical lakes Xolotlan (Erikson 1999) and George (Ganf 1974b) as well as the concept of respiration being comprised of a basal maintenance respiration rate and a respiration rate proportional to a cell's growth rate (Langdon 1988). As Figure 2.11 predicts decreasing photosynthetic rates along an increasing chl gradient, it follows that R_B will also decrease along an increasing chl gradient as depicted in Figure 2.15A. As shown in Table 2.6, average R_B in each bay conforms to this pattern; Napoleon Bay with the least chl and highest P_{BM} had the highest average R_B, while Inner Murchison Bay had the lowest P_{BM}, the highest chl and the lowest R_B.

Talling's (1965) observation that respiration rates are 'generally 1/3 of optimal photosynthetic rates', is approximately three time for a P_{BM} of 25 mg O_2.mg $chl^{-1}.hr^{-1}$ as predicted from the regression equation of Figure 2.15A. This discrepancy may be related to Lake Victoria's change in trophic status, as the values of R_B presented in Table 2.6 fall within the range of other published average measurements of R_B from other tropical eutrophic lakes: R_B (units given in Table 2.1) was 4.4 in an African soda lake (Melack 1982), 1.5 in Lake Xolotlan (Erikson 1999), 1.2 in Lake

George (Ganf 1974b), and 1.0 in Lake Awassa (Taylor and Zinabu 1989). Furthermore, detailed measurements of R_B below the euphotic zone and at night in Lake Xolotan (Erikson 1999) were lower than those measured in the photic zone (1.2 and 1.1 mg O_2.mg Chl^{-1}.hr^{-1} respectively), comparable to nocturnal R_B in Lake George (1.0 mg O_2.mg Chl^{-1}.hr^{-1}; Ganf 1974b) and assumed to represent the maintenance respiration rate. From Figure 2.15B the intercept of the regression equation of 1.34 mg O_2.mg Chl^{-1}.hr^{-1} may represent the basal maintenance respiration rate in the absence of any photosynthesis and is similar to the above reported values. The methodological calculation of AR in this chapter does not account for a basal respiration rate in the absence of photosynthesis and may therefore be an overestimation. Substitution of the inferred basal respiration rate for phytoplankton below the photic zone and at night will significantly decrease estimates of AR and this assumption is addressed in Chapter 4.

R_B was determined using whole water samples, such that it is a measurement of community respiration including bacterial respiration. Bacterial oxygen consumption in Lake Awassa was estimated as 14.9 mg O_2.m^{-3}.hr^{-1} using size fractionated samples (<2 μm; Taylor and Zinabu 1989). As bacterial abundance in Lake Victoria changes along a chl gradient comparable to Lake Awassa (Jackson and Taylor, unpublished data) a similar bacterial oxygen consumption rate would account for approximately 22% of community respiration measured in Lake Victoria as predicted by the regression equation of Figure 2.15B using an average chl of 22 mg.m^{-3} for Lake Awassa (Zinabu and Taylor 1997). Relative to other regression coefficients of relationships presented in this chapter, the r^2 of R_B with chl and P_{BM} shown in Figure 2.15A and B respectively are low. As respiration rates strongly influence estimates of AR and PP_N, the potential errors in predicting R_B from independent measurements of chl or P_{BM} can decrease the validity of AR and PP_N estimates. Some of the unexplained variance of the relationships shown in Figure 2.15 may be due to a variable contribution of bacterial respiration; quantification of R_B in size-fractionated samples across a gradient of chl may elucidate more statistically significant relationships. Furthermore, the increased correlation between R_B and chl when diurnal averages of both parameters are taken (Figure 2.15C) suggests respiration

rates can vary on short time periods such that size-fractionated samples should be taken several times during the day.

As summarized in Table 2.7 and shown in Figure 2.16, PP_G was highest in Napoleon Gulf and lowest in Inner Murchison Bay, an opposite trend from the average chl in each bay. This pattern demonstrates that deeper euphotic depths and higher photosynthetic rates offset low chl to the extent that PP_G actually decreases with increasing chl, as further examined in Chapter 4. However unlike chl, the absolute differences in PP_G between each bay are comparatively small. Temporal variability was relatively high in each bay and the c.v. increased with increasing PP_G in each bay. This finding conforms to aforementioned patterns of k_{PAR}, P_{BM} and α_B along chl gradients: The rate of change of each parameter is higher at lower concentrations of chl, such that areas including Napoleon Gulf with lower chl should experience more variable PP_G. Figure 2.20B demonstrates diurnal variance (c.v. = 11.9%) is generally less than sub-seasonal variance (c.v. = 19.6%) in Fielding Bay. The statistically significant difference for PP_G estimates derived using only data collected in the morning and late afternoon shown in Figure 2.20B demonstrates that this technique provides an overestimation and underestimation respectively for each time period, presumably due to a similar diurnal pattern in the PI parameters (Figure 2.18). Furthermore this analysis shows that in the absence of diurnal data, sample collection at midday will provide the most representative measurements of PP_G.

Table 2.7 shows that, unlike PP_G, average values of $AR_{[Zeu]}$ and $AR_{[WC]}$ adheres to the average chl pattern between bays. As shown in Figure 2.15A, the gradient of decrease of R_B along increasing chl is not as large as the parameters that influence PP_G. The relationship between chl and AR can be expressed mathematically using the regression equation of Figure 2.15A and a simple example: Station A and B are each 10 m deep and have a respective average chl of 20 and 50 $mg.m^{-3}$. Despite station B having a 83% lower R_B than station A, due to the higher chl in station B $AR_{[WC]}$ is 2.1 times greater than in station A. This pattern is exemplified in Table 2.7; despite being twice as shallow, $AR_{[WC]}$ in Inner Murchison Bay is 125% greater than in Napoleon Gulf. Temporal variability of AR also exceeds variability of PP_G and is comparable to variability of chl in each bay.

As depicted in Figure 2.16, PP_G either exceeded or was equivalent to $AR_{[Zeu]}$ in Fielding Bay and Napoleon Gulf, but fell below $AR_{[Zeu]}$ in Inner Murchison Bay on 3 of the 7 sampling days. Despite these 3 days, the average P:R ratio in the euphotic zone was greater than 1 in each bay, indicating that the euphotic zones in each bay are metabolically autotrophic. However, due to the relative consistency of PP_G in each bay and the increase of $AR_{[Zeu]}$ with increasing chl, the $P:R_{[Zeu]}$ ratio declined with increasing chl. $P:R_{[Zeu]}$ was highest in Napoleon Gulf and lowest in Inner Murchison Bay. These findings challenge the concepts that autotrophy increases with a lake's trophic status and that phytoplankton production is more variable than community respiration (del Georgio and Peters 1993), however this discrepancy may be an artifact of higher chl in Lake Victoria as compared to the measured values reported in del Georgio and Peters (1993).

Figure 2.17 and Table 2.7 show that on average when AR is computed for the entire water column all three stations are net heterotrophic. It should be noted however that the degree of metabolic balance in each bay would shift towards autotrophy in each bay if a basal maintenance respiration rate were applied for the night period. Figure 2.17 also shows Z_{cr}, the depth where PP_G is equivalent to AR, as well as the average depth of each bay within a 5 km radius of each station. A radius is used to account for the variable morphology of each bay, as each station was generally located in the deepest part of its respective bay. 5 km was chosen as a modest distance that surface currents can laterally advect in 24 hours, as this corresponds to an average current of 0.06 $m.s^{-1}$, lower than values reported by MacIntyre et al. (2002b) and Ochumba (2000) in Lake Victoria. Through comparing the Z_{cr} to the average depth of each bay, Figure 2.17 shows that in general each bay is net autotrophic and the average Z_{cr} is on average below the average depth of the respective bay. Temporal patterns in Z_{cr} closely follow temporal patterns in $AR_{[WC]}$ (Figure 2.17 versus Figure 2.16) in each bay, as PP_G shows less variability than $AR_{[WC]}$. Through comparing Figure 2.4 and Figure 2.17, when the Z_{cr} is well below or above the average depth of each bay there is usually a synchronous increase and decrease in chl respectively. Furthermore, when Z_{cr} is close to the bays average depth chl appears to reach an approximate steady state.

Overall PP_G is relatively constant in inshore areas of Lake Victoria and lateral advection with deeper areas as well as morphometry influence chl concentrations within each bay in the following manner. In the absence of strong wind events, the exchange of water with deep areas is minimized and water column temperatures and chl synchronously increase. Chl and consequently AR and Z_{cr} will continue to increase up to the point where Z_{cr} approaches the mean depth of the bay. When Z_{cr} is equivalent to the mean depth, AR and PP_G are essentially balanced with each bay, PP_N is zero and chl reaches a steady state. By this rationale the mean depth of a bay sets an approximate upper limit on chl assuming mixing occurs to depth, such that shallower bays can support lower critical depths and higher chl than deeper bays. Strong wind events favor exchange with deep areas causing synchronous decreases in water column temperatures and chl. The decrease in chl decreases AR and lowers Z_{cr} relative to the mean depth of the bay, again allowing chl to increase over time until either a steady state is again reached or an exchange with deeper water occurs. This concept is further shown in Chapter 4.

2.5 Work Cited

Allen, M.M. and F. Hutchson. 1980. Nitrogen limitation and recovery in the cyanobacterium *Aphanacapsa* 6308. Arch. Microbiol. 128: 1-7.

Asnani, G.C. 1993. Tropical Meteorology. Volume 2. Indian Institute of Tropical Meteorology.

Barlow, R.G., J. Aiken, P.M. Holligan, D.G. Cummings, S. Maritorena and S. Hooker. 2002. Phytoplankton pigment and absorption characteristics along meridional transects in the Atlantic Ocean. Deep-Sea Research. 47: 637-660.

Behrenfeld, M.J., O. Prasil, M. Babin and F. Bruyant. 2004. In search of a physiological basis for covariations in light-limited and light-saturated photosynthesis. Journal of Phycology. 40: 4-23.

Belay, A. and R.B. Wood. 1984. Primary productivity of five Ethiopian rift valley lakes. Verh. Internat. Verein. Limnol. 22:1187–1192.

Berges, J.A., D.O. Charlebios, D.C. Mauzerall and P.G. Falkowski. 1996. Differential effects on nitrogen limitation on photosynthetic efficiency of photosystems I and II in microalgae. Plant Physiology: 110: 689-696.

Bootsma, H.A. 1993. Algal dynamics in an African great lake, and their interaction to hydraulic and meteorological conditions. Ph.D. thesis, University of Manitoba. Winnipeg, Canada.

Bootsma, H.A. and R.E. Hecky. 1993. Conservation of the African Great Lakes: A limnological perspective. Conservation Biology. 3: 644-656.

Boussiba, S. and A.E. Richmond. 1980. C-phycocyanin as a storage protein in the blue-green alga *Spirulina platensis*. Arch. Microbiol. 125: 143-147.

Carignan, R., A.M. Blais and C. Vis. 1998. Measurement of primary production and community respiration in oligotrophic lakes using the Winkler method. Canadian Journal of Fisheries and Aquatic Sciences. 55: 1078-1084.

Carlson, J. 2002. Development for an optimized dissolved oxygen sensor for oceanographic profiling. International Ocean Systems. 6: 1-4.

Carpenter, E.J. and T. Roenneberg. 1995. The marine planktonic cyanobacteria *Trichodsmium* spp.: Photosynthetic rate measurements in the SW Atlantic Ocean. Marine Ecology Progress Series: 118: 267-273.

Cullen, J.J., C.M. Yentsch, T.L. Cucci and H.L. MacIntyre. 1988. Autofluorescence and other optical properties as tools in biological oceanography. In: Ocean Optics VIII. Proc. SPIE: 149-156.

De Nobel, W.T., H.C.P. Matthijs, E.V. Elert and L.R. Mur. 1998. Comparison of the light-limited growth of the nitrogen-fixing cyanobacteria Anabaena and Aphanizomenon. New Phytologist. 138: 579-589.

del Giorgio, P.A. and R.H. Peters. 1993. Balance between phytoplankton production and plankton respiration in lakes. Canadian Journal of Fisheries and Aquatic Science. 50: 282-289.

del Giorgio, P.A. and R.H. Peters. 1994. Patterns in planktonic P:R ratios in lakes. Influence of lake trophy and dissolved organic carbon. Limnology and Oceanography. 39: 772-7877.

Dubinsky, A, P.G. Falkowksi and K. Wyman. 1986. Light harvesting and utilization in phytoplankton. Plant Cell Physiology. 27: 1335-1349.

Enriquez, S., C.M. Duarte, K. Sand-Jensen and S.L. Nielsen. 1996. Broad-scale comparison of photosynthetic rates across phototrophic organisms. Oecologia. 108: 197-206.

Erikson, R. 1999. Algal respiration and the regulation of phytoplankton biomass in a polymictic tropical lake (Lake Xolotlan, Nicaragua). Hydrobiologia. 382: 17-25.

Falkowski, P.G. and J. LaRoche. 1991. Acclimation to spectral irradiance in algae. Journal of Phycology. 27: 8-14.

Falkowski, P.G. and J.A. Raven. 1997. Aquatic photosynthesis. Blackwell Science.

Fee, E.J. 1973. A numerical model for determining integral primary production and its application to Lake Michigan. J. Fish. Res. Db. Canada. 30: 1447-1468.

Fee, E.J. 1975. The importance of diurnal variation of photosynthesis vs. light curves to estimates of integral primary production. International Association of Theoretical and Applied Limnology. 19:39-46.

Fee, E.J. 1990. Computer programs for calculating in-situ phytoplankton photosynthesis. Can. Tech. Rep. Fish. Aquat. Sci. No. 1740.

Fischer, H.B., E.J. List, R.C.Y. Koh, J. Imberger and N.H. Brooks. 1979. Mixing in inland and coastal waters. Academic Press.

Flohn, H. and K. Fraedrich. 1966. Tagesperiodische zirkulation und niederschlagsverteilumn am Victoria-See (Ostafrika). Meteorol. Rundschau. 19: 157-165.

Ganf, G.G. 1974a. Diurnal mixing and the vertical distribution of phytoplankton in a shallow equatorial lake (Lake George, Uganda). Journal of Ecology. 62: 611-629.

Ganf, G.G. 1974b. Rates of oxygen uptake by planktonic community of a shallow equatorial lake (Lake George, Uganda). Oecologia15: 17-34.

Ganf, G.G. and A.J. Horne. 1975. Diurnal stratification, photosynthesis and nitrogen-fixation in a shallow, equatorial lake (Lake George, Uganda). Freshwater Biology. 5: 13-39.

Geider, R.J. 1987. Light and temperature dependence of the carbon to chlorophyll-a ratio in microalgae and cyanobacteria: Implications for physiology and growth of phytoplankton. New Phytologist. 106: 1-34.

Geider, R.J., H.L. MacIntyre and T.M. Kana. 1996. A dynamic model of photoadaptation in phytoplankton. Limnology and Oceanography. 41: 1-15.

Gilbert, M., C. Wilhelm and M. Richter. 2000. Bio-optical modeling of oxygen evolution using *in vivo* fluorescence: Comparison of measured and calculated photosynthesis/irradiance (P-I) curves in four representative phytoplankton species. Journal of Plant Physiology. 157: 307-314.

Guildford, S.J. and R.E. Hecky. 2000. Total nitrogen, total phosphorus, and nutrient limitation in lakes and oceans: Is there a common relationship. Limnology and Oceanography. 45: 1213-1223.

Guildford, S.J., R.E. Hecky, W.D. Taylor, R. Mugidde and H.A. Bootsma. 2003. Nutrient enrichment experiments in tropical Great Lakes Malawi/Nyasa and Victoria. Journal of Great Lakes Research. 29 (2): 89-106.

Harding, L.W., T.R. Fisher and M.A. Tyler. 1987. Adaptive responses of photosynthesis in phytoplankton: Specificity to time-scale change in light. Biological Oceanography. 4: 403-437.

Hare, L. and J.C.H. Carter. 1984. Diel and seasonal physico-chemical fluctuations in a small natural West African lake. Freshwater Biology. 14: 597-610.

Healey, F.P. 1985. Interacting effects of light and nutrient limitation on the growth rate of *Syenochocuccus linearis* (Cyanophyceae). Journal of Phycology. 21: 134-146.

Heaney, S.I. 1978. Some observations on the use of the *in vivo* fluorescence technique to determine chlorophyll-a in natural populations and cultures of freshwater phytoplankton. Freshwater Biology. 8: 115-126.

Hecky, R.E. 1993. The eutrophication of Lake Victoria. International Association of Theoretical and Applied Limnology. 25: 39-48.

Hecky, R.E. and E.J. Fee. 1981. Primary production and rates of algal growth in Lake Tanganyika. Limnology and Ocanography. 26: 532-547.

Hecky, R.E., F.W.B. Bugenyi, P. Ochumba, J.F. Talling, R. Mugidde, M. Gophen and L. Kaufman. 1994. The deoxygenation of Lake Victoria. Limnology and Oceanography. 39: 1476-1481.

Hecky, R.E., H.A. Bootsma, R. Mugidde and R.W.B. Bugenyi. 1996. Phosphorus pumps, nitrogen sinks, and silicon drains: Plumbing nutrients in the African Great Lakes. In. Johnson, T.C. and E. Odada [eds]. The limnology, climatology and paleoclimatology of the East African Lakes.

Henley, W.J. 1993. Measurement and interpretation of photosynthetic light-response curves in algae in the context of photoinhibition and diel changes. Journal of Phycology. 29: 729-739.

Henley, W.J., G. Levavasseur, L.A. Franklin, C.B. Osmond and J. Ramus. 1991. Photoacclimation and photoinhibition in *Ulva rotundata* as influenced by nitrogen availability. Plant. 184: 235-243.

Holmes, R.W. 1970. The Secchi disk in turbid coastal zones. Limnology and Oceanography. 15: 688-694.

Idso, S.B. and R.G. Gilbert. 1974. On the universality of the Poole and Atkins Secchi disk-light extinction equation. J. Appl. Ecol. 11: 399-401.

Imberger, 1985. The diurnal mixed layer. Limnology and Oceanography. 30: 737-770.

Imberger, J. and G. Parker. 1985. Mixed layer dynamics in a lake exposed to a spatially variable wind field. Limnology and Oceanography. 30: 473-488.

Ivey, G.N. and J. Imberger. 1991. On the nature of turbulence in a stratified fluid. Part 2: Applications to lakes. Journal of Physical Oceanography. 21: 659-680.

Jassby, A.D., and T. Platt. 1976. Mathematical formulation of the relationship between photosynthesis and light for phytoplankton. Limnology and Oceanography. 21: 540-547.

Kalff. J. 2001. Limnology: Inland water ecosystems. Prentice-Hall Publishers.

Kana, T.M., N.L. Feiwel and L.C. Flynn. 1992. Nitrogen starvation in marine *Syenchococcus* strains: Clonal differences on phycobiliprotein breakdown and energy coupling. Marine Ecology Progress Series. 88: 75-82.

Kawamuru, M., M. Mimuro and Y. Fujita. 1979. Quantitative relationship between two reaction centers in the photosynthetic sustem of blue-green algae. Plant Cell Physiology. 20: 697-705.

Kilham, P., Kilham S.S. and R.E. Hecky. 1986. Hypothesized resource relationships among African planktonic diatoms. Limnology and Oceanography. 31: 1169:1181.

Kilham, P. and R.E. Hecky. 1988. Comparitive ecology of marine and freshwater phytoplankton. Limnology and Oceanography. 33: 776-795.

Kirk, J.T.O. 1994. Light and photosynthesis in aquatic ecosystems. Cambridge University Press.

Kling, H.J., R. Mugidde and R.E. Hecky. 2001. Recent changes in the phytoplankton community of Lake Victoria in response to eutrophication. In: M. Munawar and R.E. Hecky (eds). The Great Lakes of the World (GLOW): Food-web, health and integrity. 47-65.

Krause-Jensen, D. and K. Sand-Jensen. 1998. Light attenuation and photosynthesis of aquatic plant communities. Limnology and Oceanography. 43: 396-407.

Langdon, C. 1988. On the causes of interspecific differences in the growth-irradiance relationship for phyoplantkon. II. A general review. Journal of Plankton Research. 10: 1291-1312.

Lorenzen, C.J. 1966. A method for the continuous measurement of *in-vivo* chlorophyll concentrations. Deep Sea Research. 13: 223-227.

Lorenzen, C.J. 1972. Extinction of light in the ocean by phytoplankton. J. Cons. Int. Explor. Mar. 34: 262-267.

MacIntyre, H., T.K. Kana, T. Anning and R.J. Geider. 2002a. Photoacclimation of photosynthesis irradiance response curves and photosynthetic pigments in microalgae and cyanobacteria. Journal of Phycology. 38: 17-38.

MacIntyre, S. 1998. Turbulent mixing and resource supply to phytoplankton. *In* J. Imberger [ed.], Physical processes in lakes and oceans. Coastal and estuarine studies 54. American Geophysical Union.

MacIntyre, S., Flynn, K.M., R. Jellison and J.R. Romero. 1999. Boundary mixing and nutrient fluxes in Mono Lake, California. Limnology and Oceanography. 47: 656-671.

MacIntyre, S., Romero, J.R. and G.W. Kling. 2002b. Spatial-temporal variability in surface layer deepening and lateral advection in an embayment of Lake Victoria, East Africa. Limnology and Oceanography. 47: 656-671.

Marra, J. 1978. Phytoplankton photosynthetic response to vertical movement in a mixed layer. Marine Biology. 46: 203-208.

Marra, J. 1997. Analysis of diel variability in chlorophyll fluorescence. Journal of Marine Research. 55: 767-784.

McConnell, M.D., R. Koop, S. Vail'ev and D. Bruce. 2002. Regulation of the distribution of chlorophyll and phycobilim-absorbed excitation energy in Cyanobacteria. A structure-based model for the light state transistion. Plant Physiology: 1201-1212.

Maxwell, K. and G.N. Johnson. 2000. Chlorophyll fluorescence – a practical guide. Journal of Experimental Biology. 51: 659-668.

Melack, J.M. 1979. Temporal variability of phytoplankton in tropical lakes. Freshwater Biology. 12: 381-399.

Melack, J.M. 1982. Photosynthetic activity and respiration in an equatorial African soda lake. Oecologia. 44: 1-7.

Millard, E.S., D.D. Myles, O.E. Johannson and K.M. Ralph. 1996. Seasonal phosphorus defiency of Lake Ontario phytoplankton at two index stations: light versus phosphorus limitation of growth. Canadian Journal of Fisheries and Aquatic Sciences. 53: 1112-1124.

Millard, E.S., E.J. Fee, D.D. Myles and J.A. Dahl. 1999. Comparison of phytoplankton photosynthesis methodology in Lakes Erie, the Bay of Quite and the Northwest Ontario Lake Size Series. In: Sate of Lake Eries (Sole) – Past, Present and Future. Eds. Munawar, M., T. Edsall and I.F. Munawar. 441-468.

Miskiewicz, E., A.G. Ivanov and N.P.A. Huner. 2002. Stoichiometry of the photosynthetic apparatus and phycobilisome structure of the Cyanobacterium *Plectonema boryanum* UTEX 485 are regulated by both light and temperature. Plant Physiology. 130: 1414-1425.

Monismith, S.G., J. Imberger and M.L. Morison. 1990. Convective motions in the sidearm of a small reservoir. Limnology and Oceanography. 35: 1676-1702.

Mori, T., B. Binder and C.H. Johnson. 1996. Circadian gating of cell division in cyanobacteria growing with average doubling times of less than 24 hours. Proc. Natl. Acad. Sci. 93: 10183-10188.

Mugidde, R. 1992. Changes in phytoplankton productivity and biomass in Lake Victoria (Uganda). M.Sc. Thesis, University of Manitoba. Winnipeg, Canada.

Mugidde, R. 1993. The increase in phytoplankton primary productivity and biomass in Lake Victoria (Uganda). International Association of Theoretical and Applied Limnology. 25: 846-849.

Mugidde, R. 2001. Nutrient status and phytoplankton nitrogen fixation in Lake Victoria, East Africa. Ph.D. Thesis, University of Waterloo, Waterloo, Canada.

Murakami, A. and Y. Fujita. 1991. Regulation of photosystem stoichiometry in the photosynthetic system of the cyanophyte *Synechocystis* PCC 6714 in response to light-intensity. Plant Cell Physiology. 32: 1233-1237.

Nimer, N.A., M. Warren and M.J. Merritt. 1998. The regulation of photosynthetic rate and activation of extracellular carbonic anhydrase under CO2-limiting conditions in the marine diatom Skeletonema costatum. Plant Cell and Environment - Institutional Subscription. 21: 805-813.

O'Brien, K.R., G.N. Ivey. D.P. Hamilton, A.M. Waite and P.M. Visser. 2003. Simple mixing criteria for the growth of negatively buoyant phytoplankton. Limnology and Oceanography. 48: 1326-1337.

Ochumba, P.B.O. 2002. Measurement of water currents, temperature, dissolved oxygen and winds on the Kenyan Lake Victoria. In The East African Great Lakes.

Owens, T.G. 1991. Energy transformation and fluorescence in photosynthesis. NATO ASI Series: 27: 101-137.

Owens, W.B., and R.C. Millard Jr., 1985: A new algorithm for CTD oxygen calibration. J. Physical Oceanography. 15, 621-631.

Otsuku, S., S. Suda, R. Li, M. Watanabe, H. Oyaizu, M. Hiroki, A. Mahakhant, Y. Lui, S. Matumoto and M.M. Watanabe. 1998. Phycoerythrin-containing *Microcystis* isolated from P.R. China and Thailand. Phycological Research**:** 42: 45-50.

Padan, E., B. Raboy and M. Shilo. 1971. Endogenous dark respiration of the blue green alga *Plectenema boryanum*. J. Bact. 106: 45–50.

Patterson, G., R.E. Hecky and E.J. Fee. 2000. Effect of hydrological cycles on planktonic primary production in Lake Malawi/Niassa. Advances in Ecological Research. 31: 421-430.

Powell, T., M.H. Kirkish, P.J. Neale and P.J. Richerson. 1984. The diurnal cycle of stratification in Lake Titicaca: Eddy diffusion. International Association of Theoretical and Applied Limnology. 22: 1237-1243.

Ramlal, P.S. 2002. Sources, transport and sinks of organic matter in Lake Malawi and Lake Victoria, East Africa. Ph.D. Thesis, University of Waterloo, Waterloo, Canada.

Ramlal, P.S., G.W. Kling, L.M. Ndawula, R.E. Hecky and H.J. Kling. 2001. Diurnal fluctuations in PCO2, DIC, oxygen and nutrients at inshore sites in Lake Victoria, Uganda. In Munawar and R.E. Hecky [eds]. The Great Lakes of the World (GLOW): Food-web, health and integrity. 67-82.

Reynolds, C.S. 1972. Growth, gas vaculation and buoyancy in a natural population of a planktonic blue-green alga. Freshwater Biology. 2: 87-106.

Reynolds, C.S. 1984. The ecology of freshwater phytoplankton. Cambridge University Press.

Reynolds, C.S., R.L. Oliver and A.E. Walsby. 1987. Cyanobacterial dominance: The role of buoyancy regulation in dynamic environments. New Zealand J. Mar. Fresh. Res. 21: 379-390.

Sea-bird Electronics Inc. 2001. Computing temperature and conductivity slope and offset correction coefficients from laboratory calibrations and salinity bottle samples. Application Note # 31.

Sea-bird Electronics Inc. 2002. Conversion of pressure to depth. Application Note # 69.

Seitzinger, S.P. 1988. Denitrification in freshwater and coastal marine ecosystems: Ecological and geochemical significance. 33: 702-724.

Senger, H. and P. Fleischhacker. 1978. Adaptation of the photosynthetic apparatus of *Scenedesmus obliquus* to strong and weak light conditions. Physiol. Plant. 43: 35-42.

Sentzova, O. Y., K. A. Nitikina and M. V. Gusev, 1975. Oxygen exchange of the obligate phototrophic blue-green alga *Anabaena variabilis* in darkness. Microbiologiya 4: 283–288.

Silsbe, G.M. 2003a. A revised phytoplankton production model. http://www.science.uwaterloo.ca/research/uwaeg/web/index.htm.

Silsbe, G.M. 2003b. A new digital map for Lake Victoria. Bulletin of the International Decade for East African Lakes (IDEAL). http://www.d.umn.edu/llo/Ideal/Su03.pdf.

Stainton, M.P., M.J. Capel and F.A. Armstrong. 1977. The chemical analysis of freshwater. Can. Fish. Mar. Serv. Misc. Publ. 25.

Talling, J.F. 1957a. Some observations on the stratification of Lake Victoria. Limnology and Oceanography. 2: 213-221.

Talling, J.F. 1957b. Diurnal changes of stratification and photosynthesis in some tropical African waters. Proc. Roy. Soc. B. 147: 57-83.

Talling, J.F. 1957c. The phytoplankton population as a compound photosynthetic system. New. Phyt. 56: 133-149.

Talling, J.F. 1957c. The phytoplankton population as a compound photosynthetic system. New. Phyt. 56: 133-149.

Talling, J.F. 1965. The photosynthetic activity of phytoplankton in East African lakes. Int. Revue ges. Hydrobiol. 50: 1-32.

Talling, J.F. 1966. The annual cycle of stratification and phytoplankton growth in Lake Victoria (East Africa). Int. Revue ges. Hydrobiol. 51: 545-621.

Talling, J.F. and D. Driver. 1963. Some problems in the estimation of chlorophyll-a in phytoplankton. Proc. Conf. On Primary Productivity Measurement, Marine and Freshwater. US Atomic Energy Comm. TID-7633: 142-146.

Taylor, W.D. and G. Zinabu. 1989. Size-structure and productivity of the plankton community of an Ethiopian Rift Valley Lake. Freshwater Biology. 21: 353-363.

Tilzer, M.M., N. Stambler and C. Lovengreen. 1995. The role of phytoplankton in determining the underwater light climate in Lake Constance. Hydrobiologia. 316: 161-172.

Voros, L., C. Callieri, K.V. Balogh and R. Bertoni. 1998. Freshwater picocyanobacteria along a trophic gradient and light quality range. Hydrobiologia. 369: 117-125.

Wanink, J.H. and J.J. Kashindye. 1998. Short-term variations in pelagic photosynthesis demand well-timed sampling to monitor long-term limnological changes in Lake Victoria. Hydrobiologia. 377: 177-181.

Wetzel, R.G. 2001. Limnology: Lake and river ecosystems. Academic Press.

Yin, X., S.E. Nicholson and M.B. Ba. 2000. On the diurnal cycle of cloudiness over Lake Victoria and its influence on evaporation from the lake. Hydrological Sciences. 45: 407-424.

Zinabu, G.M. and W.D. Taylor. 1997. Bacteria-chlorophyll relationships in Ethiopian lakes of varying salinity: are soda lakes different? Journal of Plankton Research. 19: 647-654.

Chapter 3: Spatial and Seasonal Patterns of Temperature, Dissolved Oxygen, Chlorophyll Fluorescence, Water Transparency and Meteorology in Lake Victoria, East Africa

3.1 Introduction

This chapter presents geospatial analyses of limnological data collected during four lakewide surveys conducted in February and August of 2000 and 2001 on Lake Victoria. As shown in Figure 3.1, approximately 50 profiles of temperature, dissolved oxygen and chlorophyll fluorescence as well as secchi depth measurements were taken at similar locations in each survey. Figure 3.1 also shows that the majority of published research on Lake Victoria examining the limnological parameters presented in this chapter have focused on their seasonal or diurnal variability at locations geographically biased by their close proximity to research institutes, whereas only two studies have performed lakewide synoptic transects. Consequently, temporal patterns of phytoplankton biomass and production (Talling 1965; Mugidde 1992), dissolved oxygen concentrations (Hecky et al. 1994; Ramlal 2002), cyanobacterial N-fixation (Mugidde 2001; Mugidde et al. 2003) and nutrient stoichiometry (Hecky 1993; Hecky and Bootsma 1993; Hecky et al. 1996; Guildford and Hecky 2000) have been spatially restricted and have also shown to be influenced by physical dynamics of Lake Victoria's thermal structure. Owing to the paucity of spatial data, extrapolation of phytoplankton production (Melack 1976) and nitrogen-fixation (Mugidde 2001; Mugidde et al. 2003) within Lake Victoria's offshore has assumed that each process is spatially homogeneous. However, synoptic temperature profiles (Kitaka 1972; Romero et al. 2001), spatial patterns of convection, rainfall, cloud-cover and evaporation (Ba and Nicholson 1998; Yin et al. 2000; Nicholson and Yin 2002) and non-dimensional hydrodynamic indices (Spigel and Coulter 1996) all suggest that physical processes in Lake Victoria are spatially heterogeneous. Thus, quantifying spatial patterns of Lake Victoria's thermal structure can greatly improve the accuracy of lakewide extrapolations of limnological processes, provided that the link between the two is well defined. The purpose of this is as follows: Spatial patterns of the

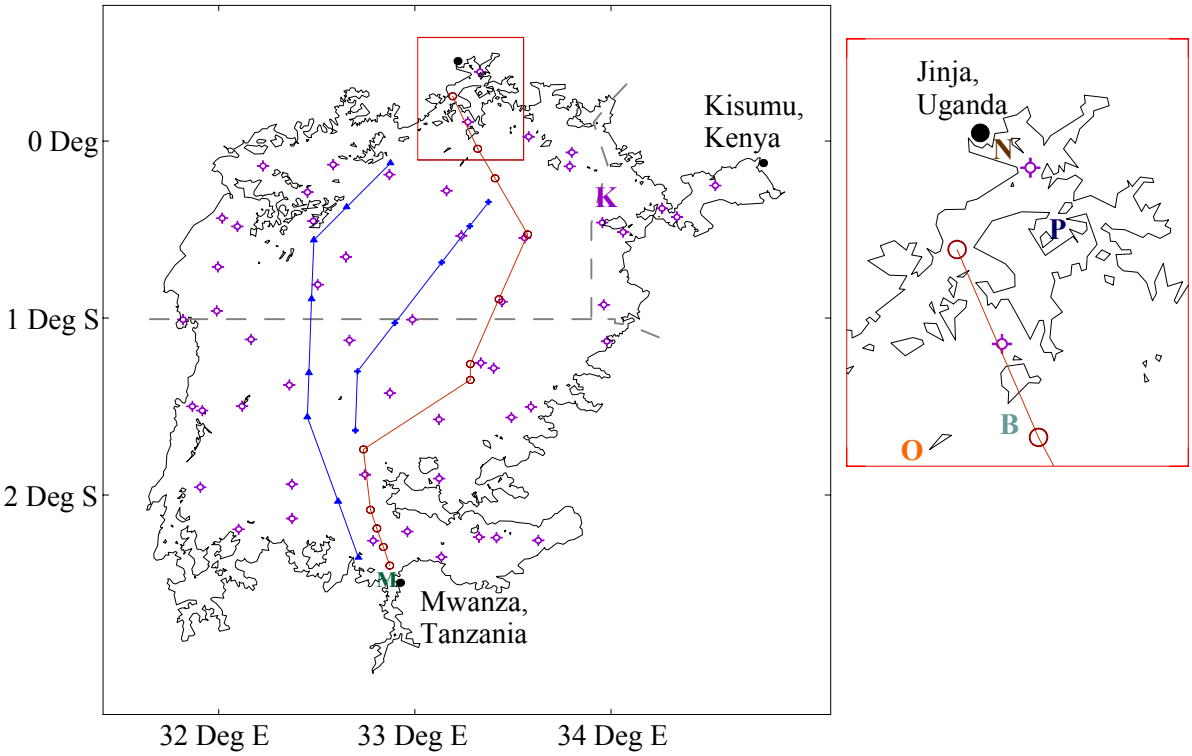

Synoptic Surveys

- This Chapter
- Romero et al. 2001
- Kitaka 1976 Transect 1
- Kitaka 1976 Transect 2

Temporal Surveys

B	Mugidde 1992, 1993, 2001 Hecky 1993; Hecky et al. 1994 Ramlal 2002
M	Wanick and Kahindye 1998
N	Mugidde 1992, 1993, 2001 Ramlal et al. 2001
O	Talling 1966
P	Mugidde 1992 Ramlal et al. 2001 MacIntyre et al. 2002
K	Hecky et al. 1994

Figure 3.1: Locations of published limnological research involving synoptic or temporal measurements through depth, including data presented in this chapter and cities with fisheries research institutes.

thermal structure from each cruise are reported and compared to historic data. Meteorological data over Lake Victoria from the National Centers for Environmental Prediction-Department of Energy Reanalysis 2 (NCEP-DOE R2) created from a complex system of programs and global datasets (Kanamistu et al. 2002), are compared to published records and further used to elucidate possible physical processes in Lake Victoria. Secchi depth measurements are used to estimate lakewide chlorophyll concentrations and light attenuation based on the equations presented in Figure 2.6, which provide critical data for lakewide phytoplankton production estimates derived in Chapter 4. Surface mixing depths are estimated from the thermal structure, dissolved oxygen concentrations and chlorophyll fluorescence profile, which are then used with light attenuation values to estimate I_{24}, the mean daily underwater irradiance exposure of the phytoplankton community.

In temperate zones, seasonal changes of the thermal structure of lakes are mainly driven by large seasonal fluctuations in solar radiation and air temperature, but in the tropics daily averages of these two parameters are comparatively stable throughout the year (solar radiation c.v. = 9.3%; air temperature c.v. = 2.3%, Nicholson and Yin 2002) and have comparatively small influence on Lake Victoria's physical limnology (Spigel and Coulter 1996). Instead, seasonality in the African Great Lakes is dominated by the annual cycle of southerly and northerly monsoon winds in the Indian Ocean and its interplay with movements of the inter-tropical convergence zone (ITCZ) (Mistry and Conway 2003). The Lake Victoria basin has a bimodal rainfall pattern; rains in March to May and November to December (as shown in Figure 3.3) coincide with the passage of ITCZ over the lake, while the months of June through August are generally drier and cooler when the ITCZ is at its maximum northerly extreme away from the lake (Asnani 1993).

The earliest comprehensive temporal study of Lake Victoria's thermal structure is Talling's (1966, Appendix II Figure 7.2) annual study of temperature profiles at the station shown in Figure 3.1, where he elucidated three phases of stratification. During September to December, Talling's first phase, the water-column exhibits rising temperatures due to successive deepening of diurnal thermoclines. By January, a prominent deep metalimnion forms and ascends in the water-column

through to May, delineating Talling's second phase. The remaining phase from mid-June to August is characterized by near isothermal conditions. These phases of thermal stratification have since been verified at a nearby station (Ramlal 2002), although isothermal conditions have occurred as early as April (Hecky 1993) and a second overturn has observed in January (Fish 1957), evidence of either inter-annual variability of Lake Victoria's thermal structure or internal seiches that can temporarily deepen the isothermal surface mixed layer at the margins of the lake (Newell 1960).

Sedimentation of organic matter through Lake Victoria's seasonal metalimnion depletes hypolimnetic oxygen and creates an oxic-anoxic interface in the water-column (Hecky et al. 1994). At the offshore stations 'O' and 'B' shown in Figure 3.1 the oxic-anoxic interface occurred contemporaneously with the seasonal metalimnion within the months of September to April (Hecky et al. 1994, Ramlal 2002). Anoxia can also occur sporadically in inshore areas when mixing is insufficient circulate the entire water-column (Mugidde 2001; Ramlal et al. 2001). The oxic-anoxic interface in Lake Victoria affects the nutrient regimes of phytoplankton through disparate modification of nitrogen (N) and phosphorus (P) pools (Hecky et al. 1996). Anoxic water acts as a N sink; at oxic-anoxic interfaces ammonification, nitrification and concurrent denitrification processes transform bioavailable N into $N_{2(g)}$ (Seitzinger, 1988), which is eventually lost to the atmosphere. Conversely P may be enriched in anoxic waters if PO_4 is released from iron oxide complexes. When Lake Victoria is stratified, N:P ratios in the epilimnion are low, N-turnover times are rapid, daily N-demand is high and the phytoplankton community is dominated by N-fixing cyanobacteria (Mugidde 2001; Mugidde et al. 2003). N-fixation is stimulated by N-limitation and requires light to generate the enzyme nitrogenase, consequently N-fixation rates in the offshore are highest when the lake is stratified and light availability is high and lowest when the lake is isothermal and light availability is low (Mugidde et al. 2003).

Despite N-deficiency in the offshore, N-fixation rates and phytoplankton biomass are 5-fold lower in the offshore than the inshore of Lake Victoria (Mugidde 2001; Mugidde et al. 2003). Offshore surface mixing depths are generally much deeper than euphotic depths, such that light-

limitation is thought to be the prominent mechanism in establishing upper limits on offshore phytoplankton production, N-fixation and algal biomass (Mugidde 1993; Kling et al. 2001; Mugidde et al. 2003). The non-dimensional I_{24}/I_k ratio (Hecky and Guildford 1984) shown in Eqn. 3.1 was developed to estimate the degree of light-limitation; I_{24} is the daily averaged irradiance in the mixed layer, where I_0 is the mean 24-hour surface insolation, k_{PAR} is the vertical extinction coefficient of PAR and z_M is the depth of the surface mixed layer. I_k is the irradiance where photosynthesis becomes light saturated for a given phytoplankton assemblage (Figure 2.1). Values of $I_{24}/I_k << 1$ are indicative of light-limited production as they correspond to a phytoplankton assemblage that has been exposed to a daily averaged irradiance below photosynthetically saturating levels; Mugidde (1992) found average offshore and inshore I_{24}/I_k values of 0.17 (n = 4) and 0.23 (n = 17) respectively, evidence of light-limitation in Lake Victoria.

Equation 3.1) $$I_{24}/I_k = I_o\,(1 - e^{-k_{PAR}\,z_m})\,(k_{PAR}\,z_m)^{-1}\,I_K^{-1}$$

Table 3.1: Sensitivity Analysis of I_{24}/I_k Variables in Lake Victoria
([1] Mugidde 1992; [2] Nicholson and Yin 2002)

Parameters	Mean (n)	Coefficient of Variance (%)	I_{24}/I_k Low	I_{24}/I_k High
I_k ($\mu mol.m^{-2}.s^{-1}$)[1]	179.6 (4)	14.4	0.12	0.16
I_0 ($\mu mol.m^{-2}.s^{-1}$)[2]	436.5 (12)	9.3	0.12	0.15
k_{PAR} (m^{-1})[1]	0.48 (4)	39.9	0.10	0.22
z_M (m)[1]	38.1 (12)	34.6	0.10	0.21

Table 3.1 presents a sensitivity analysis of the parameters that make up the I_{24}/I_k ratio to demonstrate the influence each parameter has on the ratio over its respective reported range in Lake Victoria. For each parameter, mean and standard deviations were determined from literature values allowing for the coefficients of variance to be calculated. I_{24}/I_k high and low were calculated for each parameter by inputting the mean plus or minus the standard deviation respectively, along with mean values of the other parameters into Equation 3.1. I_k, k_{PAR} and z_m are taken directly from Mugidde

1992, I_o is 45% of shortwave radiation (Kirk 1994) as calculated by the formula of Dingman (2002) with the monthly mean daytime fractional cloud cover given by Nicholson and Yin (2002).

Mugidde (1992) found I_k to have a small variance in the offshore of Lake Victoria as presented in Table 3.1, consistent with photochemical theories and other datasets that show limited variation in I_k (Behrenfeld et al. 2004). Accordingly, Table 3.1 shows that variations in I_k have little influence on the I_{24}/I_k ratio. I_0 also shows small variability and has little influence on the I_{24}/I_k ratio. As the equator bisects Lake Victoria the monthly variation of radiation outside the atmosphere is minor (coefficient of variance = 4.6%; Yin et al. 2000) such that half of the variability shown in Table 3.1 is due to monthly variability in cloud cover. k_{PAR} has a much greater variability and is correlated to the amount of phytoplankton biomass in the euphotic zone (Figure 2.6B). As phytoplankton biomass itself is a function of prior phytoplankton production, k_{PAR} is a lag variable more dependent on past I_{24}/I_k ratios. The remaining parameter, z_M, shows the largest variation and influence on the I_{24}/I_k ratio aside from the lag variable k. Deep offshore mixing depths decreases mean light exposure of phytoplankton while areal respiration of the mixed layer phytoplankton population increases through a greater depth of integration. When algal respiration exceeds gross production through deep mixing, phytoplankton biomass decreases, whereas when mixing is shallow the light climate of phytoplankton is improved such that gross production may exceed respiration and other loss processes such that phytoplankton biomass may increase.

The influence of Lake Victoria's thermal structure on phytoplankton production and biomass through light-limitation is further demonstrated by empirical datasets. Figure 3.2 shows monthly offshore chlorophyll measurements (Mugidde 1993) compared to measurements of thermal stability (Hecky 1993) acquired in the same year at a nearby offshore station. Large values of thermal stability correspond with shallow surface mixed layers (Hecky 1993) that in turn increase the I_{24}/I_k ratio. Low thermal stability corresponds with isothermal conditions, deep surface mixing and severe light limitation. An increase in chlorophyll results from positive net phytoplankton production (eg. gross phytoplankton production exceeds respiration and other loss processes) whereas a decrease in

chlorophyll is indicative of negative net phytoplankton production (eg. respiration and other loss processes exceeds gross phytoplankton production). Between August and December, both thermal stability and chlorophyll generally increase and reach their respective annual maxima. From January to April, although there is some month-to-month decoupling of thermal stability and chlorophyll, both parameters generally show a decline. Between April and July thermal stability is low and shows its greatest departure from chlorophyll in May and June, probably due to the breakdown of the oxic-anoxic interface and subsequent release of nutrients into the epilimnion (Mugidde 1992). However by July chlorophyll reaches its annual minimum concurrent with low thermal stability, presumably again due to light-limitation of phytoplankton production. The relationship between chlorophyll and thermal stability is not strong but significant ($r^2 = 0.36$, $n = 12$, $p = 0.029$) and increases if the two 'nutrient pulse' months of May and June are ignored ($r^2 = 0.54$, $n = 10$, $p < 0.01$).

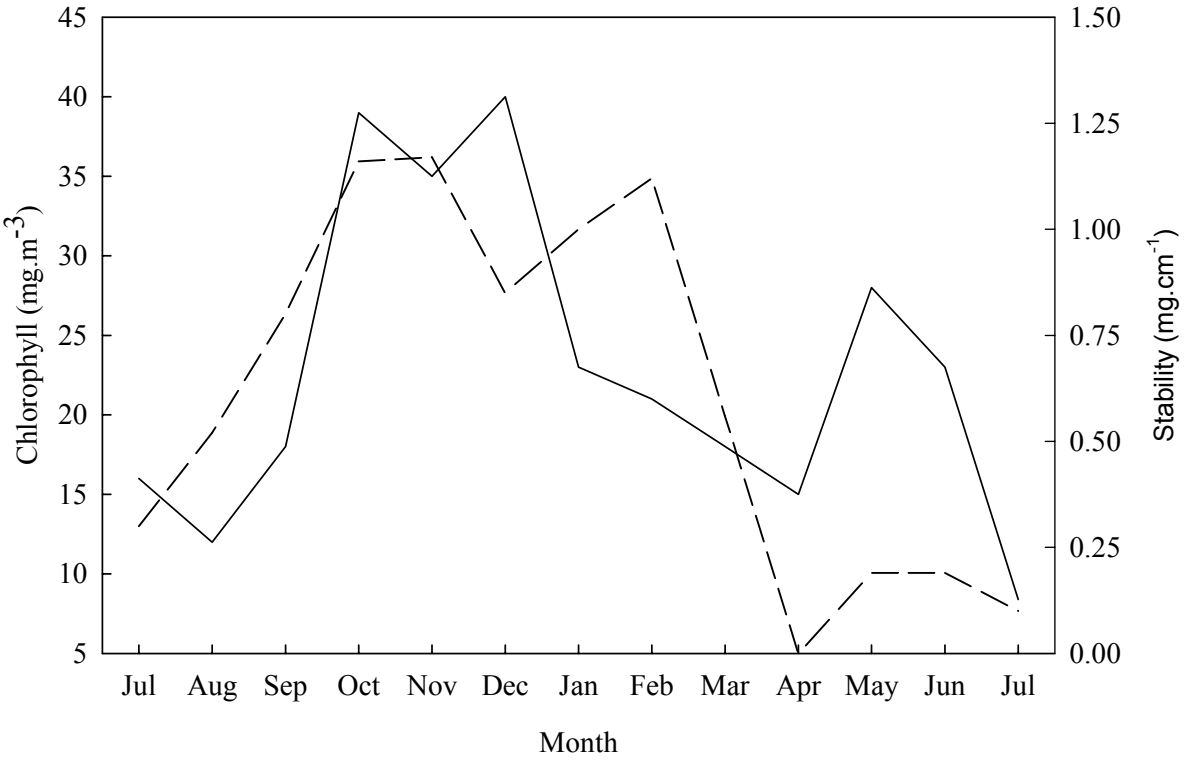

Figure 3.2: Monthly offshore variability of water-column stability (dashed line) and chlorophyll concentrations in the euphotic zone (solid line) in 1990-1991 (Mugidde 1992; Hecky 1993).

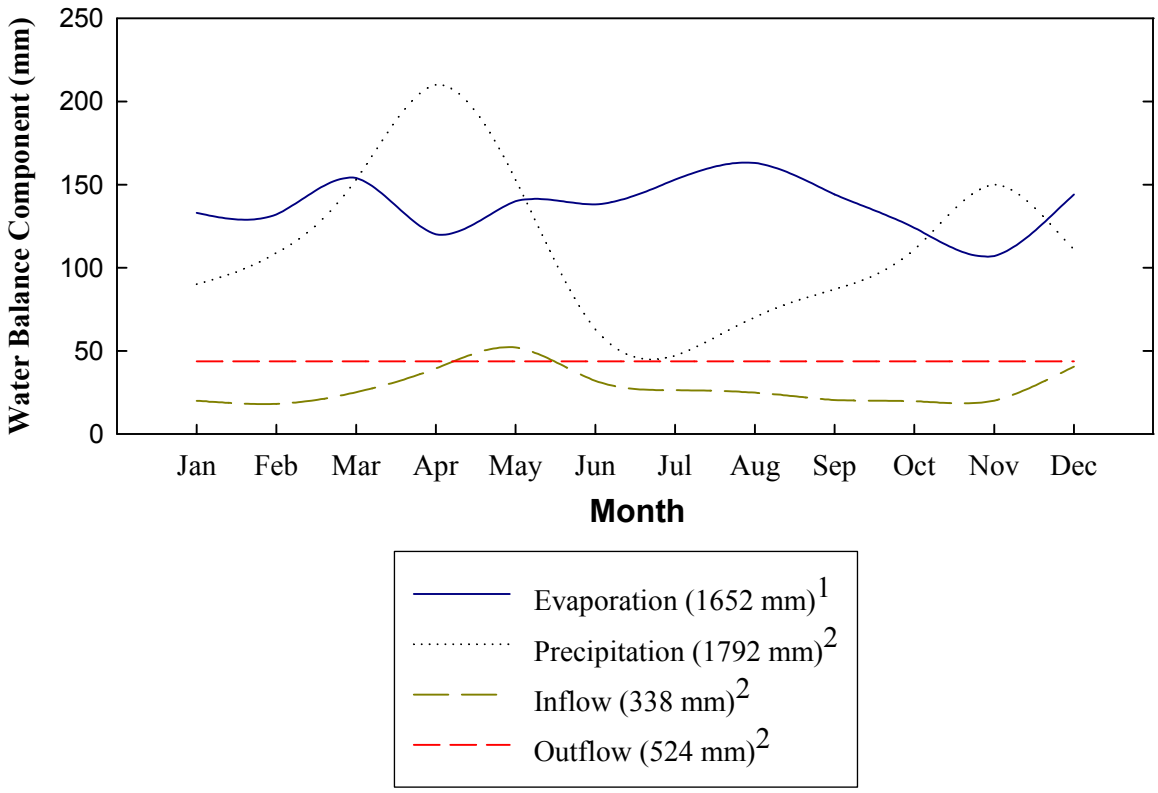

Figure 3.3: Monthly Components of Lake Victoria's Water Balance ([1]Nicholson and Yin 2002; [2]Yin and Nicholson 1998)

Several attempts to create a historical water balance to account for observed water level changes in Lake Victoria have been made in the last 40 years (Newell 1960; Kite 1981; Sene and Plinston 1994). The most recent and accurate attempts (Yin and Nicholson 1998, Yin et al. 2000; Nicholson and Yin 2002) employ spatially averaged land-based meteorological data as well as remote sensing techniques, as significant discrepancies were discovered between the frequency and timing of cloud formation over lake Victoria with the surrounding catchment. From Figure 3.3 it is apparent that precipitation and evaporation are the principle components of Lake Victoria's water balance, with riverine inflows (19 major rivers) and outflow (Nile River) having a secondary importance. This water balance is consistent with both Talling's (1966) observations and MacIntyre et al.'s (2002) surface energy budget showing that evaporation is the dominant cooling process in Lake Victoria, but cannot be further validated as continuous meteorological measurements have never been made in the open lake. This lack of data is exacerbated by substantial discrepancies between land-based wind

speed data used to calculate evaporation in Figure 3.3 with opportunistic ship-based measurements (Ochumba 1996), both in magnitude and seasonal patterns.

Annual wind speed averages from Ochumba (1996) are 2.0 $m.s^{-1}$, 3.0 $m.s^{-1}$ and 4.6 $m.s^{-1}$ for a land-based station, ship-based measurements within Nyanza Gulf and in the open lake respectively, indicating that wind speed increases with fetch length as also reported in Lake Malawi (Hamblin et al. 2003A). The land-based average wind speed is close to the annual average used by Nicholson and Yin (1998, 1.95 $m.s^{-1}$), underscoring the potential errors of employing land-based meteorological data to model open-lake processes such as evaporation. Yin and Nicholson (1998) also show wind speeds are highest in July and August and lowest in December, whereas at two open-lake stations wind speeds were highest in March and May and lowest in June and August (Ochumba 1996). This last discrepancy may be an artifact of the geographical locations of meteorological stations: Wind speed data from Yin and Nicholson (1998) are derived from stations at the north and south of the lake, whereas the data from Ochumba (1996) were collected in the east of the lake.

Further discrepancies in the literature are found concerning the direction of trade winds during the dry and rainy seasons (Hills 1979; Asnani 1993; Spigel and Coulter 1996; Nicholson and Yin 2002), perhaps arising from fact that the direction of winds change with altitude (Hills 1979) and have a tendency to shift over Lake Victoria (Nicholson and Yin 2002). Overall the findings of Hills (1979) agree with the descriptions given by Asnani (1993) as follows: The general large-scale flow over the lake is easterly, but has a southerly component when the ITCZ is north of the lake and a northerly component when the ITCZ is to the south of the lake.

Spatially differential meteorological processes across a lake cause differential heating and cooling that induce spatial heterogeneity in a lake's thermal structure and subsequent lateral advection of cool or warm water (Imberger and Parker 1985). In Lake Tanganyika, advection has strong temporal variability and is a prominent term in the lake's energy balance when latitudinal evaporation gradients create horizontal temperature gradients (Verburg and Hecky 2003; Verburg 2004). The theory of lateral advection through differential heating and cooling is supported by pronounced

diurnal spatial patterns in solar radiation (Nicholson and Yin 2002, Appendix II Figure 7.4), convection (Ba and Nicholson 1998), cloud cover (Yin et al. 2000, Appendix II Figure 7.5) and observed isotherm tilting in historic datasets (Kitaka 1976; Romero et al. 2001). Spatial disparities in meteorological processes around Lake Victoria is visually apparent by simply traveling around the lake: In the southeast of Lake Victoria the vegetation is predominantly dry shrub land which receives only 900 mm of rainfall a year; whereas 200 km to the northeast are the Sesse Islands dominated by tropical rainforests that receive over 2200 mm of precipitation a year (Asnani 1993).

The interaction between prevailing trade winds and diel thermal winds create distinct diel meteorological patterns over Lake Victoria depicted in Figure 3.4 (Flohn and Fraedrich 1966). Thermal winds have been well documented in Lake Tanganyika (Savijarvi 1997; Verburg and Hecky 2003), where they were found to contribute to approximately one third of total wind energy, however no such study has been conducted on Lake Victoria on an annual time scale (Asnani 1993). Thermal winds consist of diurnal lake winds and nocturnal land winds generated through differences in air temperature over a lake and its surrounding catchment: During the day, air temperatures over land are higher than over a lake due to the lower albedo of water (Dingman 2002). The increased buoyancy of land air forces it upwards and is replaced by lake winds that travel to the shoreline to replace buoyant land air with cooler lake air (Rotunnu 1983). At night the exact opposite wind pattern occurs, as air becomes warmer over the lake through relatively large sensible and evaporative heat fluxes. Although this process occurs over all water bodies, it is particularly prevalent over Lake Victoria whose equatorial location favors high year round solar insolation (Asnani 1993). As maximum land wind speeds occur tens of kilometers offshore (Nuemann and Mahrer 1974), it is likely that thermal winds over the large and near rectangular surface area of Lake Victoria have a greater contribution to total wind energy than Lake Tanganyika, whose narrow and long shape would favor convergence of land breeze fronts before they reach their maximum potential speed (Asnani 1993). Yin et al. (2000) illustrate distinct spatial patterns of cloud formation over Lake Victoria prominent in the months encompassing October through May caused by thermal and trade winds

(Appendix II Figure 7.5). In the east and south, both over the lake and along the adjacent shoreline, maximum cloud formation occurs in the late afternoon, whereas over the western side of the lake maximum cloud formation occurs in the early morning and slightly later along the adjacent shoreline. Divergent lake winds during the day travel away from the lake, and in the south and east they would converge with the trade winds in the late afternoon causing uplift and subsequent cloud formation. At night lake winds shift and become land winds, the clouds that were formed in the south and east are then pushed northwest by both the land and trade winds and by early morning they converge with strong westerly land winds (Flohn and Fraedrich 1968) to develop strong nocturnal cumulonimbus clusters and often intense low pressure systems that enhance over-lake rainfall (Yin and Nicholson 1998).

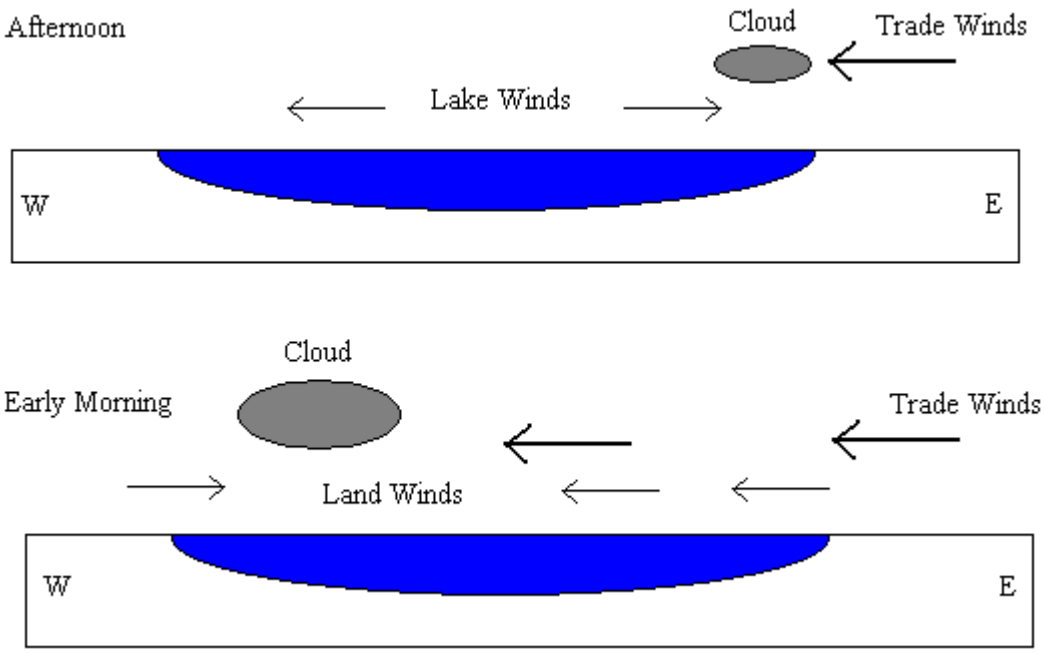

Figure 3.4: Diagram showing diel cycle of thermal winds and cloud formation along a west-east gradient over Lake Victoria.

As a direct result of the diel pattern of convection and cloud-cover eastern Lake Victoria receives greater surface insolation (Nicholson and Yin 2002, Appendix II Figure 7.4), western Lake Victoria has increased evaporation (Yin et al. 2000) and wind speeds are higher over the south than the north of the lake (Asnani 1993). The effects of differential heating and cooling on Lake

Victoria's thermal structure are apparent in synoptic transects: Kitaka (1972) provides the first synoptic spatial study of temperature in Lake Victoria by taking several vertical profiles along two predominantly north-south transects in the pelagic zone of Lake Victoria in February 1969 (Appendix II Figure 7.6). In the eastern transect metalimnetic isotherms (23.4-23.6°C) are found at a consistent depth throughout; however all isotherms above and below this temperature exhibit downward tilting towards the north. As a result of isothermal tilting, the temperature gradient is stronger in the north (25.0 to 23.0°C) than the south (24.0 to 23.0°C). Kitaka equates isotherm tilting and the subsequent gradient of stratification due to observed southeasterly winds that cause accumulation of warm water upwind with subsequent upwelling upwind. Similar wind-driven seiching has also been observed in Lakes Malawi (Hamblin et al. 2003B) and Tanganyika (Verburg 2004) and along with a latitudinal gradient of evaporation is hypothesized as Lake Victoria's dominant hydrodynamic feature (Spigel and Coulter 1996). Romero et al. (2001) also conducted two north-south transects in the pelagic zone of Lake Victoria in May 1995 and April 1996 and also found spatial heterogeneity of Lake Victoria's thermal structure (Appendix II Figure 7.7). A general downward tilting of isotherms towards the north occurred in both transects, similar to Kitaka (1972) but with the prominent metalimnetic depth rising to 40 m in the south and intersecting with the bottom of the lake in the north. The tilting of isotherms is more severe in May than April, but in both transects virtually all the warm water is confined to the north and subsequent cool water to the south of the lake. As a result the highest degree of stratification and apparent stability in Romero et al.'s (2001) transects occurs at the midpoint of each transect, where the overlap of cool and warm water is greatest.

Kitaka's second transect reveals a completely different feature: An overnight storm with a cyclonic low pressure disturbance displaced warm water away the station causing remarkable upwelling of cooler water below the centre of the storm and severe isotherm tilting to the north and south. This phenomenon, both in timing and location, is consistent with convergence of land winds that can induce localized low-pressure cells over a lake and create such a storm (Asnani 1993; Nicholson and Yin 2002). Furthermore, the remarkable influence the storm had on the lake's thermal

structure, presumably through high rates of evaporation mitigated by an unstable boundary layer, suggest that these events occurring in the west of the lake may be an even more prominent feature of Lake Victoria's physical limnology than a north-south gradient of evaporation and seiching. This hypothesis is supported by the fact that the frequency of these storms are at their highest in the months of March through May (Nicholson and Yin 2002), the period in which heat content and thermal stability in the lake decrease rapidly (Talling 1966; Hecky 1993). Regardless of the mechanism, spatial variations in meteorological forcings over Lake Victoria would induce the spatial heterogeneity of the lake's thermal structure shown in lakewide transects (Kitaka 1976; Romero et al. 2001). Accordingly, surface mixing depths are expected to vary spatially, as well as the depth of the oxic-anoxic interface and nutricline when the lake is stratified. As these two features affect the light and nutrient regimes of phytoplankton, both phytoplankton biomass and production should also display a degree of spatial variability. This chapter makes use of novel lakewide data on limnological conditions to demonstrate and analyze such spatial variability.

3.2 Materials and Methods

A SBE-19 CTD profiler (Sea-Bird Electronics Inc., Bellevue WA), equipped with a Beckman dissolved oxygen sensor and a WetStar chlorophyll fluorometer (WetLabs, Philomath OR), was used to collect approximately 50 profiles during each of four lakewide hydroacoustic cruises in February and August of 2000 and 2001 conducted by the Lake Victoria Fisheries Research Project (LVFRP). The CTD samples at a 2 Hz interval and was lowered at a descent rate of 1.0 $m.s^{-1}$ allowing for measurements of temperature, conductivity, oxygen and chlorophyll inferred fluorescence every 0.5 m. Site selection for profiles was chosen during the first cruise to maximize spatial coverage given the time allotted by the cruise supervisor, and a GPS allowed participating limnologists in subsequent cruises to revisit these sites.

The conductivity, temperature and pressure (depth) sensors on the CTD have very sensitive resolutions (0.0001°C) and are extremely stable (0.0002°C per month; Seabird 2001, 2002), however the dissolved oxygen sensor required calibration: The internal electrochemistry of the oxygen sensor changes with successive measurements, thus recorded values undergo a linear and gradual departure from the actual concentrations (Carlson 2002). To accommodate for this sensor drift, independent measurements of dissolved oxygen using the Winkler method were performed in duplicate at the beginning and end of each cruise. The observed departures in sensor and Winkler measurements were processed in an algorithm (Owens and Millard 1985) designed to perform post-collection calibration.

The WetStar fluorometer measures *in-vivo* phytoplankton fluorescence and can be used to estimate chlorophyll concentrations. A thorough theoretical explanation of this measurement is provided in Chapter 2.

Water transparency was measured with a white secchi disk with a 25 cm diameter. The secchi depth (SD) was determined to be the average depth at which the disk was no longer visible upon lowering and raising the disk in the water column on the shaded side of the boat.

Geostatistical analysis is an increasingly used tool in aquatic ecology (Johnson and Gage 1997). Kriging is a geostatistical method for spatial interpolation of data and is employed in this chapter at its most basic level: Kriging assumes that variables are continuous matter and that values from points nearer each other are more correlated than those further apart; interpolation of spatial temperature distributions by means of kriging has been successfully validated in the Baltic Sea (Toompuu and Wulff 1996). Historically, linear interpolation has been used for drawing isotherms between profiles taken at different locations or at different times. Kriging performs this task, but with the added advantage that it can be done quickly while statistically accounting for more than one profile, even if these profiles do not lie along a linear transect.

Kriging is used to construct cruise-specific spatial maps of temperature and dissolved oxygen presented in this chapter in the following fashion. XYZ (longitude, latitude, variable) files were created for each successive metre through depth for both temperature and dissolved oxygen for a total of 75 files per measurement per cruise. For example, data from a profile that extended to a depth of 18 m would contribute to the first 18 files while data from a profile 68 m depth would contribute to 68 files. As profiles in the dataset were taken at a variety of times throughout the day, the temperature below any observed diurnal thermocline (Imberger 1985) was extrapolated to the surface. Each depth-specific file was then geospatially interpolated to a 100 x 100 m grid and imported into a Microsoft Access database. Within the database, planimetric grid points outside the depth-specific area of Lake Victoria (using the digital map presented by Silsbe 2003) were removed (shown as grey regions in the preceding figures), while an algorithm extracted data along latitudinal and longitudinal planes to create cross-sections of the lake. Overall, 75 horizontal, 39 longitudinal and 36 latitudinal maps were created and plotted for each cruise and parameter using the Surfer graphing program. All maps are available on the accompanying CD in the folder ‘Chapter 3>Spatial Maps’, while all profiles and Secchi depth measurements are provided in the folder ‘Chapter 3>Profiles’. Spatial maps for 0, 20, 40 and 60 m are given in the results along with two longitudinal and one latitudinal transects whose geographical location are shown in Figure 3.5. Also shown in the results are the

average temperature profiles within the four quadrants of the lake (delineated by 33°E abd 1°S) as well as box and whisker plots quantifying the interpolated lakewide distribution of temperature at 0, 20, 40 and 60 m depth. Table 7.1 to 7.8 provides two numerical summaries per cruise for the spatial temperature distribution. The first table for each cruise documents the spatially interpolated temperature distribution for the four depth layers through presenting the mean, 5^{th} and 95^{th} percentile of temperature with the difference between percentiles indicating the temperature range. Also presented in the first table for each cruise is the average temperature gradient along each depth and the direction of the gradient presented as degrees clockwise from north. Specifically, the direction of the temperature gradient indicates the direction cool water would flow through a gravitational adjustment in an unperturbed system. The second table for each cruise shows the average temperature of the lake for the four depth layers for each quadrant of the lake as well as the average thermal stability of the respective quadrant, a simple rank is also assigned to each quadrant where 1 and 4 correspond to the most and least thermally stable quadrant respectively.

Geospatial maps of temperature through depth were used to calculate thermal stability following the formula of Kling (1988). Density was calculated as a function of temperature, salinity and depth using the formula of Zeeb and Wolf-Gladrow (2001). A constant salinity of 0.055 PSU was employed throughout as its small variability (0.05 – 0.06 PSU) as determined using conductivity and temperature (Fofonoff and Millard 1983) had a negligible effect on density.

From the geospatial analysis of the dissolved oxygen distribution, the areal coverage of oxic-hypoxic and oxic-anoxic interface were calculated as percent of total lake area. In this chapter hypoxia is defined as concentrations < 6 mg.L^{-1} or $\approx 80\%$ saturation as calculated by Mortimer (1974) while anoxia is defined as concentrations < 1 mg.L^{-1}. This analysis also facilitates volumetric estimates of water containing hypoxic and anoxic water. Following the equations of Charlton (1980), areal hypolimnetic oxygen depletion rates (AHOD) were calculated with the following assumptions: Dissolved oxygen concentrations below 6 mg.L^{-1} contribute to AHOD and oxygen depletion commences in September when the lake begins to stratify (Talling 1966, Hecky 1993).

In this chapter mixed depth refers to the depth to which surface phytoplankton may be mixed on a diel cycle such that diurnal mixed depths (Chapter 2) are ignored. Mixed depths were determined numerically and through a visual inspection of each individual profile. Specifically, individual depths where the gradient of chlorophyll fluorescence decreased by more than 1 $mg.m^{-3}/m$ were identified within each profile and a visual inspection then determined which of these identified gradients corresponded with noticeable temperature and/or oxygen gradients. In most profiles the temperature gradient that coincided with the mixed depth was the first temperature gradient below the diurnal thermocline, and mixed depths were significantly correlated to the depth of 6 $mg.L^{-1}$ oxycline ($r^2 = 0.89$, $p < 0.0001$, $n = 95$) when present. Two examples of this procedure are shown in Figure 7.9 and 7.10 in Appendix II. The profile shown in Figure 7.9 lacks a well-defined thermocline, however the presence of an oxycline and a decrease in the chlorophyll fluorescence profile suggests that mixing can occur to 45 depth. The profile shown in Figure 7.10 shows a pronounced diurnal thermocline at 5 m and another thermocline between 18 and 20 m. This second thermocline corresponds with decreases in both oxygen and chlorophyll fluorescence such that 18 m is taken as the mixed layer. Mixed depths were then geospatially extrapolated using the kriging method for each cruise, and an algorithm was used to identify areas where mixing occurred to the bottom depth.

As mixed depths were significantly correlated to secchi depths in each cruise (Figure 7.7), the following analysis was employed to determine their lakewide distributions. Secchi depths at each geographic location are the product of the mixed depth and the ratio of predicted Secchi depths according to the cruise specific regression equation (Figure 7.8) to actual Secchi depths (Figure 7.9). From this method, actual Secchi depths are accurately adhered to while geospatial extrapolations to areas where Secchi depths were not measured account for both changes in the mixed depth and observed departures from mixed depth inferred Secchi depths with actual Secchi depths.

Meteorological data from the NCEP-DOE R2 project uses a state-of-the-art analysis/forecast system to perform data assimilation using global datasets (Kanamistu et al. 2002). 6-hourly surface wind speed and direction data from 10 m height for 2000 and 2001 were downloaded from the

Climate Diagnostic Center (http://www.cdc.noaa.gov/cdc/data.ncep.reanalysis2.html) from an area delineated by 30°E, 40°E, 5°S and 5°N with a spatial grid of 2.5 x 2.5°. Wind speeds and direction for each grid point and temporal observation were geospatially interpolated on a 10 x 10 km grid using the kriging technique from which mean monthly wind speeds were spatially extracted over Lake Victoria with corresponding monthly wind direction frequencies computed for every 22.5°. To facilitate a comparison to historic data, wind speeds were converted from 10 m to 2 m using the formula $U_{10} = U_2 [\ln (10/z_o)].[\ln(2/z_o)]^{-1}$ (Brutseart 1982) where U_Z = wind speed measurement at height z and z_o = roughness height (0.1 mm, Chow et al. 1988).

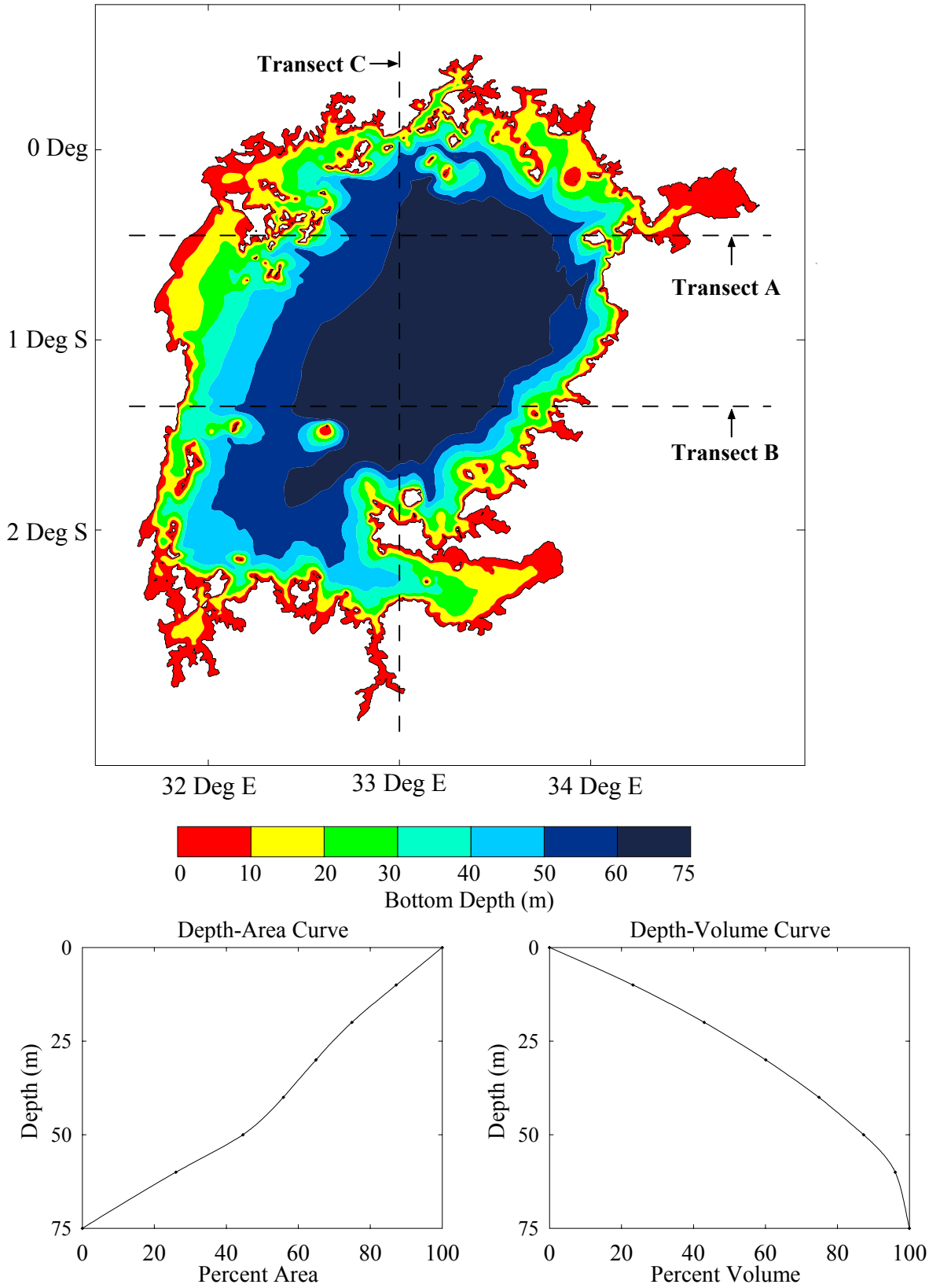

Figure 3.5: Bathymetry and hypsographic curves of Lake Victoria (Silsbe 2003). Dashed lines indicate location vertical cross-sections.

3.3 Results

3.3.1 Meteorology

Figure 3.6 shows the monthly averaged wind speed data over Lake Victoria from NCEP-DOE R2 and historic wind speeds averaged from six land-based stations presented by Yin and Nicholson (1998) used to estimate the water balance of Lake Victoria. There is comparable annual variability between years; the average wind speed of 3.54 $m.s^{-1}$ in 2000 is higher than the 2001 average of 2.73 $m.s^{-1}$. Wind speeds in 2000 were highest in February and March and lowest in October, whereas wind speeds in 2001 are highest in December, February and May and lowest from June through September. The average wind speed from Yin and Nicholson (1998) is much lower (1.95 $m.s^{-1}$), shows less monthly variability with a minor peak in June and July.

Figure 3.7 presents the average monthly wind direction frequencies over Lake Victoria in 2001. Angular direction and distance from the origin represent wind direction (going to as opposed to coming from) and % frequency respectively. As shown in Figure 3.7 the dominant wind direction over Lake Victoria are easterlies (blowing to the west). There is an increasing northerly component from February to June/July coinciding with the passage of the ITCZ to the north of Lake Victoria, that begins to subside in September when the ITCZ begins to move southward (Hills 1979). The northerly wind component is minimal during November through December, when the ITCZ is to the south of the lake (Hills 1979). The frequency of wind direction in westerly and southerly directions is negligible each month, despite overwhelming evidence suggesting thermal winds over Lake Victoria can propagate in these directions (Flohn and Fraedrich 1966; Asnani 1993; Yin et al. 2000). As the wind direction frequencies correspond with seasonal movements of the ITCZ but do not adequately account for thermal winds, application of these data to Lake Victoria is limited to general mesoscale processes.

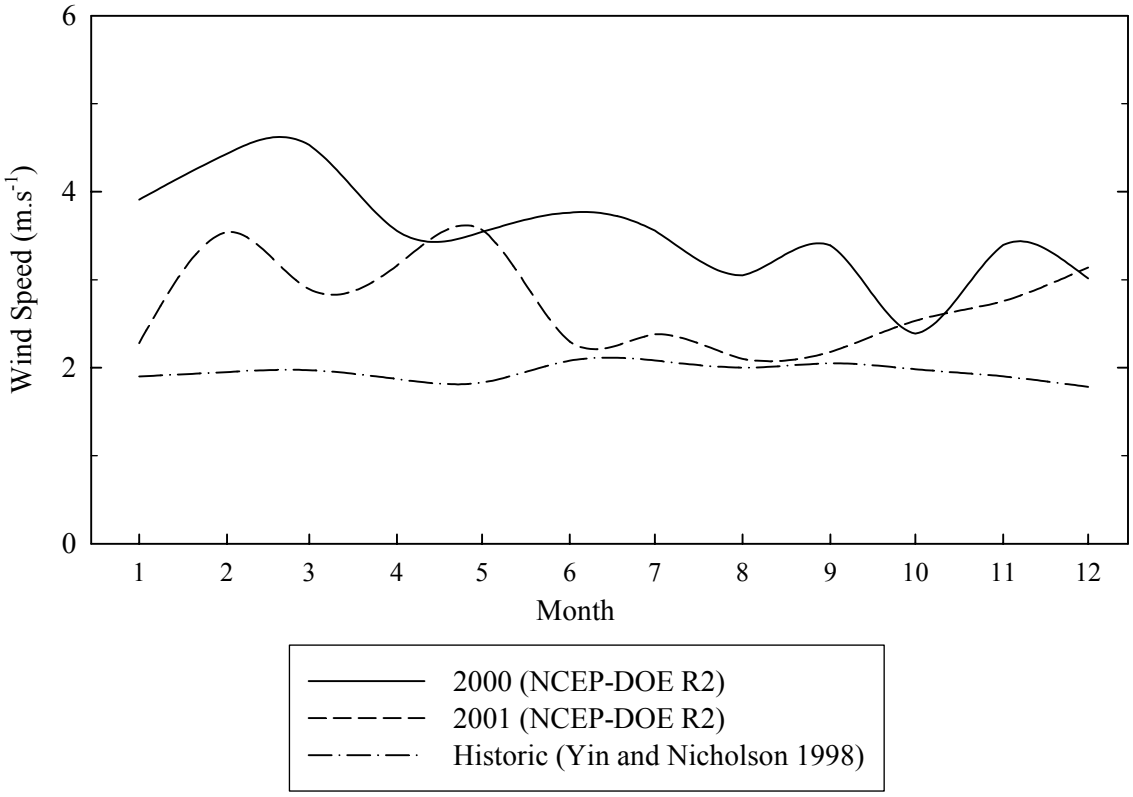

Figure 3.6: Monthly modeled wind speed at 2 m height over Lake Victoria during 2000 and 2001 from NCEP-DOE R2 and wind speed data from Yin and Nicholson (1998).

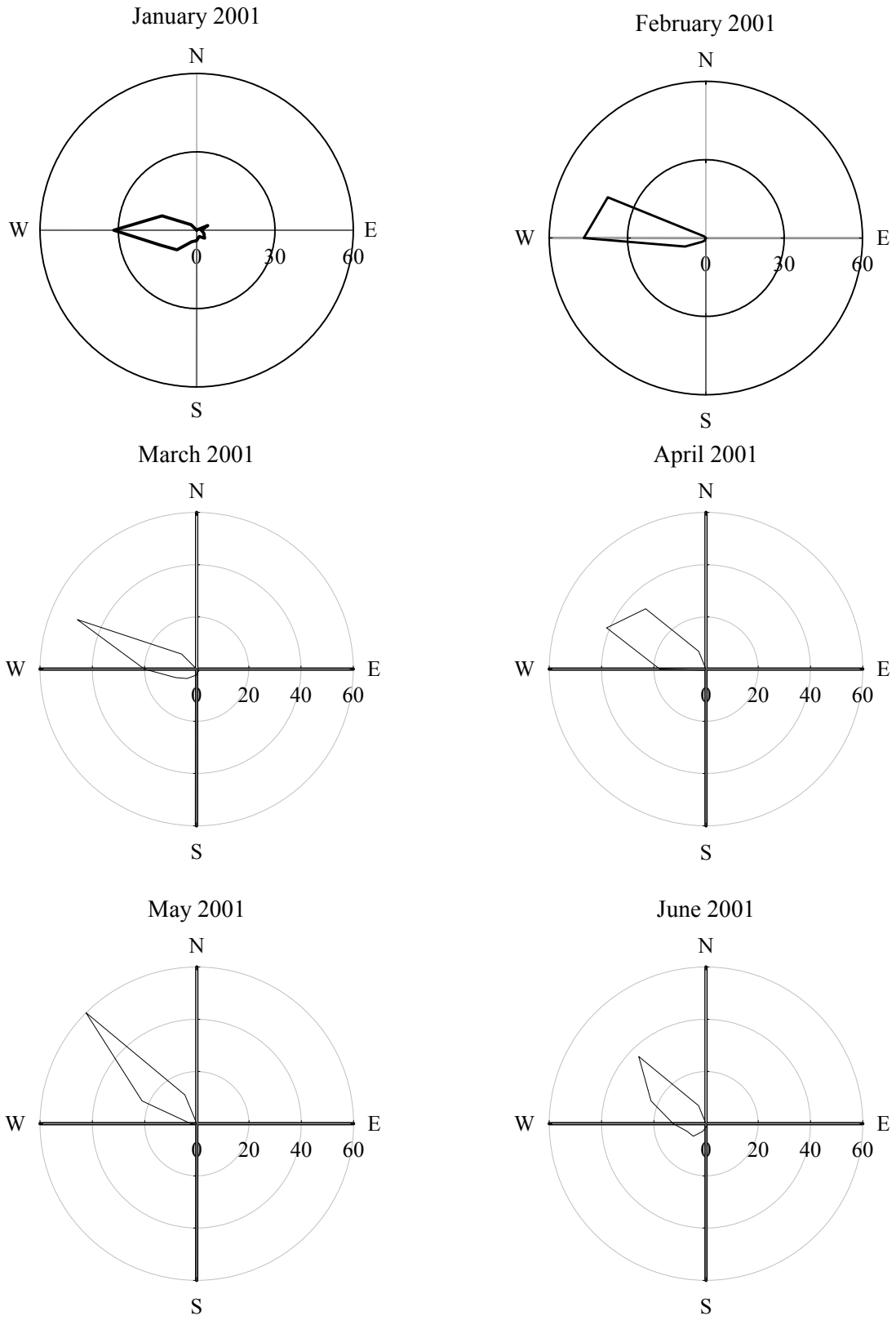

Figure 3.7: Monthly modeled wind direction frequencies over Lake Victoria from NCEP-DOE R2.

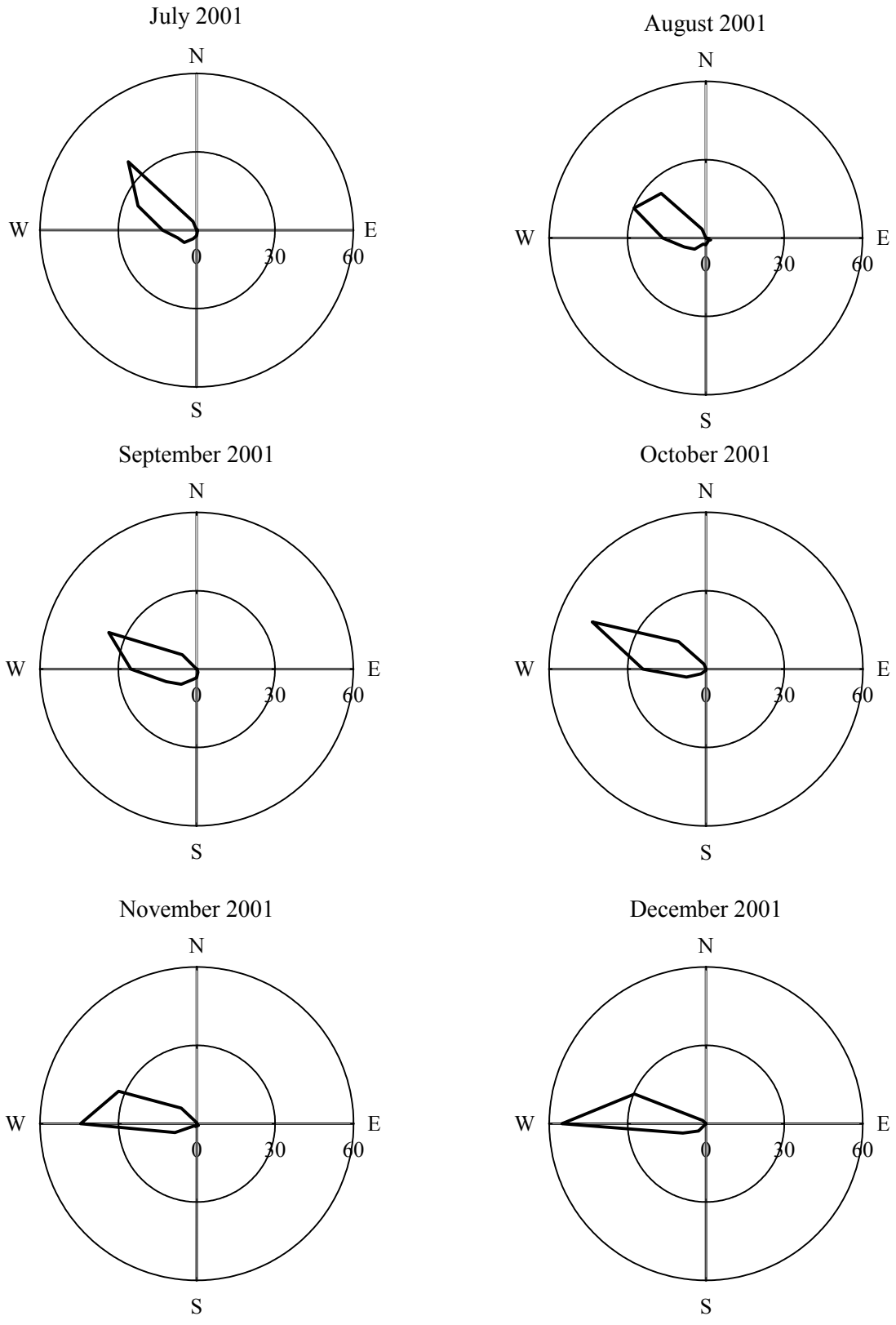

Figure 3.7 Continued: Monthly modeled wind direction frequencies over Lake Victoria from NCEP-DOE R2.

3.3.2 Temperature

February 2000

Figure 3.8 depicts the temperature distribution along four planimetric depths. At the surface, coolest water is located along the western shore of the lake south of the Sesse Islands and the warmest water is confined to the shallow regions along the north of the lake. By 20 m the cool surface water (<24.0°C) is no longer present, however the volume of water between 24.0-25.0°C increases in both the west and southern regions of Lake Victoria covering approximately 50% of the lake while spatially constraining warmer waters in the northeast of the lake. Isotherms delineating the warmer water at 20 m have comparable orientations and Table 7.1 shows the direction of the average temperature gradient is 39.1°. The direction and magnitude of temperature change is nearly identical in the 40m layer, although the average temperature decreases by 0.39°C. Despite the conspicuous absence of water in the <24.0°C range from the 20 m layer, this cool water mass reappears in the southwest of the lake in the 40 m layer. By 60 m spatial heterogeneity of temperature has substantially decreased, with all water at or below this depth between 23.6-24.0°C and the direction of the average temperature gradient is 359°.

The spatial distribution of temperature is further evident in the three cross-sections: Along the northernmost transect shown in Figure 3.9A, a strong temperature gradient is present between 40 and 50 m deep and epilimnetic isotherms downwell towards the east. The easternmost Nyanza Gulf is approximately 2.5°C warmer than the westernmost Sango Bay, where the severity of isotherm tilting enacts greater horizontal temperature gradients than through depth. One degree to the south along the transect shown in Figure 3.9B, the same pattern of warm water in the east and cool water in the west exists. However at this latitude water column temperatures decrease and the temperature gradient is more vertically diffuse. The transition between these two transects is apparent in the north-south transect along the 33°E shown in Figure 3.9C: North of 1°S, a strong temperature gradient is found at approximately 45 m with an increasingly warmer epilimnion moving northwards. South of 1°S, cool water isotherms (24.0 to 24.8°C) are more vertically diffuse but do not upwell to

the surface, while the increase in epilimnetic temperature southwards is smaller compared to the north.

As shown in Figure 3.10 and summarized in Table 7.2, horizontal temperature variability is greatest at the surface, is similar at 20 and 40 m and small at 60 m depth. Figure 3.20A demonstrates that thermal stability is highest in the northeast corner of the central basin (1400 $J.m^{-2}$) and remains high (> 1000 $J.m^{-2}$) down along the eastern edge of the basin. Notwithstanding shallow areas where stability is low, the greatest decrease in thermal stability occurs in a westward direction.

August 2000

As shown in Figure 3.11A, the distribution of surface temperature reveals interesting contrasts to February 2000: Whereas the coolest surface waters in the previous cruise are located along the western shore, cool surface water temperature in the 23.0-23.6°C range occurs in Mwanza Gulf in the southeastern corner of the lake and the direction of the average temperature gradient is 19°. Within the deep central basin, the coolest waters are in the southwest that become progressively warmer to the northeast. On average and as shown in Table 7.3, surface water temperatures are 0.66°C cooler than in February 2000. At 20 m depth, the average temperature has decreased by 0.37°C and the direction of the average temperature gradient is 44°. The cold mass of water in Mwanza Gulf is still present but does not extend further to the west, while water in the 23.6-24.0 °C range occupies a greater spatial range extending from the southwest of the lake along the western side of the central basin up to the Sesse Islands. By 40 m this mass of water is further extended to the north and east, and as summarized in Table 7.3 the direction of the overall temperature gradient is 97°, in other words isotherms are generally aligned in a north-south direction. At 60 m, there is still horizontal temperature variability with the warmest water located in the southeast of the deep central basin.

In contrast to February 2000, isotherms in Figure 3.12A do not exhibit appreciable vertical deflection. One degree to the south along the transect shown in Figure 3.12B, horizontal heterogeneity of temperature increases with cooler water in the west and warmer water in the east.

Along the north-south transect shown in Figure 3.12C, the 24.0°C isotherm rapidly plunges from 25 m depth to intersect the bottom of the lake around 1.25°S; this plunge is not an artifact of spatial interpolation, two profiles taken within three hours and 30 nautical miles exhibited this phenomenon. Figure 3.12C shows that within the central basin, warmer epilimnetic and cooler hypolimnetic water are located in the north such that the water-column in Mwanza Gulf is on average approximately 1.6°C cooler than the water-column at the northern extent of the transect.

Overall during this month, as depicted in Figure 3.13, the two northern quadrants had the warmest surface waters and the two western quadrants had the coolest hypolimnetic water. As shown in Table 7.3, the average temperature at the surface and the 60 m layer is 0.66°C cooler and 0.11°C warmer compared to the same respective layers in February 2000. Accordingly, an approximate two-fold decrease in thermal stability compared to February 2000 further shows the lake is much more isothermal during this month. Table 7.4 and Figure 3.20B show that the northeast quadrant is the most thermally stable, followed by the northwest, and the southeast quadrant is the least thermally stable.

February 2001

Figure 3.14A illustrates that warm surface temperatures are confined to the north of the lake except for a warm plume extending out easterly 50 km from Bukoba, Tanzania. Similar to February 2000, cool water is again present in Sango Bay, although the coolest surface water is located in Mwanza Gulf. In contrast to February 2000, the mean temperature of surface water is cooler (a decrease of 0.23°C) and as shown in Table 7.5 isotherms are orientated in a more north-south gradient (351.5° versus 60°). By 20 m depth, the east-west alignment of isotherms is now consistent and cooler water in the 24.0-24.6°C range occupies the entire southern half of the lake. By 40 m, water in the 23.6-24.0°C range appears south of 1.5°S, with water between 24.6-25°C diametrically constrained to the northeast and the direction of the average temperature gradient is 26°. At 60m, the

24.0°C isotherm is approximately delineated by 1°15'S with cooler water to the south and warmer water to the north.

Upon examining the northernmost transect shown in Figure 3.15A, there are some similarities to the same transect shown in February 2000: The greatest temperature gradient is again located east of 33°E between 40 and 50 m, epilimnetic isotherms are found at deeper depths moving eastward, but unlike February 2000 the vertical deflection of isotherms west of 33°E is small. One degree to the south along the transect shown in Figure 3.15B, isotherms are generally vertically homogeneous with shallow warmer surface waters in the extreme east and west of the transect. The most significant isotherm tilting occurs along the north-south transect shown in Figure 3.15C. Similar to the transect performed by Romero et al. (2001, Figure 7.6) in May 1995, isotherms downwell in the north and upwell in the south and water > 25.0°C is only found north of 1°S. The latitudinal heterogeneity of temperature also causes a north-south gradient in thermal stability. As seen in Figure 3.20C, thermal stability in the northernmost extent of the central basin exceeds 1000 $J.m^{-2}$ whereas thermal stability in the southern extent of the central basin is around 400 $J.m^{-2}$.

The degree of interannual variability can be inferred by comparing average temperatures in February 2001 (Table 7.5) to February 2000 (Table 7.1): In 2001, surface temperatures are on average 0.23°C cooler while the average temperature at 60 m is 0.23°C warmer. With respect to thermal stability, comparing Table 7.6 shows the average thermal stability of each quadrant is lower than in February 2000 and slightly higher than August 2000.

August 2001

Planimetric temperature distributions during August 2001 as presented in Figure 3.17 are similar to patterns described for August 2000. Cool surface waters in the 24.0-24.6°C range are found in the south of Lake Victoria and along the western half of the pelagic zone, while warmer waters are once again located in the north central part of the lake. By 20 m, a cool mass of water between 24.0-24.2°C is seen more prominently in the south and southwest, and all areas experience a drop in temperature except along the eastern coast. The planimetric maps show strong west-east

gradients and as summarized in Table 7.7, the direction of the average temperature gradient is 70.1, 94.7 and 107.1° for 20, 40 and 60 m depth respectively.

Figure 3.18A shows very little horizontal variability of isotherms, except Nyanza Gulf is slightly warmer than areas to the west. As was also shown in August 2000, one degree to the south along the transect shown in Figure 3.18B horizontal temperature heterogeneity has increased with cooler water in the west and warmer water in the east. The north-south transect shown in Figure 3.18C demonstrates an pattern also documented in Figure 3.9C in February 2000: Water between 24.2 and 24.4°C upwells in the centre of the central basin with warmer water located both to the north and south. Furthermore, as shown in August 2000 epilimnetic water along the northern extent of the transect is approximately 1.5°C warmer than in Mwanza Gulf.

Similar to other cruises, Figure 3.20D illustrates that thermal stability is highest (900 $J.m^{-2}$) in the north of the central basin and decreases to the south and west. However unlike the other cruises, thermal stability again increases in the extreme southeast of the central basin and remains relatively high (700 $J.m^{-2}$) through Nabuyongo and Ukerewe islands towards the southwest.

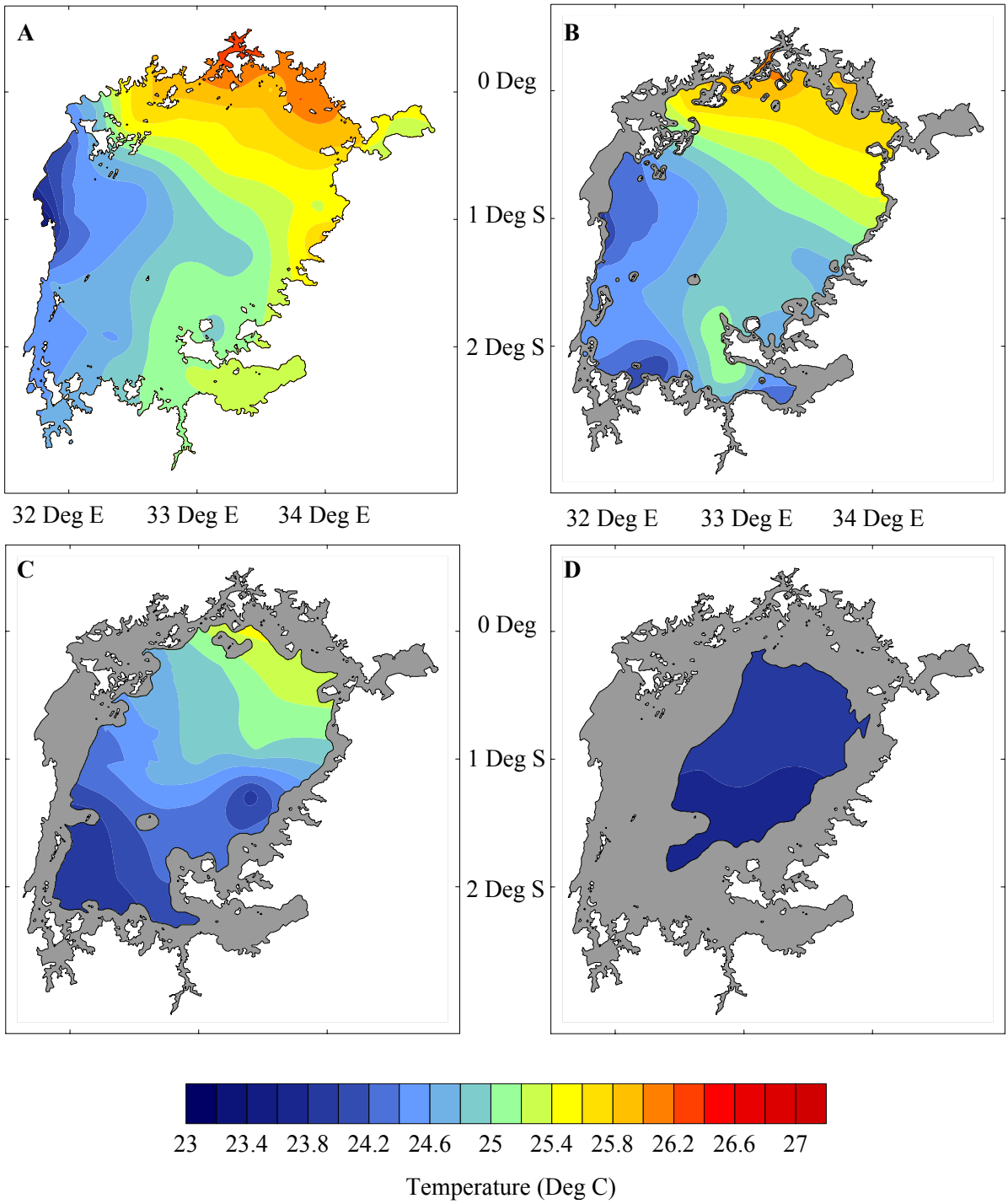

Figure 3.8: Horizontal distribution of temperature at A) 0 m, B) 20 m, C) 40 m and D) 60 m depth. Grey regions correspond to areas shallower than specified depth. February 2000.

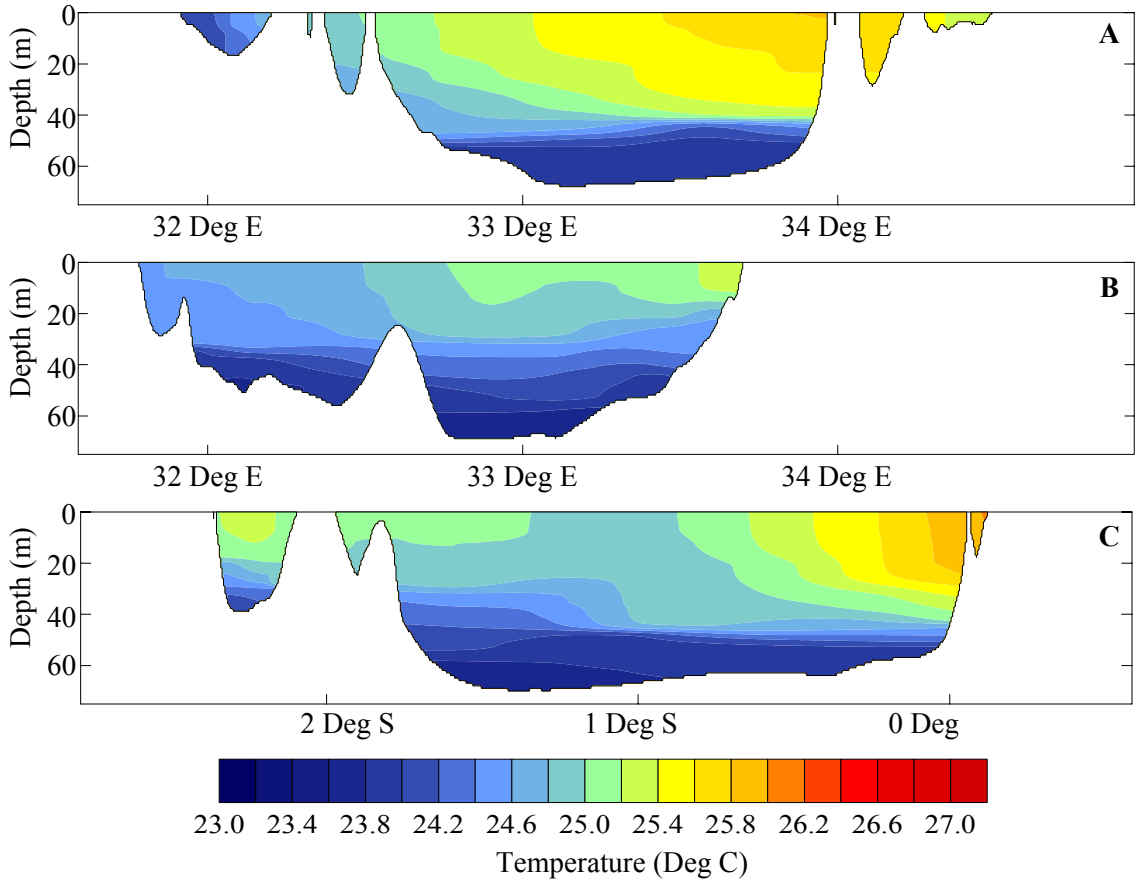

Figure 3.9: Vertical temperature distribution along west-east cross-sections at A) 0.5°S and B) 1.5°S and C) a south-north transect along 33°E. February 2000.

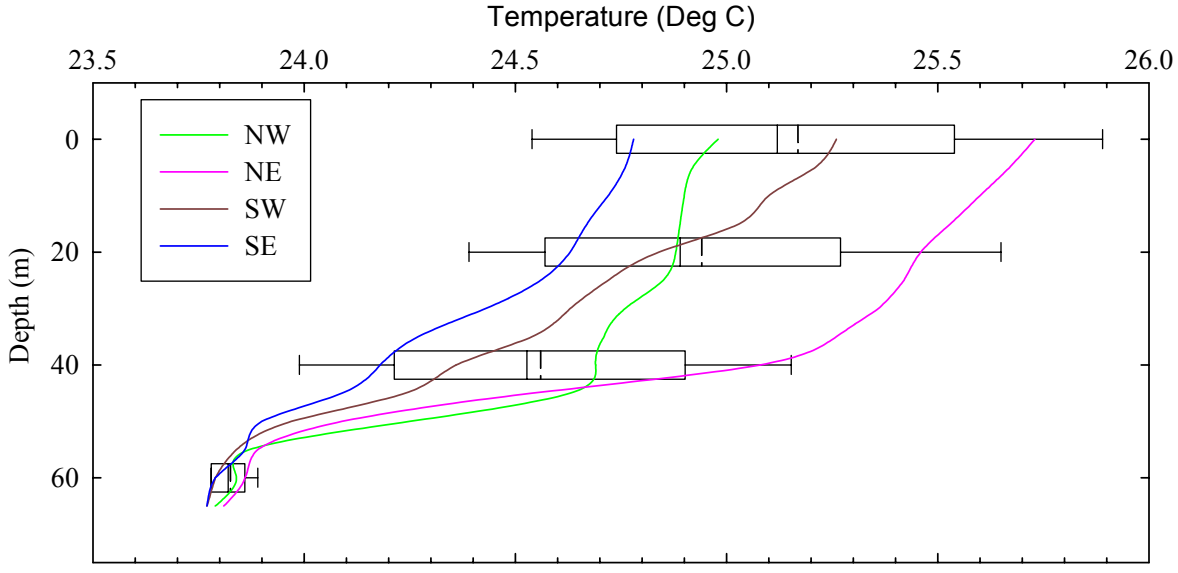

Figure 3.10: Average temperature profile by quadrant delineated by 33°E and 1.5°S. Box plot corresponding to 25th, 50th and 75th percentiles and whiskers corresponding to 5th and 95th percentile of spatially extrapolated lakewide temperature at 0 m, 20 m, 40 m and 60 m. February 2000.

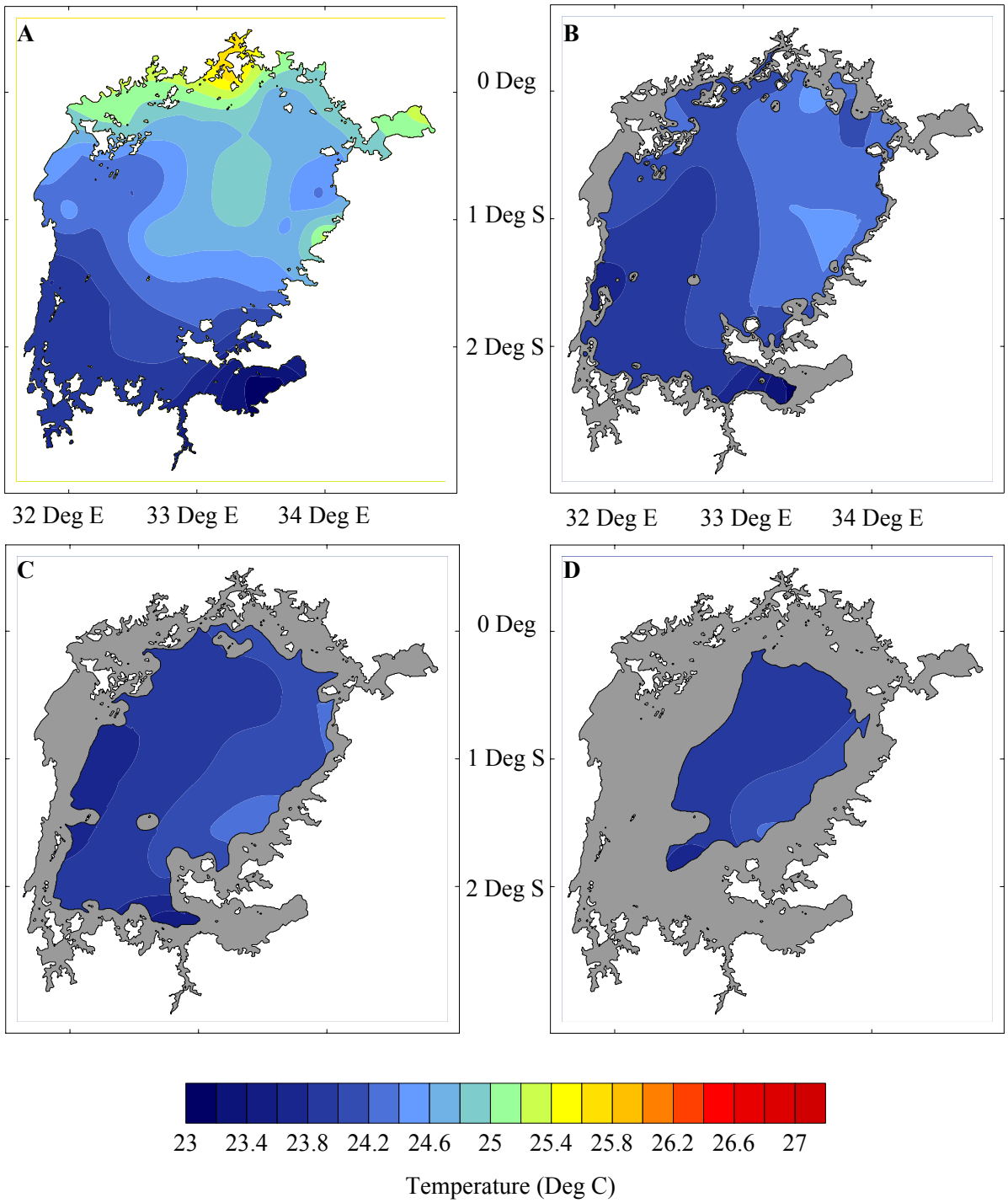

Figure 3.11: Horizontal distribution of temperature at A) 0 m, B) 20 m, C) 40 m and D) 60 m depth. Grey regions correspond to areas shallower than specified depth. August 2000.

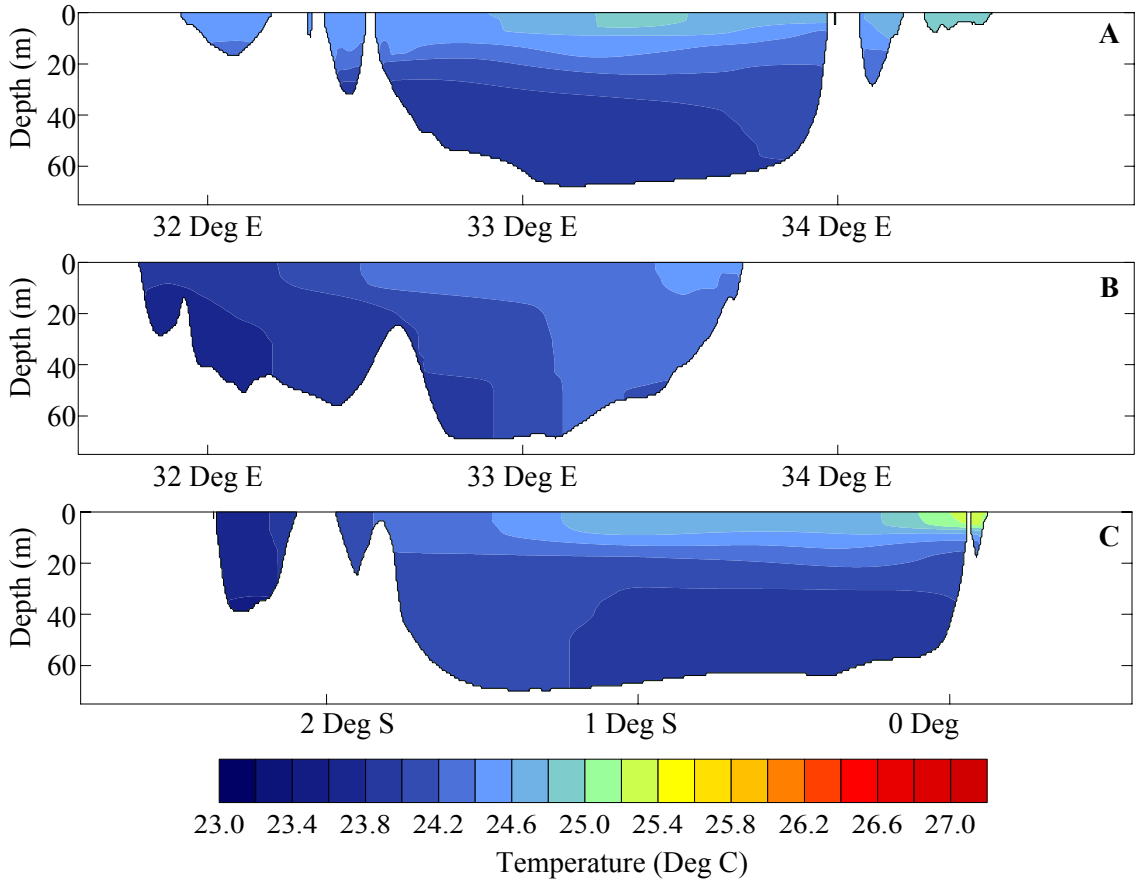

Figure 3.12: Vertical temperature distribution along west-east cross-sections at A) 0.5°S and B) 1.5°S and C) a south-north transect along 33°E. August 2000.

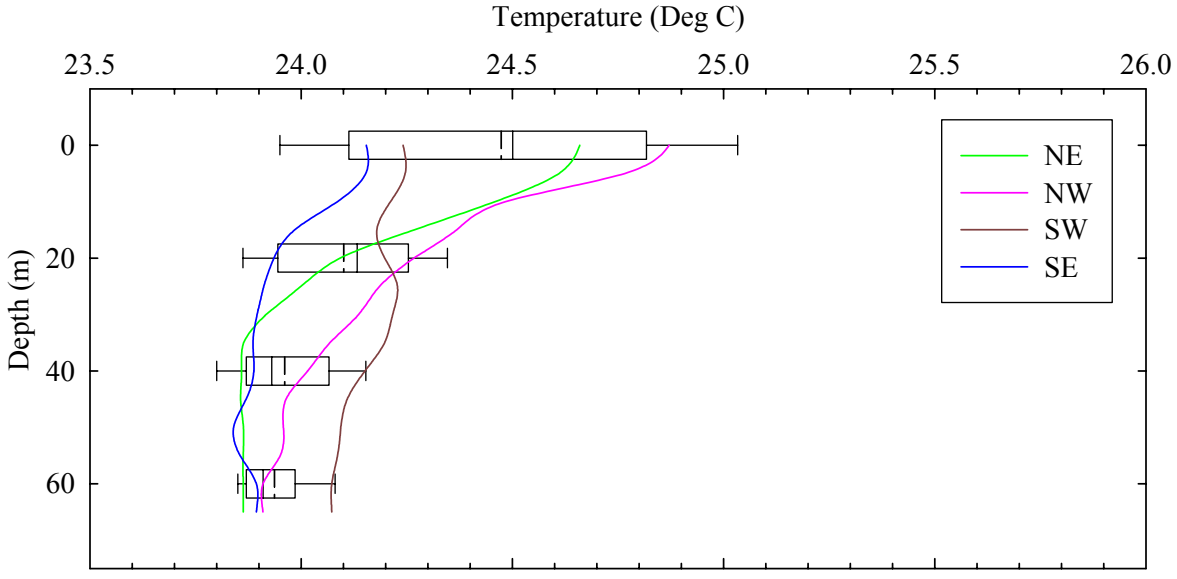

Figure 3.13: Average temperature profile by quadrant delineated by 33°E and 1.5°S. Box plot corresponding to 25th, 50th and 75th percentiles and whiskers corresponding to 5th and 95th percentile of spatially extrapolated lakewide temperature at 0 m, 20 m, 40 m and 60 m. August 2000.

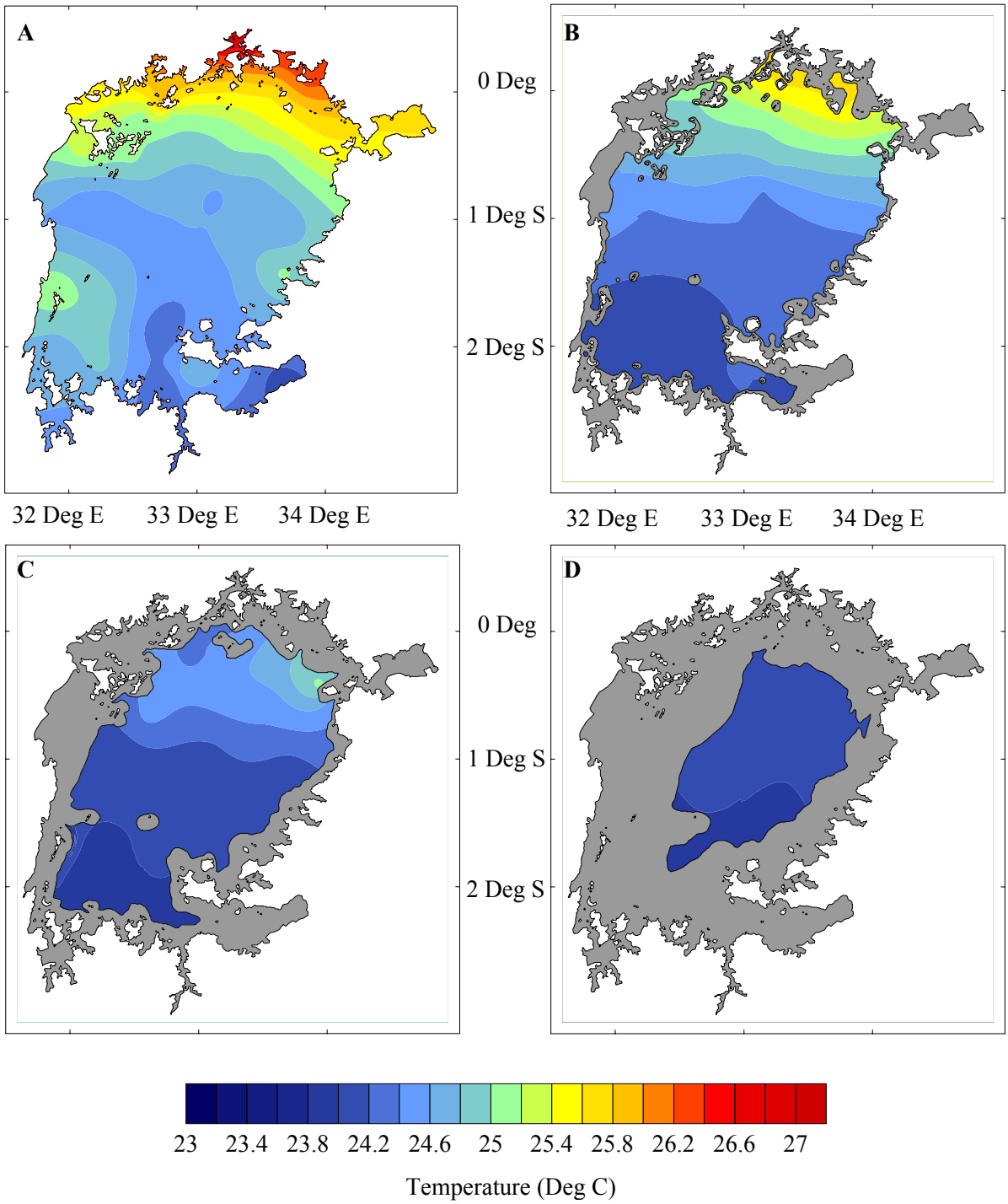

Figure 3.14: Horizontal distribution of temperature at A) 0 m, B) 20 m, C) 40 m and D) 60 m depth. Grey regions correspond to areas shallower than specified depth. February 2001.

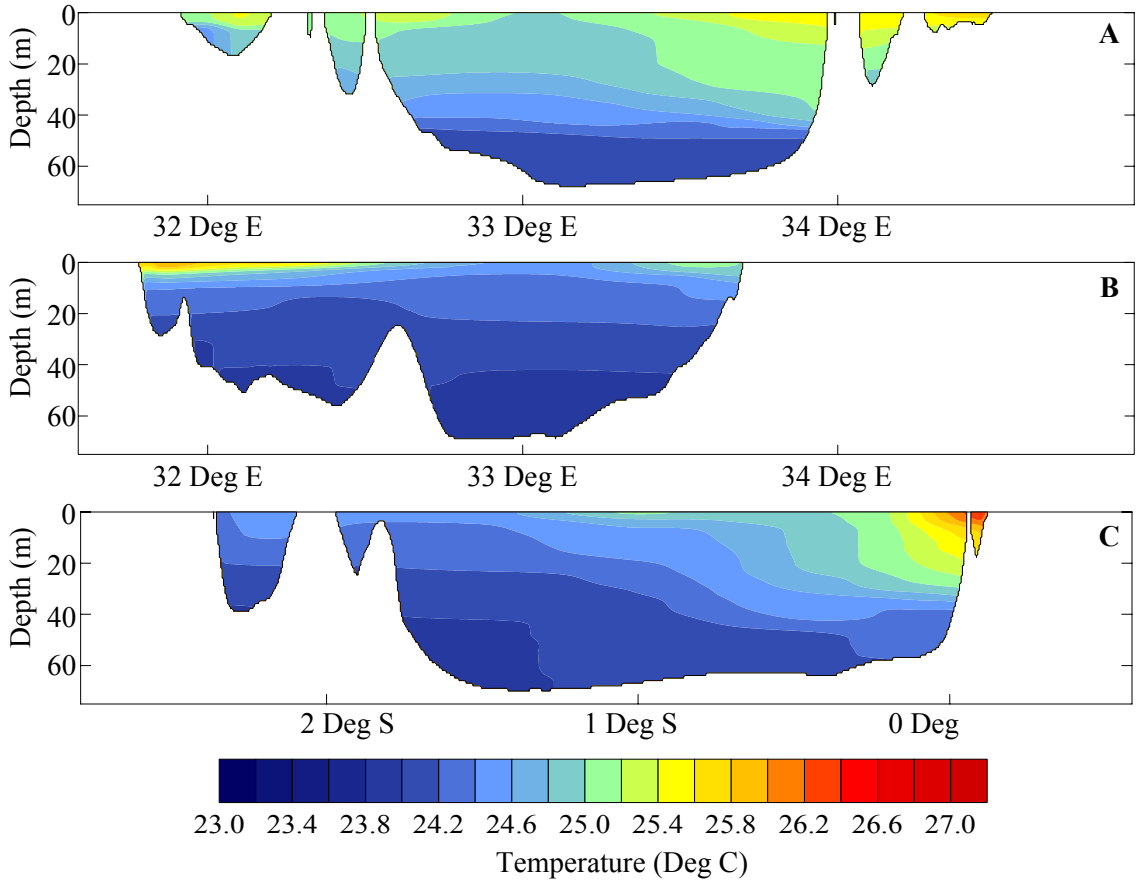

Figure 3.15: Vertical temperature distribution along west-east cross-sections at A) 0.5°S and B) 1.5°S and C) a south-north transect along 33°E. February 2001.

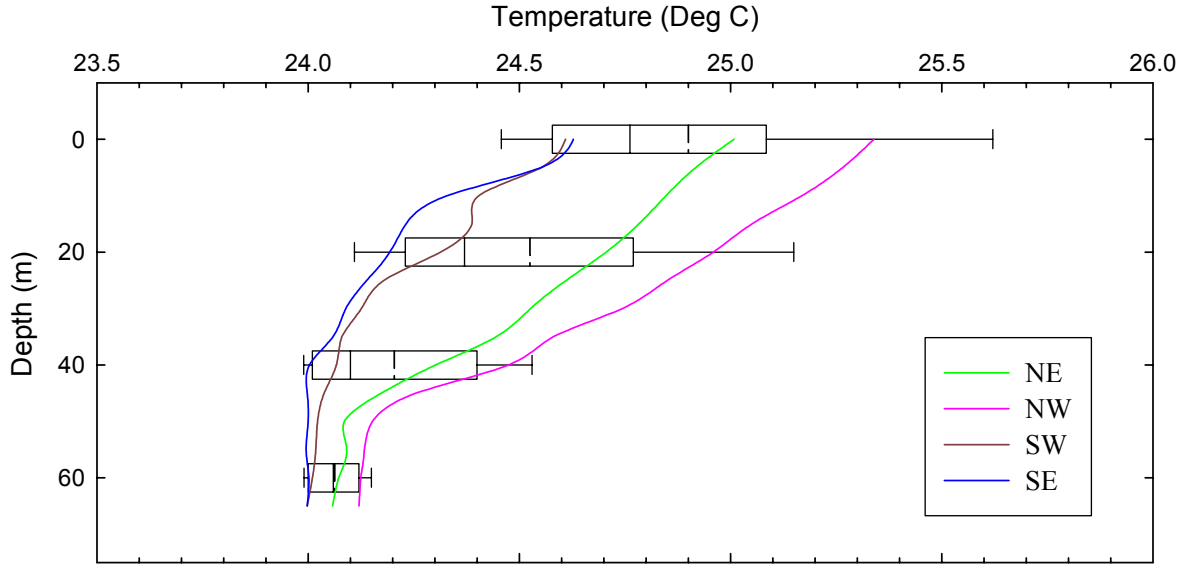

Figure 3.16: Average temperature profile by quadrant delineated by 33°E and 1.5°S. Box plot corresponding to 25th, 50th and 75th percentiles and whiskers corresponding to 5th and 95th percentile of spatially extrapolated lakewide temperature at 0 m, 20 m, 40 m and 60 m. February 2001.

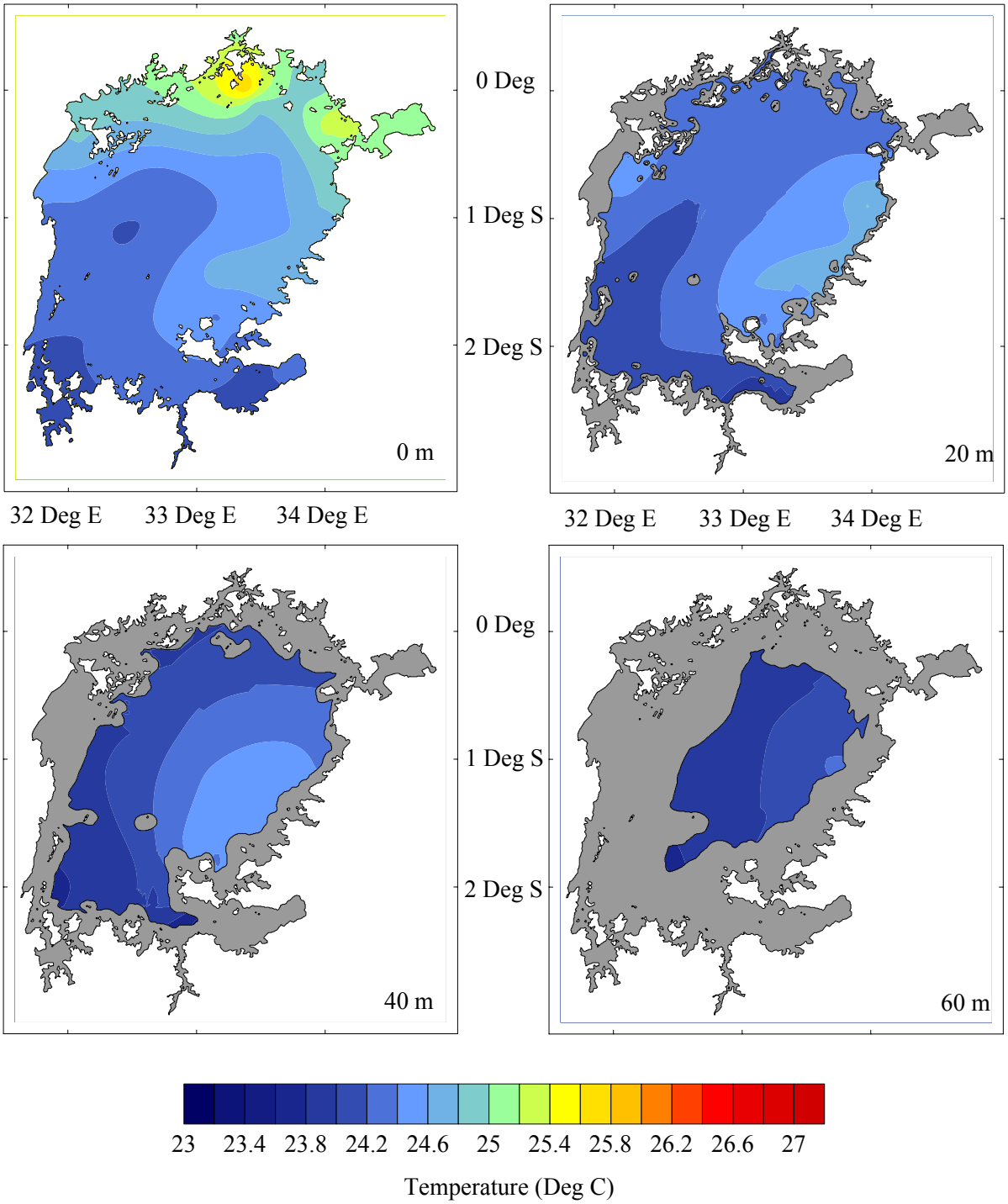

Figure 3.17: Horizontal distribution of temperature at A) 0 m, B) 20 m, C) 40 m and D) 60 m depth. Grey regions correspond to areas shallower than specified depth. August 2001.

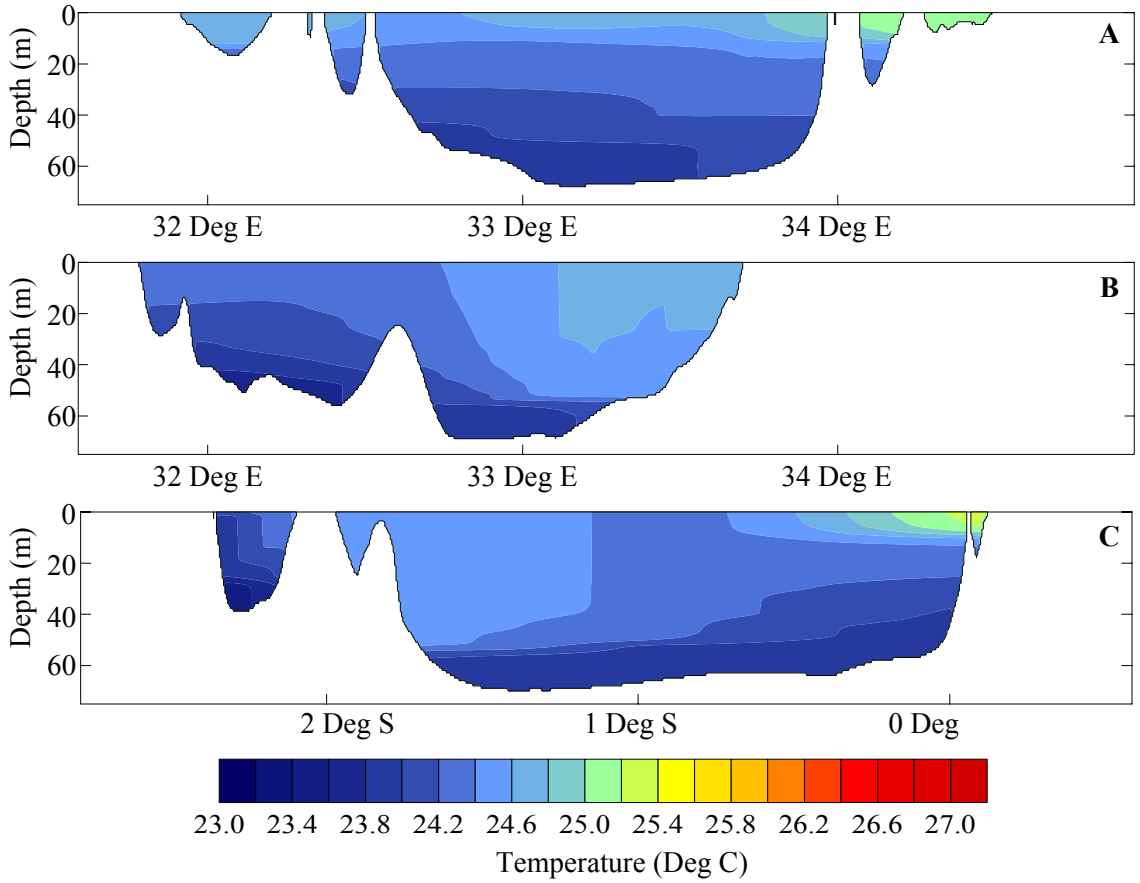

Figure 3.18: Vertical temperature distribution along west-east cross-sections at A) 0.5°S and B) 1.5°S and C) a south-north transect along 33°E. August 2001.

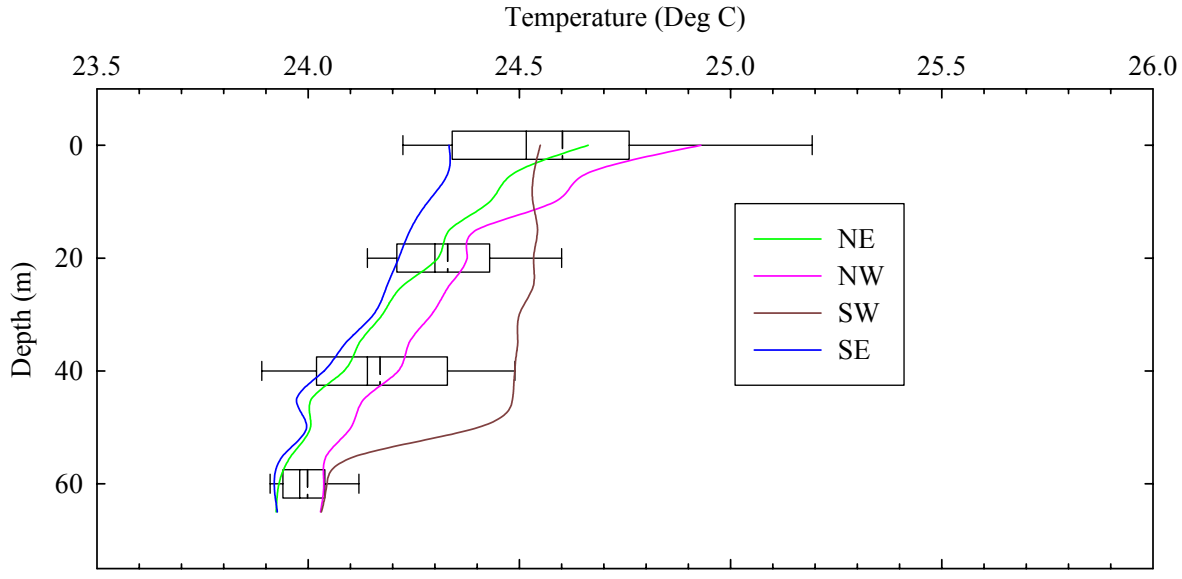

Figure 3.19: Average temperature profile by quadrant delineated by 33°E and 1.5°S. Box plot corresponding to 25th, 50th and 75th percentiles and whiskers corresponding to 5th and 95th percentile of spatially extrapolated lakewide temperature at 0 m, 20 m, 40 m and 60 m. August 2001.

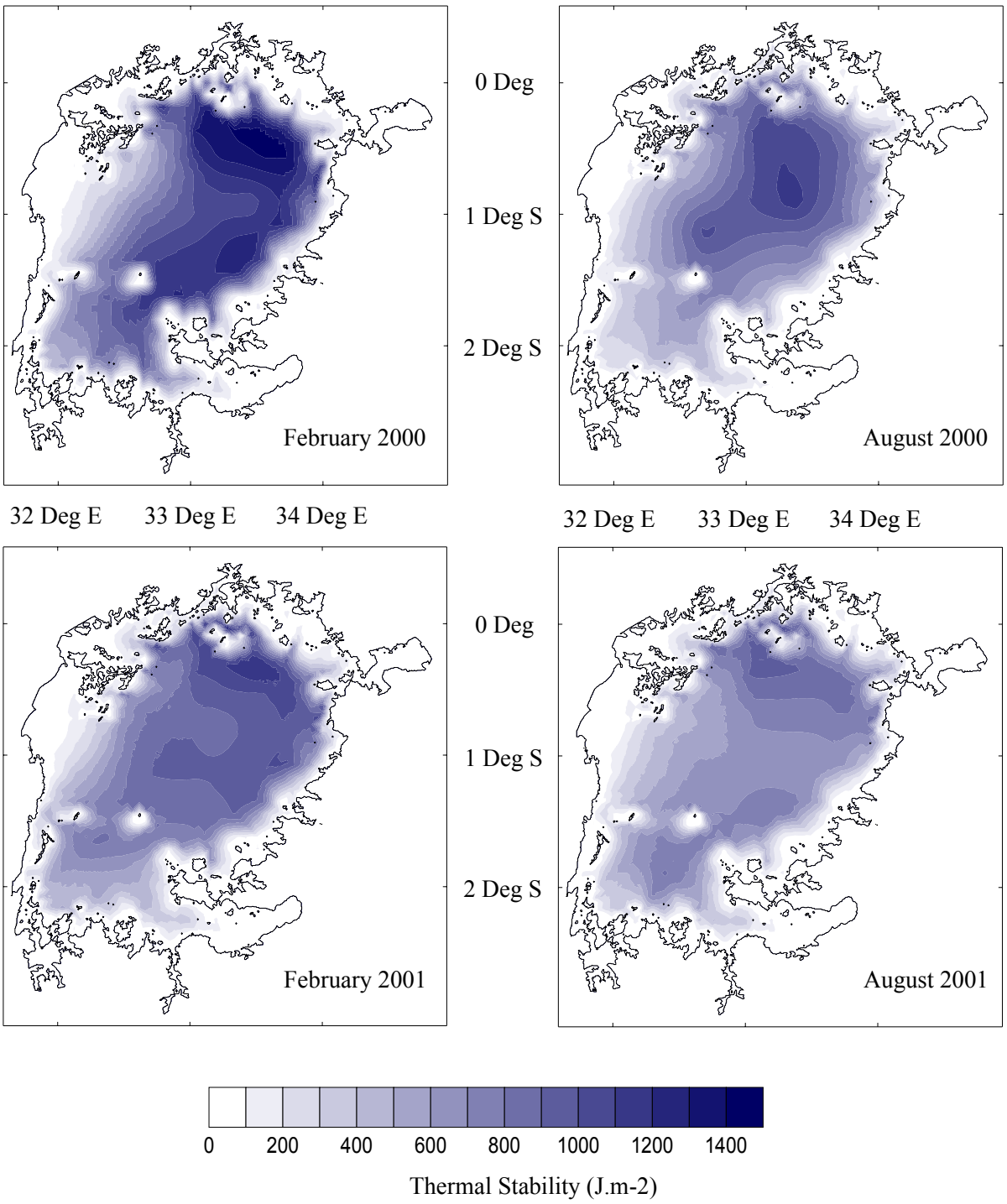

Figure 3.20: Spatial patterns of thermal stability in Lake Victoria in A) February 2000, B) August 2000, C) February 2001 and D) August 2001

Dissolved Oxygen

Figure 3.21and Figure 3.21 document dissolved oxygen concentrations along the three cross-sections shown in Figure 3.5 for February 2000 and 2001 respectively, as well as the percentage of total lake volume within a range of dissolved oxygen concentrations. Figure 3.22 and Figure 3.24 show planimetric distributions of minimum dissolved oxygen concentrations in the water column and the percentage of total lake area that the minimum dissolved oxygen isopleths occupy for the same range of concentrations as in the preceding figures. The planimetric distribution of minimum dissolved oxygen concentrations for August 2000 is shown in Figure 3.25. Similar to August 2001 (data not shown), only profiles in the open lake showed marginal hypoxia (as defined as < 6 mg.L^{-1} or $\approx 80\%$ saturation as calculated by Mortimer 1974) while no profiles detected any anoxia.

As seen in Figure 3.21 the spatial distribution of dissolved oxygen in February 2000 corresponds with spatial pattern of the thermal structure shown in Figure 3.9. Within the deep central basin in Transect A, dissolved oxygen concentrations < 5.0 mg.L^{-1} are found below the strong temperature gradient where most of the water is anoxic (as defined as < 1 mg.L^{-1}). In Figure 3.9A the 25.0°C isotherm was found at shallower depths in a westward direction, and Figure 3.21A shows that dissolved oxygen between 5.0 and 6.0 mg.L^{-1} also exhibits the same spatial pattern. One degree to the south, Figure 3.21B shows that hypoxic and anoxic water are found at shallower depths in the water column, especially east of 33°E. This feature corresponds with isotherms of cooler water ($<$ 25.0 °C) that are also shallower east of 33°E in Figure 3.9B as well as being more vertically diffuse along this longitudinal gradient. From this analysis, it is apparent that anoxic isopleths generally coincide with isotherms around 24.4°C, while hypoxic water is dependent on the degree of stratification above the 24.4°C isotherm. This observation is further shown along the north-south transect of Figure 3.21C: Similar to the 24.4°C isotherm shown in Figure 3.9C, the onset of anoxia occurs at deeper depths in the north and shows marginal upwelling to the south. Furthermore, both anoxic water and the 24.4°C isotherm are found at relatively shallower depths within Mwanza Gulf.

The onset of hypoxia along Figure 3.21C occurs deepest around 1°S and is shallower with increased vertical diffusivity of isopleths to both the north and south. From Figure 3.9C and Figure 3.20A, hypoxic isopleths correspond with upwelling of isotherms between 24.4-24.8°C, while to the north shallower hypoxic isopleths coincide with increasing thermal stability as influenced by a progressively warmer epilimnion. Overall, 22% of Lake Victoria's volume is anoxic, and 43% or the lake volume is hypoxic during February 2000. To further illustrate the magnitude of oxygen depletion, compared to data from Table 1.1, the absolute volume of anoxic water in Lake Victoria (anoxia = 583 km^3) exceeds the total volume of Lake Erie.

Figure 3.22 illustrates that the areal magnitude of oxic-hypoxic and oxic-anoxic interfaces in February 2000 occupy 75% and 58% of Lake Victoria's entire surface area respectively. Through a comparison of the lake's bathymetry in Figure 3.5, approximately 25% of the lake is shallower than 20 m and corresponds to regions where dissolved oxygen concentrations that are either saturated or near saturated through depth. Furthermore, all areas at least 40 m deep are anoxic with the exception of an area to the south of Sesse Islands that are only marginally hypoxic. In general, areas with only an oxic-hypoxic interface are regions with maximum depths between 20 and 40 m.

Based on the observed link between spatial patterns in the thermal structure and dissolved oxygen concentrations described above as well as observed inter-annual variability in Lake Victoria's thermal structure, there are notable differences between the spatial distribution of dissolved oxygen between February 2001 and February 2000. As shown in Figure 3.23A, upward tilting of the 6.0 $mg.L^{-1}$ isopleth in the west corresponds with similar tilting of isotherms shown in Figure 3.15A, while the oxic-anoxic interface coincides with the 24.4°C isotherm; two features readily apparent in February 2000. However in February 2001, Figure 3.15C shows higher vertical seperation of isotherms towards the south corresponding with relatively lower thermal stability shown in Figure 3.20. Accordingly as shown in Figure 3.23C, the vertical orientation of dissolved oxygen isopleths are more vertically diffuse while the overall degree of oxygen depletion decreases in a southward direction. A close comparison between Figure 3.23C, Figure 3.15C and Figure 3.20C reveals that

oxygen isopleths along a north-south gradient are not correlated with any isotherms and severe oxygen depletion in this month seems to be governed by thermal stability. Interestingly, the volume of hypoxic water in February 2001 is higher (49%), but the percentage of anoxic water has decreased to 2% of total lake volume. Figure 3.24 illustrates that the areal magnitude of oxic-hypoxic and oxic-anoxic interfaces in February 2001 occupy 69% and 10% of Lake Victoria's entire surface area respectively. Unlike February 2000, the oxic-anoxic interface is spatially constrained in the northern section of the deep central basin while the oxic-hypoxic interface is again found at areas up to 20 m deep. AHOD in February 2001 is approximately 36% less than February 2001 (4.88 g $O_2.m^{-2}.day^{-1}$ as compared to 6.66 g $O_2.m^{-2}.day^{-1}$).

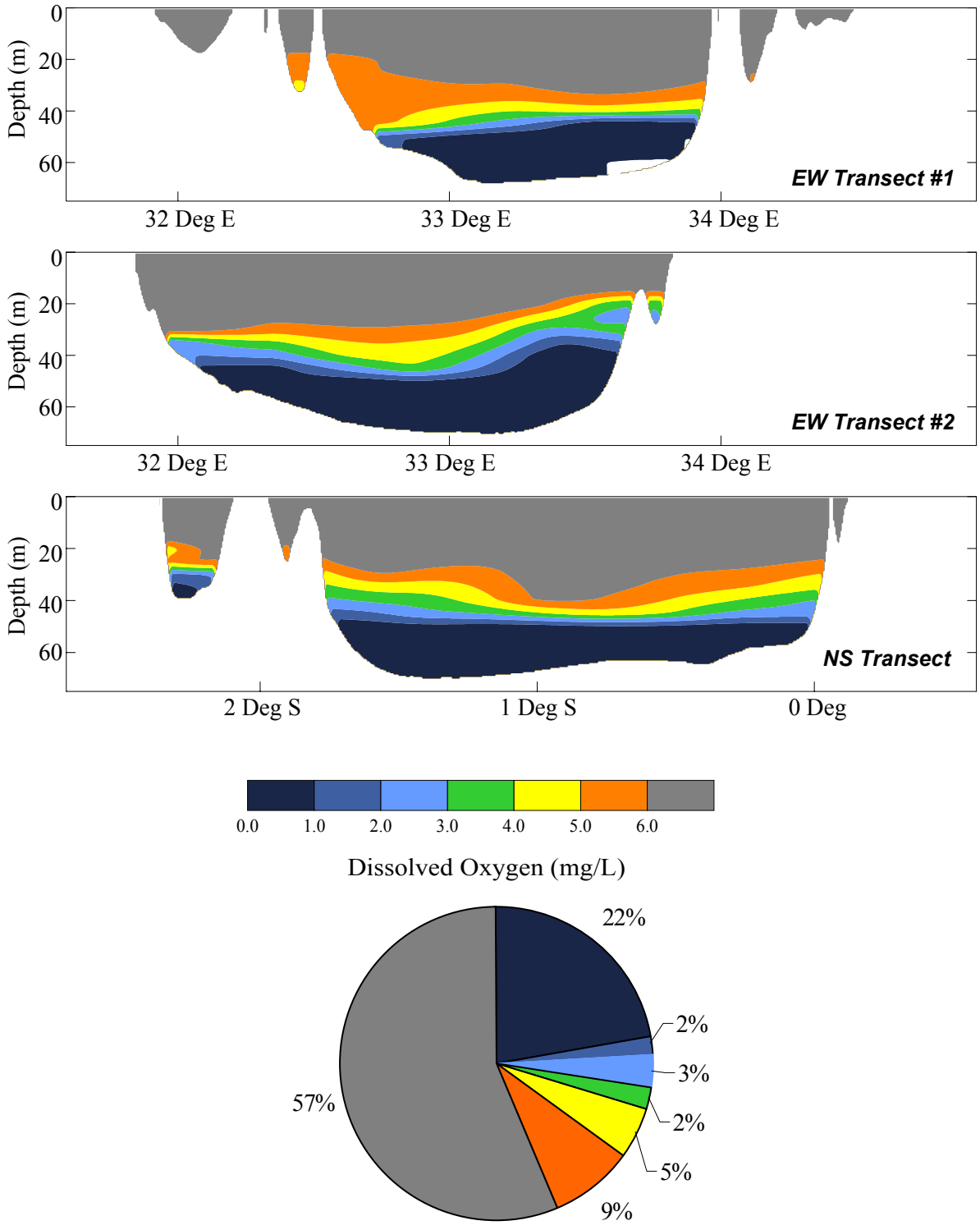

Figure 3.21: Vertical dissolved oxygen distribution along west-east cross-sections at A) 0.5°S and B) 1.5°S and C) a south-north transect along 33°E with corresponding volumes of dissolved oxygen concentrations as a percentage of total lake volume. February 2000.

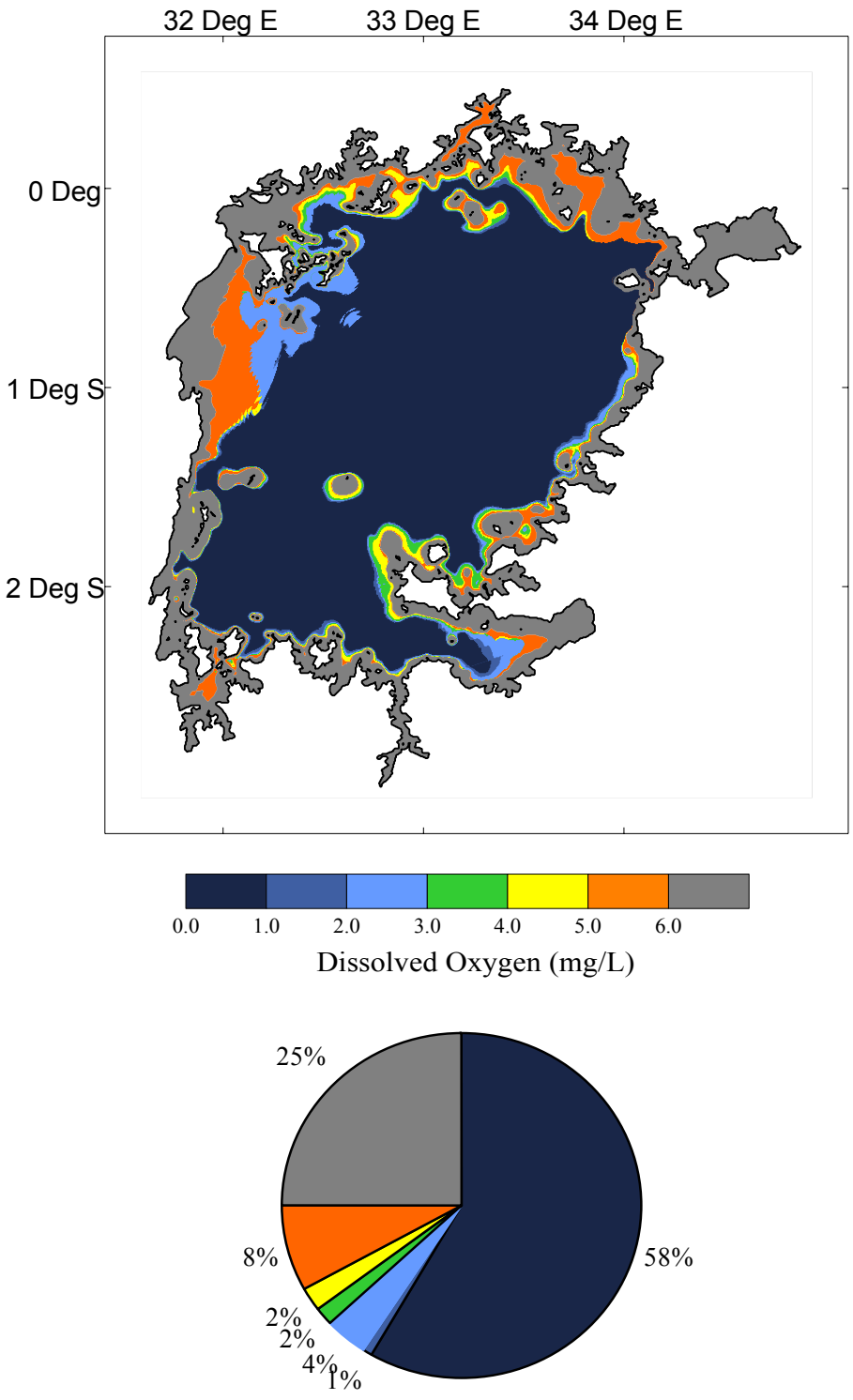

Figure 3.22: Planimetric Minimum Dissolved Oxygen with Corresponding Minimum Concentrations as a Percentage of Total Lake Area. February 2000.

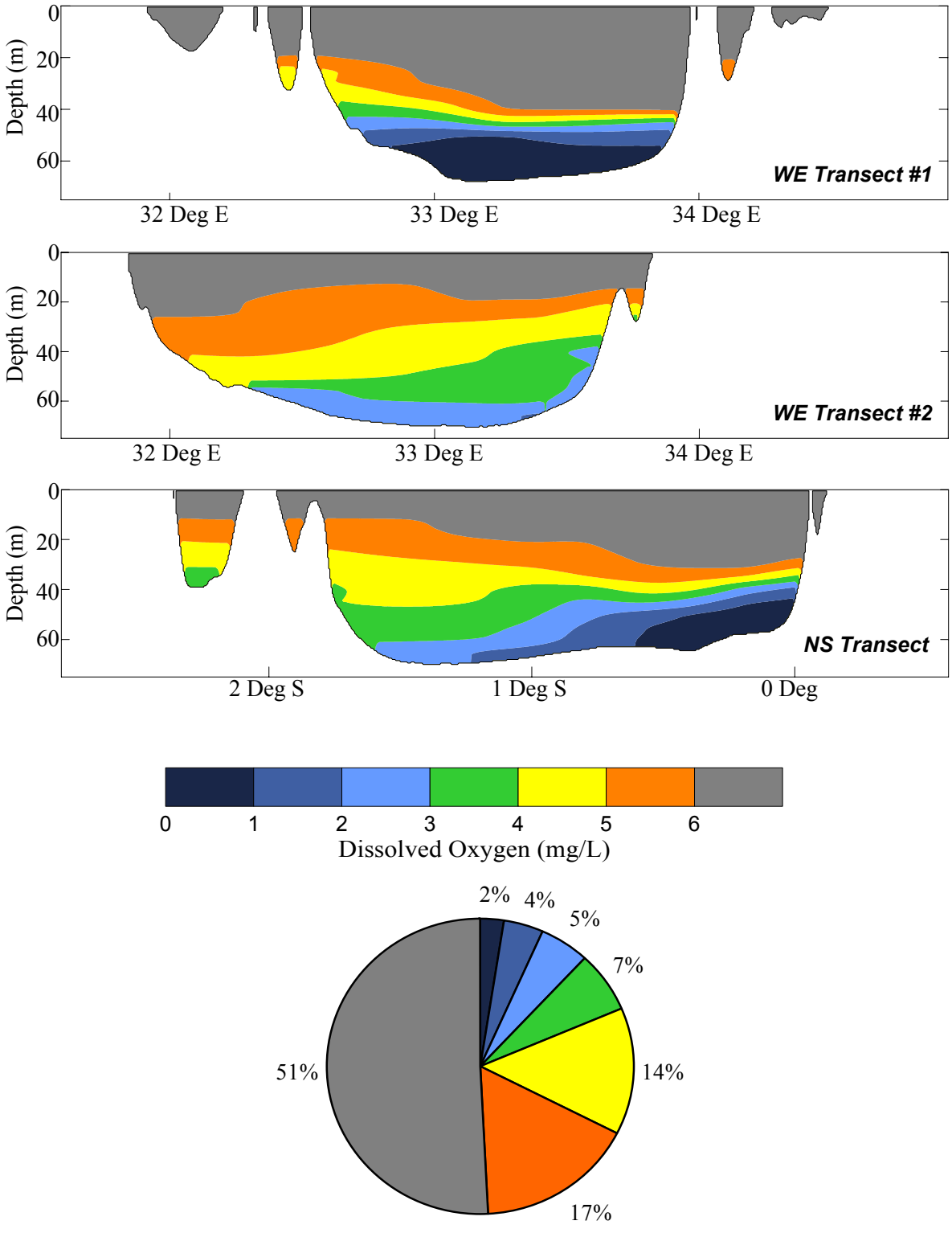

Figure 3.23: Vertical dissolved oxygen distribution along west-east cross-sections at A) 0.5°S and B) 1.5°S and C) a south-north transect along 33°E with corresponding volumes of dissolved oxygen concentrations as a percentage of total lake volume. February 2001.

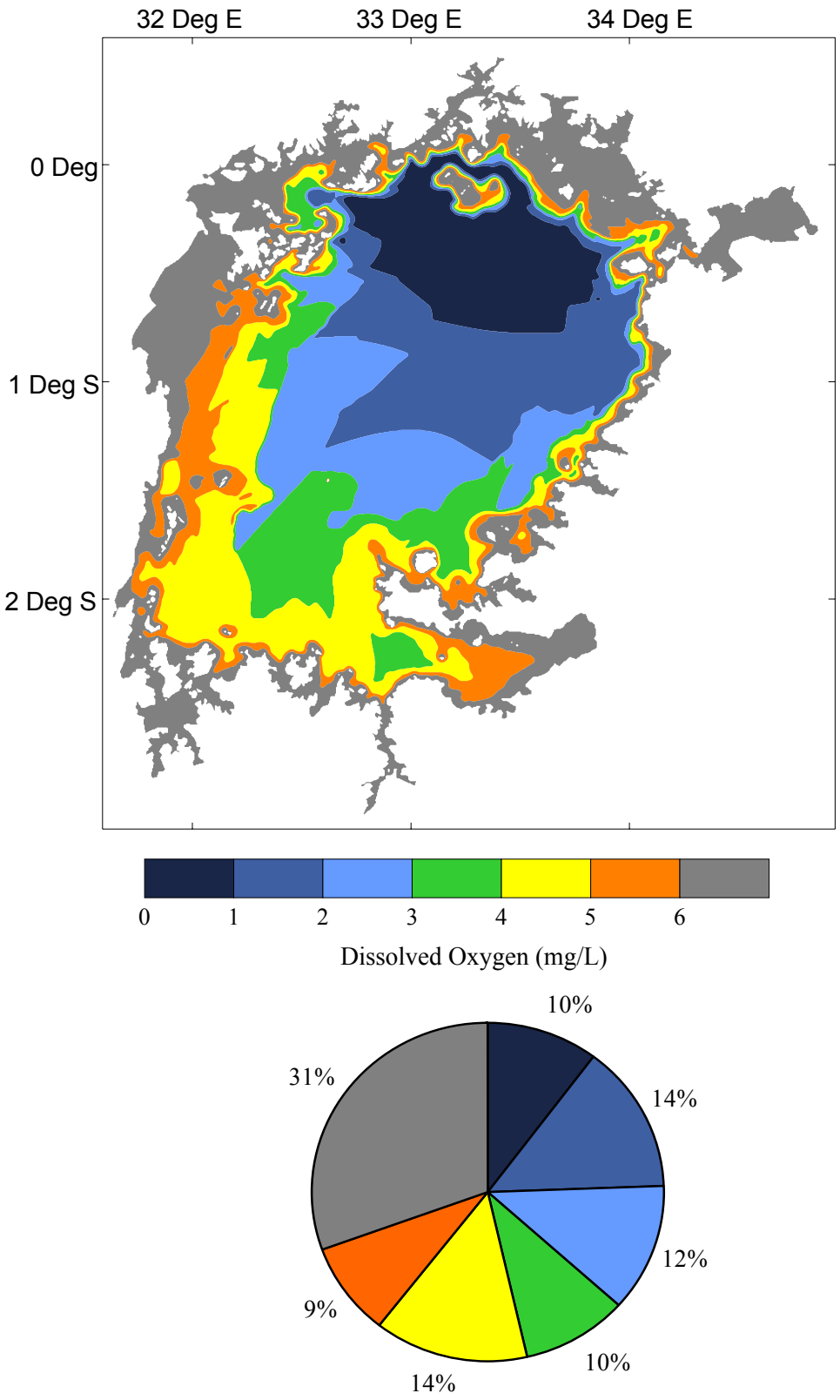

Figure 3.24: Planimetric Minimum Dissolved Oxygen with Corresponding Minimum Concentrations as a Percentage of Total Lake Area. February 2001.

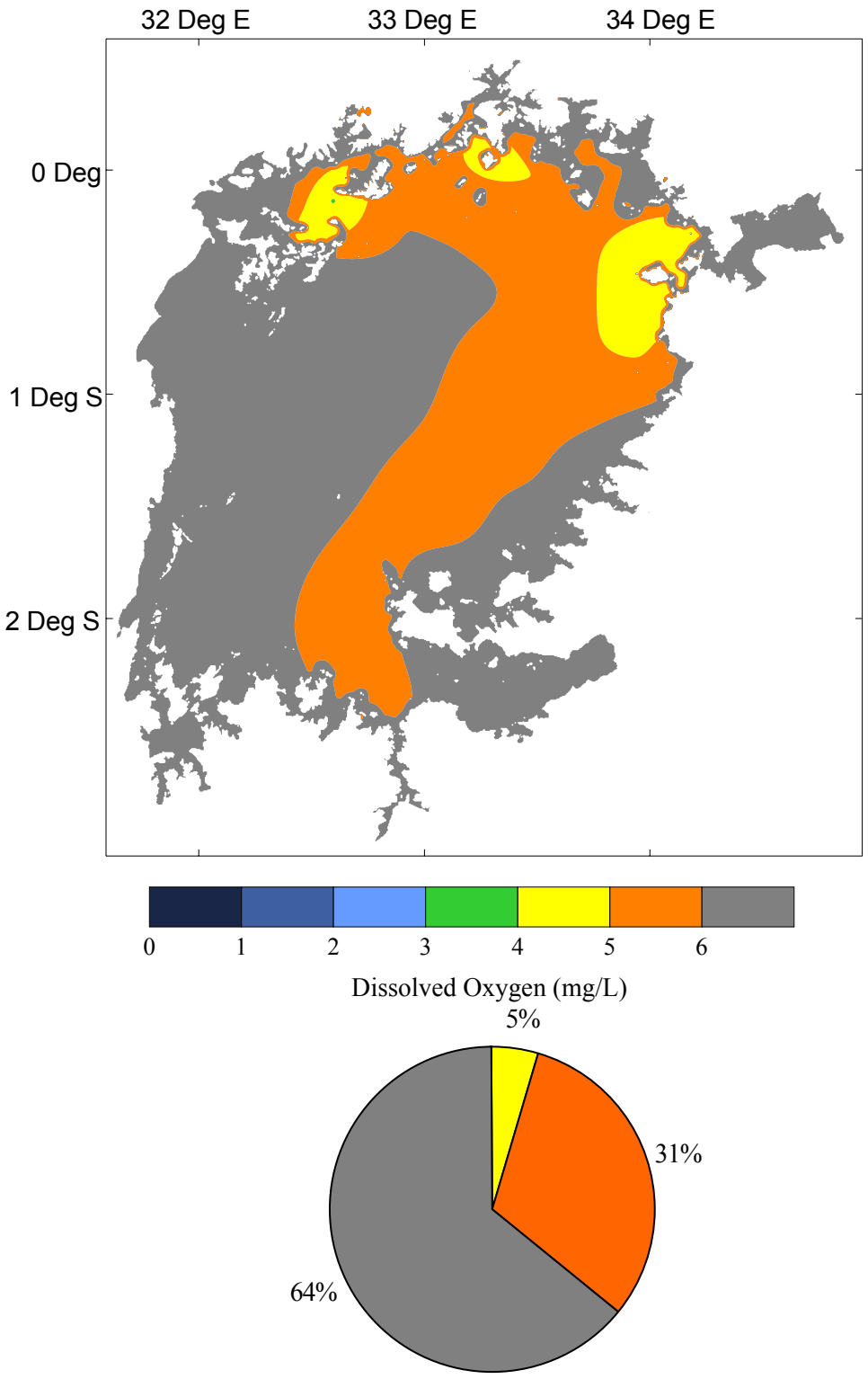

Figure 3.25: Planimetric Minimum Dissolved Oxygen with Corresponding Minimum Concentrations as a Percentage of Total Lake Area. August 2000.

3.3.3 Mixed and Secchi Depths, with Modeled Estimates of Chlorophyll and the I_{24}/I_k Ratio

Figure 3.26 illustrates spatial patterns of mixed depths for each of the four cruises. The average lakewide mixed depths, excluding areas where complete water column mixing occurs, are 29.9, 32.3, 30.5 and 34.8 m for February 2000, August 2000, February 2001 and August 2001 respectively. Complete mixing occured in regions where bottom depths do not exceed 20 m in each cruise, and areas delineating this occurrence are similar to regions where dissolved oxygen was near saturation throughout the water column (Figure 3.22 and Figure 3.24). Figure 3.26A shows that the deepest mixing (40 – 50 m) occurs along 1°S in the central basin in February 2000, and mixed depths become progressively shallower to the north and south. During August 2000, areas in the southwest and east have the greatest mixed depths (50- 60 m) while most of the northwest of the central basin has mixed depths less than 30 m as illustrated in Figure 3.26B. Figure 3.26C shows that the deepest mixing (40 – 50 m) in February 2001 occurs in the northern-middle of the central basin, while most other areas in the open basin mix to at least 30 m except for the southeast where mixed depths are shallower and between 20 and 30 m. In August 2001, the deepest mixing areas (50 – 60 m) are found in the southeast of the central basin and gradually decrease in all directions as shown in Figure 3.26D. The shallowest offshore mixed depths also are found during this cruise; in northern section of the central basin mixed depths are between 10 and 20 m.

Figure 3.27 and Figure3.29A depict the spatial distribution and statistical range of Secchi depths for each cruise. Spatial patterns in Secchi depths are similar to the above-described spatial patterns of mixed depths. In February 2000, the average Secchi depth was 2.57 m with a maximum of 4.2 m in the western half of the central basin. Figure 3.29A shows that in August 2000 the average Secchi depth was the deepest of all four cruises with an average depth of 3.63 m where the maximum of 8.0 m was observed in the southwestern region of the lake as shown in Figure 3.27B. During this month, Secchi depths became progressively shallower moving to the northwest of Lake Victoria. Figure3.29A illustrates that the average lakewide Secchi depth was 2.91 m in February 2001, where a

maximum Secchi depth of 5.1 m was observed in the north-central area of the lake shown in Figure 3.27C. Similar to February 2000, the western half of Lake Victoria has deeper Secchi depths than the eastern half. As shown in Figure3.30A, the average lakewide Secchi depth in August 2001 was 2.73 m where a maximum of 5.0 m was observed in the southwestern region of the lake as depicted in Figure 3.27D. Similar to August 2000, Secchi depths become progressively shallower moving north in August 2001. Secchi depths in each cruise also show a linear relationship with surface temperature, such that deep Secchi depths area associated with cool water and shallow Secchi depths are associated with warm water. The regression coefficients for these relationships are not strong but significant ($p < 0.01$), with r^2 of 0.28, 0.18, 0.11 and 0.36 for February 2000, August 2000, February 2001 and August 2001 respectively.

Extracted chlorophyll measurements were not possible to obtain during any cruise, but chlorophyll in the euphotic zone (chl_{Zeu}) and in the mixed layer (chl_{ML}) are required to calculate gross phytoplankton production and areal respiration respectively. In order to get approximate spatial representations of these parameters, chl_{Zeu} is derived from spatial patterns of Secchi depths (Figure 3.27) and the regression equation in Figure 2.6A that provides an estimation of chl_{Zeu} from a Secchi depth measurement. As chlorophyll fluorescence profiles are not necessarily uniform within the mixed layer, the maximum chlorophyll fluorescence within the euphotic depth and the estimated chl_{Zeu} provides the chl_F:chl ratio. Similar to Chapter 2, the chl_F:chl ratio is then applied to chlorophyll fluorescence measurements within the mixed layer to provides a more accurate representation of chl_{ML} than simply assuming chlorophyll is evenly distributed within the mixed layer.

By these methods, spatial patterns in chl_{Zeu} are necessarily similar to Secchi depths for each cruise, as shown in Figure 3.28. As shown in Figure 3.29B, the spatially averaged chl_{Zeu} is 12.3, 9.0, 9.1 and 11.9 $mg.m^{-3}$ for February 2000, August 2000, February 2001 and August 2001 respectively. Through averaging only data in the offshore (> 50 m), chl_{Zeu} decreases to 6.1, 5.4, 4.2 and 5.2 $mg.m^{-3}$ for February 2000, August 2000, February 2001 and August 2001 respectively. The spatially averaged chl_{ML} is 10.6, 6.3, 8.8 and 10.8 $mg.m^{-3}$ for February 2000, August 2000, February 2001 and

August 2001 respectively. On average chl_{Zeu} is 16% higher than chl_{WC}, where the average difference is smallest in February 2001 (3.4%) and highest in August 2000 (43%). Figure 3.31 illustrates that the average chl_{ML} is significantly related to the mixed layer depth during each cruise. The regression curves shown in Figure 3.31 illustrate that as the mixed depth decreases, chl_{ML} increases. Furthermore, student t-tests revealed that the slopes of the linearly transformed regression curves were statistically similar ($\alpha_{(2)} = 0.05$), with the exception of August 2001 versus August 2000 and August 2001 versus February 2001 which were not statistically similar.

Figure 3.32 and Figure 3.29C depict the spatial distribution and statistical range of the I_{24}/I_k ratio for each cruise. The spatial distribution of the I_{24}/I_k ratio was determined for each cruise according to Equation 3.1. This method employs the spatial distribution of mixed depths (Figure 3.26), while the attenuation coefficient, k_{PAR}, was estimated from the spatial distribution of Secchi depths and the regression equation presented in Figure 2.6C. I_k was estimated from the spatially inferred chlorophyll distribution with the quotient of the regression equations provided in Figure 2.11B and Figure 2.11A respectively. I_o is taken as the annual average of presented in Table 3.1.

As shown in Figure 3.29C, the average I_{24}/I_k ratio is 0.27, 0.36, 0.32 and 0.25 for February 2000, August 2000, February 2001 and August 2001 respectively. The spatial patterns of the I_{24}/I_k ratio for each cruise shown in Figure 3.32 are more complex than either mixed or Secchi depths, but some generalizations can be made. With the exception of shallow inshore areas, the I_{24}/I_k ratio is often below 0.5 for the entire lake. Figure 3.32A shows that in February 2000 the ratio is predominantly between 0.2 and 0.4 but falls below 0.2 along the northern part of the central basin, where mixed depths are deep, as well as within Mwanza Gulf. In contrast to the other cruises, Figure 3.29C shows that the I_{24}/I_k ratio is higher throughout the lake in August 2000. Figure 3.32B illustrates I_{24}/I_k ratios greater than 0.5 and 0.4 along the western and southern parts of Lake Victoria respectively, corresponding to areas with deep Secchi depths. In February 2001, Figure 3.32C shows that, like February 2000, the I_{24}/I_k ratio is generally between 0.2 and 0.4 for most of the lake. Areas in February 2001 where the ratio falls below 0.2 correspond with areas where Secchi depths were

shallower than nearby waters with similar depths. Figure 3.32D illustrates that in August 2001 the I_{24}/I_k ratio is between 0.2 and 0.3 for most of the lake, while small areas in the open basin, around the Sesse Islands and extending out from Mwanza Gulf have a ratio below 0.2.

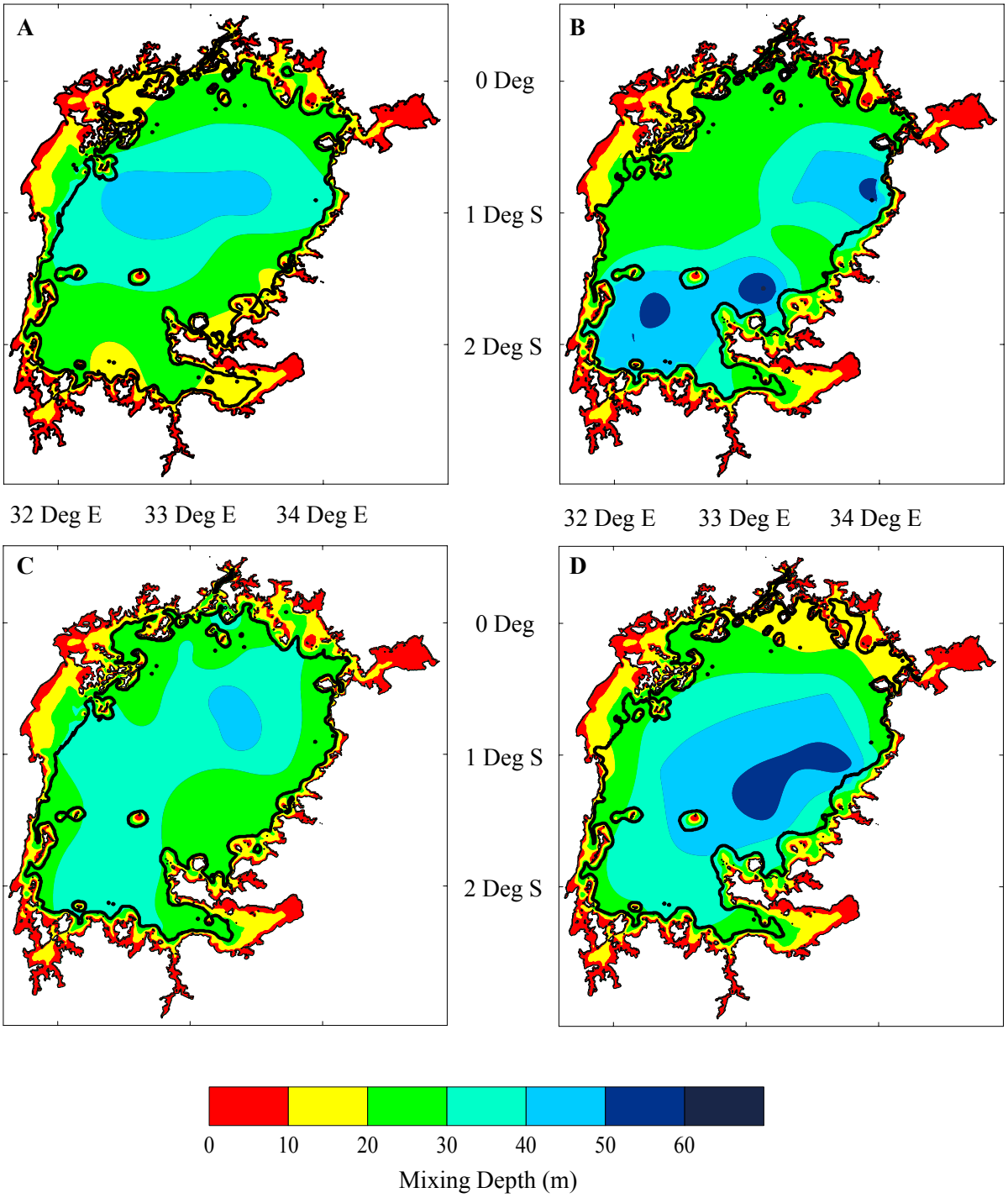

Figure 3.26: Spatial patterns of mixed depths in A) February 2000, B) August 2000, C) February 2001 and D) August 2001. Areas outside solid black lines correspond to regions where mixing occurs to the bottom depth.

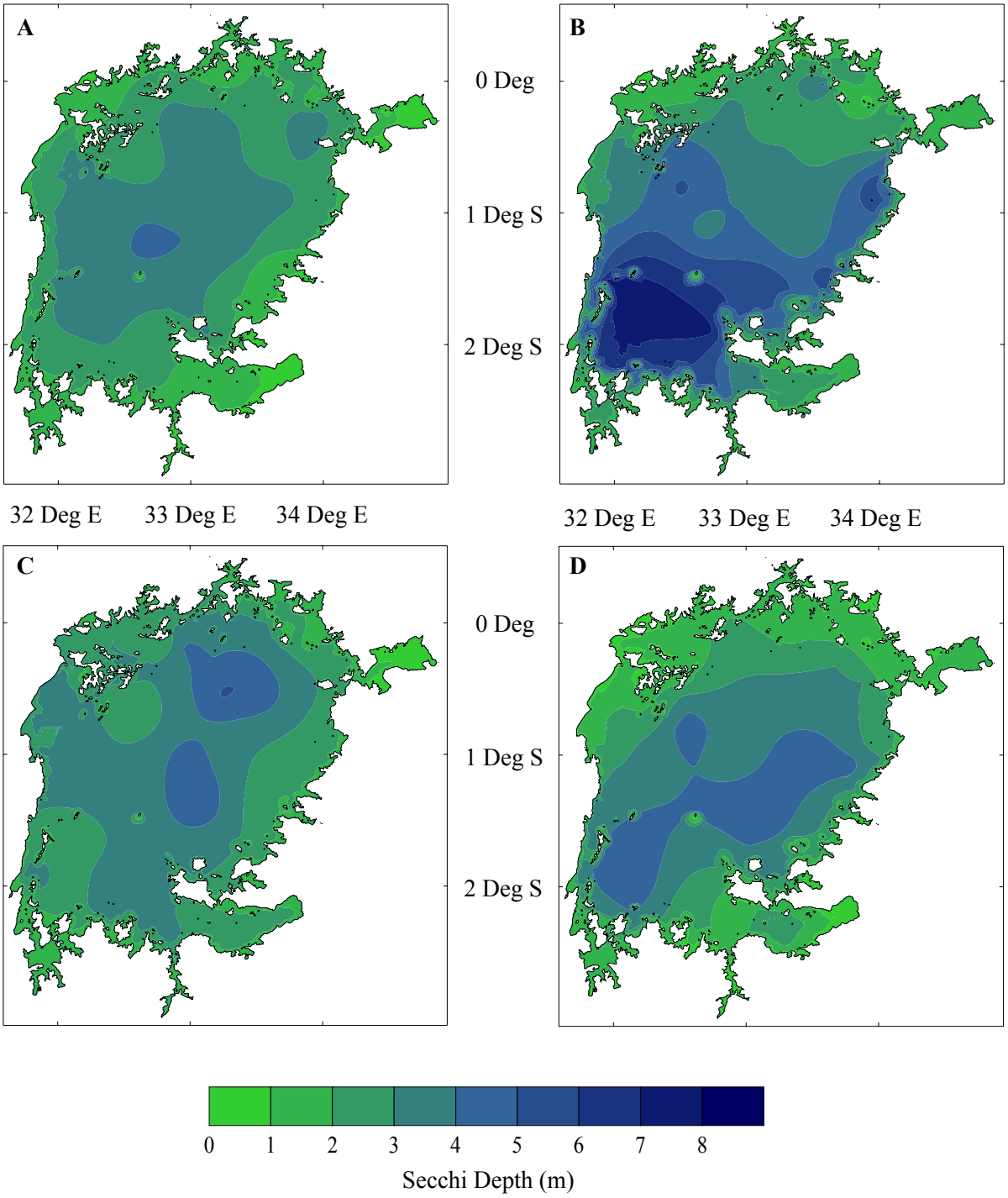

Figure 3.27: Spatial patterns of Secchi depth in Lake Victoria in A) February 2000, B) August 2000, C) February 2001 and D) August 2001.

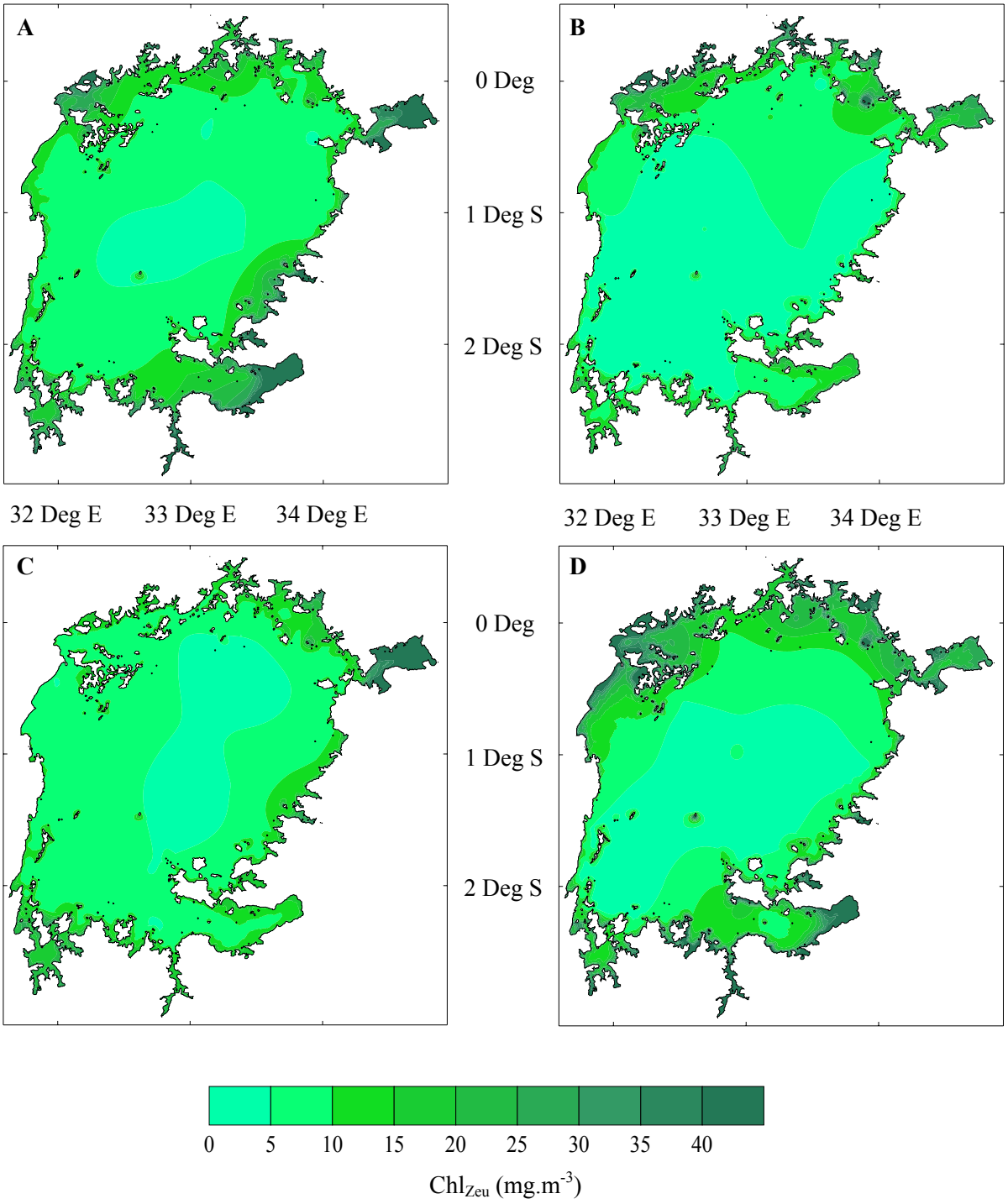

Figure 3.28: Spatial patterns of chlorophyll in Lake Victoria calculated from the secchi depth distribution (Figure 3.27) with the regression equation relating the two parameters (Figure 2.6A) for A) February 2000, B) August 2000, C) February 2001 and D) August 2001.

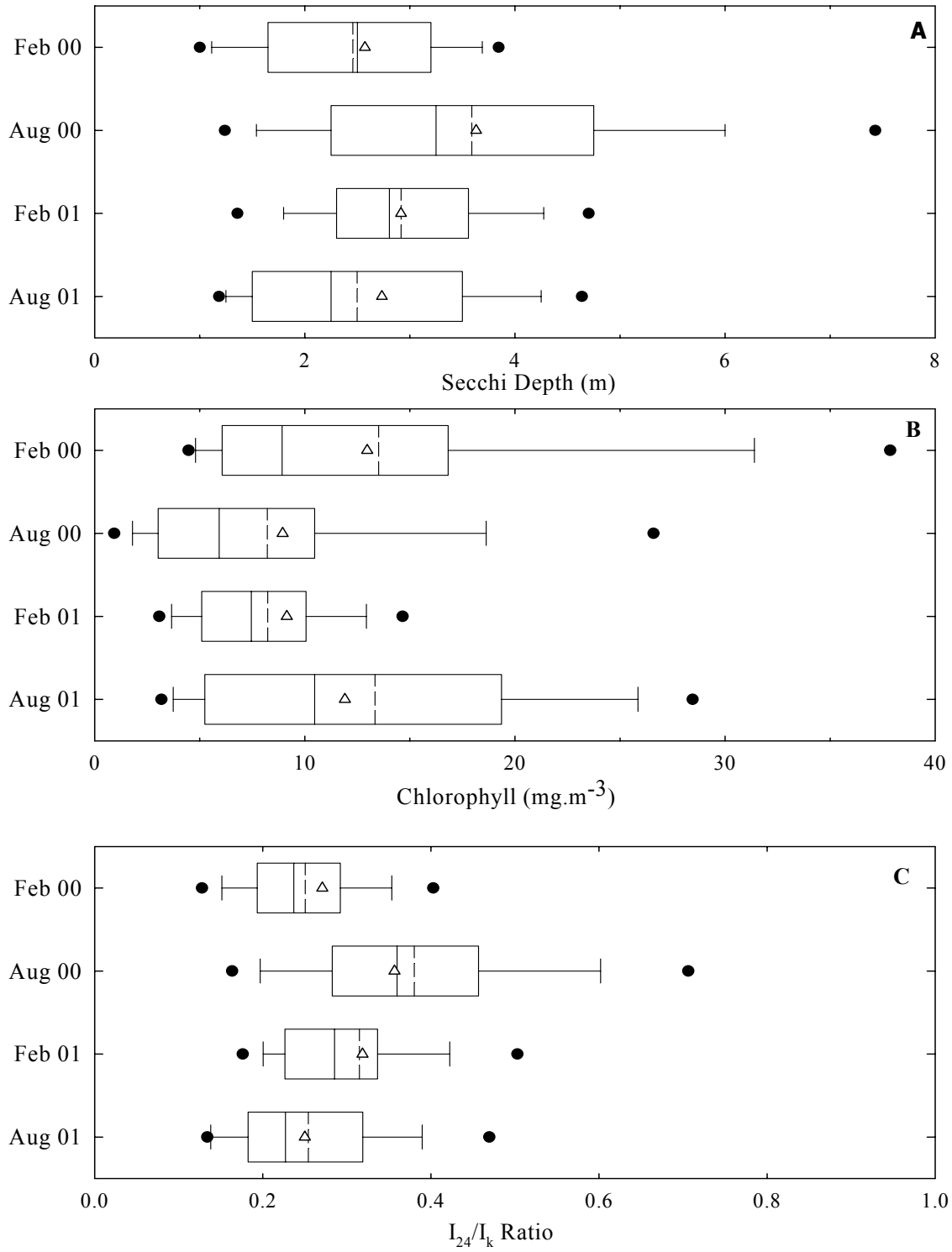

Figure 3.29: Statistical range of A) Secchi depth (m), B) chlorophyll ($mg.m^{-3}$) and C) the I_{24}/I_k ratio for cruises with dates shown. Circles represent minimum and maximum values, whiskers represent 5th and 95th percentile, solid box line indicates 25th, mode and 75th percentile and dashed line indicates the mean. Hollow triangles correspond to the spatially interpolated mean.

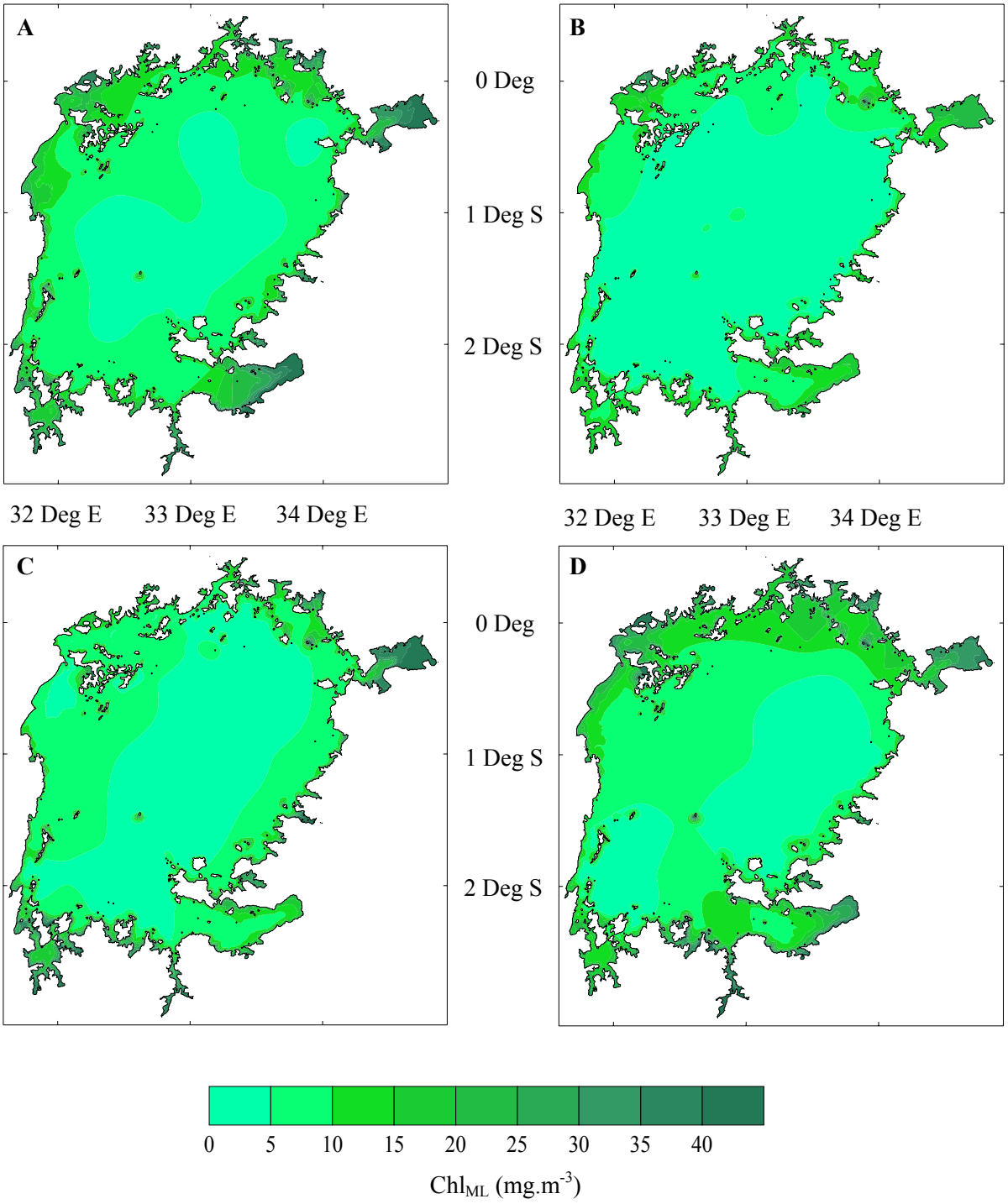

Figure 3.30: Spatial patterns of the average chl concentration within the mixed layer in A) February 2000, B) August 2000, C) February 2001 and D) August 2001.

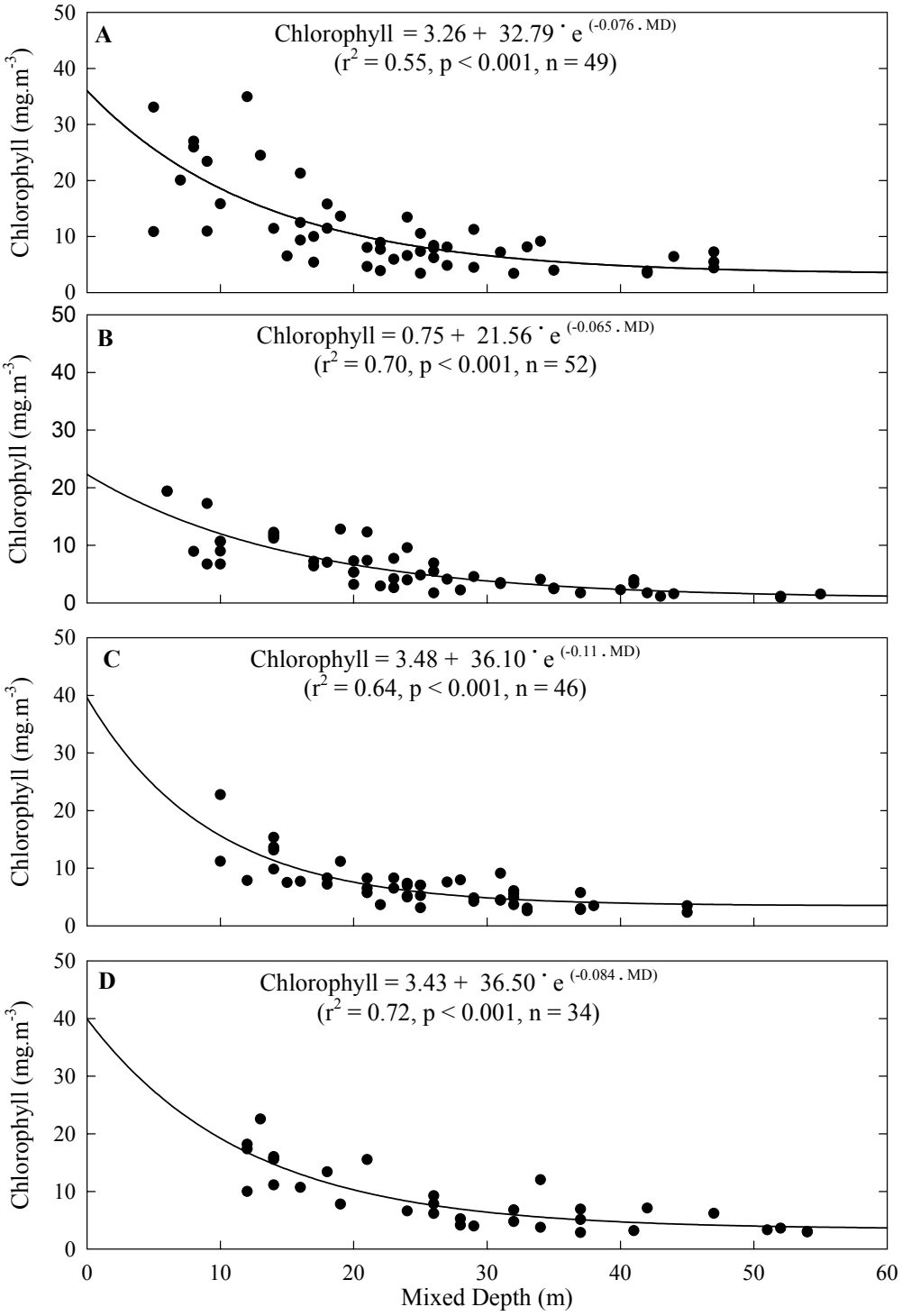

Figure 3.31: Regression of mixed depth versus the average volumetric chlorophyll concentration in the mixed layer for A) February 2000, B) August 2000, C) February 2001 and D) August 2001.

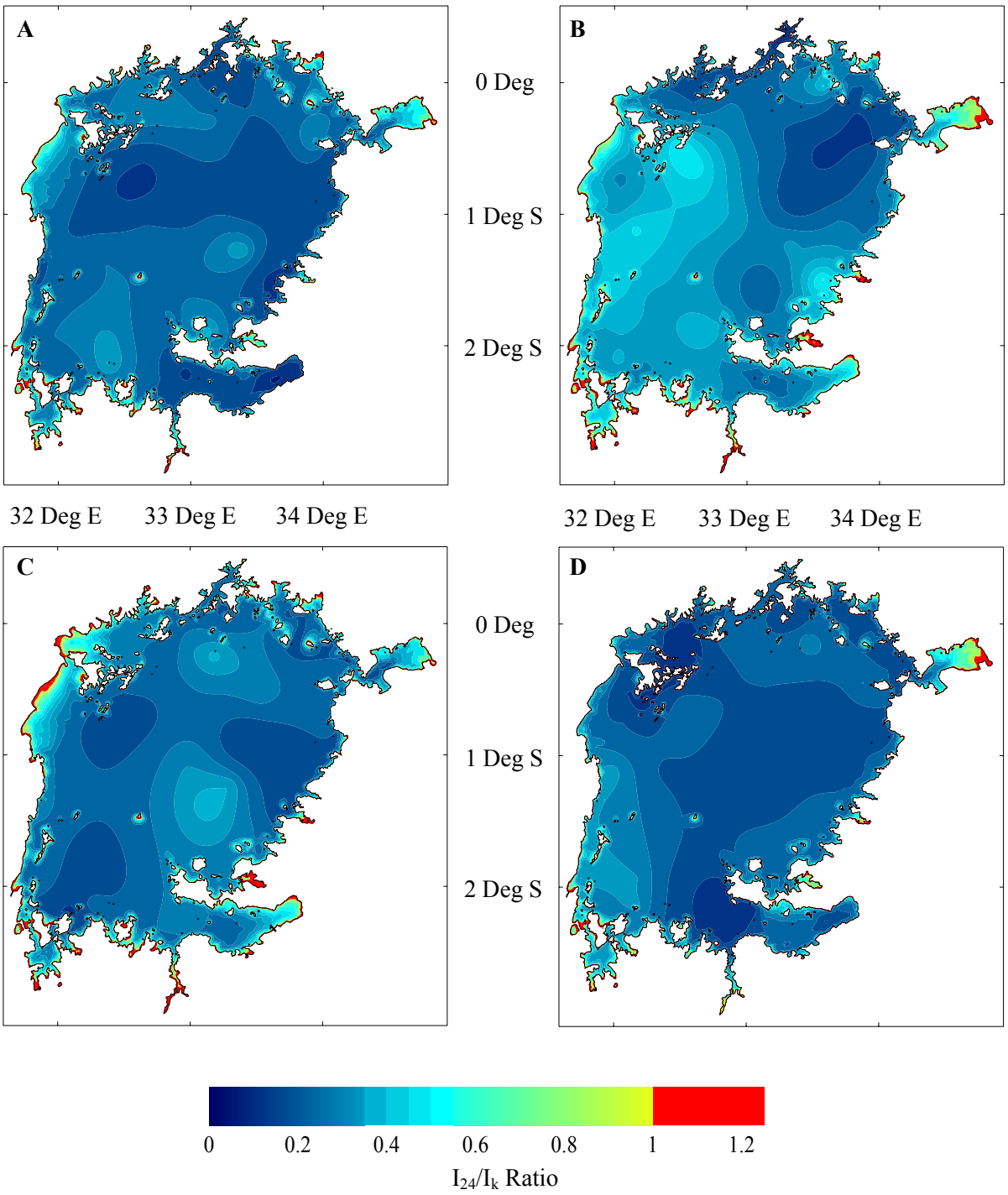

Figure 3.32: Spatial patterns of the I_{24}/I_k ratio in Lake Victoria in A) February 2000, B) August 2000, C) February 2001 and D) August 2001.

3.4 Discussion

Figure 3.9 to Figure 3.27 show that the thermal structure, dissolved oxygen isopleths and Secchi depths are spatially heterogeneous and that these patterns are at times more complex than the unidirectional hypothesis of warmer water in the north and cooler water in the south (Spigel and Coulter 1996) that has been observed in historic latitudinal transects (Kitaka et al. 1972; Romero et al. 2001). This spatial complexity demonstrates that previous research conducted in the northern offshore waters of Lake Victoria cannot be considered representative of the entire offshore region; therefore spatial extrapolations of temporal offshore studies of phytoplankton production (Mugidde 1993), hypolimnetic deoxygenation (Hecky et al. 1994) and algal N-fixation (Mugidde et al. 2003) will not yield accurate lakewide annual estimates. Owing to this spatial complexity, only a three-dimensional hydrodynamic model could predict temporal lakewide thermal structure dynamics. Unfortunately, the absence of measured meteorological data over Lake Victoria and discrepancies amongst reported mean meteorological forcings, specifically wind speed and direction, inhibits any realistic attempt to model the lake's physical limnology until offshore data becomes available. However, lakewide limnological patterns presented in this chapter can be applied to the derived limnological relationships presented in Chapter 2 to facilitate time and space specific estimates of gross and net phytoplankton production for the cruise months in 2000 and 2001, as shown in Chapter 4. Furthermore, by assuming general meteorological patterns over Lake Victoria in conjunction with thermal structure patterns shown in this chapter, alternative hypotheses concerning prominent processes in Lake Victoria's water balance and thermal structure can now be proposed. Aside from providing a new conceptual framework for Lake Victoria's physical limnology, this task assists future assumptions of spatial and temporal extrapolation of relevant limnological processes.

The general agreement between wind speed magnitudes acquired from NCEP-DOE R2 (Figure 3.6) with open-lake measurements (Ochumba 1996) suggest that the lower wind speeds used to model Lake Victoria's water balance (Yin and Nicholson 1998) may be underestimating evaporation. Furthermore, the observed increase in wind speed with fetch length follows the theory

that thermal land winds do not reach maximum speeds until approximately 50 km offshore (Asnani 1993), further validating the hypothesis that land-based meteorological stations underestimate wind speed. As the water balance model of Yin and Nicholson (1998) has been successfull in hindcasting changes in historic water levels, supposed higher evaporation must be offset by another hydrologic term. As rainfall stations in the northwest of the lake, where most precipitation occurs (Asnani 1993) were not used in the water balance (Yin and Nicholson 1998), higher evaporation is most likely offset by increased over-lake precipitation. Fortunately, Yin and Nicholson (1998) provide sensitivity graphs showing anticipated changes in evaporation for specific wind speeds. NCEP-DOE R2 wind speeds for 2000 and 2001 increase evaporation to approximately 1950 and 1800 mm per year from the original value of 1743 mm as calculated using the Penman method according to the sensitivity graph (Yin and Nicholson 1998). Increases in annual evaporation and precipitation over Lake Victoria carry important consequences. Wet deposition of nutrients through rainfall is a major source of P into Lake Victoria (Tamatamah 2002), such that nutrient budgets require an accurate estimate of precipitation. Secondly, the increase in both wind speed and evaporation estimates with fetch length can result in differential cooling over Lake Victoria, providing a mechanism for observed horizontal temperature variability. The effect of cloud cover on incoming radiation may also reinforce such patterns (Yin and Nicholson 2000).

Historical latitudinal transects have shown horizontal temperature variability from February through April (Kitaka 1972, Figure 7.6; Romero et al. 2001, Figure 7.7) with cooler water in the south and warmer water in the north, while thermal stability in the northern offshore waters of Lake Victoria decreases through these months (Hecky 1993). Northward surface seiching and a latitudinal gradient of evaporation decreasing from the south has been hypothesized to cause horizontal temperature variability (Spigel and Coulter 1996), while a seasonal increase in evaporative cooling remains the most current explanation for the temporal decrease in thermal stability leading to an isothermal water-column around or after April (Talling 1965; Spigel and Coulter 1996). What has not been explicitly noted in the literature is that from February through April horizontal temperature

variability increases and the decrease in thermal stability is not only reached through a cooling of the epilimnion but also warming of the hypolimnion, as shown by Ramlal (2002, Figure 7.3) whose offshore temperature profiles were taken in the same year as the transects of Romero et al. (2001). The following interpretation of these observations is validated with spatial patterns of temperature and dissolved oxygen presented in this chapter: Isothermal conditions in the northern offshore waters in Lake Victoria are not reached simply through a seasonal increase in evaporative cooling; higher concurrent evaporation elsewhere causes hypolimnetic water in the north of the lake to laterally advect away leading to downwelling of epilimnetic isotherms in the north and hypolimnetic upwelling elsewhere. Furthermore, the orientation of these processes is not only along a latitudinal gradient (as hypothesized by Spigel and Coulter 1996) but can vary spatially due to thermal winds. Areas of upwelling have increased water transparency due to lower phytoplankton biomass, as shown with the correlations between Secchi depths and surface temperature during each cruise.

During February and August, seasonal winds have a substantial easterly component (Figure 3.7, Hills 1978, Yin and Nicholson 1998). If seiching and a decreasing evaporation gradient upwind are the prominent hydrodynamic mechanisms in Lake Victoria (Spigel and Coulter 1996), the coolest waters will be along the upwind eastern coastline and the warmest water will be along the downwind western shore (Imberger and Patterson 1990). However as shown in Figure 3.9A, Figure 3.9B, Figure 3.12B, Figure 3.15A, and Figure 3.18B Lake Victoria's thermal structure has gradients of increasing temperature from west to east, contradictory to the above stated prediction, assuming the wind field is accurate. As the increased presence of cool water in the west coincides with a shallower oxic-hypoxic interface westward shown in Figure 3.21A and Figure 3.23A, and deeper Secchi depths relative to other areas during individual cruises, the physical mechanism causing these horizontal gradients also creates spatial variability of limnological parameters. The presence of cool westerly water supports the hypothesis that high rates of evaporation coincide with frequent and strong convection localized over western Lake Victoria during the rainy seasons (Kitaka 1972, Figure 7.5; Asnani 1993; Yin et al. 2000, Figure 7.4). Furthermore, nocturnal westerly land winds often

associated with these convective events (Yin et al. 2000) would induce eastwards surface currents with concurrent westward currents at depth (Stevens and Imberger 1996; Figure 3.33). This hydrodynamic circumstance would cause the observed westerly oxycline upwelling and could also transport phytoplankton from deep waters to the surface. As profiles have shown that phytoplankton biomass generally decreases with depth, an upwelling event could explain the deeper Secchi depths in western Lake Victoria. Increased precipitation over western Lake Victoria (Asnani 1993; Nicholson and Yin 1998) may also be responsible for cooler water in this area. Precipitation falls at temperature approximately equivalent to air temperature (Dingman 2002), which can be lower than 20°C at night when most precipitation over western Lake Victoria occurs.

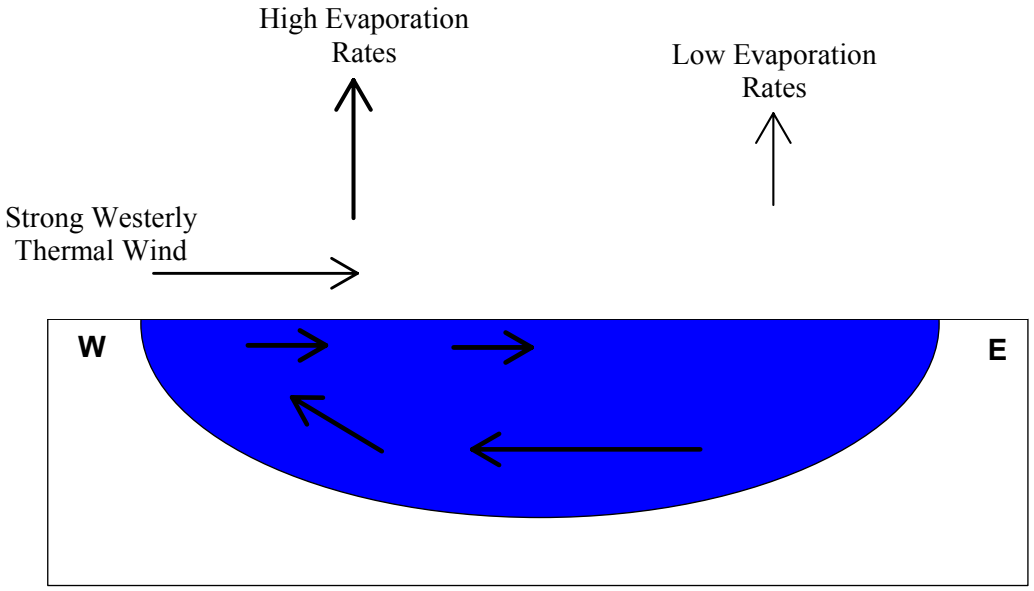

Figure 3.33: Idealized diagram showing a strong westerly thermal wind that causes eastward surface waters, increased evaporative cooling in the west and westward currents from depth.

A second prominent feature of the planimetric and cross-section temperature diagrams is the presence of a north-south gradient, with the warmest surface water always located in the north of Lake Victoria. A latitudinal evaporation gradient may be partially responsible for this feature (Spigel and Coulter 1996), although there is also strong evidence suggesting lateral advection of warm water to the offshore also contributes to this pattern: As shown in Figure 3.5, shallower archipelagos and

embayments dominate the morphometry of the northern extent of Lake Victoria. Similar to Nyanza Gulf, where the dominant water currents indicate advection to open waters (Ochumba 1996), these shallow areas are more sheltered from seasonal and thermal winds and are therefore anticipated to be warmer than the open central basin (Imberger and Parker 1985) as confirmed in Lake Victoria by MacIntyre et al. (2002). The warmest epilimnetic waters in the open central basin for all four cruises are located near these shallow areas, specifically evident along the eastern extent of Figure 3.9A, Figure 3.15A and Figure 3.18A as well as the northern extent of Figure 3.9C, Figure 3.12C, Figure 3.15C and Figure 3.18C. Lateral advection from shallower protected areas may serve as an important transport mechanism to offshore epilimnetic waters. This is particularly evident in the cross-lake chlorophyll measurements of Mugidde (2001), where offshore values were highest closest to the north of the lake, perhaps indicating advection of chl rich water from warmer inshore areas. North-south temperature gradients are also associated with upwelling of oxyclines, particularly pronounced in February 2001 as shown in Figure 3.23C, and spatial patterns in Secchi depths. Southerly upwelling is associated with deeper Secchi depths, this feature is particularly pronounced during the August cruises where warm northerly and cool southerly water (Figure 3.11A and Figure 3.17A) occur with a general pattern of shallower Secchi depths northwards.

The cold mass of surface water in Sango Bay observed in February 2000 corresponds with the entry point of the Kagera River, by far the largest river flowing into Lake Victoria. As inflows are generally cooler than lakes (Imberger and Patterson 1990) and can be up to 6°C colder than surface water temperatures in Lake Victoria (Ochumba and Manyala 1992), it is probable that this cool water mass originates from the Kagera River, whose flow is particularly high in February. When vertical turbulence in the water column is sufficient, gravity currents formed by cooler denser water become entrained with warmer water and create a horizontal density gradient (Linden and Simpson 1986). As this cool water mass is not apparent in the 20 m temperature distribution (Figure 3.9B), it is likely that the cool riverine water is being actively mixed with the lake, thereby decreasing the water temperature and contributing to the observed horizontal temperature gradients in this area. This

feature is also present in Sango Bay in February 2001 (Figure 3.14A), although as water temperatures in Sango Bay are approximately 0.5°C warmer compared to February 2000, riverine flow may have been lower in 2001.

Aside from the general thermal structure patterns and suspected processes outlined above, there are also differences between the two years. Interannual differences are particularly pronounced through the comparison of February 2001 with February 2000 and August 2001 with August 2000. In February 2001, epilimnetic waters are cooler, hypolimnetic waters are warmer, thermal stability is lower, Secchi depths are deeper, meaning algal biomass is lower, while AHOD is 36% less compared to February 2000. In August 2001, epilimnetic and hypolimnetic waters are warmer, thermal stability is higher, Secchi depths are shallower and mixed depths are deeper causing a lower lakewide average of the I_{24}/I_k ratio compared to August 2000. Published descriptions of climatic variability in East Africa are limited, where most researchers have analyzed the relationship between El-Nino events with sea surface temperatures (SSTs) in the Indian Ocean and how this affects precipitation within East Africa. The most significant impact on climactic variability in the Lake Victoria basin through El-Nino events or SST anomalies is an increase in precipitation during the short rainy season in November to December (Birkett et al. 1999), and reports indicate that areas of Kenya, Uganda and Tanzania experienced the highest amount of precipitation since 1961 during the short rainy season of 2000 (WMO Bulletin 2001). The effect of increased seasonal precipitation on Lake Victoria's thermal structure is unknown, although a similar event in 1961 substantially increased the water level (Yin and Nicholson 1998). As rainy seasons in the Lake Victoria basin are associated with increased cloudiness and convective events, it is likely that increased cloudiness during the short rains (October to December of 2000) decreased heating of the lake while evaporation increased cooling of the lake, explaining the cooler surface waters in February 2001. Furthermore, as it has been hypothesized that hydrodynamic events associated with convective storms in the rainy season increase hypolimnetic upwelling, lower AHOD and warmer hypolimnetic temperatures observed in February 2001 may be attributed to hypothesized increased upwelling.

Aside from thermal structure features and hypothesized physical processes, several features relevant to phytoplankton production are illustrated in this chapter. Lakewide averages of the I_{24}/I_k ratio, used to estimate the degree of light-limitation on phytoplankton production (Hecky and Guildford 1984), range from 0.27 in February 2000 to 0.40 in August 2000. These values are slightly higher than both the offshore and inshore averages presented by Mugidde (1992) of 0.17 and 0.23 respectively. This small discrepancy infers that light limitation is less severe than originally hypothesized and probably reflects a methodological discrepancy. Mugidde (1992) used the metalimnion to delineate the mixed depth, where in this study the maximum gradient of chlorophyll fluorescence coinciding with any discernable temperature or oxygen gradient delineates an equivalent or shallower mixed depth than Mugidde (1992). Furthermore, the highest spatially averaged I_{24}/I_k ratio in August 2000 does not occur with the shallowest average mixed depth. Aside from suggesting that phytoplankton production may be highest in August 2000 through the least severe light limitation, this finding contradicts the hypothesis that the mixed depth is the most critical term determining the I_{24}/I_k ratio. Instead, deep euphotic depths in August 2000 inferred from deep Secchi depths causes the higher I_{24}/I_k ratio relative to the other months. Low chl inferred from deep Secchi depths may be due to deeper mixed depths in previous months following the concept that k_{PAR}, which is related to Secchi depths (Figure 2.6C), is a lag variable.

Average offshore chl concentrations in each cruise are slightly lower than the offshore annual average of 13.5 $mg.m^{-3}$ measured by Mugidde et al. (2003) at Bugaia Island. However measurements from a cross-lake transect in December 1994 revealed that chl concentrations in the offshore are predominantly between 5 and 10 $mg.m^{-3}$ (Mugidde 2001), close to the offshore spatial averages presented in this chapter. Higher offshore chl at Bugaia Island may be due to advection of chl rich water from warmer inshore areas but may also be attributed to shallower mixed depths at Bugaia Island relative to the rest of the offshore (Figure 3.26). Figure 3.31 illustrates that chl_{ML} is highly correlated to the mixed depth indicating that, similar to the bottom depth of inshore areas in Chapter 2, the depth of mixing sets an upper limit on chlorophyll. Furthermore, the statistical similarity of the

regression equations for each cruise presented in Figure 3.31 suggests that the relationship between mixed depths and chl_{WC} has small temporal and spatial variance. Some of the unexplained variability in the relationships presented in Figure 3.31 probably occurs when Secchi depths are small relative to mixed depths, which as already noted may occur through hypolimnetic upwelling. This observation is again similar to a conclusion drawn in Chapter 2, that is hydrodynamic exchange of water masses with areas of differing depths can temporarily decouple the relationship between mixed depths (bottom depth in Chapter 2) and chlorophyll. Concepts and data from both Chapter 2 and this chapter are combined in Chapter 4 to further validate the relationship between mixed depths and chl_{WC} while the I_{24}/I_k ratio provides further insights into phytoplankton production.

3.5 Work Cited

Asnani, G.C. 1993. Tropical Meteorology. Volume 2. Indian Institute of Tropical Meteorology.

Ba, M.B. and S.E. Nicholson. 1998. Analysis of convective activity and its relationship to the rainfall over the Rift Valley Lakes of East Africa during 1983-90 using the metosat infrared channel. Journal of Applied Meteorology. 37: 1250-1264.

Behrenfeld, M.J., O. Prasil, M. Babin and F. Bruyant. 2004. In search of a physiological basis for covariations in light-limited and light-saturated photosynthesis. Journal of Phycology. 40: 4-23.

Birkett, C., R. Murtugudde and T. Allan. Indian Ocean climate event brings floods to East Africa's lakes and the Sudd Marsh. Geophysical research letters. 26: 1031-1034.

Brutseart, W.H. 1982. Evaporation into the atmosphere: Theory, history and applications: Dordrecht: D. Reidel.

Carlson, J. 2002. Development for an optimized dissolved oxygen sensor for oceanographic profiling. International Ocean Systems. 6: 1-4.

Charlton, M.N. 1980. Hypolimnion oxygen consumption in lakes: Discussion of productivity and morphometry effects. Canadian Journal of Fisheries and Aquatic Sciences. 37: 1531-1539.

Chow, V.T., Maidment, D.R. and L.W. Mays. 1988. Applied Hydrology. New York: McGraw-Hill.

Dingman, L. 2002. Physical Hydrology. Prentice Hall.

Fish, G.R. 1957. A seiche movement and its effects on the hydrology of Lake Victoria. Fish. Publ. Lond. 10: 1-68.

Flohn, H. and K. Fraedrich. 1966. Tagesperiodische zirkulation und niederschlagsverteilumn am Victoria-See (Ostafrika). Meteorol. Rundschau. 19: 157-165.

Fofonoff, N.P. and R.C. Millard. 1983. Algorithms for computation of fundamental properties of seawater. UNESCO technical papers in marine science #44.

Guildford, S.J. and R.E. Hecky. 2000. Total nitrogen, total phosphorus, and nutrient limitation in lakes and oceans: Is there a common relationship. Limnology and Oceanography. 45: 1213-1223.

Hamblin, P.F., H.A. Bootsma and R.E. Hecky. 2003A. Surface meteorological observations over Lake Malawi/Nyasa. Journal of Great Lakes Research. 29: 19-33.

Hamblin, P.F., H.A. Bootsma and R.E. Hecky. 2003B. Modeling nutrient upwelling in Lake Malawi/Nyasa. Journal of Great Lakes Research. 29: 34-47.

Hecky, R.E. 1993. The eutrophication of Lake Victoria. International Association of Theoretical and Applied Limnology. 25: 39-48.

Hecky, R.E., F.W.B. Bugenyi, P. Ochumba, J.F. Talling, R. Mugidde, M. Gophen and L. Kaufman. 1994. The deoxygenation of Lake Victoria. Limnology and Oceanography. 39: 1476-1481.

Hecky, R.E., H.A. Bootsma, R. Mugidde and R.W.B. Bugenyi. 1996. Phosphorus pumps, nitrogen sinks, and silicon drains: Plumbing nutrients in the African Great Lakes. In. Johnson, T.C. and E. Odada [eds]. The limnology, climatology and paleoclimatology of the East African Lakes.

Hecky, R.E., P. Campbell and L.L. Hendzel. 1993. The stoichiometry of carbon, nitrogen and phosphorus in particulate matter of lakes and oceans. Limnol. Oceanogr. 38: 709-724.

Hecky, R.E. and S.J. Guildford. 1984. Primary productivity of Southern Indian Lake before, during, and after impoundment and Churchill River diversion. Canadian Journal of Fisheries and Aquatic Sciences. 41: 591-604.

Hecky, R.E. and P. Kilham. 1988. Nutrient limitation of phytoplankton in freshwater and marine environments: A review of recent evidence on the effects of enrichment. Limnology and Oceanography. 33: 796-822.

Hills, R.C. 1979. The structure of the Inter-Tropical Convergence Zone in Equatorial Africa and it relationship to East African rainfall. Transactions of the Institute of British Geographers, New Series. 4: 329-352.

Imberger, 1985. The diurnal mixed layer. Limnology and Oceanography. 30: 737-770.

Imberger, J. and G. Parker. 1985. Mixed layer dynamics in a lake exposed to a spatially variable wind field. Limnology and Oceanography. 30: 473-488.

Imberger, J. and Patterson, J.C. 1990. Physical limnology. Advances in Applied Mechanics. 27: 303-475.

Johnson, L.B. and S.H. Gage. 1997. Landscape approaches to the analysis of aquatic ecosystems. Freshwater Biology. 37: 113-132.

Kanamitsu, M., W. Ebisuzaki, J. Woollen, S-K Yang, J.J. Hnilo, M. Fiorino, and G. L. Potter. 2002. NCEP-DEO AMIP-II Reanalysis (R-2). Bul. of the Atmos. Met. Soc. 83: 1631-1643.

Kirk, J.T.O. 1994. Light and photosynthesis in aquatic ecosystems. Cambridge University Press.

Kitaka, G.E.B. 1972. An instance of cyclonic upwelling in the southern offshore waters of Lake Victoria. African Journal of Tropical Hydrobiology and Fisheries. 2: 85-92.

Kite, G.W. 1981. Recent changes in level of Lake Victoria. Hydrology Science Bulletin. 26: 233-243.

Kling, G.W. 1988. Comparative transparency, depth of mixing, and stability of stratification in lakes of Cameroon, West Africa. Limnology and Oceanography. 33: 27-40.

Kling, H.J., R. Mugidde and R.E. Hecky. 2001. Recent changes in the phytoplankton community of Lake Victoria in response to eutrophication. In: M. Munawar and R.E. Hecky (eds). The Great Lakes of the World (GLOW): Food-web, health and integrity. 47-65.

Linden, P.F. & Simpson, J.E. 1986. Gravity driven flows in a turbulent fluid. J. Fluid Mech. 172: 481-497.

MacIntyre, S., Romero, J.R. and G.W. Kling. 2002. Spatial-temporal variability in surface layer deepening and lateral advection in an embayment of Lake Victoria, East Africa. Limnology and Oceanography. 47: 656-671.

Melack, J.M. 1976. Primary productivity and fish yields in tropical lakes. Transactions of the American Fisheries Society. 105: 575-560.

Mistry, V.V. and D. Conway. 2003. Remote forcing of East African rainfall and relationships with fluctuations in levels of Lake Victoria. International Journal of Climatology. 23: 67-89.

Mortimer, C.H. 1974. The oxygen content of air-saturated fresh waters over ranges of temperature and atmospheric pressure of limnological interest. Mitte. Internat. Verien. Limnol. 22: 1-17.

Mugidde, R. 1992. Changes in phytoplankton productivity and biomass in Lake Victoria (Uganda). M.Sc. Thesis, University of Manitoba. Winnipeg, Canada.

Mugidde, R. 1993. The increase in phytoplankton primary productivity and biomass in Lake Victoria (Uganda). International Association of Theoretical and Applied Limnology. 25: 846-849.

Mugidde, R. 2001. Nutrient status and phytoplankton nitrogen fixation in Lake Victoria, East Africa. Ph.D. Thesis, University of Waterloo, Waterloo, Canada.

Mugidde, R., R.E. Hecky, L.L. Hendzel and W.D. Taylor. 2003. Pelagic nitrogen fixation in Lake Victoria (East Africa). Journal of Great Lakes Research. 29: 76-88.

Newell, B.S. 1960. The hydrology of Lake Victoria. Hydrobiologia. 15: 363-383.

Nicholson, S.E. and X. Yin. 2002. Mesoscale patterns of rainfall, cloudiness and evaporation over the Great Lakes of East Africa. In Odada, E.O. and D.O. Olago [eds]. The limnology, climatology and paleoclimatology of the East African Lakes.

Ochumba, P.B.O. 1996. Measurement of water currents, temperature, dissolved oxygen and winds on the Kenyan Lake Victoria. In The East African Great Lakes.

Ochumba, P.B.O. and J.O. Manyala. 1992. Distribution of fishes along the Sondu-Miriu River of Lake Victoria, Kenya with special references to upstream migration, biology and yield. Journal of Aquac. Fish. Man. 23: 701-719.

Owens, W.B., and R.C. Millard Jr., 1985: A new algorithm for CTD oxygen calibration. J. Physical Oceanography. 15, 621-631.

Ramlal, P.S. 2002. Sources, transport and sinks of organic matter in Lake Malawi and Lake Victoria, East Africa. Ph.D. Thesis, University of Waterloo, Waterloo, Canada.

Ramlal, P.S., G.W. Kling, L.M. Ndawula, R.E. Hecky and H.J. Kling. 2001. Diurnal fluctuations in PCO2, DIC, oxygen and nutrients at inshore sites in Lake Victoria, Uganda. In Munawar and R.E. Hecky [eds]. The Great Lakes of the World (GLOW): Food-web, health and integrity. 67-82.

Romero, J., J. Imberger, S. MacIntyre and G.W. Kling. 2001. Persistent spatial and temporal patterns in lakes and reservoirs. http://www.cwr.uwa.edu.au/Presentations/index.html.

Rotuuno, R. 1983. On the linear theory of the land and sea breeze. Journal of Atmospheric Science. 40: 1999-2009.

Savijarvi, H. 1997. Diurnal winds around Lake Tanganyika. Q.J. R. Meteorol. Soc. 123: 901-918.

Sea-bird Electronics Inc. 2001. Computing temperature and conductivity slope and offset correction coefficients from laboratory calibrations and salinity bottle samples. Application Note # 31.

Sea-bird Electronics Inc. 2002. Conversion of pressure to depth. Application Note # 69.

Sene, K.J. and D.T. Plinston. 1994. A review and update of the hydrology of Lake Victoria in East Africa. Hydrological Sciences. 39: 47-63.

Seitzinger, S.P. 1988. Denitrification in freshwater and coastal marine ecosystems: Ecological and geochemical significance. 33: 702-724.

Silsbe, G.M. 2003. A new digital map for Lake Victoria, East Africa. Bulletin of the International Decade for East African Lakes.

Spigel, R.H. and G.W. Coulter. 1996. Comparison of hydrology and physical limnology of the East African Great Lakes: Tangyanika, Malawi, Victoria, Kivu and Turkana (with reference to some North American Great Lakes. In Johnson, T.C. and E. Odada [eds]. The limnology, climatology and paleoclimatology of the East African Lakes.

Stevens, C. and J. Imberger. 1996. The initial response of a stratified lake to a surface shear stress. Journal of Fluid Mechanics. 312: 39-66.

Talling, J.F. 1965. The photosynthetic activity of phytoplankton in East African lakes. Int. Revue ges. Hydrobiol. 50: 1-32.

Talling, J.F. 1966. The annual cycle of stratification and phytoplankton growth in Lake Victoria (East Africa). Int. Revue ges. Hydrobiol. 51: 545-621.

Talling, J.F. and I.B. Talling. 1965. The chemical composition of African lake waters. Internationale Revue der gesamten Hydrobiologie. 50: 421-463.

Tamatamah, R.A. 2002. Nonpoint source loading of phosphorus to Lake Victoria from the atmosphere and rural catchments in Tanzania, East Africa. Ph.D. Thesis, University of Waterloo, Waterloo, Canada.

Toompu, A. and F. Wulff. 1996. Optimum spatial analysis of monitoring data on temperature, salinity and nutrient concentrations in the Baltic proper. Environmental Monitoring and Assessment. 43: 283-306.

Verburg, P. 2004. Climate effects on lake circulation and its importance to the pelagic ecosystem in Lake Tanganyika, East Africa. Ph.D. Thesis, University of Waterloo, Waterloo, Canada.

Verburg, P. and R.E. Hecky. 2003. Wind patterns, evaporation, and related physical variables in Lake Tanganyika (East Africa). Journal of Great Lakes Research. 29: 48-61.

World Meteorological Organization. 2001. World Climate News. Bulletin 19. Geneva, Switzerland.

Yin, X., S.E. Nicholson and M.B. Ba. 2000. On the diurnal cycle of cloudiness over Lake Victoria and its influence on evaporation from the lake. Hydrological Sciences. 45: 407-424.

Yin, X. and S.E. Nicholson. 1998. The water balance of Lake Victoria. Hydrological Sciences: 43: 789-811.

Zeeb, R.E. and D. Wolf-Gladrow. 2001. CO2 in seawater : equilibrium, kinetics and isotopes. Elsevier. New York, USA.

Chapter 4: Lakewide Phytoplankton Production Estimates for Lake Victoria, East Africa

4.1 Introduction

Lake Victoria's fishery increased seven-fold between 1968 to its peak in 1990 when an estimated 787,899 tonnes of fish were landed (Mkumbo and Cowx 1999), making it the world's largest freshwater fishery. The enormity of this fishery is largely attributed to two introduced species, *Lates niloticus* and *Oreochromis niloticus*, which along with the endemic *Rastrineobola argentea* compromise the three dominant species in Lake Victoria in terms of biomass and economic value (Ogutu-Owayo 1990). By 1995 there had beeen a 48% decline in the fish landed from the 1990 maximum (Mkumbo and Cowx 1999), while a fourfold increase in fishing boats during the past decade (FSTC 2000) and the continual emergence of new fish processing plants are leading to growing concern amongst stakeholders that Lake Victoria's present-day fishery may not be sustainable (Ntiba et al. 2001). As the increase in the lake's fishery between 1968 and 1990 is estimated to have created 150,000 new jobs and a three-fold increase in net economic benefits (Greboval 1990) while providing the region's most inexpensive source of dietary protein, a collapsed fishery would be detrimental to the Lake Victoria basin.

Many models are available to estimate a fisheries maximum sustainable yield (MSY) from an array of limnological and morphometric parameters, for example mean depth (Rawson 1955), surface area (Rounsefell 1946), total dissolved solids (Northcote and Larkin 1956) and a morphoedaphic index of total dissolved solids divided by mean depth (Ryder et al. 1974). Current estimates for the MSY of Lake Victoria's fishery range from 93,000 to 690,000 Mg per year as determined using several models with 300,000 Mg per year considered as the 'best-guess' MSY (Pitcher and Bundy 1994). Phytoplankton production has also been used as a correlative predictor of MSY (Oglesby 1977). A log-linear model relating gross phytoplankton production (PP_G) to fish yield proposed by Melack (1976) provides a better empirical fit to 9 large African lakes including Lake Victoria (r^2 =

0.82) than the commonly used morphoedaphic index ($r^2 = 0.004$). Melack's (1976) estimates from Lake Victoria are based on pre-eutrophication PP_G from only one inshore and offshore station (Talling 1966) and now outdated estimates of fisheries yield (Kudhongania and Cordone 1974), however past success of this approach warrants current data.

Unlike other models, the relationship between phytoplankton production and fish yield is based on theoretical food web principles. Specifically, the amount of production at one trophic level is related to another trophic level through a coefficient describing the efficiency of carbon transfer between different trophic levels. This concept has been formalized as a mass balance food web model (Pauly et al. 2000), and the transfer efficiency of carbon to the next highest trophic level is on average 10% (Pauly and Christensen 1995) but may be higher in efficient ecosystems such as tropical Lake Tanganyika (Hecky et al. 1981). Equation 4.1 summarizes the use of the transfer efficiency of carbon in this chapter. $P_{[N]}$ refers to net production at trophic level n, and is related to net production at trophic level n+x through the product of itself and TE^X where TE is the transfer efficiency of carbon (0.10) and x is the number of trophic levels above n.

Equation 4.1) $P_{[N]} = P_{[N+X]} \cdot TE^X$

This chapter presents a novel model allowing estimates of PP_G and net phytoplankton production (PP_N) based on empirical relationships developed and discussed in Chapter 2, and applies this model to lakewide data presented in Chapter 3 to generate lakewide monthly estimates of PP_G and PP_N for February and August 2000 and 2001. These estimates are temporally extrapolated to provide the first spatially-explicit estimates of annual lakewide PP_G and PP_N in Lake Victoria that are in turn used to estimate an MSY using both the relationship of Melack (1976) and the carbon transfer efficiency approach of Pauly et al. (2000). Estimates of MSY for different trophic levels are then compared to recent estimates of production of prevalent species in Lake Victoria for which there are available data. Table 4.1 shows the trophic level of some relevant species as elucidated through stomach content and isotopic fractionation, where phytoplankton are set to the first trophic level. (Balirwa 1998; Wanink 1998; Campbell et al. 2003). The freshwater shrimp *Caridina niloticus* is

assigned trophic level 2 based on their diet of benthic algae and algal detritus (Ignatow et al. 1996; Campbell et al. 2003). The Nile tilapia *Oreochromis niloticus* is predominantly a planktivore but can also feed on *Caridina* and chironomids (Balirwa 1998) and its isotopic $\delta^{15}N$ value changes with maturity with an average value indicating a trophic level of 2.2 (Campbell et al. 2003). The diet composition of *Rastrineobola argentea* consists of zooplankton and invertebrates, while its trophic level as determined by its mean isotopic $\delta^{15}N$ value of 4 (Campbell et al. 2003) may indicate its food source passes through the microbial food web. Finally, the $\delta^{15}N$ value of the top piscivore *Lates niloticus* increases linearly with body length (Campbell et al. 2003) reflecting its change of diet with age (Ogutu-Owhayo 1994). The average $\delta^{15}N$ value of 12 samples indicate a trophic level of 3.9 that corresponds to a body length of 52 cm, close to the mean length of 50-60 cm reported in recent commercial catches by (Hecky pers. comm.). Net production of *C. niloticus* is taken from Ignatow et al. (1996), and net production estimates of *R.. argentea*, *L. niloticus* and *O. niloticus* are derived from annual commercial yields as presented by Pitcher et al. (1996), Mkumbo and Cowx (1999) and Goudswaard et al. (2002) respectively. In the case of the *O. niloticus*, only data from Tanzania and Kenya were available, so in order to estimate lakewide biomass the commercial yield was multiplied by 1.8 to reflect that 45% of Lake Victoria's surface area is within Uganda. Annual commercial yields were converted to net production by assuming carbon is 5% of fish wet weight (Kitchell et al. 1997), dividing by the Lake Victoria's surface area (Table 1.1) and 365 days per year. This method provides a minimum estimation of fish net production as it assumes loss terms such as fish mortality and respiration are negligible and biomass is equivalent to the commercial harvest. However in the absence of published data on any of these terms, these assumptions are currently required.

Table 4.1: Notable species in Lake Victoria with associated diet, trophic level and estimated net production.
([1] Ignatow et al. (1996), [2] Goudswaard et al. (2002), [3] Pitcher et al. (1996), [4] Mkumbo and Cowx (1999))

Species	Trophic Level	Production (mg $C.m^{-2}.day^{-1}$)
Caridina niloticus	2.0	11.40[1]
Oreochromis niloticus	2.2	0.58[2]
Rastrineobola argentea	4.0	0.17[3]
Lates niloticus	3.9	0.44[4]

4.2 Model Description

Figure 4.1 describes the framework of the model used to estimate PP_G and PP_N. The top of the figure shows all relevant parameters with arrows denoting statistically significant relationships with regression coefficients as derived in Chapter 2. Chlorophyll (chl) is the central parameter of this model as all other parameters show a significant relationship to it allowing their prediction based on a chl measurement alone. The bottom of Figure 4.1 illustrates the predicted distribution of three parameters along a chl gradient according to their respective regression equations presented in Chapter 2. Interpretation of each curve is given in Chapter 2. These parameters, along with incident irradiance, provied the required input data of Fee's model (1990) needed to calculate PP_G. As the equator bisects Lake Victoria, the annual variation of the daily averaged surface insolation is minor as noted by the small coefficient of variance in Table 3.1. A constant daily average incident irradiance of 436.5 $\mu mol.m^{-2}.s^{1}$ based on the reported annual average over Lake Victoria (Nicholson and Yin 2002) is therefore used in this model.

Figure 4.1 also shows predicted values of PP_G along a chl gradient. This curve is derived by calculating PP_G with the adapted program of Fee (Silsbe 2003) with incremental values of chl and associated values of maximum photosynthetic rate per unit biomass (P_{BM}), light-limited photosynthetic rate per unit biomass (α_B) and the vertical attenuation coefficient of photosynthetically active radiation (k_{PAR}) as predicted by the regression curves also shown in Figure 4.1 and a daily average incident irradiance described above. The empirical curve predicts that PP_G increases in a near linear fashion between chl of 0 to 10 $mg.m^{-3}$, begins to flatten out as chl approaches 20 $mg.m^{-3}$ and then slightly decreases when chl exceeds 40 $mg.m^{-3}$ where the maximum PP_G of 13.1 g $O_2.m^{-2}.day^{-1}$ is reached. This empirical model is in close agreement with a theoretical argument proposed by Talling (1965). When chl is high, Talling (1965) states that PP_G reaches an upper limit as algal pigments become the dominant cause of light attenuation in the water column and the chlorophyll-specific attenuation coefficient (k_{chl}) sets a maximum population limit of phytoplankton within the euphotic zone. Talling's model (1957) for calculating PP_G, which is theoretically and empirically

similar to Fee's (1990), predicts that phytoplankton with a P_{BM} of 25 mg O_2.mg chl^{-1}.hr^{-1} that reach their maximum euphotic population have a maximum PP_G of 12.5 g $O_2.m^{-2}.day^{-1}$, similar to the maximum of 13.1 mg $O_2.m^{-2}.day^{-1}$ derived empirically in Figure 4.1.

The linear decoupling between chl and PP_G shown in Figure 4.1 illustrates the most critical finding of this thesis; high quantities of algal biomass (> 20 $mg.m^{-3}$) do not lead to increased PP_G and are therefore not necessarily advantageous to Lake Victoria's fishery. In other words, excessive nutrient loading does not translate into increased fish production as is often assumed. This statement is further exemplified by the decline in PP_G above chl concentrations of 40 $mg.m^{-3}$ where light-limitation through self-shading decrease the photosynthetic rates per unit biomass shown in Figure 4.1. Furthermore, Chapter 3 illustrates the large degree of hypolimnetic deoxygenation which, together with harmful algal blooms, hinder Lake Victoria's fishery (Hecky et al. 1994; Ochumba and Kibaara 1989). As both of these features are attributed to excessive nutrient loading, effective management of nutrient loading can improve fish habitat and water quality without decreasing production at the base of the food web. This finding is supported by the general agreement of this new empirical model with the theoretical model of Talling (1965), however small discrepancies between Talling's (1965) assumptions and empirical data presented in Chapter 2 cause some minor differences between the two. Data from Lake Victoria suggests that PI parameters are not constant as assumed by Talling (1965), and decrease along an increasing chlorophyll gradient presumably through increased light limitation, a taxonomic shift from diatoms to cyanobacteria and an increasing need for biologically fixed nitrogen (Chapter 2; Mugidde 2001; Kling et al. 2001). Furthermore, k_{chl} is not constant in Lake Victoria and decreases along an increasing chl gradient (Chapter 2). Due to these reasons, PP_G in this empirical model declines after reaching its maximum level whereas Talling (1965) assumes it plateaus.

The empirical curve of PP_G versus chl shown in Figure 4.1 illustrates the importance of offshore chl data when generating lakewide estimates of PP_G. Inshore chl values invariably exceed 20 $mg.m^{-3}$ (Chapter 2; Mugidde 1993, 2001; Ramlal et al. 2001) such that modeled estimates of PP_G

will not significantly vary in these areas. However as offshore chl values are often below 20 $mg.m^{-3}$ in Lake Victoria (Mugidde 2001; Chapter 3), large temporal and spatial variability of PP_G can occur as the empirical curve shows increasing sensitivity of PP_G as chl decreases below 20 $mg.m^{-3}$.

The model derivation of areal respiration (AR) and consequently PP_N cannot be derived from chl alone as is done for PP_G. In the case of PP_G the depth of integration is the euphotic depth set by k_{PAR}, which can be statistically derived from chl. Although respiration per unit biomass (R_B) can be estimated from chl, the depth of integration for AR is the mixed depth and is not determined by chl. Figure 4.2A shows that predicted values of AR increase with both chl and mixed depth. AR as a function of chl can be plotted given a specific mixed depth (10 m) as shown in Figure 4.2B. PP_G as a function of chl is also shown in Figure 4.2B where the intersection of the PP_G and AR is the critical depth ($PP_N = 0$) that in turn corresponds to a specific chl concentration. By combining Figure 4.2A with the empirical model describing PP_G as a function of chl, critical depths can be determined for incremental chl values by assuming chl is uniform in the water column. The resultant curve is shown in Figure 4.2C, the solid line represents the critical depth when a nocturnal respiration rate of 1.34 mg $O_2.mg\ chl^{-1}.hr^{-1}$ is assumed (as derived and discussed in Chapter 2) while the dashed line assumes nocturnal and diurnal respiration rates are equivalent. Figure 4.2C illustrates that, when a nocturnal respiration rate is assumed, AR is smaller and the critical depth is deeper. Figure 4.2B and C further illustrate how excessive nutrient loading can hinder fish production. As chl increases, PP_N generally decreases as PP_G reaches an upper limit while AR continues to linearly increase. Furthermore the critical depth decreases with increased chl such that given a fixed mixed depth, PP_N will be generally be higher for lower chl concentrations.

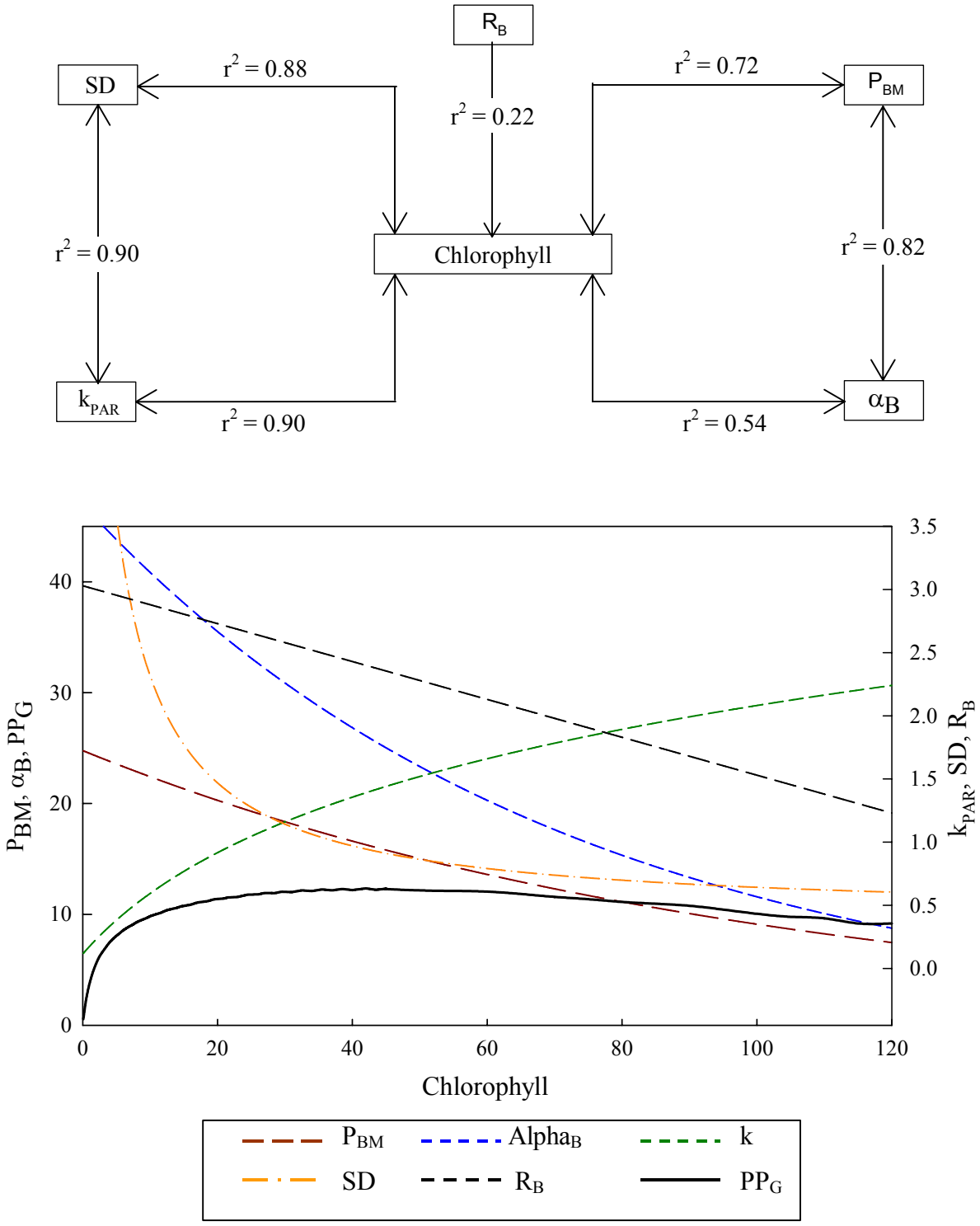

Figure 4.1: Model framework showing regression coefficients relating relevant parameters as derived in Chapter 2 and predicted distribution of these parameters along a chlorophyll gradient according to their respective regression equation with chlorophyll presented in Chapter 2 and the empirically derived PP_G plotted against chl. Units and definitions of symbols are given in Table 2.1.

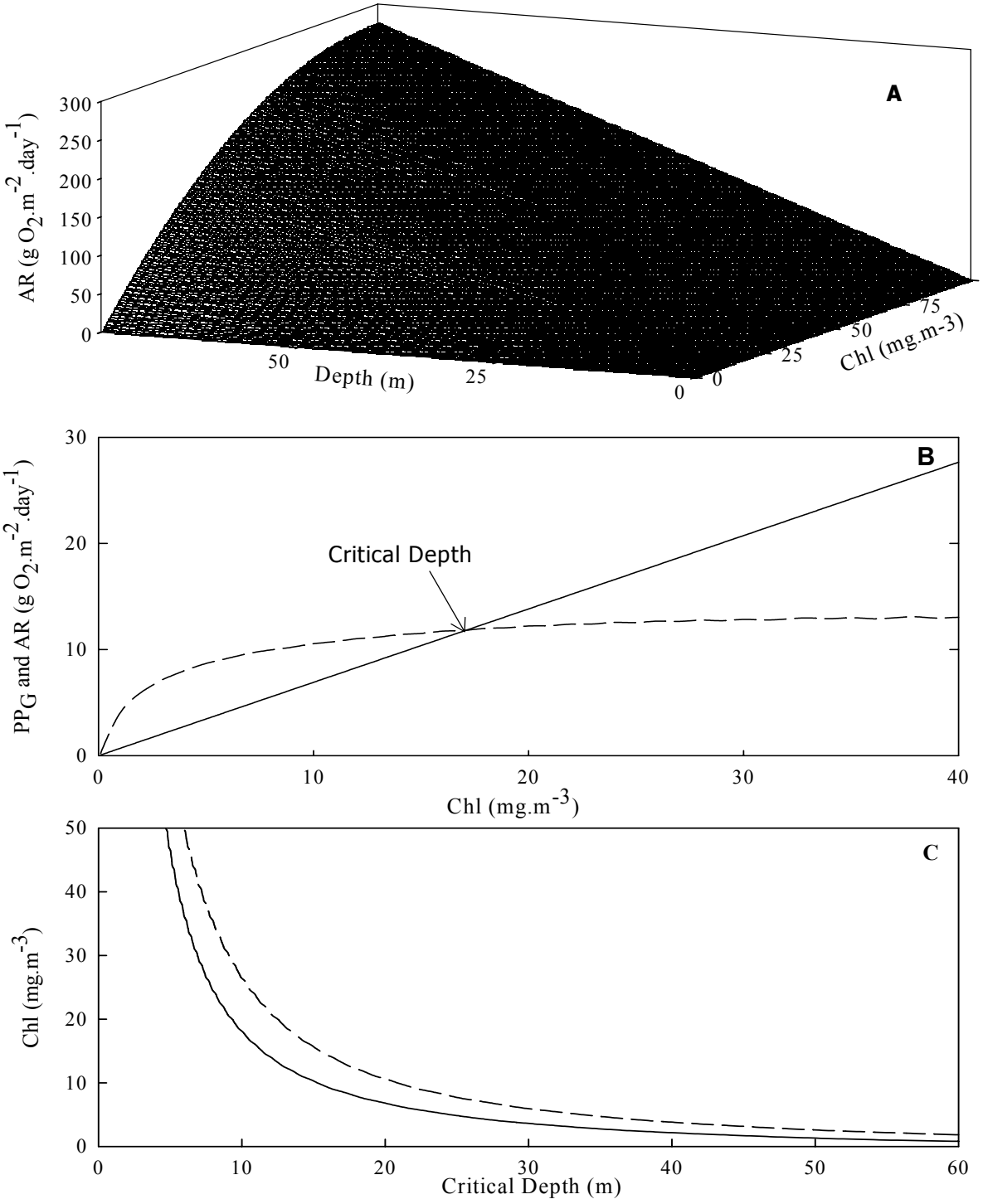

Figure 4.2: Model Description showing A) predicted AR along a chl and integrated depth interval, B) predicted PP_G (dashed line) and AR (solid line) integrated through 10 m along a chl gradient and C) the critical depth corresponding to an average volumetric chl concentration above the specified depth, the solid line corresponds to a critical depth where a nocturnal respiration rate of 1.34 mg O_2.mg $chl^{-1}.hr^{-1}$ is assumed while the dashed line assumes nocturnal and diurnal respiration are equivalent.

4.3 Model Validation

Figure 4.3A shows calculated PP_G from Chapter 2, adjusted to a constant incident irradiance described above and plotted against measured diurnally averaged chl. Figure 4.3A also shows the historic data of Talling (1965). The model prediction is significant and the regression coefficient increases (r^2 = 0.54 to 0.85) when spatial averages are taken for each region as shown in Figure 4.3B. The increase of r^2 illustrates that although calculations of PP_G on individual days can show considerable scatter around the predicted curve, temporally intensive studies increase the validity of the model. Figure 4.3C shows published measurements of PP_G against chl for Lake Malawi in 1992 and 1993 (Patterson et al. 2000), Lake Tanganyika (Hecky and Fee 1981) and Lake George (Ganf 1974). In the case of Lakes Malawi and Tanganyika, the C14 method was employed so values were converted to oxygen assuming a photosynthetic quotient (PQ) of 1.2. The apparent fit of these data to the empirical curve provides further validation and suggests a similar modeling approach may be useful to other African Lakes.

Figure 4.4A and B document the regressions of predicted and measured AR and PP_N respectively as well as the 1:1 line. Measured AR is from Chapter 2, and predicted AR is derived by substituting measured respiration rates with predicted respiration rates according to measured chl values and the relationship between R_B and chl shown in Figure 4.1. Measured PP_N is from Chapter 2, and predicted PP_N is derived from predicted AR calculated for Figure 4.4A as well as predicted PP_G for each day from Figure 4.3. Both relationships are significant, and r^2 increases to 0.75 and 0.56 for Figure 4.4A and B respectively if a nocturnal respiration rate is assumed (data not shown).

Figure 4.4C shows measured mixed depths and with corresponding estimates of the average mixed layer chl concentration presented in Chapter 3. Also shown in Figure 4.4C are the model's predicted critical depths along a chl gradient developed from Figure 4.2. Values taken from Figure 3.31 are more significantly related to the critical depth that assumes a basal nocturnal respiration rate than equivalent nocturnal and diurnal respiration rates; the critical depth derived by assuming a nocturnal respiration rate explains 51% of the variance of this dataset. Along with previously

reported studies that have documented a distinct nocturnal basal respiration rate (Ganf 1974; Erikson 1999), the statistical significance of the critical depth curve when a nocturnal respiration rate is assumed suggests that until these measurements are available this assumption will provide a more realistic estimate of AR and consequently PP_N in Lake Victoria. Furthermore, the considerable scatter in Figure 4.4C is expected; if all values were found along the critical depth curve, PP_N would be zero throughout the lake. If the axis of Figure 4.4C were reversed, it becomes apparent that the majority of data points have mixed depths above the critical depth for their respective chl concentrations. This suggests that most data points correspond to an area and time for which PP_N is positive.

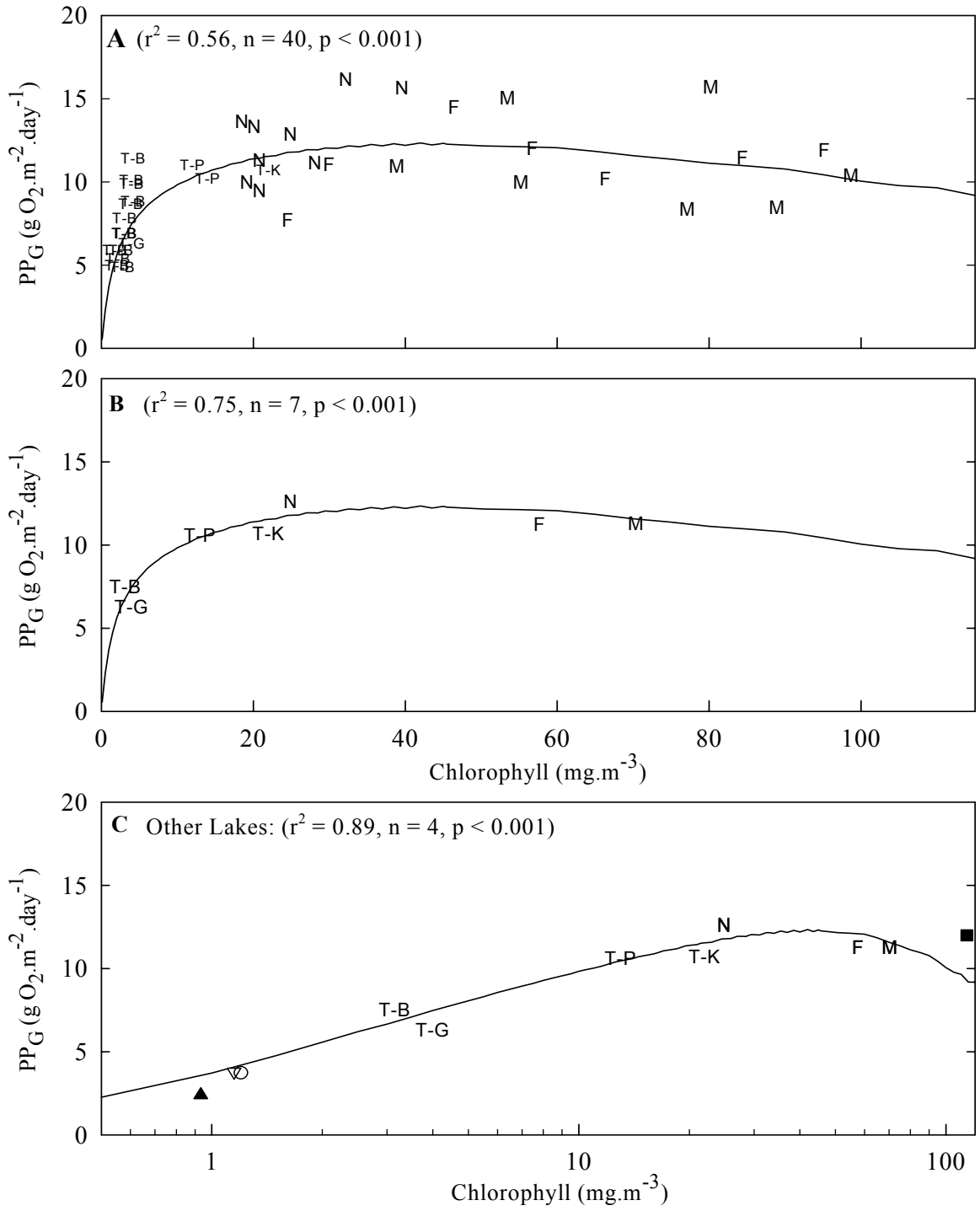

Figure 4.3: Model validation showing predicted PP_G versus chl (solid line) with A) calculated PP_G from M – Inner Murchison Bay, F – Fielding Bay, N- Napoleon Gulf and T–B Bugaia Island, T-P Pilkington Bay, T-G Grant Bay and T-K Kavirondo Gulf where T denotes source of data (Talling 1965), B) spatial averages of calculated PP_G from A and C) spatial averages along with data from Lake Malawi (closed triangle 1992, open triangle 1993; Patterson et al. 2000), Lake Tanganyika (open circle; Hecky and Fee 1981) and Lake George (closed square; Ganf 1974).

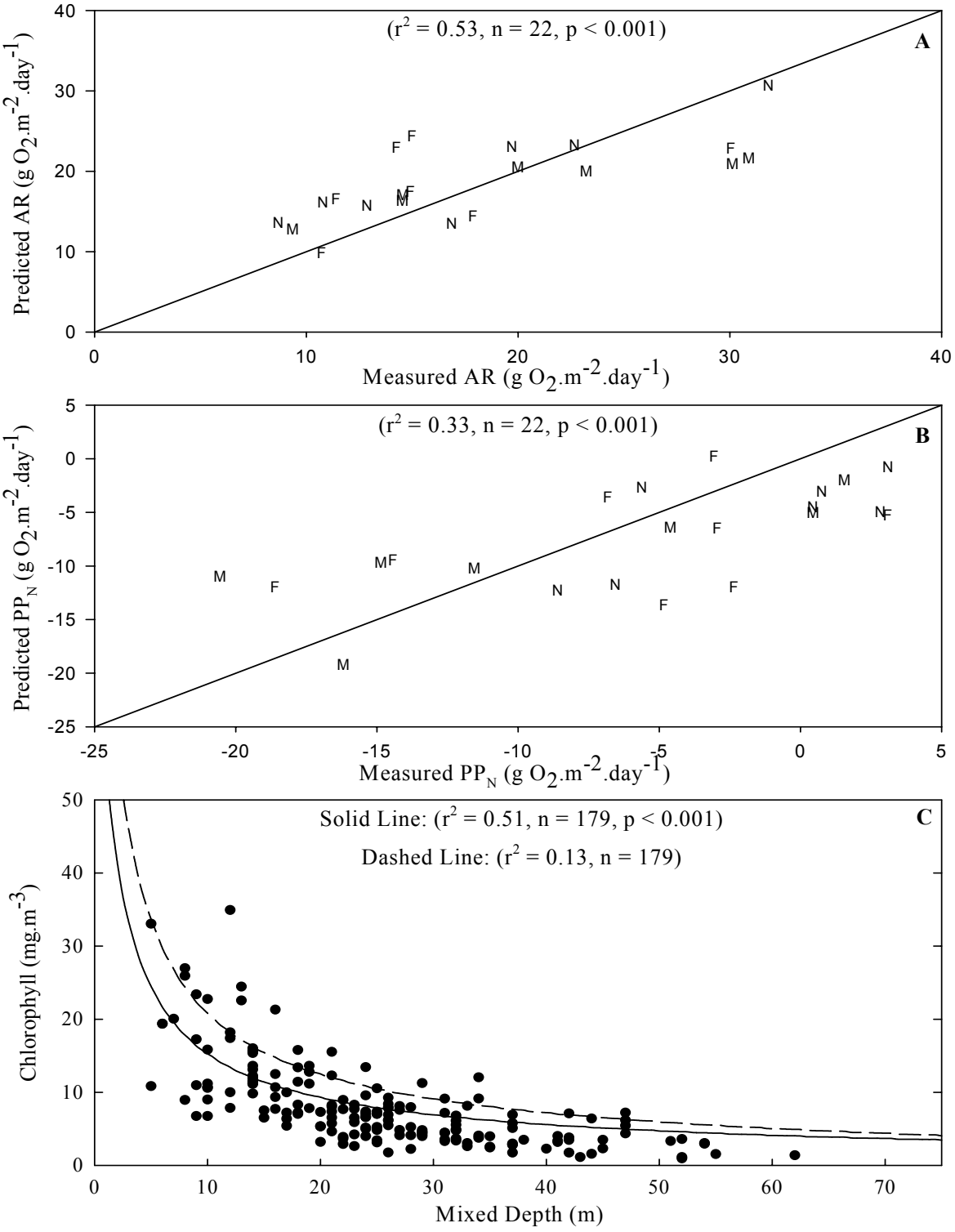

Figure 4.4: Model validation showing A) measured AR versus predicted AR, B) measured PP_N versus predicted PP_N and C) mixed depth versus the average chlorophyll concentration in the mixed layer, the solid line corresponds to a critical depth where a nocturnal respiration rate of 1.34 mg $O_2.m^{-3}.hr^{-1}$ is assumed while the dashed line assumes nocturnal and diurnal respiration are equivalent. F- Fielding Bay, M – Inner Murchison Bay, N – Napoleon Gulf.

4.4 Model Application

Figure 4.5 shows the frequency distribution of PP_G in Lake Victoria as a percentage of total lake area for each of the four cruises presented in Chapter 3. The empirical model in Figure 4.3 was applied to the spatially inferred chlorophyll distribution shown in Figure 3.28 for each cruise to derive an estimate of monthly mean lakewide PP_G that are summarized in Table 4.2. Overall, lakewide PP_G for each cruise follows the same pattern described for the lakewide chl distribution (Figure 3.28). A minimum of 18% of lakewide PP_G during each cruise exceeds 11 g $O_2.m^{-2}.day^{-1}$. Areas where this high production generally occurs are in the inshore (< 20 m) where the bottom depth sets a finite mixed depth that can more readily support higher chl concentrations (Figure 4.4C). The lowest modeled PP_G estimates occur in August 2000 where deep Secchi depth measurements were made (Figure 3.27). On average, PP_G is highest in February 2000 and lowest in August 2000 and similar in February and August 2001. An absence of temporally distributed offshore chl or production data inhibits an accurate temporal extrapolation of these values; however owing to their lack of strong temporal variance (16% and 3% difference between February and August of 2000 and 2001 respectively) and published studies showing offshore chl is usually relatively high in February and low in August (Hecky 1993, Figure 3.2), a simple average of the two months may yield an acceptable estimate. The annual averages for 2000 and 2001 are 9.51 and 9.86 g $O_2.m^{-2}.day^{-1}$ respectively, indicating that of inter-annual variability of lakewide PP_G is small. Assuming an annual PP_G average of 9.68 g $O_2.m^{-2}.day^{-1}$, the regression equation of Melack (1976) predicts that fish yield for Lake Victoria is approximately 670,000 Mg per year. This value is below the peak commercial yield found in 1990, but substantially higher than the 'best-guess' MSY of 300,000 Mg per year (Pitcher and Bundy 1994).

Lakewide AR was computed by constructing geospatial maps of respiration rates based on lakewide distributions of euphotic zone chl concentrations (Figure 3.27) with the relationship between R_B and chl shown in Figure 4.1 then multiplying these rates with the corresponding mixed layer depths (Figure 3.26) and the average chl concentration within the mixed layer depth (Figure 3.30).

AR was then subtracted from PP_G to determine the spatial distributions of PP_N during each cruise shown in Figure 4.6. As summarized in Table 4.2, the coefficient of variance is higher for AR than PP_G and the lakewide average is highest in August 2001 and lowest in August 2000.

Spatial patterns of AR, and consequently PP_N, are similar to patterns of the I_{24}/I_k ratio shown in Figure 3.28. In February 2000, PP_N is negative across a large swath along the centre of the lake (Figure 4.6A), inspection of the I_{24}/I_k spatial map reveals that this region corresponds to an area where the I_{24}/I_k ratio is below 0.2. During February 2000, the I_{24}/I_k ratio is also below 0.2 in the southeast corner of Mwanza Gulf and the north central extent of the lake, region that correspond to negative PP_N. Similar patterns can be seen throughout the rest of the cruises. In August 2001 a large latitudinal area of negative PP_N from the southern to the northern extent of Lake Victoria is shown in Figure 4.6D, again matching an area where the I_{24}/I_k ratio is below 0.2 (Figure 3.28D). In February 2001, AR exceeds PP_G in a region to the south of the Sesse Islands where the I_{24}/I_k ratio is below 0.2. Figure 4.7 validates this observation by illustrating the statistically significant relationship between the I_{24}/I_k ratio derived from individual profiles presented in Chapter 3 with corresponding estimates of PP_N derived in this chapter.

Table 4.2: Lakewide means of PP_G, AR and PP_N during each cruise with mean values and coefficients of variance (CV).

Cruise	PP_G (g $O_2.m^{-2}.day^{-1}$)	AR (g $O_2.m^{-2}.day^{-1}$)	PP_N (g $O_2.m^{-2}.day^{-1}$)
February 2000	10.22	8.49	1.73
August 2000	8.79	5.17	3.62
February 2001	9.71	6.09	2.83
August 2001	10.00	9.58	0.62
Mean (CV)	9.68 (6.5%)	7.33 (28.0%)	2.2 (59.4%)

The lack of temporal algal respiration and mixed depth data throughout Lake Victoria inhibits a precise interpolation of lakewide AR to assess an annual mean PP_N value, therefore a mean annual PP_N is derived by simply using the average of all four cruises. Again as published studies have shown offshore chl is usually relatively high in February and low in August while mixed depths

exhibit the opposite seasonal pattern (Hecky 1993), a simple average of PP_N may yield a relatively accurate estimate. Converting the mean PP_N shown in Table 4.2 to units of C by assuming a PQ of 1.2 yields an average annual value of 688 mg $C.m^{-2}.day^{-1}$. The mean PP_N value can be used to generate MSY for incremental trophic levels using Equation 4.1. For example, the amount of PP_N available to the fourth trophic level is 0.68 mg $C.m^{-2}.day^{-1}$. This value is in close proximity to the calculated combined net production of *Lates niloticus* (Nile Perch) and *Rastrineobola argentea* shown in Table 4.1 as 0.61 mg $C.m^{-2}.day^{-1}$. The estimated biomass for the fourth trophic level (using the reverse procedure employed in Table 4.1) is 330,000 Mg, close to the value of 300,000 Mg estimated by Pitcher and Bundy (1994) as the MSY for the Nile perch fishery.

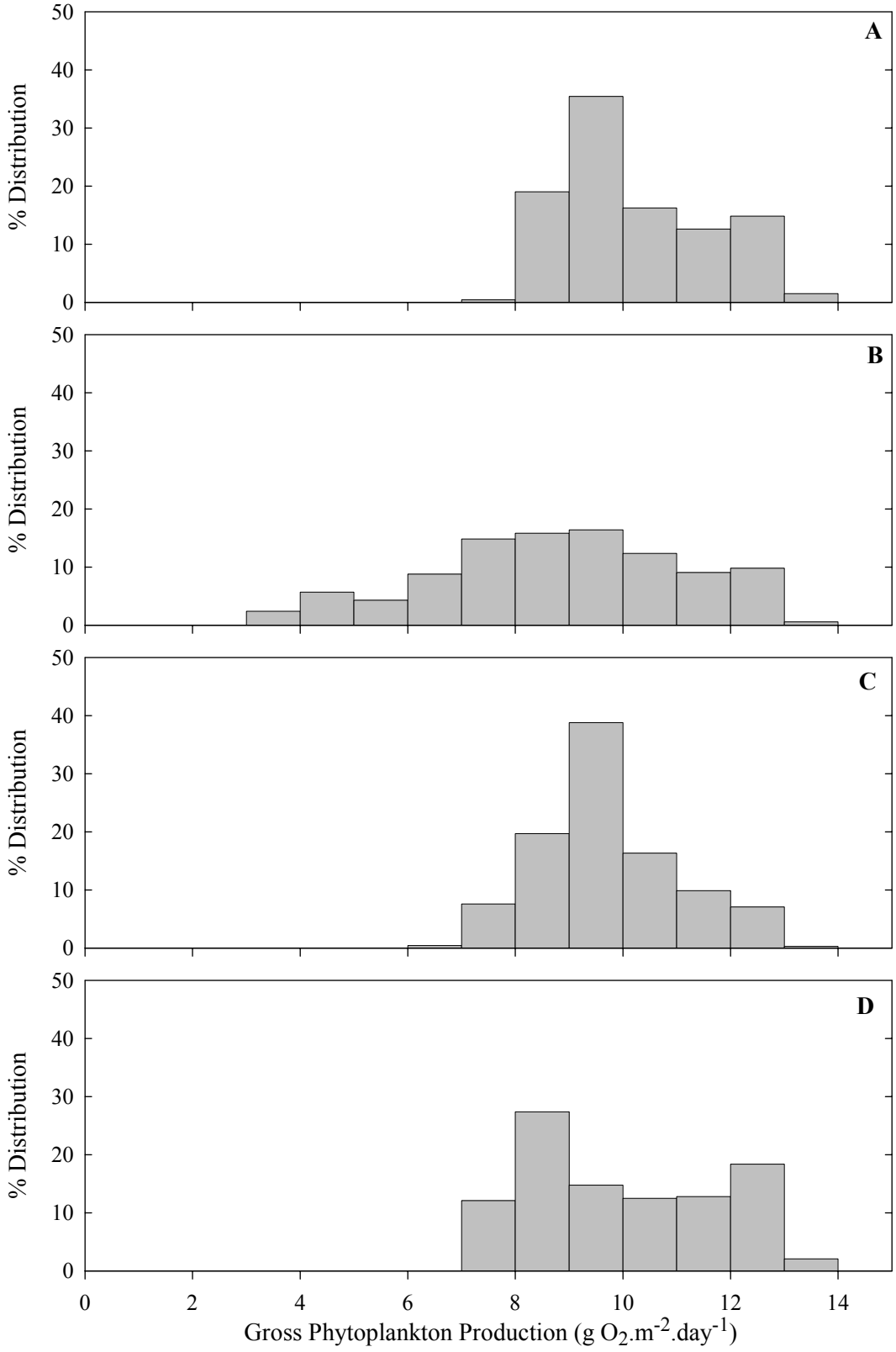

Figure 4.5: Percent distribution of modeled lakewide gross phytoplankton production for A) February 2000, B) August 2000, C) February 2001 and D) August 2001.

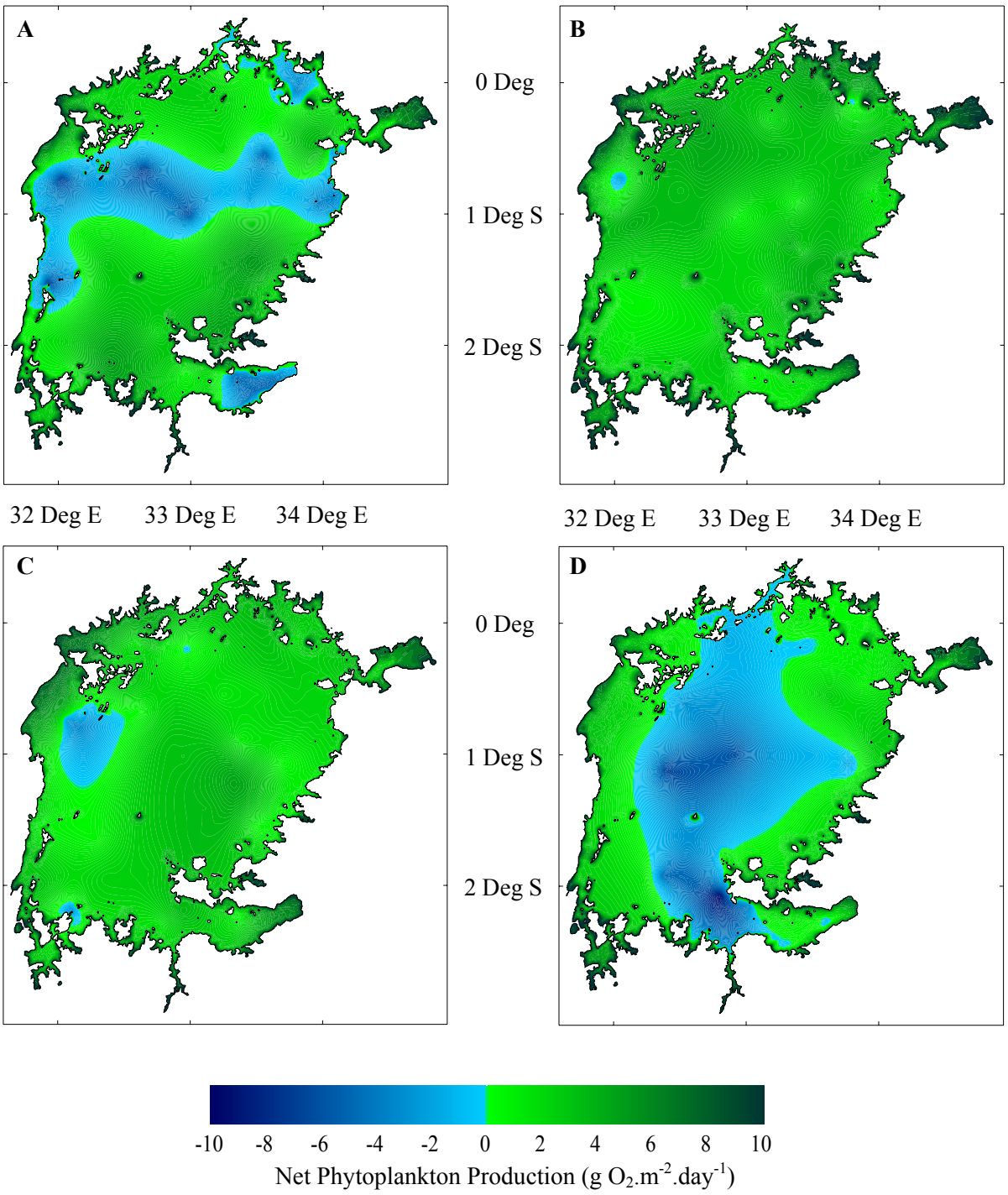

Figure 4.6: Net Phytoplankton Production in A) February 2000, B) August 2000, C) February 2001 and D) August 2001.

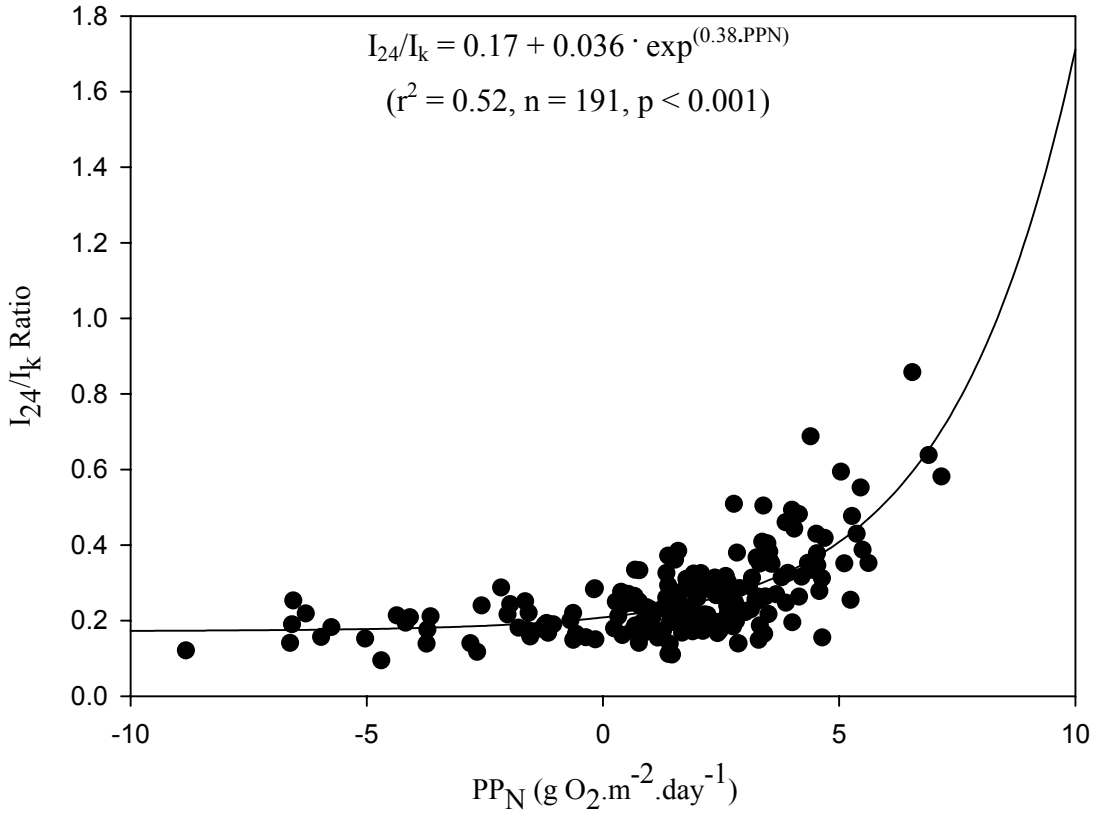

Figure 4.7: The relationship between the measured values of the I_{24}/I_k ratio and modeled estimates of PP_N in Lake Victoria.

4.5 Model Caveats

The close agreement between MSY from PP_N estimates with other studies (Pitcher and Bundy 1994) suggests the using phytoplankton production as a surrogate to estimate MSY is valid. Still, further research may eliminate some of the assumptions of this approach to further enhance its validity. AR estimates require more research relative to PP_G. Unlike PP_G with its small temporal variance in lakewide estimates (Table 4.1) and its finite range along a large chl gradient (Figure 4.1), AR has a much wider range and is very sensitive to mixed depths and respiration rates. A 3-D hydrodynamic model similar to that employed for Lake Erie (Leon et al. 2003) may provide accurate temporal and spatial patterns in mixed depths. Furthermore, remotely-sensed data can provide excellent spatial and temporal coverage of chl, from which PP_G estimates can be derived. As k_{PAR} can be derived from remotely-sensed chl data, the I_{24}/I_k ratio can be derived in conjunction with modeled mixed depths to provide an estimate of PP_N following Figure 4.7. However, in view of the paucity of meteorology data over Lake Victoria and the lack of temperature data to validate a hydrodynamic model output, this option is currently unfeasible. Wind fields and surface temperature derived from remote-sensing may provide the most plausible means to construct and validate a hydrodynamic model at this time.

Several assumptions concerning production within higher trophic levels also need to be resolved. Specifically, the assumption that annual commercial harvest is equivalent to biomass which can then be converted to production is ingrained with several assumptions. This approach does not account for loss processes such as fish mortality, fish respiration and assumes that turnover rates are equivalent to exactly one year. These assumptions aside, the lakewide estimates of PP_N presented in this chapter may help to assist future attempts to model Lake Victoria's food web.

4.6 Work Cited

Balirwa, J.S. 1998. Lake Victoria Wetlands and the ecology of the Nile tilapia, *Oreochromis niloticus Linne*. Ph.D. thesis. Wageningen Agricultural Univ., Wageningen, NL.

Campbell, L.M., R.E. Hecky and S.B. Wandera. 2003. Stable isotope analyses of food web structure and fish diet in Napoleon and Winalm gulfs, Lake Victoria, East Africa. Journal of Great Lakes Research. 29: 258-266.

Erikson, R. 1999. Algal respiration and the regulation of phytoplankton biomass in a polymictic tropical lake (Lake Xolotlan, Nicaragua). Hydrobiologia. 382: 17-25.

Fee, E.J. 1990. Computer programs for calculating in-situ phytoplankton photosynthesis. Can. Tech. Rep. Fish. Aquat. Sci. No. 1740.

FSTC. 2000. Frame survey technical committee draft report on Lake Victoria fisheries frame survey. Part 1: Main Report. Lake Victoria Fisheries Organization. Jinja. Pp. 63-87.

Ganf, G.G. 1974. Rates of oxygen uptake by planktonic community of a shallow equatorial lake (Lake George, Uganda). Oecologia15: 17-34.

Goudswaard, P.C., F. Witte and E.F.B. Katunzi. 2002. The tilapiine fish stock of Lake Victoria before and after the Nile Perch upsurge. Journal of Fish Biology. 60: 838-856.

Greboval, D. 1990. Socio-economic issues for planning in support of fisheries management. *In* CIFA report of the 5th session of the Sub-committee for the Development and Management of the Fisheries of Lake Victoria. FAO Fisheries Report 430: 75-97.

Hecky, R.E. and E.J. Fee. 1981. Primary production and rates of algal growth in Lake Tanganyika. Limnology and Ocanography. 26: 532-547.

Hecky, R.E., E.J. fee, H.J. Kling and J.W. M. Rudd. 1981. Relationship between primary production and fish production in Lake Tanganyika. Transactions of the American Fisheries Society. 110: 336-345.

Hecky, R.E., F.W.B. Bugenyi, P. Ochumba, J.F. Talling, R. Mugidde, M. Gophen and L. Kaufman. 1994. The deoxygenation of Lake Victoria. Limnology and Oceanography. 39: 1476-1481.

Ignatow, M. G. Mbahinzireki and J.T. Lehman. 1996. Secondary production and energetics of the shrimp *Caridina niloticus* in Lake Victoria, East Africa: Model development and application. Hydrobiologia. 332: 175-181.

Kitchell, J.F., D.E. Schindler, R. Ogutu-Ohwayo and P.N. Reinthal. 1997. The Nile perch in Lake Victoria: Interactions between predation and fisheries. Ecological Applications. 7: 653-664.

Kudhongania, A.W., and A.J. Cordone. 1974. Batho-spatial distribution patterns and biomass estimates of the major demersal fishes in Lake Victoria. Afr. J. Trop. Hydrobiol. Fish. 3: 15-31.

Melack, J.M. 1976. Primary productivity and fish yields in tropical lakes. Transactions of the American Fisheries Society. 105: 575-560.

Mkumbo, O.C. and I.G. Cowx. 1999. Catch trends from Lake Victoria. In: Cowx, I.G. and D. Tweddle (Eds.). Report of the Fourth FIDAWOG Workshop held at Kisumu. LVFRP/TECH/99/07. Lake Victoria Fisheries Research Project, Jinja, pp. 99-102.

Mugidde, R. 1993. The increase in phytoplankton primary productivity and biomass in Lake Victoria (Uganda). International Association of Theoretical and Applied Limnology. 25: 846-849.

Mugidde, R. 2001. Nutrient status and phytoplankton nitrogen fixation in Lake Victoria, East Africa. Ph.D. Thesis, University of Waterloo, Waterloo, Canada.

Northcote, T.G. and P.A. Larkin. 1956. Indices of productivity in British Columbia lakes. J. Fish. Res. Board. Can. 13: 515-540.

Ntiba, M.J., W.M. Kudoja and C.T. Mukasa. 2001. Management issues in the Lake Victoria watershed. Lakes and Reservoirs: Research and Management. 6: 211-216.

Ochumba, P.B. and D.I. Kibaara. 1989. Observations on blue-green algal blooms in the open waters of Lake Victoria, Kenya. African Journal of Ecology. 27: 23-34.

Oglesby, R.T. 1977. Relationships of fish yield to lake phytoplankton standing crop, production and morphoedaphic factors. Journal of the Fisheries Research Board of Canada. 34: 2271-2279.

Ogutu-Ohwayo, R. 1990. The decline of the native fishes of lakes Victoria and Kyoga (East Africa) and the impact of introduced species, especially the Nile perch, *Lates niloticus*, and the Nile tilapia, *Oreochromis niloticus*. Environmental Biology of Fishes. 27: 81-96.

Patterson, G., R.E. Hecky and E.J. Fee. 2000. Effect of hydrological cycles on planktonic primary production in Lake Malawi/Niassa. Advances in Ecological Research. 31: 421-430.

Pauly, D. and V. Christensen. 1995. Primary production required to sustain global fisheries. Nature. 374: 255-257.

Pauly, D., V. Christensen and C. Walters. 2000. Ecopath, Ecosim, and Ecospace as tools for evaluating ecosystem impact of fisheries. ICES Journal of Marine Sciences. 57: 697-706.

Pitcher, T.J. and A. Bundy. 1994. Successful species introduction in the African lakes: Assessment, uncertainties and strategies for fishery management. *In* B. David and E. Baldwin [eds]. Proceedings of the International Symposium on Management Strategies for Exploited Fish Populations. AK-SG-93-02. Alaska Sea Grant Program. Fairbanks, Alaska, USA.

Ramlal, P.S., G.W. Kling, L.M. Ndawula, R.E. Hecky and H.J. Kling. 2001. Diurnal fluctuations in PCO2, DIC, oxygen and nutrients at inshore sites in Lake Victoria, Uganda. In Munawar and R.E. Hecky [eds]. The Great Lakes of the World (GLOW): Food-web, health and integrity. 67-82.

Rawson, D.S. 1955. Morphometry as a dominant factor in the productivity of large lakes. Int. Ver. Theor. Angew. Limnol. Verh. 12: 164-175.

Rounsefell, G.A. 1946. Fish production in lakes as guide for estimating production in proposed reservoirs. Copeia. 1946: 29-40.

Ryder, R.A. 1965. A metod for estimating the potential fish production of north-temperatre lakes. Trans. Am. Fish. Soc. 94: 214-218.

Silsbe, G.M. 2003. A revised phytoplankton production model. http://www.science.uwaterloo.ca/research/uwaeg/web/index.htm.

Talling, J.F. 1957. The phytoplankton population as a compound photosynthetic system. New. Phyt. 56: 133-149.

Talling, J.F. 1965. The photosynthetic activity of phytoplankton in East African lakes. Int. Revue ges. Hydrobiol. 50: 1-32.

Talling, J.F. 1966. The annual cycle of stratification and phytoplankton growth in Lake Victoria (East Africa). Int. Revue ges. Hydrobiol. 51: 545-621.

Wanink, J.H. 1998. The pelagic cyprinid *Rastrineobola argentea* as a crucial link in the discrupted ecosystem of Lake Victoria. Ph.D. thesis. Sociale Wetenschappn. Univ. of Leiden, NL.

Chapter 5: General Summary and Conclusions

5.1 Summary

1. Secchi depth (SD) and the vertical attenuation of photosynthetic active radiation (PAR) (k_{PAR}) are statistically related to chlorophyll (chl) and to each other as shown in Figure 2.6, and the relationship between SD and k_{PAR} with chl is not linear. As chl increases SD decreases and k_{PAR} increases, however both curves become increasingly asymptotical along an increasing chl gradient.

2. The photosynthetic parameters that define the photosynthesis irradiance curve, the maximum photosynthetic rate per unit chl (P_{BM}) and the light-limited slope of photosynthesis per unit chl (α_B), linearly covary. The covariance of these parameters is stronger on sub-seasonal scales than on diurnal scales, although both parameters generally decrease through the day.

3. P_{BM} and α_B decrease along an increasing chl gradient. The regression equation between chl and photosynthetic parameters from published datasets on Lake Victoria (Talling 1965; Mugidde 1993) exhibit a statistically similar relationship with chl to that derived in this thesis.

4. The partial attenuation of irradiance due to chl (k_{chl}) as well as the ratio of inferred photosystem II to photosystem I (PSII:PSI) also decrease along an decreasing P_{BM} gradient as shown in Figure 2.12A and Figure 2.13C respectively. These relationships, as well as decreased phytoplankton growth rates, are expected to occur with a taxonomic shift from diatoms to cyanobacteria (Kirk 1994; Heaney 1978; Kilham and Hecky 1988), as well as within a cyanobacteria dominated community under increasing nitrogen (N) and light-limitation (Berges et al. 1996; Barlow et al. 2002).

5. Respiration per unit biomass (R_B) decreases with chl and increases with P_{BM}. The derived offset between R_B and P_{BM} (eg. where P_{BM} is zero) may be indicative of a basal maintenance

respiration rate. R_B has no discernable diurnal pattern (Figure 2.18C), however the regression coefficient between chl and R_B increases if diurnal averages of both parameters are taken (Figure 2.15B and C).

6. The parameters P_{BM}, α_B and k_{PAR} can be predicted from chl, along with incident irradiance (which has little annual variability as shown in Table 3.1), provide the input required to calculate gross phytoplankton production (PP_G) using the model developed by Fee (1990). In other words, one measurement of chl within the euphotic zone allows other parameters to be predicted to give an estimate of PP_G. Furthermore, R_B can be predicted from chl, which along with mixing depth determines areal respiration (AR), where the difference between PP_G and AR is net phytoplankton production PP_N.

7. Inshore spatial patterns of chl generally change with the average depth of the study site, deep areas have lower chl than shallower areas. The relationship between nocturnal wind speed and water temperature (Table 2.8) and the correlation between chl and the average early morning water temperature (T_{WC}) in each bay (Page 59) suggests that temporal patterns of chl are influenced by hydrodynamic events. Based on the direction of winds during strong nocturnal events observed during the 2002 study period, water from Fielding Bay may laterally advect to the south with a return current from depth that essentially flushes Fielding Bay causing observed decreases in chl and T_{WC} (Monismith et al. 1990).

8. Lakewide spatial patterns of the thermal structure in February and August 2000 and 2001 are more complex than the unidirectional hypotheses of warm water in the north and cold water in the south. Each lakewide cruise demonstrates that an east-west gradient of decreasing water column temperature as well. Increased evaporation, the dominant cooling process in Lake Victoria (Talling 1966; MacIntyre et al. 2002), may occur in the west due to frequent and strong convection localized over western Lake Victoria (Ba and Nicholson 1998). Nocturnal westerly land winds often associated with these convective events (Yin et al. 2000) would

induce eastwards surface currents with concurrent westwards currents at depth (Stevens and Imberger 1996). The combination of increased westerly evaporation and westward currents from depth offers an explanation for upwelling of oxyclines towards the west of Lake Victoria.

9. The warmest epilimnetic waters in the open central basin for all four cruises are located near shallow areas, suggesting that lateral advection of warmer inshore water to the offshore contributes to observed spatial patterns.

10. Interannual differences in the thermal structure and dissolved oxygen concentrations are also apparent. In February 2001, epilimnetic waters are cooler, hypolimnetic waters are warmer, thermal stability is lower and the areal hypolimnetic oxygen deficit (AHOD) is 36% less compared to February 2000. These interannual differences may be attributed to anomalously high precipitation in the short rainy season (October through December) of 2000 (WMO Bulletin 2001). As rainy seasons in the Lake Victoria basin are associated with increased cloudiness and convective events, it is likely that increased cloudiness during the short rains decreased heating of the lake while evaporation increased cooling of the lake, while hypothesized increased upwelling associated with convective storms in the rainy season may be responsible for the lower AHOD and warmer hypolimnetic temperatures observed in February 2001.

11. Spatial patterns of secchi depths are used to estimate spatial patterns of euphotic zone chl using the regression equation presented in Figure 2.6. Average offshore chl concentrations in each cruise are slightly lower than the offshore annual average of 13.5 $mg.m^{-3}$ measured by Mugidde et al. (2003) at Bugaia Island, but fall within the range of chl measurements acquired during a cross-lake transect in December 1994 (Mugidde 2001).

12. The average chl in the mixed layer (chl_{ML}) (as derived using chl in the euphotic zone, chlorophyll fluorescence and a mixed depth inferred from temperature profiles) is highly

correlated to the mixed depth as shown in Figure 3.31. This correlation suggests that, similar to the bottom depth of inshore areas in Chapter 2, the depth of mixing sets an upper limit on chl. Furthermore, the statistical similarity of the regression equations for each cruise presented in Figure 3.31 suggests that the relationship between mixed depths and chl_{WC} has small temporal and spatial variance.

13. An empirical model developed from the relationships developed in Chapter 2 predicts that PP_G increases in a near linear fashion when chl is between 0 and 10 $mg.m^{-3}$, begins to flatten out as chl approaches 20 $mg.m^{-3}$ and then slightly decreases when chl exceeds 40 $mg.m^{-3}$ where the maximum PP_G of 13.1 g $O_2.m^{-2}.day^{-1}$ is reached. This empirical model is in close agreement with a theoretical argument proposed by Talling (1965) who predicts that self-shading of a phytoplankton community occurs when chl is high, and this self-shading eventually sets an upper limit on PP_G. Figure 4.3 demonstrates that PP_G can be adequately estimated from the empirical model given a single measurement of chl.

14. AR and consequently PP_N are sensitive to chl within the mixed layer as well as mixed layer depths. From Figure 4.3, specific values of chl correspond to critical depths, where the PP_N is zero. Figure 4.4 demonstrates that the derived curve of chl versus critical depth accounts for 51% of the variance in chl_{ML} versus mixed depth when a basal respiration rate is assumed, if a basal maintenance respiration rate is not assumed the modeled critical depth accounts for only 13% of the variance.

15. The I_{24}/I_k ratio moderately predicts ($r^2 = 0.52$) PP_N. Generally, when the I_{24}/I_k ratio is below 0.2, phytoplankton production is light-limited as AR exceeds PP_G and $PP_N < 0$.

5.2 Conclusions and Recommendations

This thesis has developed an empirical model from which PP_G, AR and consequently PP_N estimates can be derived from simple measurements. Predicted values from the model are in close agreement with measured values from Chapter 2, historical data of Talling (1965) as well as primary

production measurements from other tropical lakes. This thesis confirms Mugidde's (1993) hypothesis that phytoplankton production in Lake Victoria is light-limited. Data from Chapter 3 demonstrates that, through the link between the I_{24}/I_k ratio and PP_N as well as the fact that individual estimates of chl_{ML} closely match ($r^2 = 0.51$) corresponding critical depths in each cruise, that light-limitation is widespread through space and time.

This thesis provides an example how simple Secchi depth and thermal structure measurements through space and time in conjunction with the empirical model can provide annual lakewide estimates of PP_G and PP_N. Overall, the annual lakewide estimates of PP_G and PP_N are 9.68 and 2.20 g $O_2.m^{-2}.day^{-1}$. This thesis also demonstrates how annual lakewide estimates of PP_G and PP_N can be used to estimate the maximum sustainable yield (MSY) for higher trophic levels where an estimated 330,000 Mg MSY of the fourth trophic level (approximately that of the average Nile perch) is close to the value of 300,000 Mg estimated by Pitcher and Bundy (1994) using fishing effort models.

This thesis identifies improvements that can be made to the model with respect to validation and application. As the model adequately predicts PP_G, and is in close agreement with a theoretical model (Talling 1965), the most imperative need for model validation concerns AR. Key assumptions that can be addressed concern the contribution of bacterial respiration to community respiration as well as the differences between nocturnal and diurnal respiration. Measurements of respiration rates using size-fractionated samples and measurements of respiration rates over several 24-hour periods may eliminate the two aforementioned assumptions respectively. This thesis computes annual lakewide PP_G and PP_N using snapshots of the lake in space and time. Remotely-sensed chl can be acquired on a daily frequency with a spatial resolution of 4 km^2 (O'Reilly et al. 1998). Provided remotely-sensed data can be validated for Lake Victoria, this method offers unparalleled spatial and temporal resolution from which PP_G can be computed. Computation of AR and consequently PP_N on an equally high resolution requires precise knowledge of mixed depths throughout the lake. A 3-dimensional hydrodynamic model may offer such resolution, but requires precise over-lake

meteorological processes as data input and temperature measurements through depth for model validation. The potential scientific benefit from such *in-situ* data may greatly outweigh the associated cost of the equipment.

5.3 Work Cited

Ba, M.B. and S.E. Nicholson. 1998. Analysis of convective activity and its relationship to the rainfall over the Rift Valley Lakes of East Africa during 1983-90 using the metosat infrared channel. Journal of Applied Meteorology. 37: 1250-1264.

Barlow, R.G., J. Aiken, P.M. Holligan, D.G. Cummings, S. Maritorena and S. Hooker. 2002. Phytoplankton pigment and absorption characteristics along meridional transects in the Atlantic Ocean. Deep-Sea Research. 47: 637-660.

Berges, J.A., D.O. Charlebios, D.C. Mauzerall and P.G. Falkowski. 1996. Differential effects on nitrogen limitation on photosynthetic efficiency of photosystems I and II in microalgae. Plant Physiology: 110: 689-696.

Heaney, S.I. 1978. Some observations on the use of the *in vivo* fluorescence technique to determine chlorophyll-a in natural populations and cultures of freshwater phytoplankton. Freshwater Biology. 8: 115-126.

Kilham, P. and R.E. Hecky. 1988. Comparitive ecology of marine and freshwater phytoplankton. Limnology and Oceanography. 33: 776-795.

Kirk, J.T.O. 1994. Light and photosynthesis in aquatic ecosystems. Cambridge University Press.

MacIntyre, S., Romero, J.R. and G.W. Kling. 2002. Spatial-temporal variability in surface layer deepening and lateral advection in an embayment of Lake Victoria, East Africa. Limnology and Oceanography. 47: 656-671.

Monismith, S.G., J. Imberger and M.L. Morison. 1990. Convective motions in the sidearm of a small reservoir. Limnology and Oceanography. 35: 1676-1702.

Mugidde, R. 1993. The increase in phytoplankton primary productivity and biomass in Lake Victoria (Uganda). International Association of Theoretical and Applied Limnology. 25: 846-849.

Mugidde, R. 2001. Nutrient status and phytoplankton nitrogen fixation in Lake Victoria, East Africa. Ph.D. Thesis, University of Waterloo, Waterloo, Canada.

Oreilly, J.F., S. Maritorena, B.G. Mitchell, D.A. Siegel, S.A. Garver and M. Kahru. 1998. Ocean color chlorophyll algorithms for SeaWiFS. Journal of Geophysical Research. Part C – Oceans. 103: 24891-24902.

Pitcher, T.J. and A. Bundy. 1994. Successful species introduction in the African lakes: Assessment, uncertainties and strategies for fishery management. *In* B. David and E. Baldwin [eds]. Proceedings of the International Symposium on Management Strategies for Exploited Fish Populations. AK-SG-93-02. Alaska Sea Grant Program. Fairbanks, Alaska, USA.

Stevens, C. and J. Imberger. 1996. The initial response of a stratified lake to a surface shear stress. Journal of Fluid Mechanics. 312: 39-66.

Talling, J.F. 1965. The photosynthetic activity of phytoplankton in East African lakes. Int. Revue ges. Hydrobiol. 50: 1-32.

Talling, J.F. 1966. The annual cycle of stratification and phytoplankton growth in Lake Victoria (East Africa). Int. Revue ges. Hydrobiol. 51: 545-621.

World Meteorological Organization. 2001. World Climate News. Bulletin 19. Geneva, Switzerland.

Yin, X., S.E. Nicholson and M.B. Ba. 2000. On the diurnal cycle of cloudiness over Lake Victoria and its influence on evaporation from the lake. Hydrological Sciences. 45: 407-424.

APPENDIX I

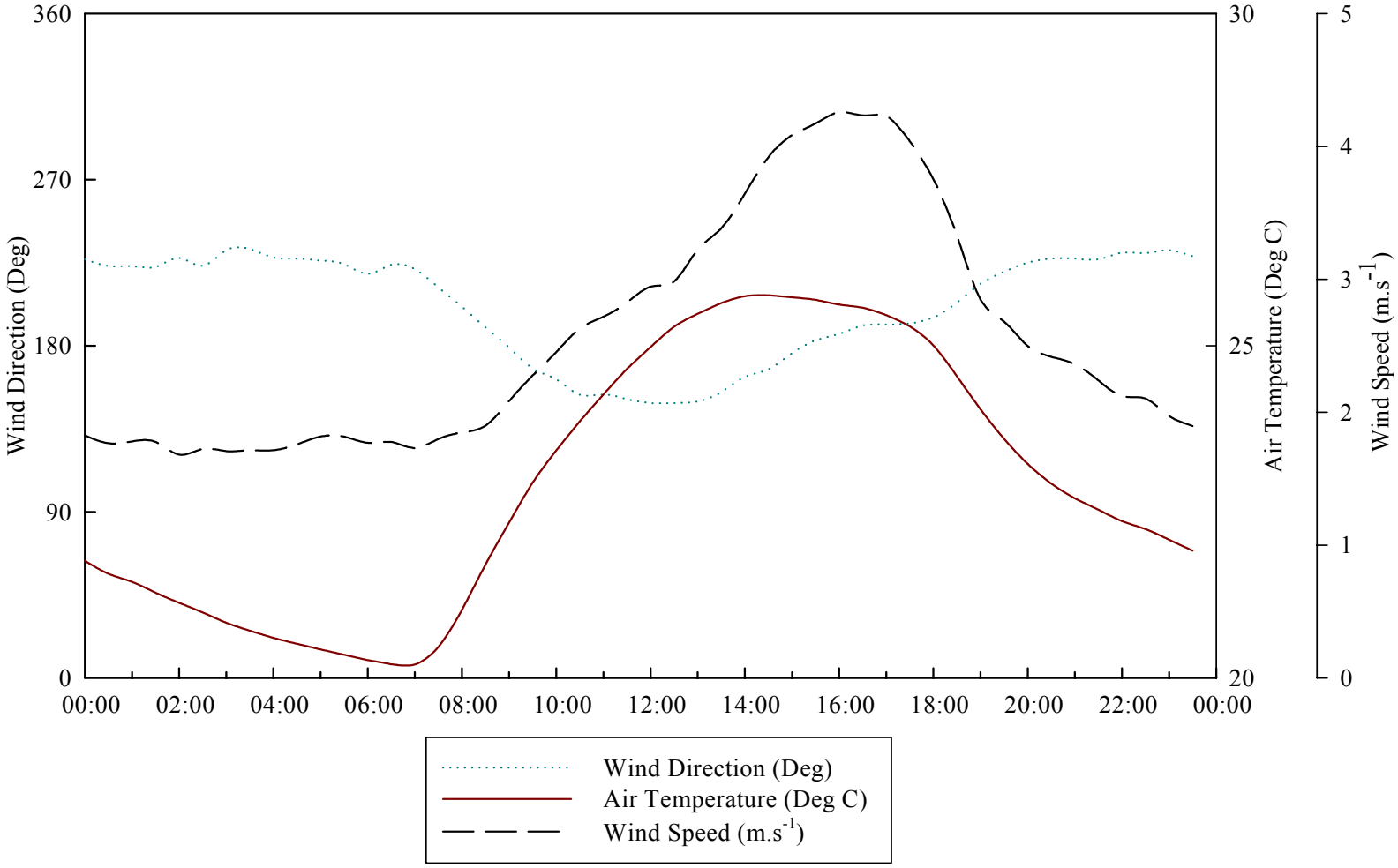

Figure 6.1: Diel averaged meteorological record for Jinja Pier. 2002.

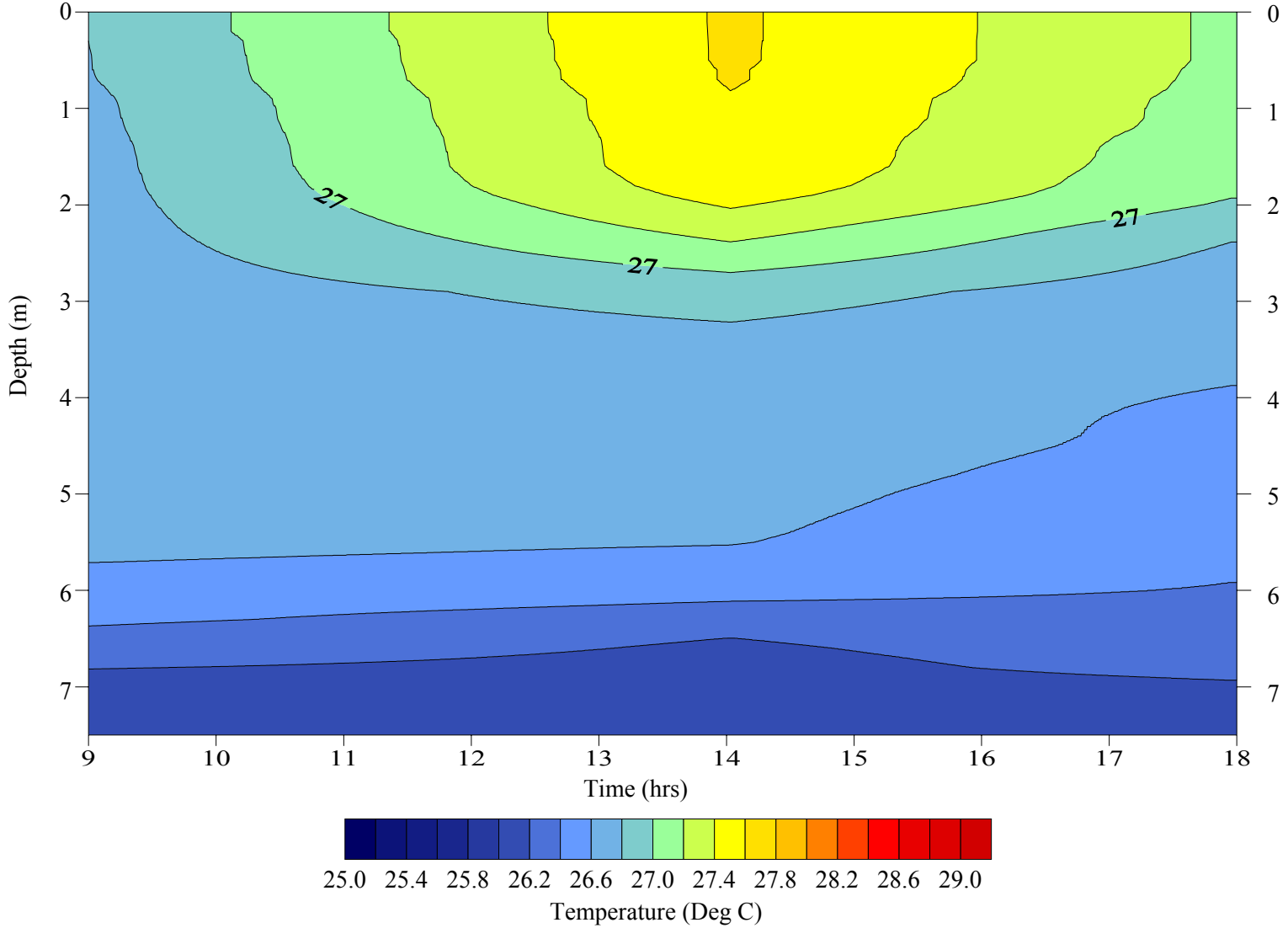

Figure 6.2: Diurnal Temperature in Fielding Bay for day of the year 270.

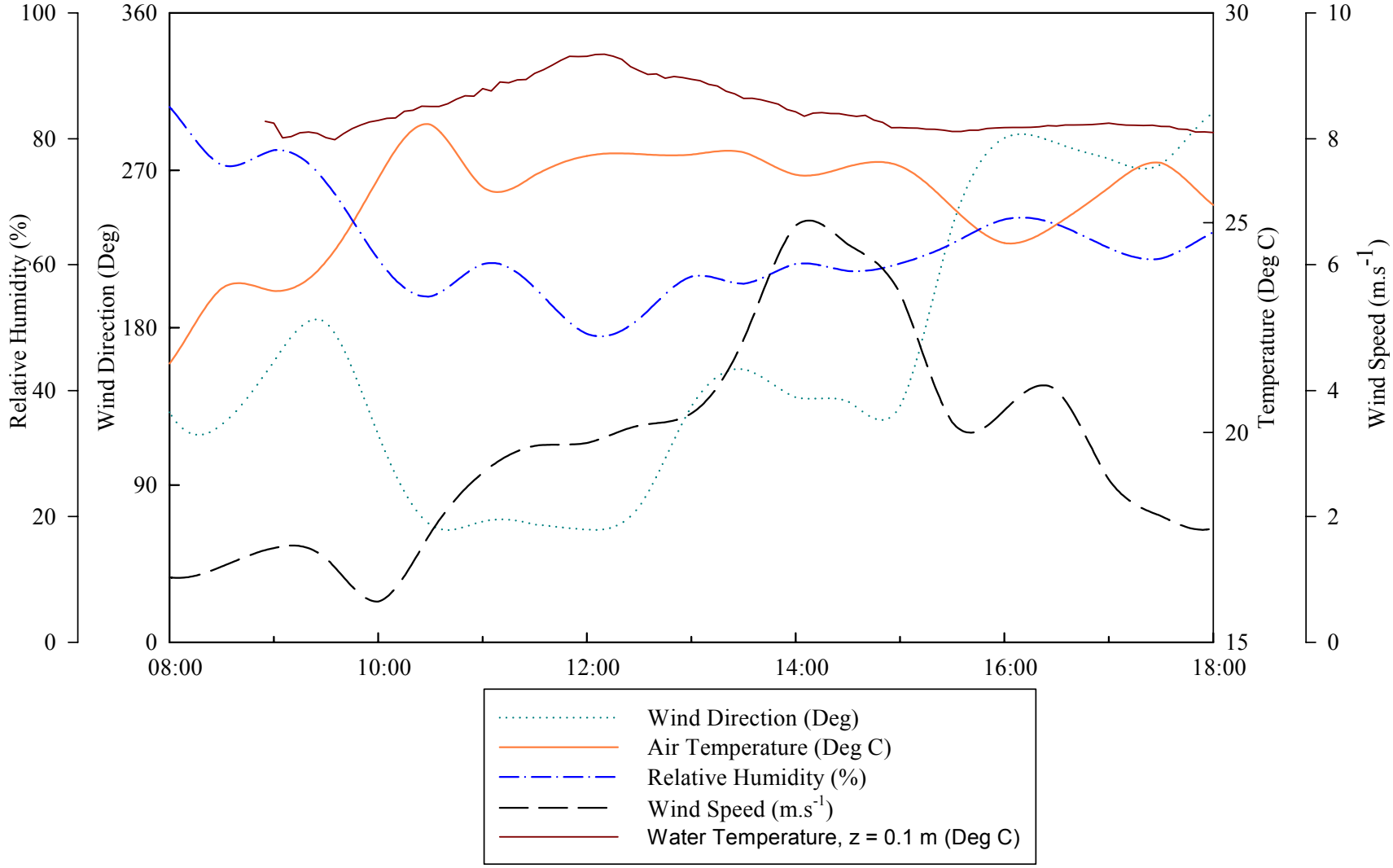

Figure 6.3: Meteorological Data for day of the year 270.

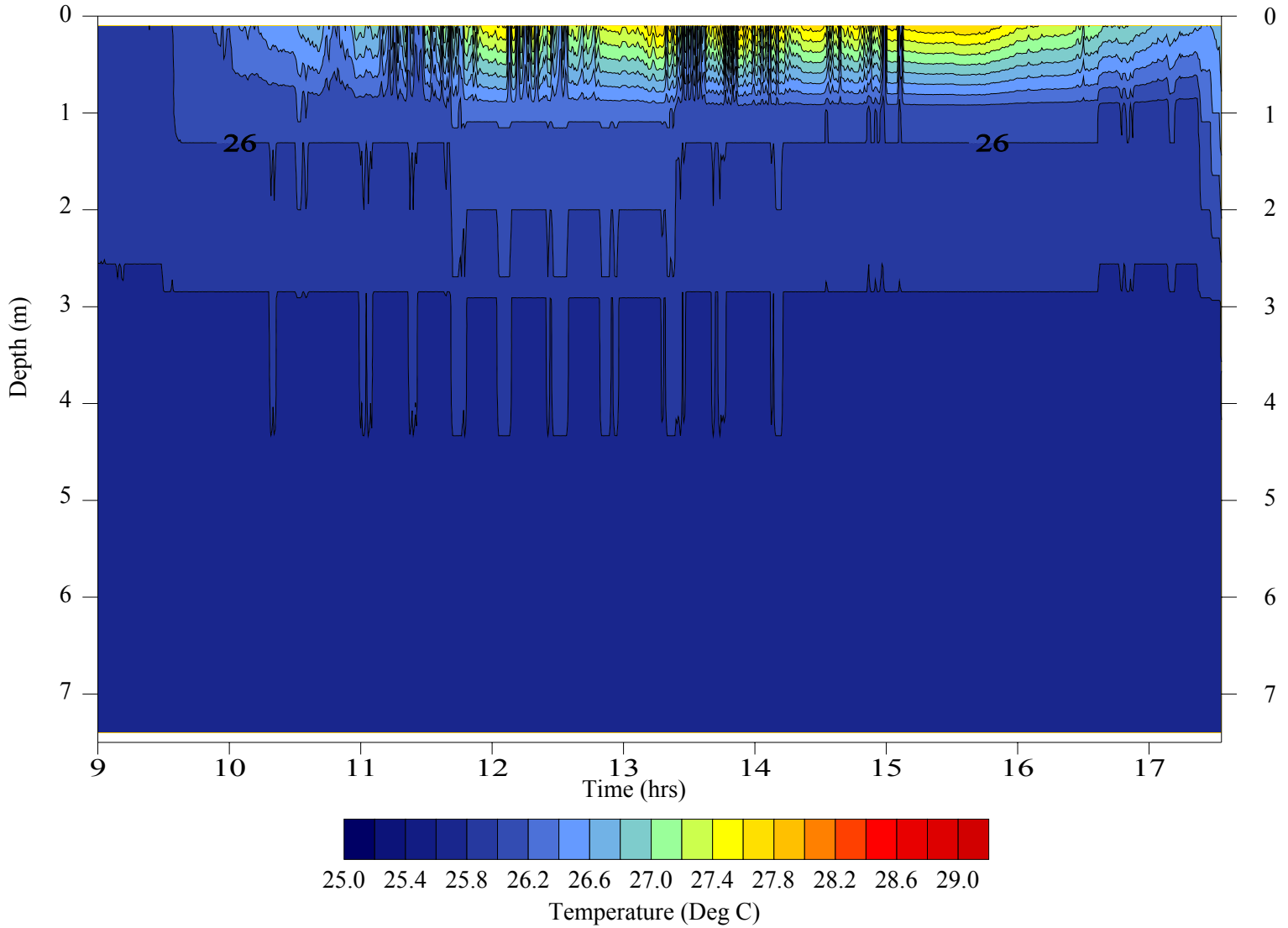

Figure 6.4: Diurnal Temperature in Fielding Bay for day of the year 276.

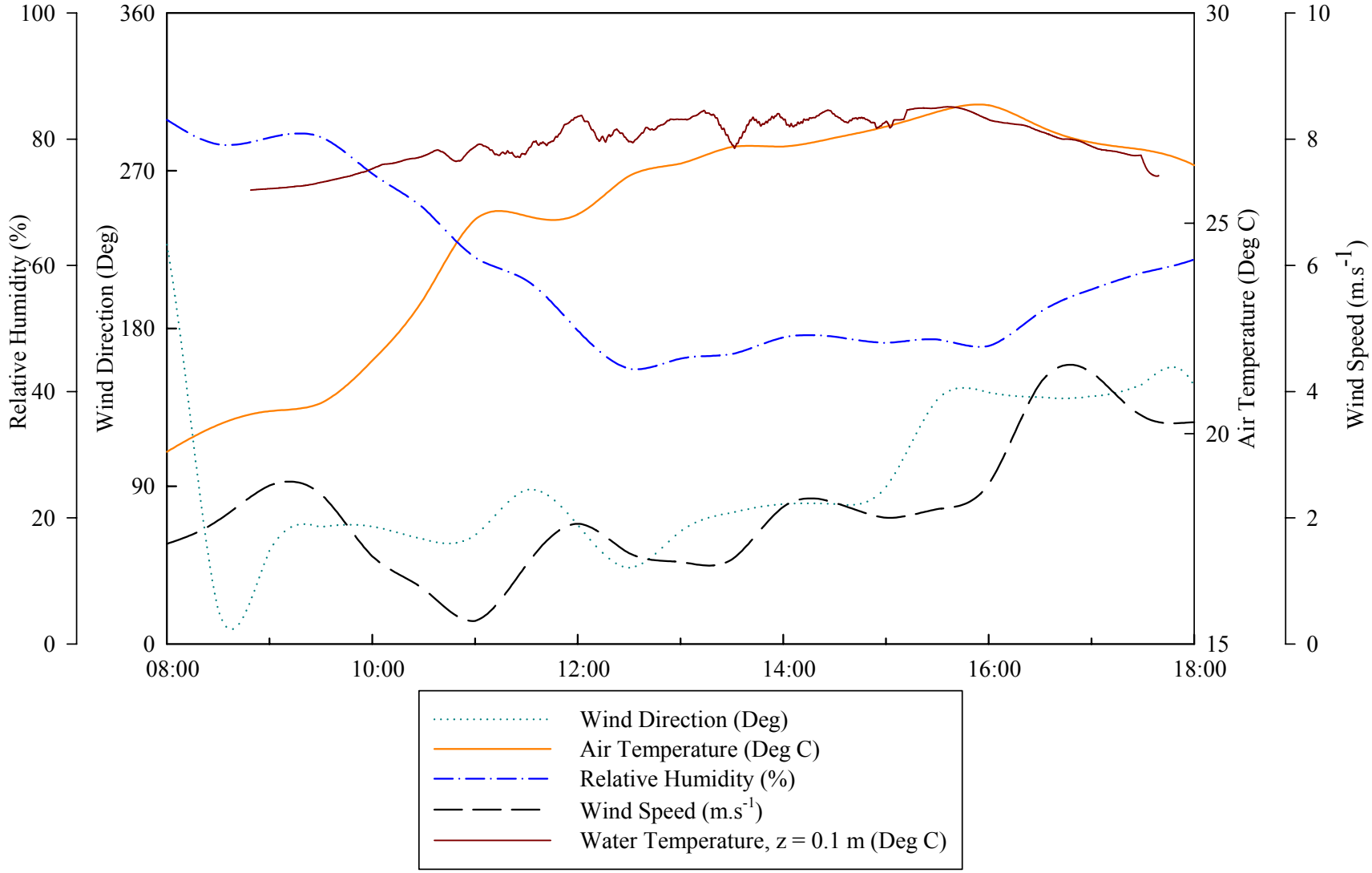

Figure 6.5: Meteorological Data for day of the year 276.

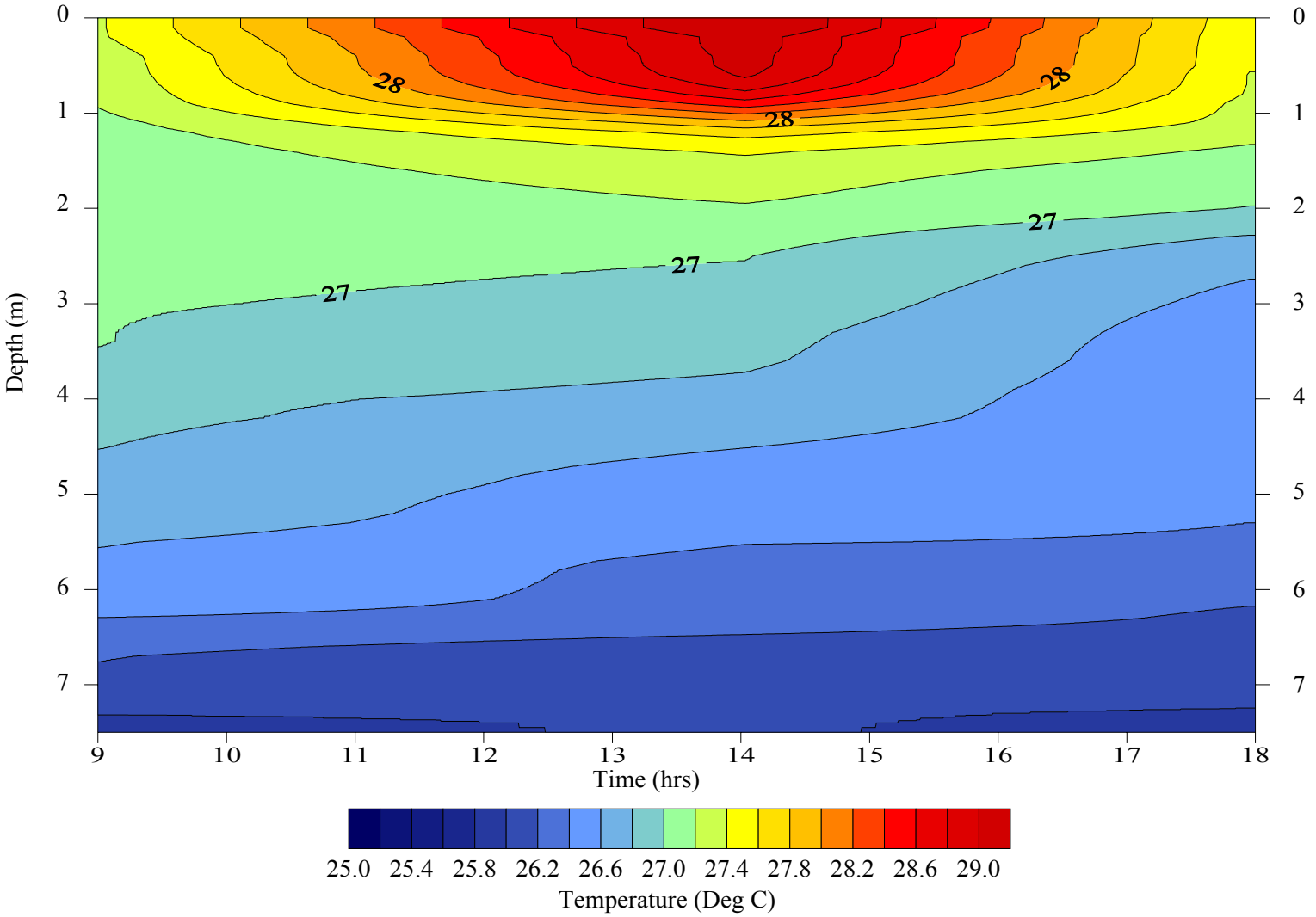

Figure 6.6: Diurnal Temperature in Fielding Bay for day of the year 289.

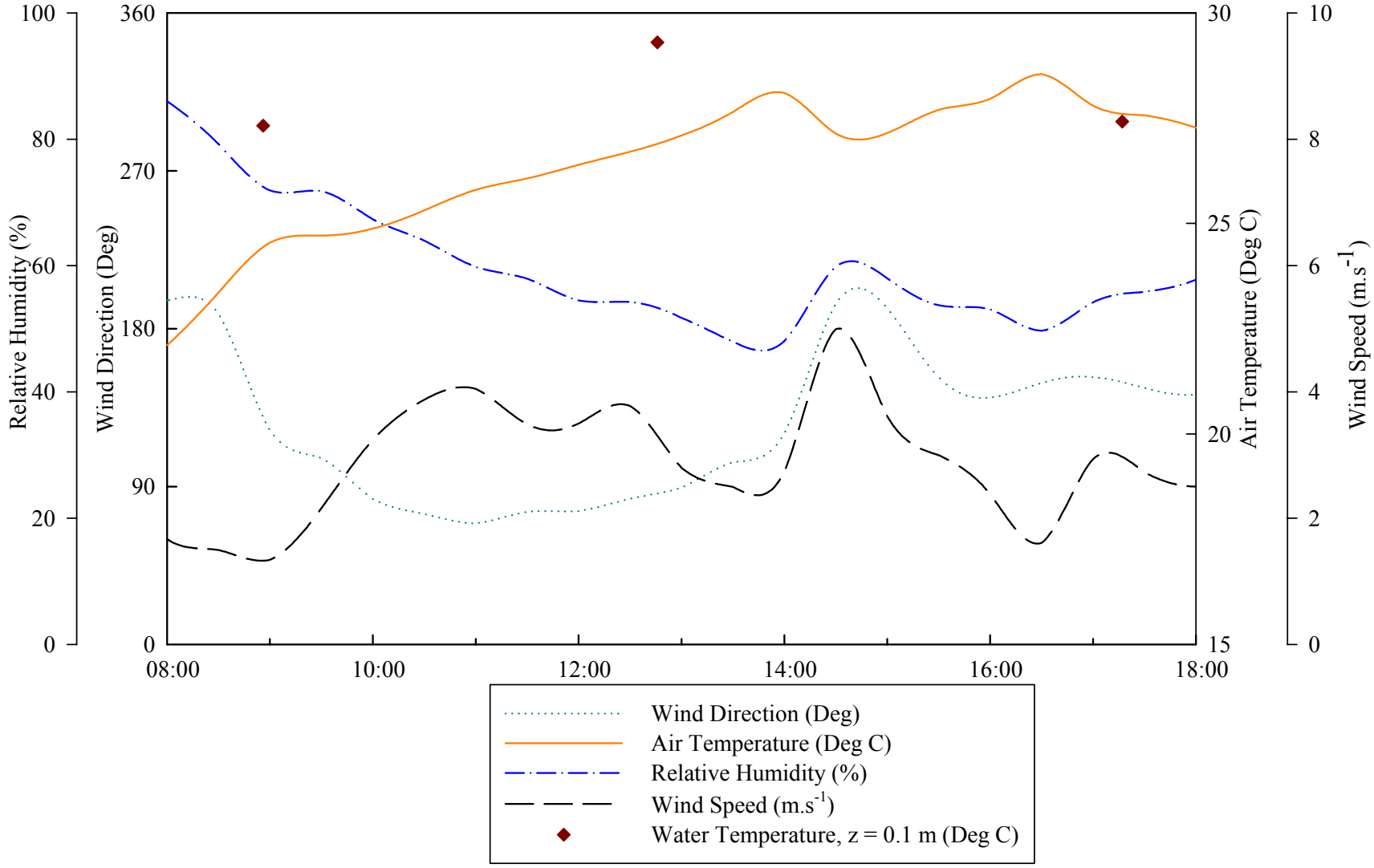

Figure 6.7: Meteorological Data for day of the year 289.

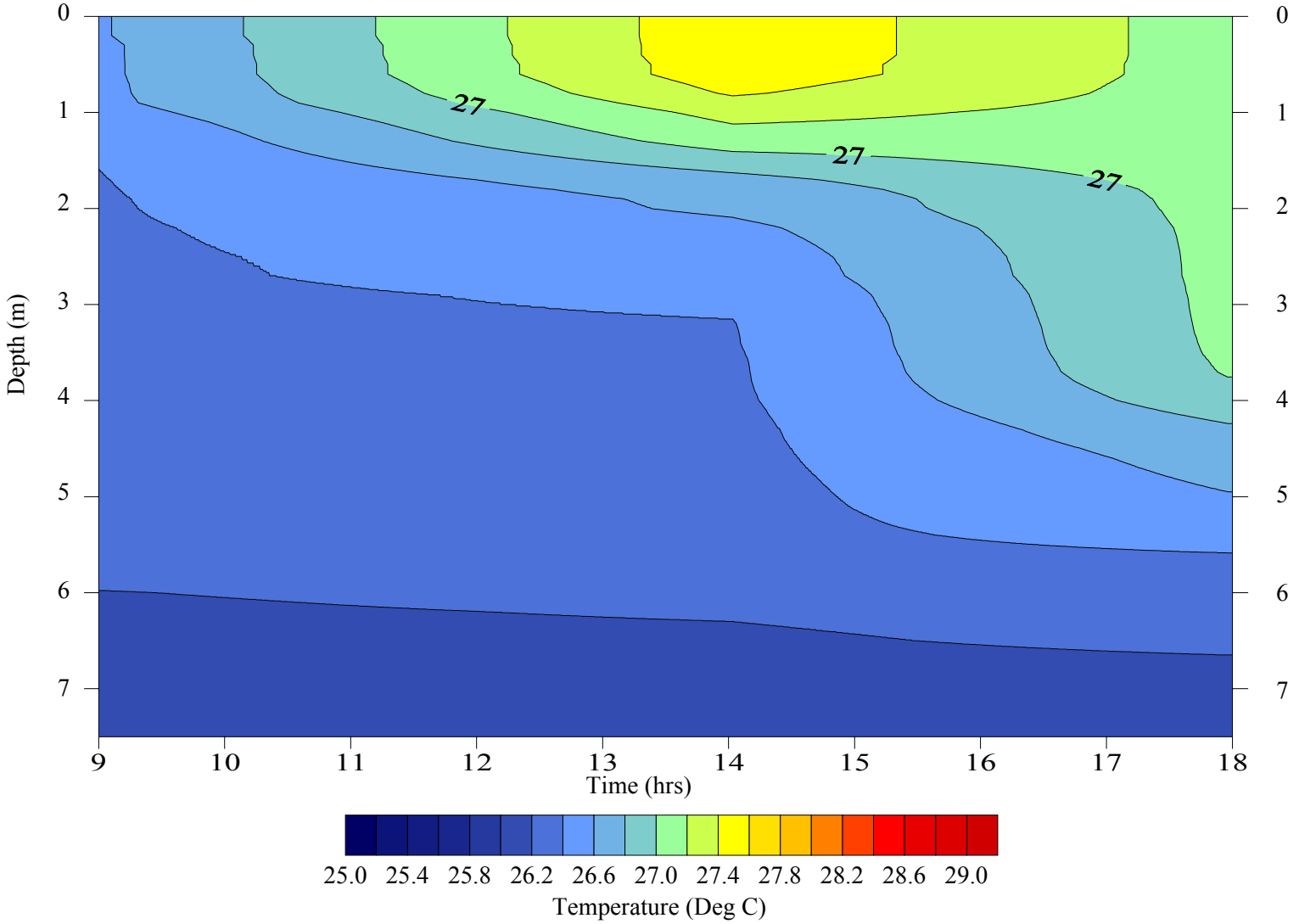

Figure 6.8: Diurnal Temperature in Fielding Bay for day of the year 296.

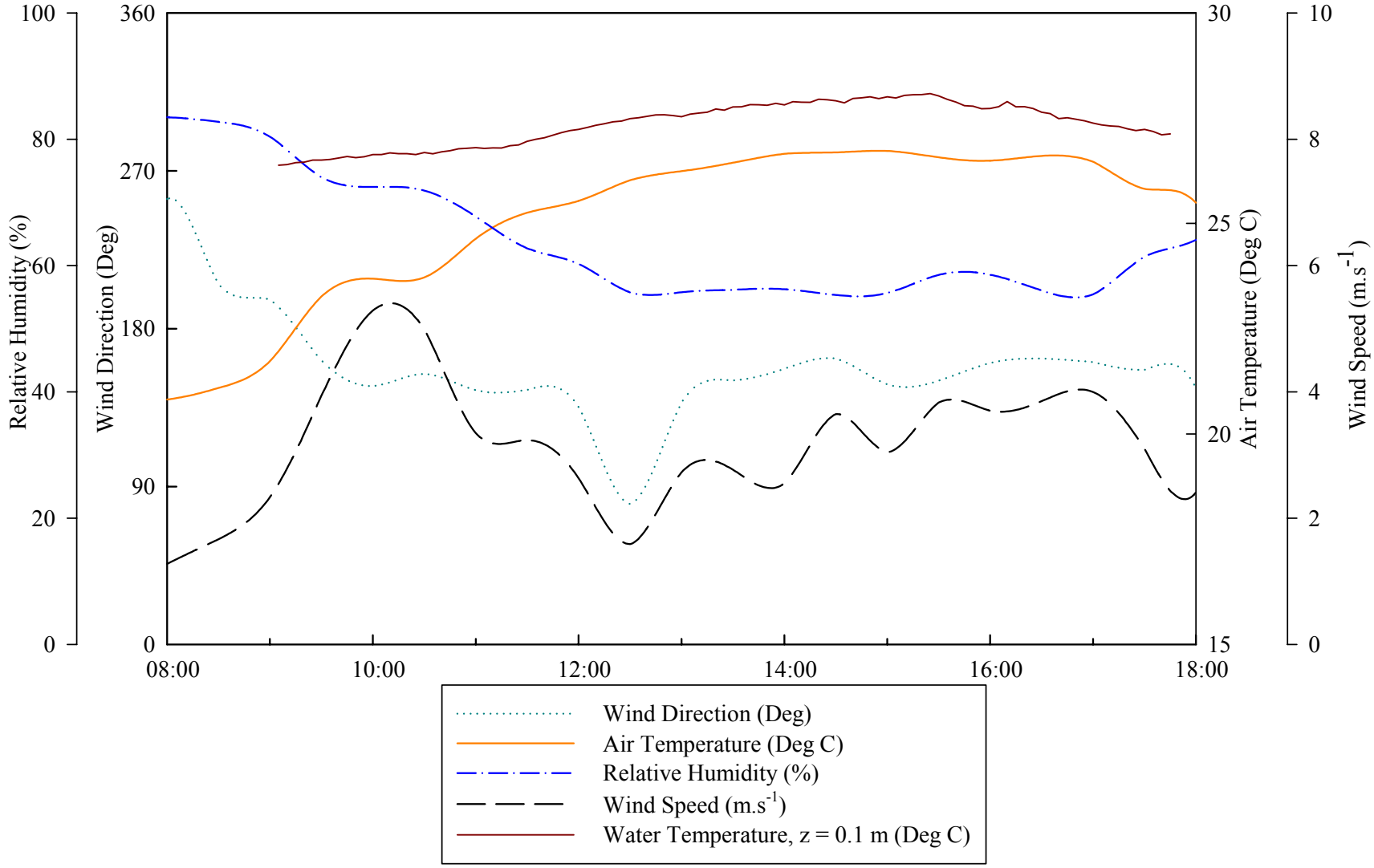

Figure 6.9: Meteorological Data for day of the year 296.

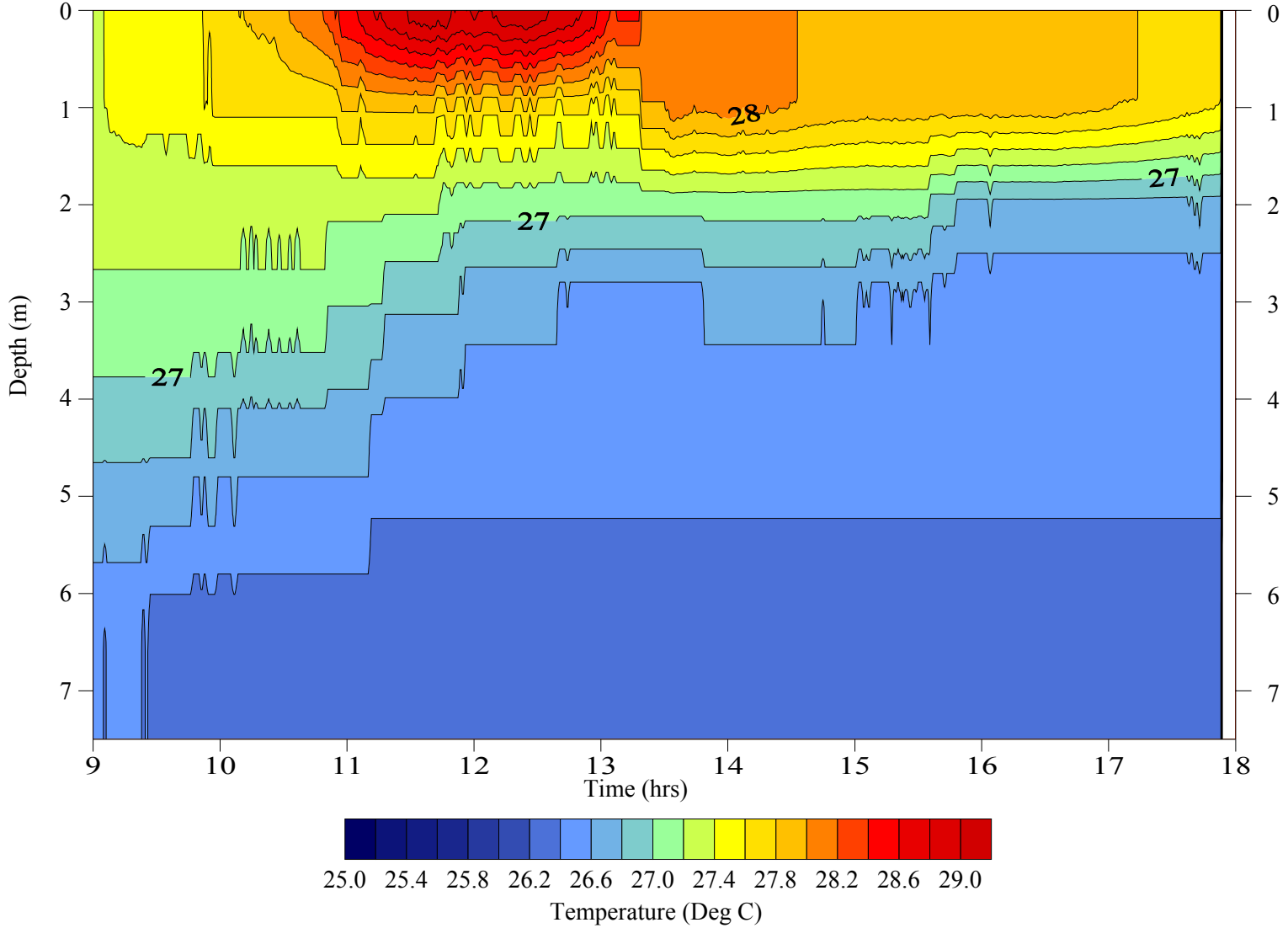

Figure 6.10: Diurnal Temperature in Fielding Bay for day of the year 302.

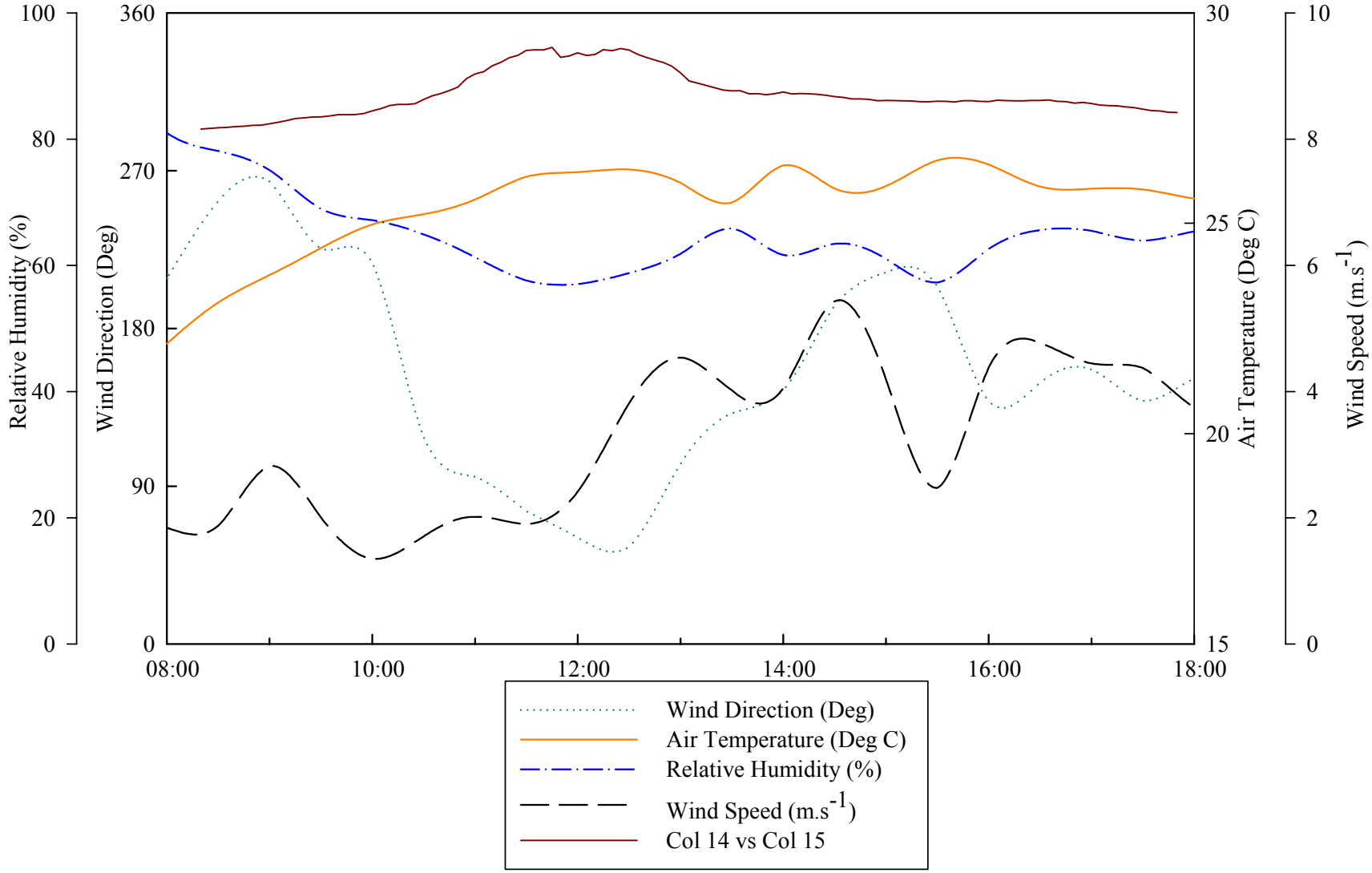

Figure 6.11: Meteorological Data for day of the year 302.

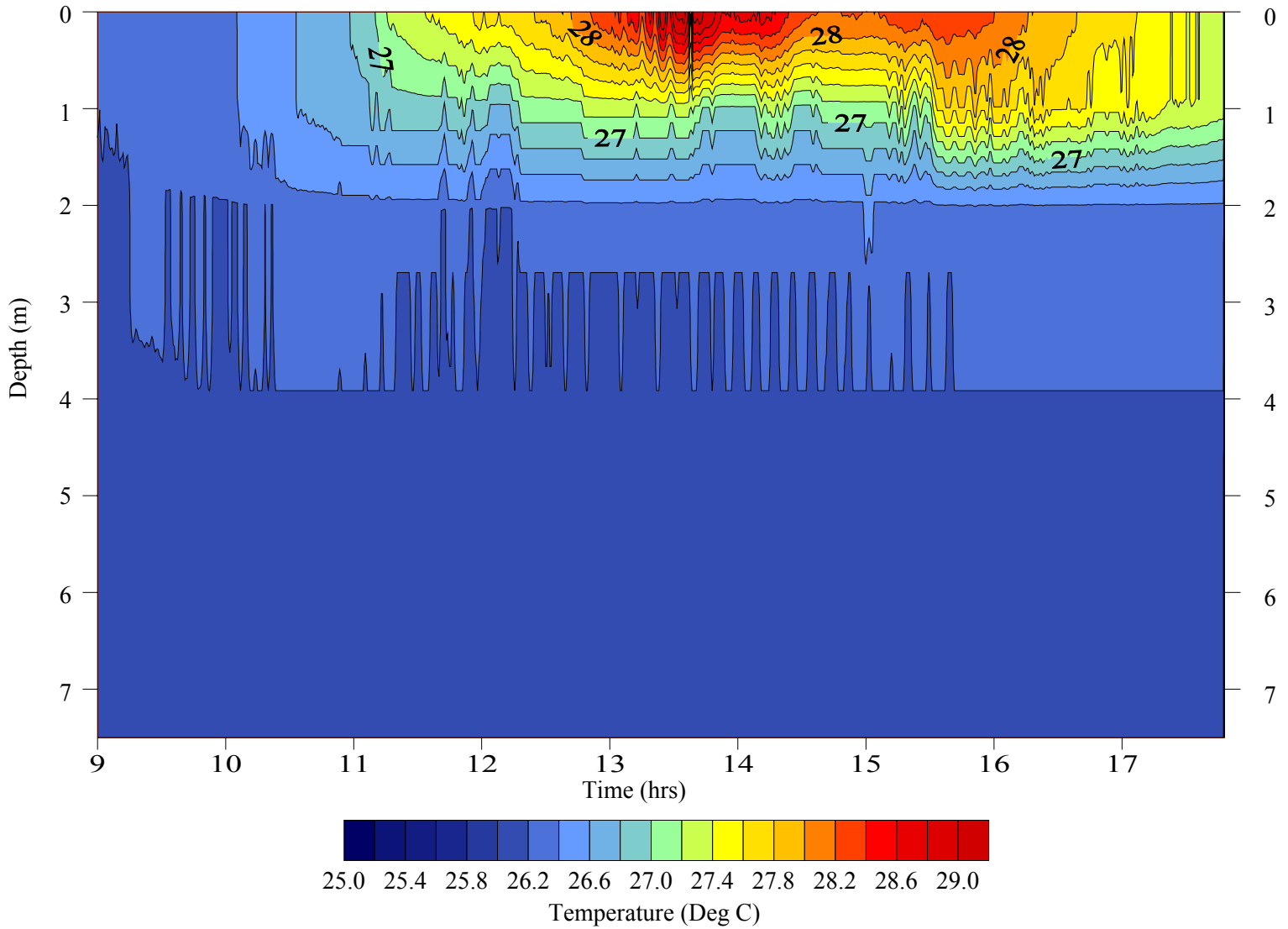

Figure 6.12: Diurnal Temperature in Fielding Bay for day of the year 309.

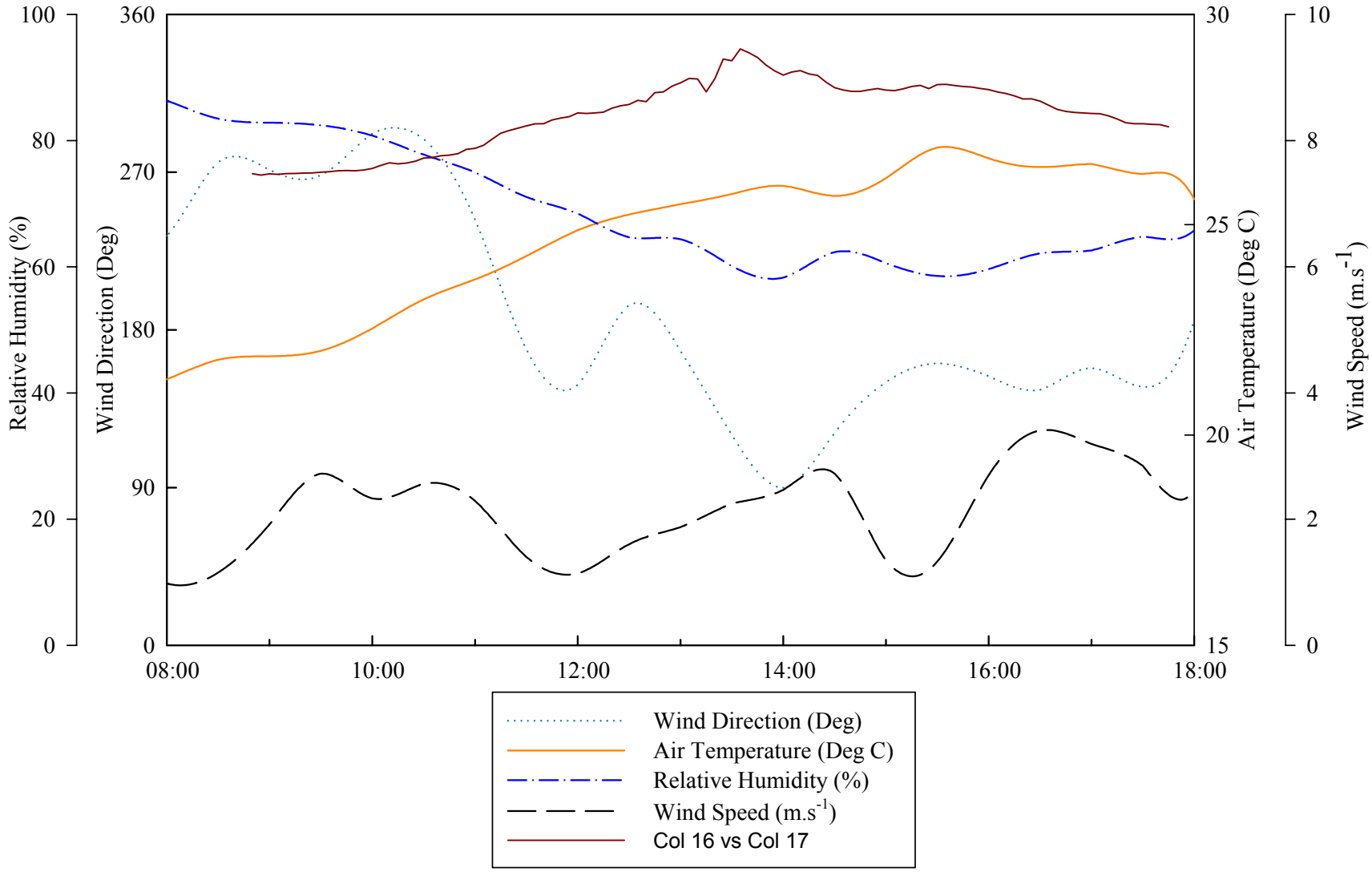

Figure 6.13: Meteorological Data for day of the year 309.

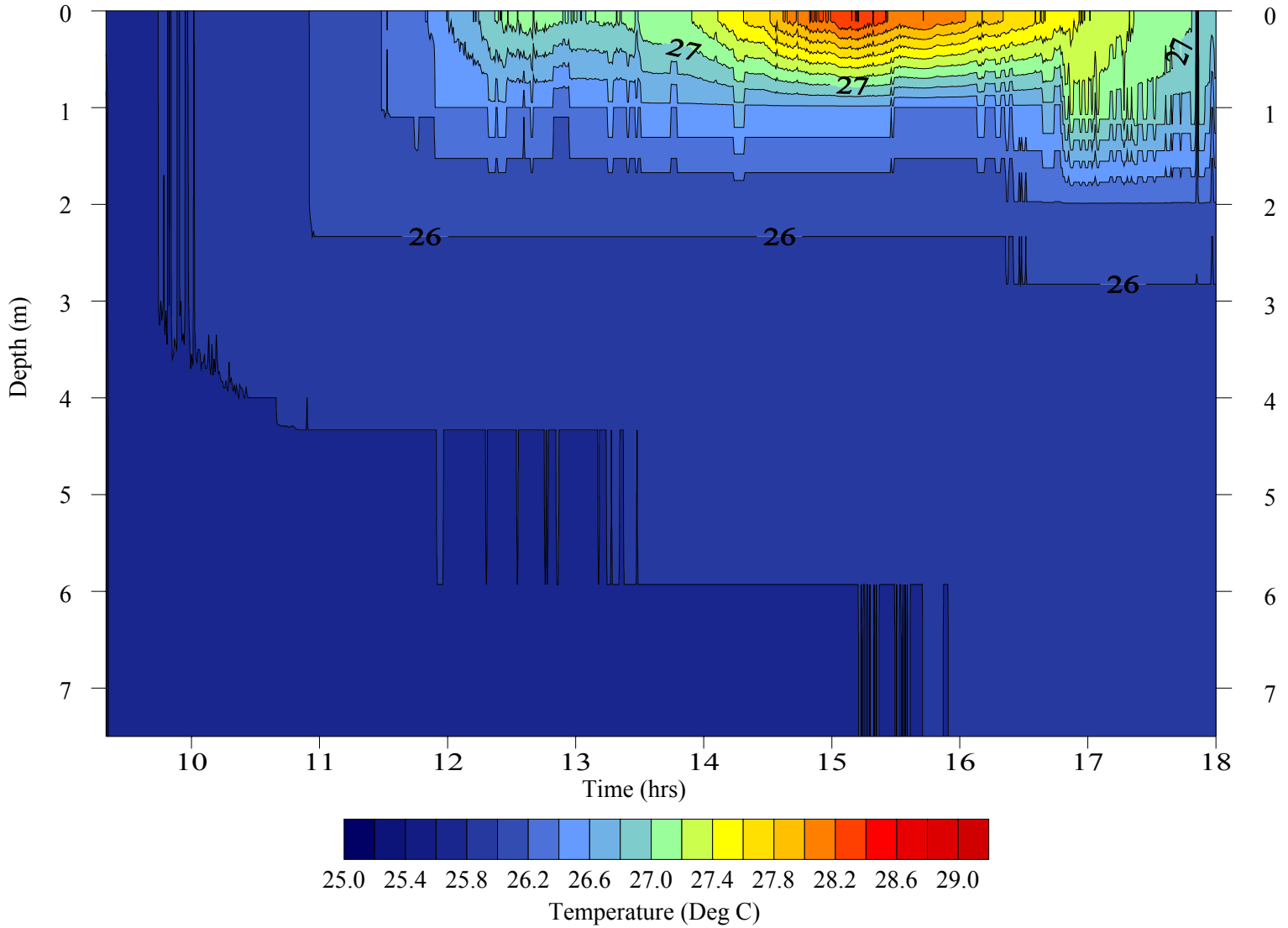

Figure 6.14: Diurnal Temperature in Fielding Bay for day of the year 330.

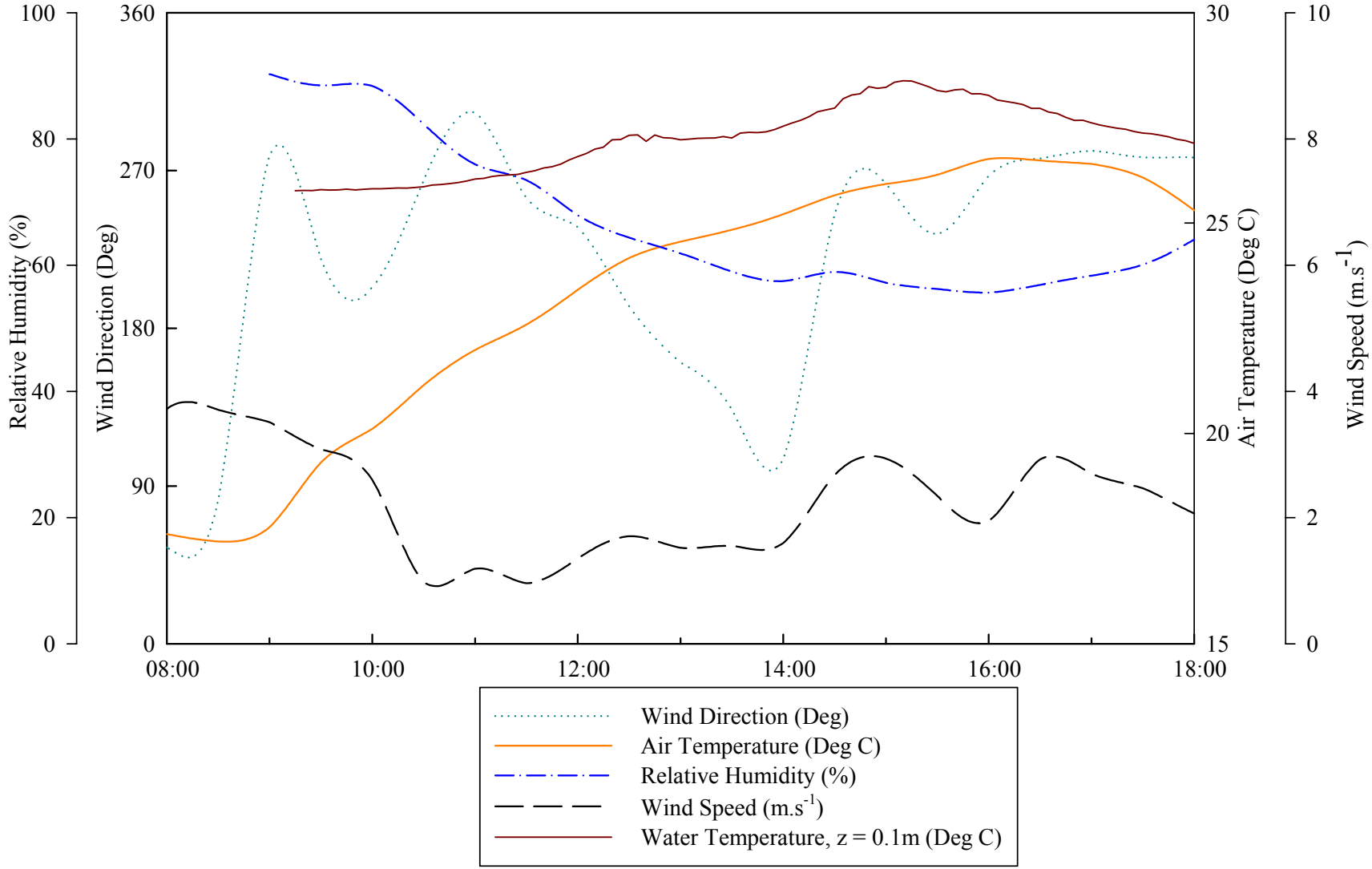

Figure 6.15: Meteorological Data for day of the year 330.

Table 6.1: Sampling Locations in Fielding Bay

Station	UTM EW	UTM NS	Max Depth (m)
FBS	529,400	49,500	9.5
FBC	528,600	49,750	7.5
FBW	528,178	49,366	3.0
FBN	527,818	50,188	3.0
FBE	529,578	50,888	5.0

Table 6.2: Spatial and Temporal Values of k_{PAR} in Fielding Bay

Date	Time	Station	k_{PAR} (m^{-1})
27-Sep-02	9:06	FBC	1.92
27-Sep-02	13:27	FBS	1.78
27-Sep-02	13:39	FBW	1.61
27-Sep-02	13:48	FBN	2.22
27-Sep-02	13:56	FBC	1.76
27-Sep-02	14:02	FBE	1.96
27-Sep-02	17:29	FBS	1.93
27-Sep-02	17:40	FBW	1.83
27-Sep-02	17:49	FBN	1.97
27-Sep-02	17:55	FBC	1.88
27-Sep-02	18:16	FBE	1.86
03-Oct-02	8:54	FBS	1.14
03-Oct-02	9:02	FBW	1.26
03-Oct-02	9:10	FBN	1.25
03-Oct-02	9:20	FBC	1.18
03-Oct-02	9:40	FBE	1.28
03-Oct-02	13:23	FBS	1.32
03-Oct-02	13:33	FBW	1.46
03-Oct-02	13:42	FBN	1.29
03-Oct-02	13:50	FBC	1.30
03-Oct-02	14:11	FBE	1.40
03-Oct-02	17:21	FBS	1.44
03-Oct-02	17:30	FBW	1.31
03-Oct-02	17:40	FBN	1.39
03-Oct-02	17:47	FBC	1.38
03-Oct-02	18:02	FBE	1.51
16-Oct-02	8:51	FBS	1.59
16-Oct-02	9:03	FBW	1.70
16-Oct-02	9:14	FBN	1.42
16-Oct-02	9:20	FBC	1.76
16-Oct-02	9:44	FBE	1.22
16-Oct-02	12:42	FBS	1.54
16-Oct-02	12:51	FBW	1.66

Table 6.2(Continued): Spatial and Temporal Values of k_{PAR} in Fielding Bay

Date	Time	Station	k_{PAR} (m^{-1})
16-Oct-02	12:59	FBN	1.87
16-Oct-02	13:07	FBC	1.90
16-Oct-02	13:29	FBE	1.45
23-Oct-02	17:10	FBS	1.55
23-Oct-02	17:18	FBW	1.47
23-Oct-02	17:31	FBN	1.77
23-Oct-02	17:39	FBC	1.80
23-Oct-02	18:01	FBE	1.65
23-Oct-02	9:09	FBS	1.81
23-Oct-02	9:19	FBW	1.62
23-Oct-02	9:29	FBN	1.60
23-Oct-02	9:38	FBC	1.89
23-Oct-02	10:14	FBE	1.83
23-Oct-02	12:43	FBS	1.66
23-Oct-02	12:51	FBW	1.73
23-Oct-02	13:00	FBN	1.74
23-Oct-02	13:08	FBC	1.81
23-Oct-02	13:31	FBE	1.81
29-Oct-02	17:15	FBS	1.79
29-Oct-02	17:26	FBW	1.69
29-Oct-02	17:34	FBN	1.63
29-Oct-02	17:43	FBC	1.85
29-Oct-02	17:59	FBE	2.11
29-Oct-02	8:25	FBS	1.64
29-Oct-02	8:36	FBW	1.92
29-Oct-02	8:44	FBN	1.80
29-Oct-02	8:51	FBC	1.88
29-Oct-02	9:10	FBE	1.76
29-Oct-02	12:42	FBS	1.82
29-Oct-02	12:52	FBW	1.57
29-Oct-02	13:00	FBN	1.70
29-Oct-02	13:14	FBC	1.67
29-Oct-02	13:30	FBE	1.80
05-Nov-02	17:14	FBS	0.68
05-Nov-02	17:25	FBW	0.81
05-Nov-02	17:34	FBN	0.97
05-Nov-02	17:49	FBC	1.86
05-Nov-02	18:01	FBE	2.37
05-Nov-02	8:55	FBS	1.56
05-Nov-02	9:05	FBW	1.54
05-Nov-02	9:15	FBN	1.47
05-Nov-02	9:24	FBC	1.43
05-Nov-02	9:42	FBE	1.30

Table 6.2 (Continued): Spatial and Temporal Values of k_{PAR} in Fielding Bay

Date	Time	Station	k_{PAR} (m^{-1})
05-Nov-02	12:55	FBS	1.50
05-Nov-02	13:05	FBW	1.35
05-Nov-02	13:13	FBN	1.40
05-Nov-02	13:21	FBC	1.88
05-Nov-02	13:21	FBE	1.13
05-Nov-02	17:14	FBS	1.83
05-Nov-02	17:24	FBW	1.22
05-Nov-02	-	FBN	Unavailable
05-Nov-02	17:43	FBC	1.72
05-Nov-02	-	FBE	Unavailable
26-Nov-02	9:18	FBS	1.31
26-Nov-02	9:29	FBW	1.39
26-Nov-02	9:37	FBN	1.62
26-Nov-02	9:46	FBC	1.27
26-Nov-02	10:10	FBE	1.25
26-Nov-02	12:44	FBS	1.39
26-Nov-02	12:57	FBW	1.54
26-Nov-02	13:06	FBN	1.40
26-Nov-02	13:19	FBC	1.55
26-Nov-02	13:33	FBE	1.56
26-Nov-02	17:26	FBS	2.22
26-Nov-02	17:36	FBW	1.57
26-Nov-02	17:44	FBN	1.51
26-Nov-02	17:57	FBC	1.59
26-Nov-02	18:14	FBE	1.50

APPENDIX II

Table 7.1: Planimetric Temperature Distribution. February 2000.

	Temperature Distribution (°C)				Average Gradient of Change	
Layer	5%	Mean	95%	$T_{95\%}$-$T_{5\%}$	Angle (°CW)	Slope (°C.100 km^{-1})
0 m	24.52	25.13	25.84	1.32	60.0	0.60
20 m	24.43	24.96	25.65	1.12	39.1	0.55
40 m	23.99	24.57	25.16	1.17	39.1	0.56
60 m	23.78	23.83	23.90	0.12	359.1	0.08

Table 7.2: Stability and Temperature by Quadrant. February 2000.

	Stability (Rank)	Temperature (°C)			
Section	($J.m^{-2}$)	0 m	20 m	40 m	60 m
NW	970 (3)	24.97	24.91	24.72	23.85
NE	1225 (1)	25.71	25.47	25.08	23.87
SW	992 (2)	25.83	24.84	24.37	23.79
SE	839 (4)	24.79	24.65	24.17	23.79

Table 7.3: Planimetric Temperature Distribution. August 2000.

	Temperature Distribution (°C)				Average Gradient of Change	
Layer	5%	Mean	95%	$T_{95\%}$-$T_{5\%}$	Angle (°CW)	Slope (°C.100 km^{-1})
0 m	23.95	24.47	25.03	1.08	18.9	0.34
20 m	23.86	24.10	24.35	0.49	43.9	0.11
40 m	23.80	23.96	24.15	0.35	97.4	0.23
60 m	23.85	23.94	24.08	0.23	118.0	0.22

Table 7.4: Stability and Temperature by Quadrant. August 2000.

	Stability (Rank)	Temperature (°C)			
Section	($J.m^{-2}$)	0 m	20 m	40 m	60 m
NW	619 (2)	24.65	24.27	23.86	23.86
NE	670 (1)	24.87	24.37	24.07	23.95
SW	493 (3)	24.24	24.18	24.20	24.09
SE	481 (4)	24.15	23.98	23.89	23.86

Table 7.5: Planimetric Temperature Distribution. February 2001.

	Temperature Distribution (°C)				Average Gradient of Change	
Layer	5%	Mean	95%	$T_{95\%}$-$T_{5\%}$	Angle (°CW)	Slope (°C.100 km^{-1})
0 m	24.46	24.90	25.62	1.16	357.5	0.56
20 m	24.11	24.52	25.15	1.03	8.3	0.53
40 m	23.99	24.20	24.53	0.54	25.7	0.29
60 m	23.99	24.06	24.15	0.16	9.9	0.11

Table 7.6: Stability and Temperature by Quadrant. February 2001.

	Stability (Rank)	Temperature (°C)			
Section	($J.m^{-2}$)	0 m	20 m	40 m	60 m
NW	752 (2)	25.01	24.71	24.30	24.07
NE	855 (1)	25.34	24.96	24.47	24.12
SW	595 (3)	24.61	24.31	24.07	24.01
SE	567 (4)	24.63	24.19	24.00	24.00

Table 7.7: Planimetric Temperature Distribution. August 2001.

	Temperature Distribution (°C)				Average Gradient of Change	
Layer	5%	Mean	95%	$T_{95\%}$-$T_{5\%}$	Angle (°CW)	Slope (°C.100 km^{-1})
0 m	24.21	24.60	25.19	0.98	28.7	0.41
20 m	24.14	24.33	24.60	0.46	70.1	0.11
40 m	23.89	24.17	24.47	0.60	94.7	0.23
60 m	23.91	24.00	24.12	0.21	107.1	0.19

Table 7.8: Stability and Temperature by Quadrant. August 2001.

	Stability (Rank)	Temperature (°C)			
Section	($J.m^{-2}$)	0 m	20 m	40 m	60 m
NW	627 (3)	24.66	24.31	24.09	23.93
NE	641 (2)	24.93	24.38	24.21	24.03
SW	674 (1)	24.55	24.53	24.49	24.11
SE	572 (4)	24.33	24.21	24.04	23.91

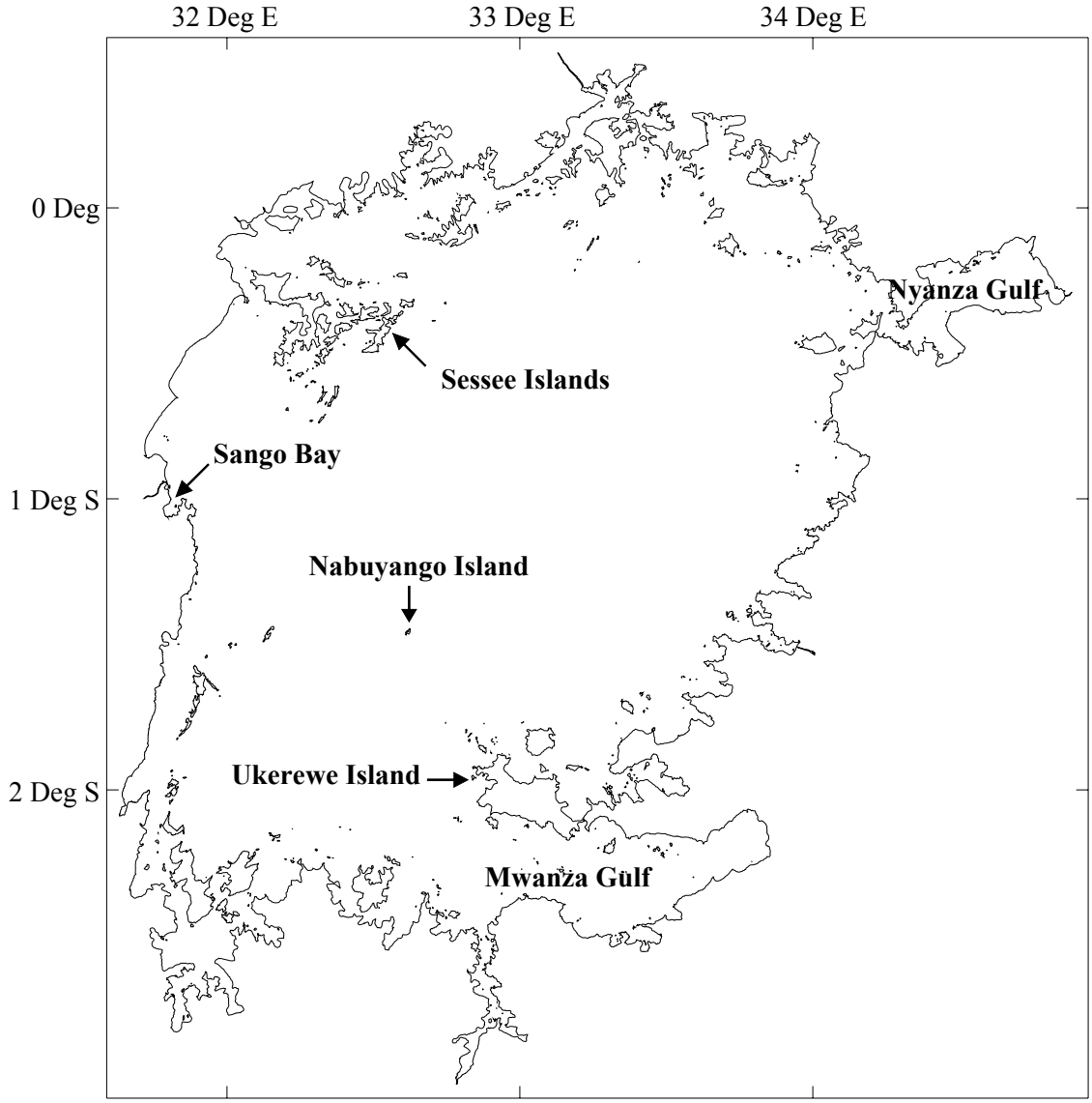

Figure 7.1: Map of Lake Victoria with georeferences of notable areas.

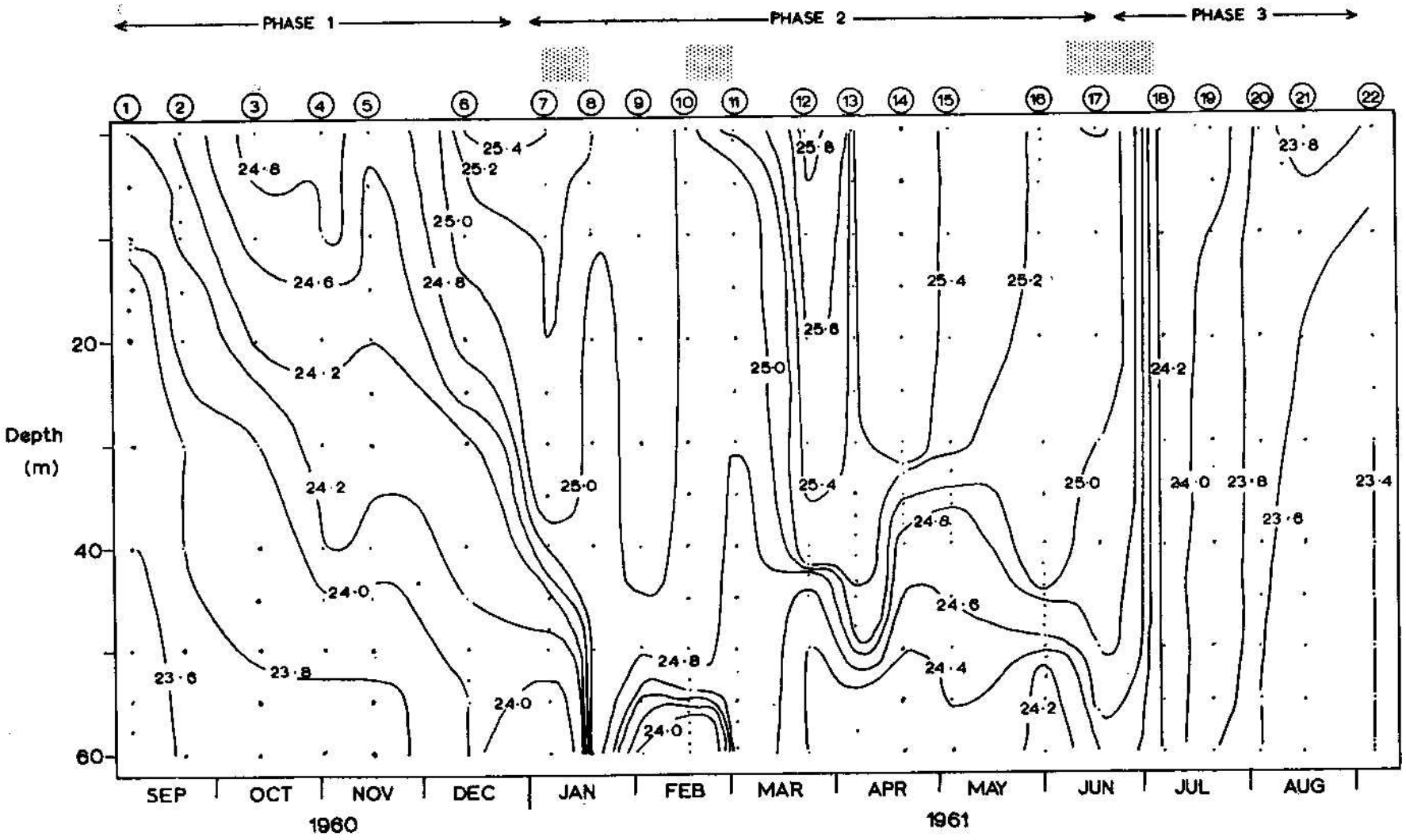

Figure 7.2: Temperature distribution with depth and time at the offshore station 'O' shown in Figure 3.1. From Talling 1966.

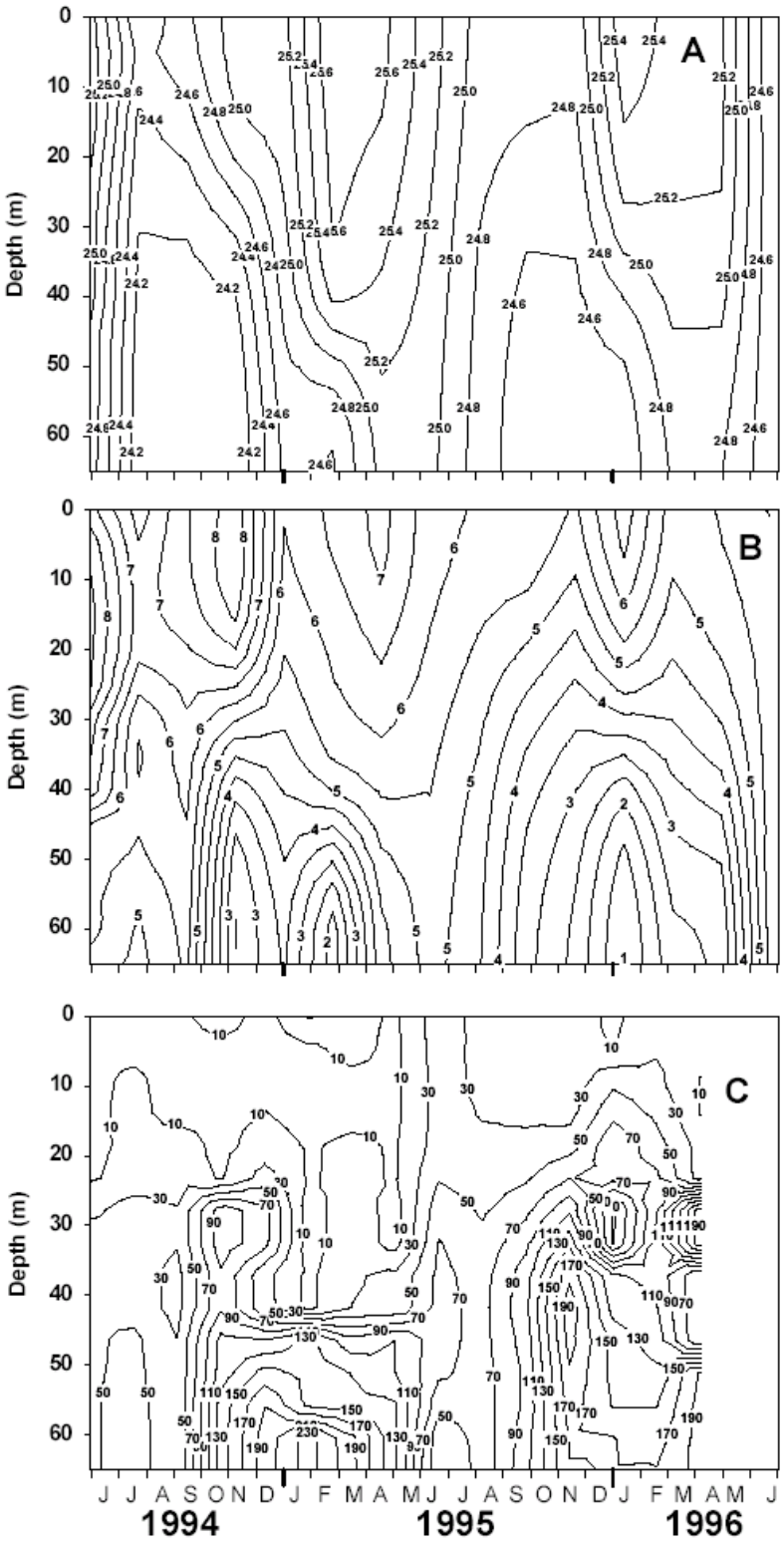

Figure 7.3: Temporal patterns of A) temperature (Deg C), B) dissolved oxygen ($mg.L^{-1}$) and C) CO_2 concentration ($\mu mol.L^{-1}$) at station B shown in Figure 3.1. From Ramlal 2002.

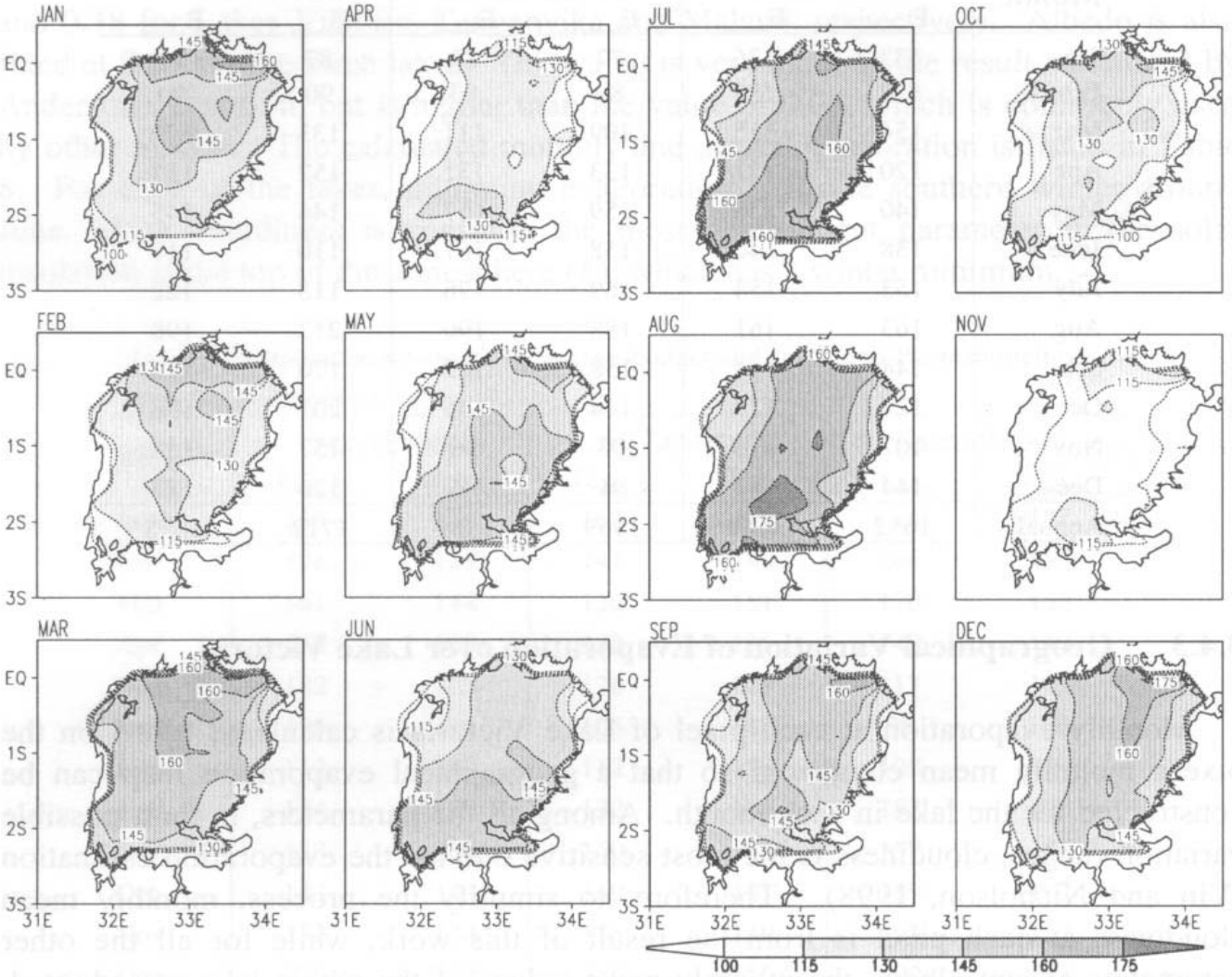

Figure 7.4: Monthly mean evaporation (solar irradiance) over Lake Victoria. From Nicholson and Yin 2002.

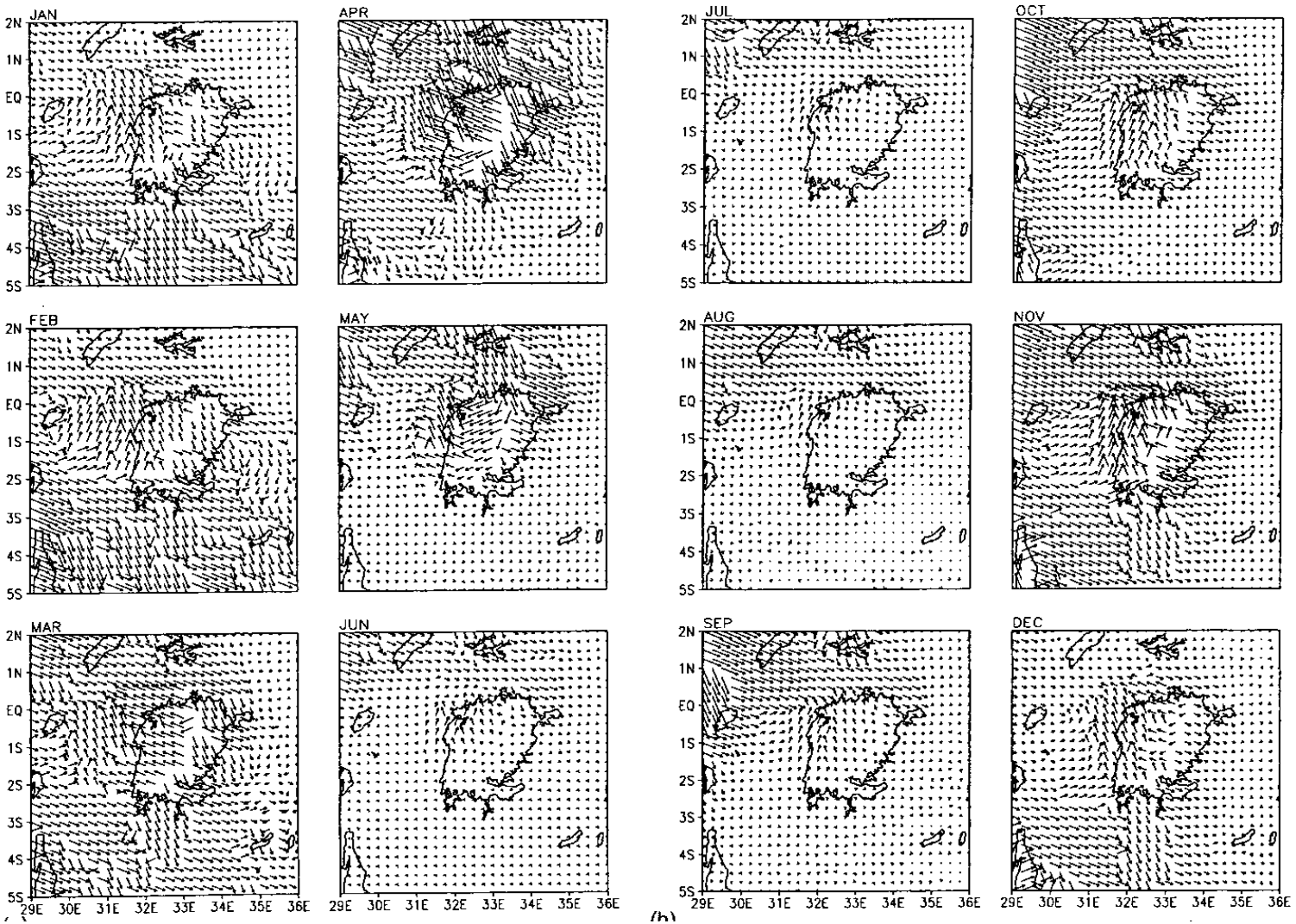

Figure 7.5: Phase of the coherent diurnal variations of cold cloud occurrences for each month of the year. The head of the arrow points to the time (UTC) of the maximum occurrence, such that a vertical arrow would be indicative of 04:00 UTC. From Yin et al. 2000.

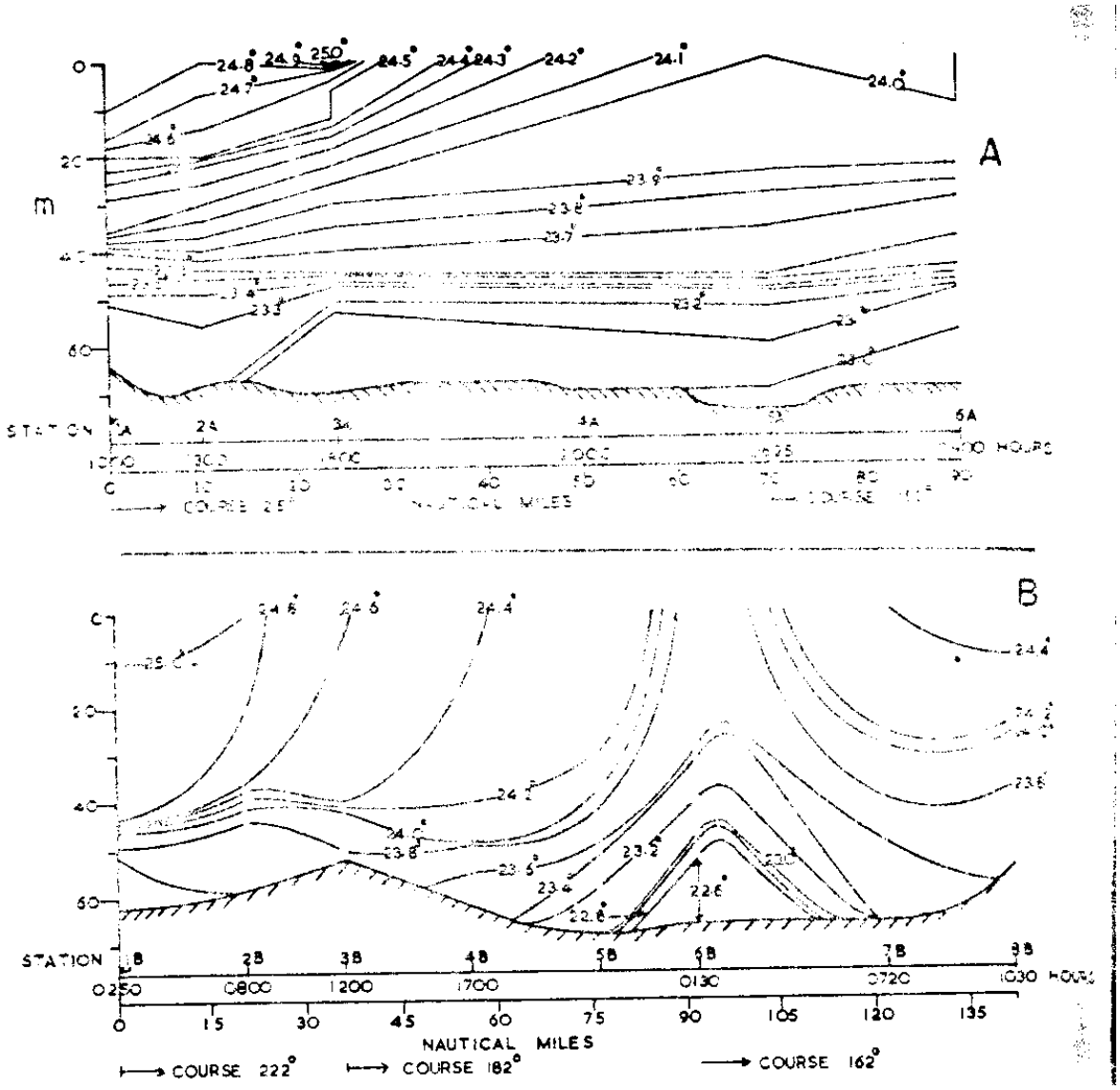

Figure 7.6: Distribution of isotherms along transects shown in Figure 3.1. From Kitaka 1972.

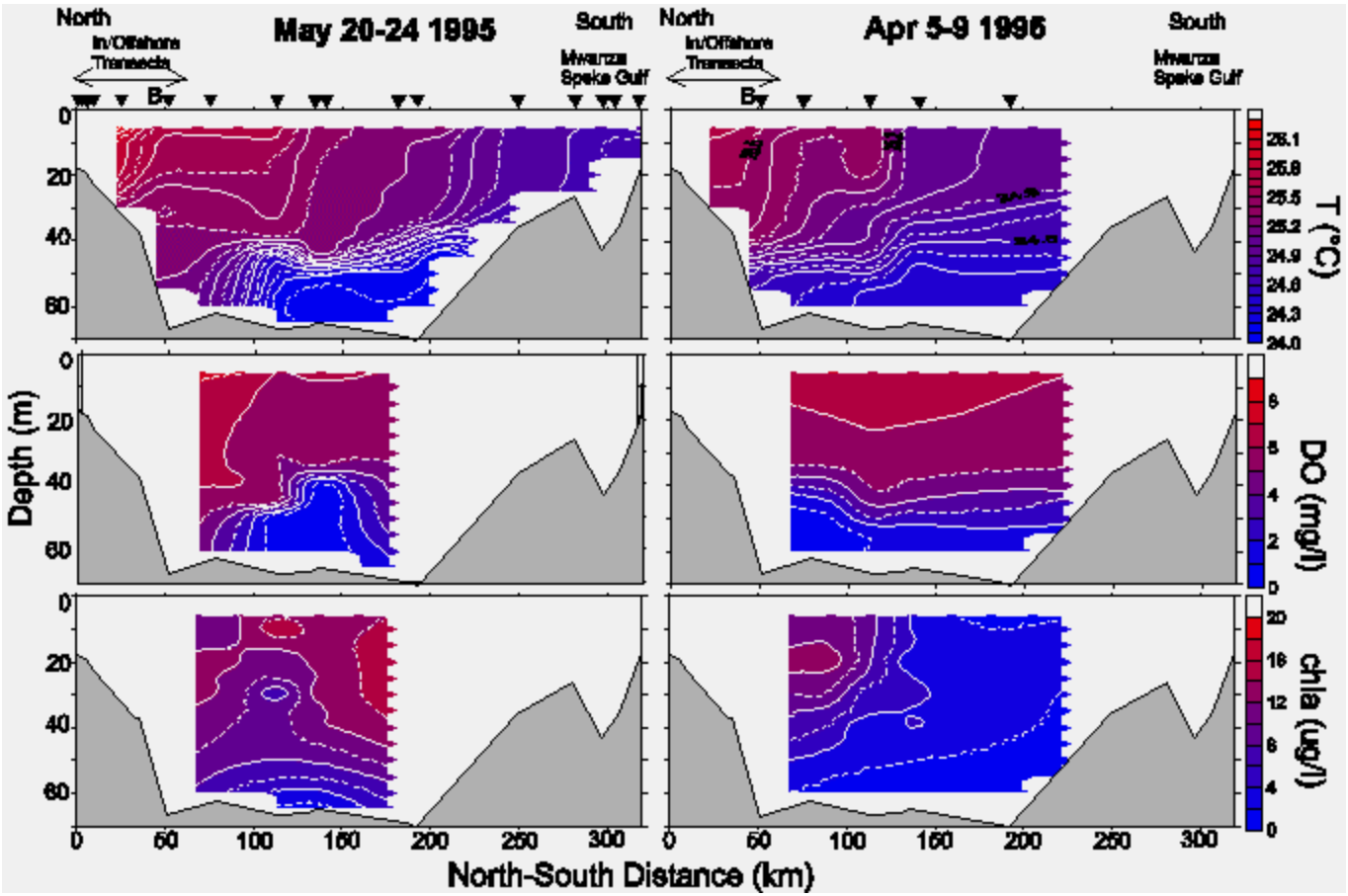

Figure 7.7: Temperature (Deg C), dissolved oxygen ($mg.L^{-1}$) and chlorophyll-a fluorescence ($\mu g.L^{-1}$) along the transect shown in Figure 3.1. From Romero et al. 2001.

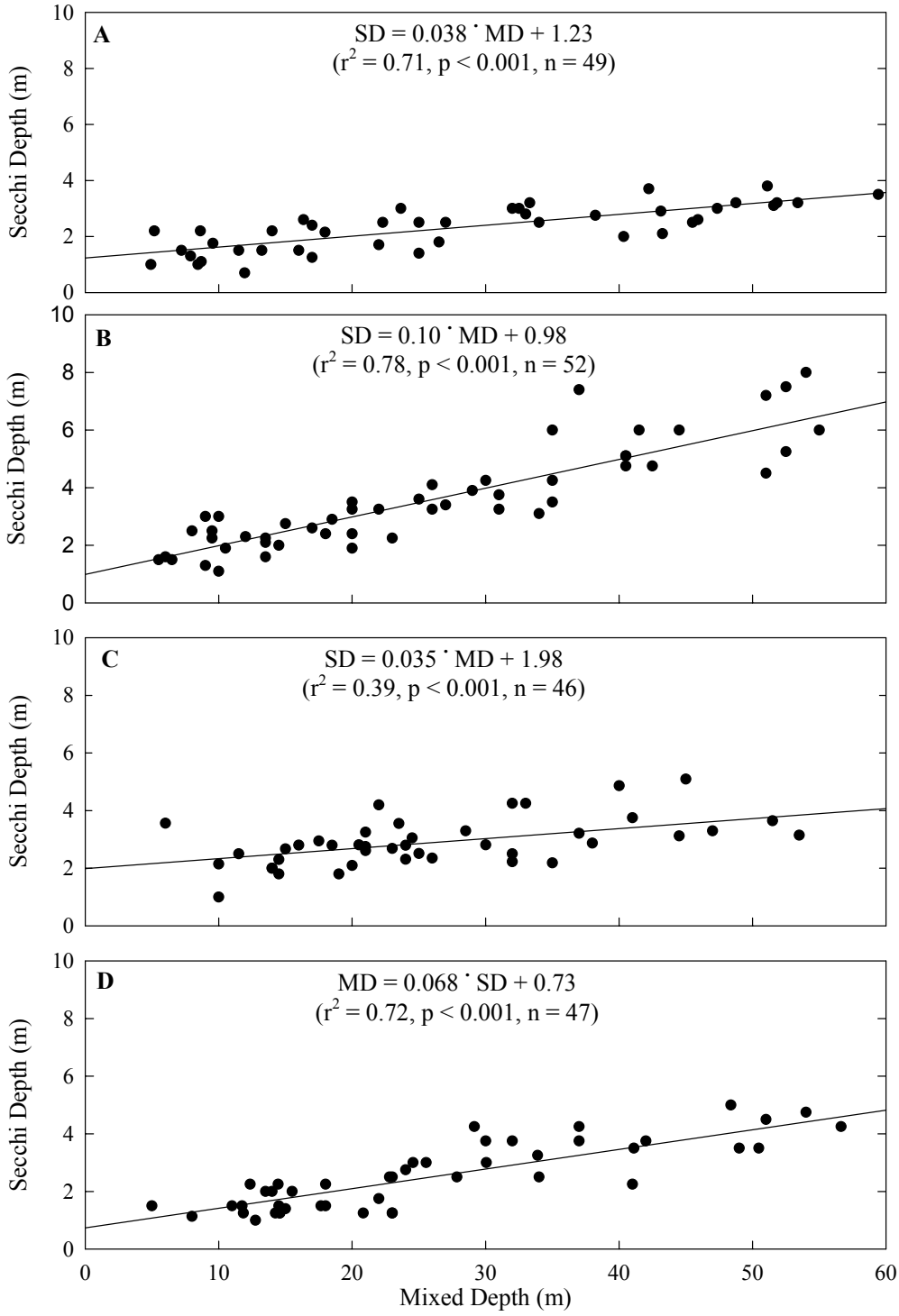

Figure 7.8: Regression of mixed depth versus Secchi depth for A) February 2000, B) August 2000, C) February 2001 and D) August 2001.

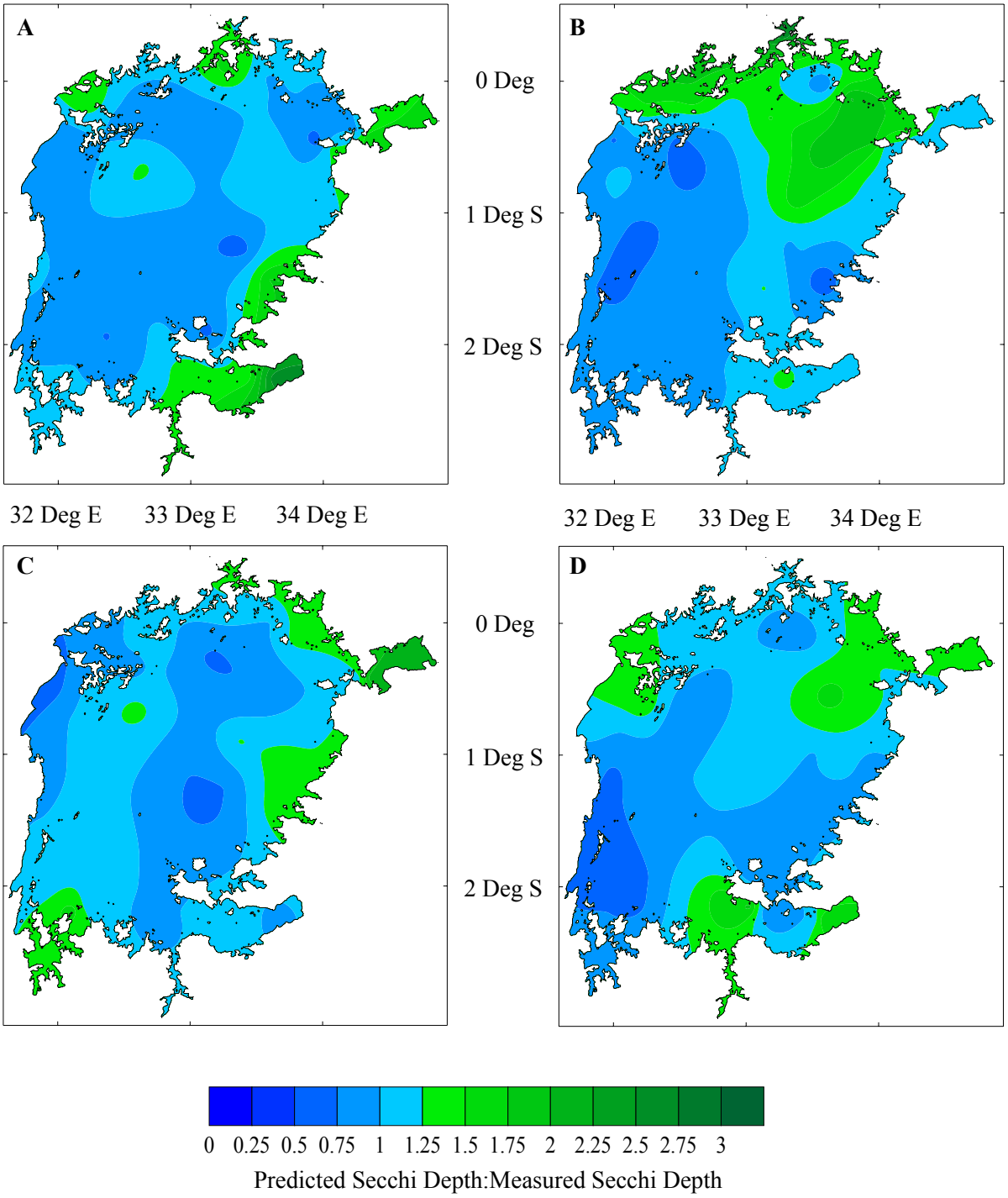

Figure 7.9: Spatial distribution of the ratio of predicted Secchi depth (Figure 7.7) to actual Secchi depth (Figure 3.26) for A) February 2000, B) August 2000, C) February 2001 and D) August 2001.

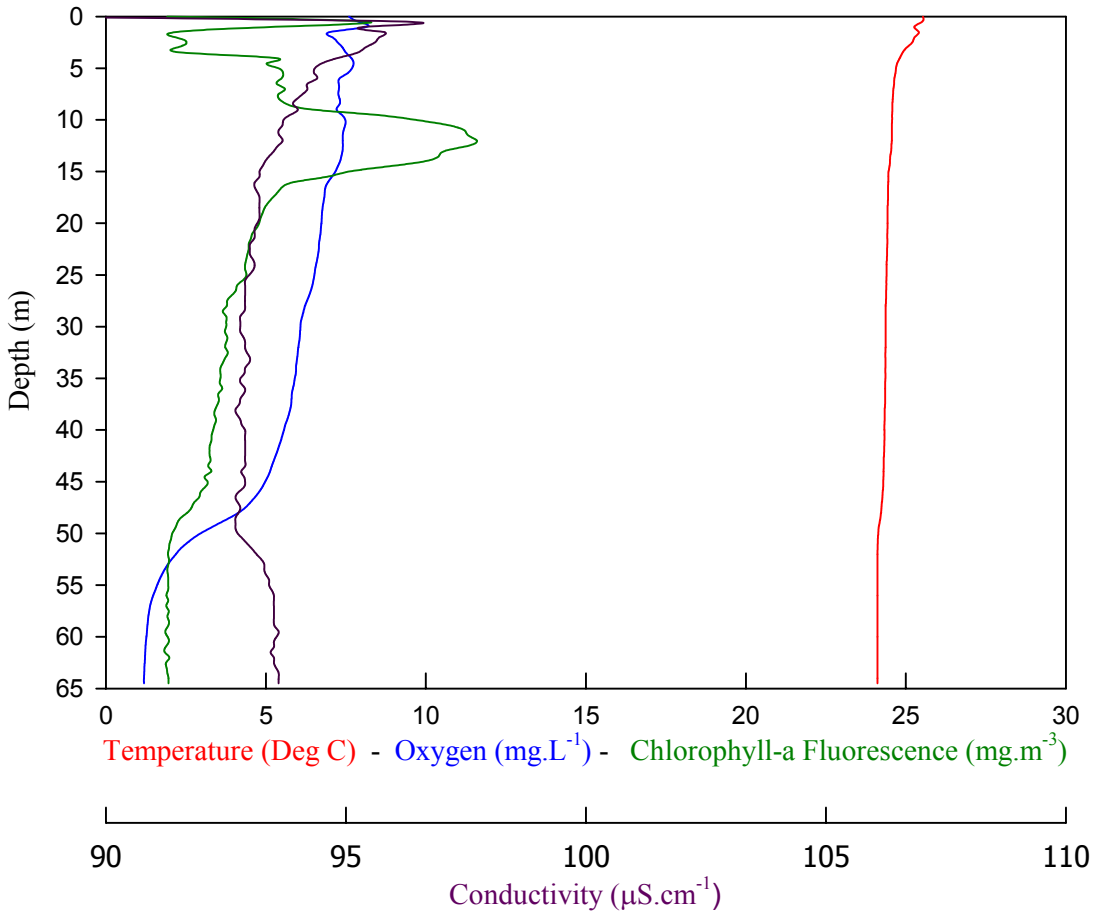

Date:	10-Feb-2001	UTM EW:	539,742
Time:	14:01	UTM NS:	-100,010
Secchi Depth (m):	3.29	Maximum Depth (m):	64.50

Figure 7.10: Profile showing an inferred mixed depth of 45 m.

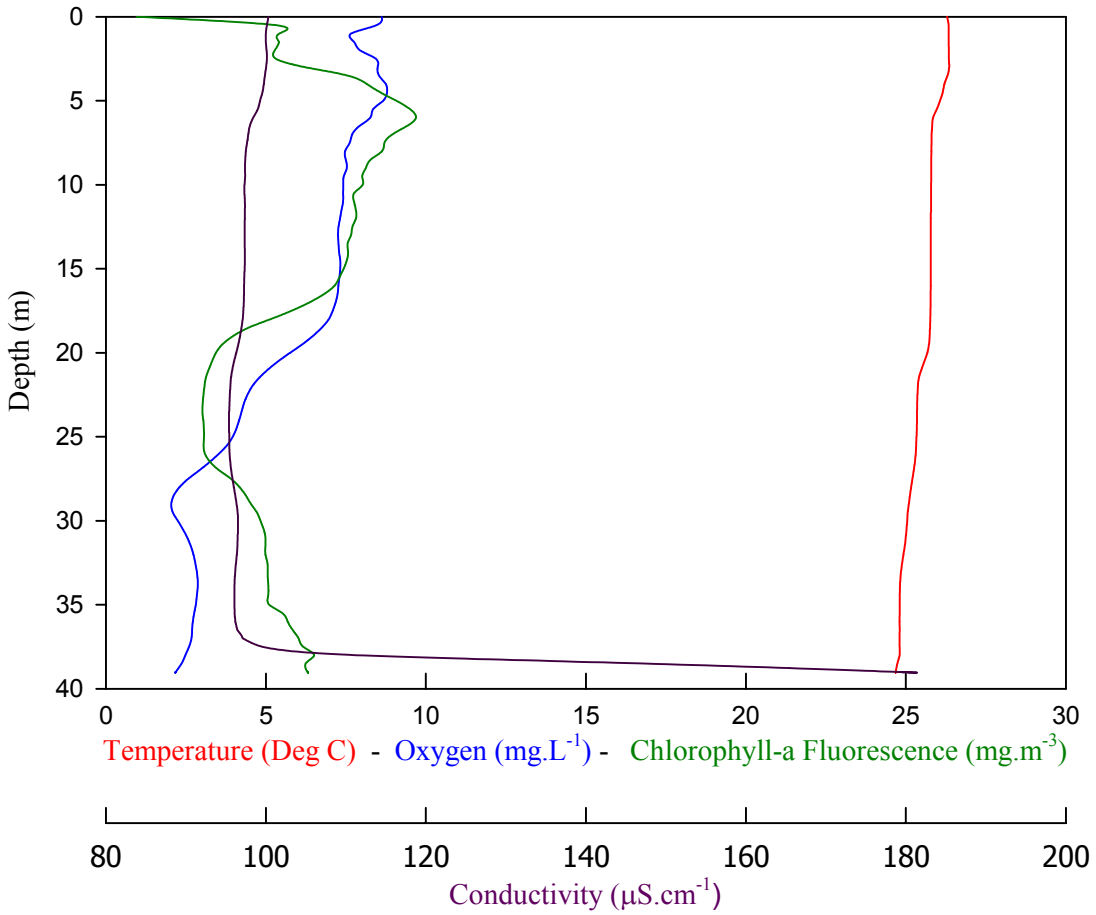

Date:	17-Feb-2000	UTM EW:	451,272
Time:	14:55	UTM NS:	-14,894
Secchi Depth (m):	2.4	Maximum Depth (m):	39.01

Figure 7.11: Profile showing an inferred mixed depth of 18 m.